ADAPTIVE CHANNEL MEASUREMENT STUDY

Phillip A. Bello, et al

CNR, Incorporated

Prepared for:

Rome Air Development Center

September 1975

RADC-TR-75-243
Final Technical Report
September 1975

ADAPTIVE CHANNEL MEASUREMENT STUDY

CMR, Inc.

Approved for public release;
distribution unlimited.

Laboratory Directors' Fund No. 01717413

Rome Air Development Center
Air Force Systems Command
Griffiss Air Force Base, New York 13441

DISCLAIMER NOTICE

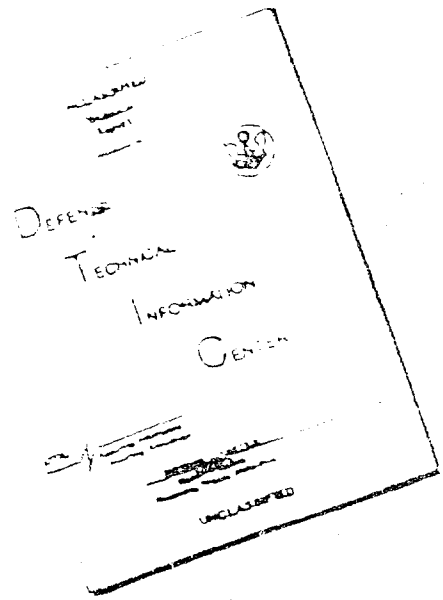

THIS DOCUMENT IS BEST QUALITY AVAILABLE. THE COPY FURNISHED TO DTIC CONTAINED A SIGNIFICANT NUMBER OF PAGES WHICH DO NOT REPRODUCE LEGIBLY.

UNCLASSIFIED

SECURITY CLASSIFICATION OF THIS PAGE *(When Data Entered)*

REPORT DOCUMENTATION PAGE		READ INSTRUCTIONS BEFORE COMPLETING FORM
1. REPORT NUMBER RADC-TR-75-243	2. GOVT ACCESSION NO.	3. RECIPIENT'S CATALOG NUMBER
4. TITLE *(and Subtitle)* ADAPTIVE CHANNEL MEASUREMENT STUDY		5. TYPE OF REPORT & PERIOD COVERED Final Technical Report June 1974 - February 1975
		6. PERFORMING ORG. REPORT NUMBER N/A
7. AUTHOR(s) Phillip A. Bello Charles J. Boardman Louis E. Jankauskas		8. CONTRACT OR GRANT NUMBER(s) F30602-74-C-0283
9. PERFORMING ORGANIZATION NAME AND ADDRESS CNR, Inc. 20 Wells Avenue Newton MA 02159		10. PROGRAM ELEMENT, PROJECT, TASK AREA & WORK UNIT NUMBERS 61101F 01717413
11. CONTROLLING OFFICE NAME AND ADDRESS Rome Air Development Center (DCLD) Griffiss AFB NY 13441		12. REPORT DATE September 1975
		13. NUMBER OF PAGES 332
14. MONITORING AGENCY NAME & ADDRESS*(if different from Controlling Office)* Same		15. SECURITY CLASS. *(of this report)* UNCLASSIFIED
		15a. DECLASSIFICATION/DOWNGRADING SCHEDULE N/A

16. DISTRIBUTION STATEMENT *(of this Report)*

Approved for public release; distribution unlimited.

17. DISTRIBUTION STATEMENT *(of the abstract entered in Block 20, if different from Report)*

Same

18. SUPPLEMENTARY NOTES

RADC Project Engineer:
Arnold E. Argenzia (DCLD)

This effort was funded totally by the Laboratory Directors' Fund.

19. KEY WORDS *(Continue on reverse side if necessary and identify by block number)*

Performance Assessment; Technical Control; Fault Location;
PCM/TDM-FM Microwave Relay Digital Communications

20. ABSTRACT *(Continue on reverse side if necessary and identify by block number)*

This study is concerned with performance assessment, fault location, and degradation trending for PCM/TDM-FM digital transmission over DCS microwave relay systems. The reported work complements and integrates previous work to provide a comprehensive new systems-theoretic approach to channel quality monitoring called the parametric approach. In this approach, three basic quality measurement units are defined - the TQU, MQU, and RQU - which measure channel parameters at the transmitter output, receiver input, and receiver output interfaces. The potentialities of adaptive channel parameter measurement

DD FORM 1 JAN 73 1473 EDITION OF 1 NOV 65 IS OBSOLETE

UNCLASSIFIED

SECURITY CLASSIFICATION OF THIS PAGE *(When Data Entered)*

techniques are investigated with the aid of computer simulation and analysis. Consideration was given to the use of different adaptation algorithms, multipath fading, the accuracy of parameter measurement, adaptation time constants, and the estimation of error rates from the measured channel parameters. For the channel disturbance model chosen, the calculations indicate that the adaptive channel parameter measurement technique represents a viable basis for performance assessment.

This report has been reviewed by the RADC Information Office (OI) and is releasable to the National Technical Information Service (NTIS). At NTIS it will be available to the general public, including foreign nations.

This technical report has been reviewed and is approved for publication.

APPROVED: Arnold E Argenzia

ARNOLD E. ARGENZIA
Project Engineer

APPROVED: Fred I Diamond

FRED I. DIAMOND
Technical Director
Communications & Control Division

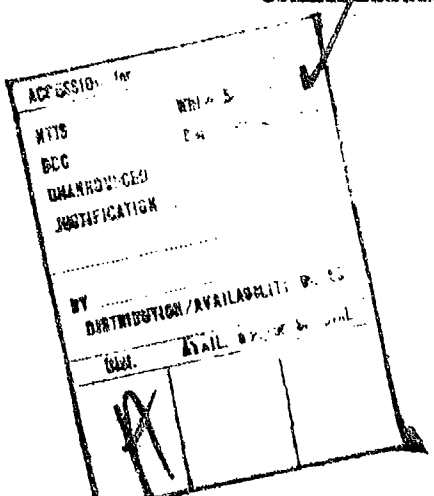

FOR THE COMMANDER: John P. Huss

JOHN P. HUSS
Acting Chief, Plans Office

This effort was funded totally by the Laboratory Directors' Fund.

Do not return this copy; retain or destroy.

PREFACE

This final report covering the period June 1974 to February 1975 was prepared by CNR, Inc., of Newton, Massachusetts, under Contract No. F30602-74-C-0283, Job Order No. 01717413.

This study was carried out primarily by Dr. P. A. Bello, Dr. L. E. Jankauskas, and Mr. C. J. Boardman. Additional services were provided by Mr. R. Pinto, Mr. D. Goldfein, Mr. M. Bello, and Mr. A. Joffe. The program was directed by Dr. P. A. Bello.

The authors wish to acknowledge the ready and willing assistance of Mr. A. Argenzia, RADC (DCLD) Project Engineer. Also, discussions with Mr. Donald Iram, head of the Digital Technical Control Group, were helpful.

TABLE OF CONTENTS

TABLE OF CONTENTS (CONTINUED)

TABLE OF CONTENTS (CONTINUED)

LIST OF ILLUSTRATIONS

LIST OF ILLUSTRATIONS (CONTINUED)

LIST OF ILLUSTRATIONS (CONTINUED)

LIST OF ILLUSTRATIONS (CONTINUED)

LIST OF ILLUSTRATIONS (CONTINUED)

LIST OF TABLES

EVALUATION

The objective of this effort was to develop adaptive digital processing techniques for Communications Performance Monitoring Assessment (CPMAS, of digital communications systems that were determined to be most applicable to the future high speed digital environment of the Defense Communications System (DCS). In order to provide a thorough analysis on a program of fixed scope, it was determined that a line-of-sight megabit communications system should be used to best evaluate the adaptive technique concept. Therefore, primary attention was given to a line-of-sight digital communications upgrade system within the European DCS known as the Frankfurt-Koenigstuhl-Vaihingen (FKV) system. This system employs a 3-level partial response modem in conjunction with an FM radio. For the case of propagation media disturbances and the modem techniques studied, the simplest parameterized model adequate for performance assessment involves a quadratic frequency representation of the complex channel transfer function, together with an expansion of the discriminator output such that the first two linear distortion terms and the first nonlinear distortion term only are retained. The parameters P_1 and P_3 characterizing the first-order linear and nonlinear distortion, respectively, were shown to be of major importance in performance assessment. These parameters may be measured and used for degradation trending well before any distortion is detectable by examination of the eye-pattern (e.g., eye-opening).

The Least Mean Square (LMS) algorithm used with appropriately normalized parameters (called Variance Equalization) was found to require the minimum

number of iterations to measure the desired channel parameters with the required amount of accuracy for performance assessment.

On the order of 9000 iterations are more than adequate to provide parameter estimates of sufficient accuracy for performance assessment, assuming that changes in bit sync timing are determined relative to a reference established under nondispersive conditions. Given the slowness of fading on LOS links, it should be satisfactory to update parameter measurements every second, which leads to a sampling rate of around 9000 per second. The sampling rate is low enough that inexpensive 12-bit A/D converters and modestly-priced multipliers may be used in the digital processing.

Because of the sharp threshold behavior of error rate with the parameters P_1 and P_3, high accuracy in measurement of P_1 and P_3 is required only if it is desired to estimate error rates from P_1 and P_3 in the vicinity of the threshold. To achieve error rate estimates to within a fraction of a decade of probability in this threshold region requires 1% accuracy in measurement of P_1 and a few percent accuracy in measurement of P_3, both of which are achievable with 9000 iterations.

The convergence time for the parameter estimates depends upon the rate at which iterations for parameter adjustment are made. Since (conservatively) 9000 iterations are required and iterations can occur at the bit rate of 14 Mb/s, convergence could take place in less than one millisecond. However, the implementation would be very expensive and would require analog processing. Since an update rate of 1 per second is satisfactory, 9000 iterations/second can be assumed in practice. For the

LMS algorithm, 13 multiplications are required per iteration, yielding a requirement of 117,000 multiplications/second.

Due to the positive results obtained on the quadratic frequency selective fading model for the case of propagation medium distortions, it is recommended that this effort be expanded to include equipment induced distortions. Since the parameters P_1 and P_3 can be used to give a precursor indication of system health even before distortion is detectable by an eye-pattern monitor, the adaptive concept as a CPMAS tool is quite valuable and should be expanded further.

Arnold L. Argenzia

ARNOLD L. ARGENZIA
Project Engineer

SECTION 1

SUMMARY

This study is concerned with channel quality monitoring for digital transmission over radio channels. While the detailed calculations are for terrestrial microwave relay LOS systems appropriate to the DCS (Defense Communication System), the approach introduced has general applicability. Present DCS microwave LOS systems use conventional analog transmission by frequency modulation of frequency-division-multiplexed voice channels (FDM-FM). Plans for changing from the existing analog FDM-FM plant to a digital PCM-TDM-FM or PM plant have been set forth by the Defense Communication Agency (DCA). Among the problems associated with this changeover is the development of appropriate performance assessment, fault location, and degradation trending techniques applicable to digital systems.

This study complements and integrates previous work on this problem by CNR [1.1] to provide a comprehensive new approach to channel quality monitoring called the parametric approach. The study includes detailed analysis and simulation, illustrating the application of adaptive channel measurement to this approach. In this first section of the final report, we present a brief summary of the results of the study, recommendations for further work, and an outline of the contents of the report.

1.1 Summary and Conclusions

From the point of view of system theory, a communications link or channel consists of a cascade of linear and nonlinear signal processing operations which transform the "input" signal into the "output" signal, where suitable interfaces at baseband, intermediate frequency (IF), or radio frequency (RF) have been defined to make the terms "input signal" and "output signal" explicit. A systems-theoretic approach to channel quality monitoring is taken in the study. In this connection, it is found that a most effective subdivision of the communication system is into:

- Transmitter channels
- Propagation channels
- Receiver channels
- Nodes

The first three items include the analog processing common to both the existing analog FDM-FM system and the PCM-TDM-FM digital communications approach. The latter system is regarded as the first evolutionary change from the existing plant. Baseband digital modems in the nodes provide the transition from the common analog processing to the digital NRZ signals of the PCM-TDM-FM system.

Sources of performance impairment and resulting channel disturbances are tabulated for the signal processing constituents of the transmitter, propagation, and receiver channels. These disturbances can be classified into one of the four categories:

- Signal reduction or loss
- Increased noise or interference level
- Linear signal distortion
- Nonlinear signal distortion

The "threshold" characteristics of the performance of a digital communication system as a function of these disturbances is pointed out. It is concluded that to obtain a means of performance assessment that will provide a basis for meaningful degradation trending with advance warning of impending faults, it is essential that channel parameters characterizing the four classes of disturbances be continually measured and related to estimated and extrapolated system performance.

Channel parameter measurement techniques are reviewed. It is concluded that the use of the demodulated data signal as if it were a channel probing signal can provide an effective basis for channel measurement on DCS LOS microwave systems. This is based upon the observation that standard system design is for high performance per link, e.g., 5×10^{-9} error rate at 12.6 Mb/s, while considerably higher error rates may be expected to allow effective functioning of data derived channel measurement techniques. For example, for the impairments studied, error rates as high as 10^{-3} had a small effect on channel parameter measurement (see 4.4.2.4 and Appendix G). The diurnal two-state character of microwave LOS links, i.e., nonfading vs. fading, is particularly convenient for isolating the effect on channel parameters of slowly deteriorating equipment from multipath and flat fading.

A detailed examination of the linear and nonlinear input-output signal processing relationships for the various modulation/demodulation, RF/IF filtering, and propagation media operations in the LOS system is carried out as a prelude to demonstrating methods of parameterizing the input-output behavior of the

transmitter, propagation, and receiver channels. Several methods for the characterization of input-output behavior are presented with particular attention given to representations of the frequency discriminator output in terms of linear and nonlinear distortion terms completely specified except for a set of parameters. These representations apply equally to the analog FDM-FM system and to the digital PCM-TDM-FM system because they are concerned with the transmitter, propagation, and receiver channels, which are common. However, the relative importance of particular channel parameters in reflecting degradation need not be the same at all for the two systems.

Given a parameterized representation of the input-output behavior from the transmitted NRZ baseband signal to any interface, it is possible to employ the approach of adaptive filtering to measure these parameters. The output data signal is used as a replica of the transmitted data signal and passed through a model of the parameterized system. Automatic adjustment of the parameters of the model are made until the output of the adaptive filter matches the channel signal as close as possible.

Several algorithms are available for these adjustments, among which the LMS (least mean squared) algorithm is frequently used. This algorithm attempts to adjust the parameters until the reconstructed channel signal differs from the actual channel signal in a minimum mean-squared error sense. There is a trade-off between the speed of adaptation and the closeness to which the actual error approaches the minimum mean-squared error — the slower the adaptation, the closer the approximation. Fortunately, the rate of fading on LOS links, even for deep fades, is sufficiently slow (sizable fractions of a second) and the data rates sufficiently high (12.6 Mb/s) that little difficulty will be encountered in achieving close to optimum performance if a sufficiently good parameterized model is used.

Specific calculations of the performance of adaptive channel parameter measurement have been carried out in the study to illustrate the effectiveness of this approach to performance assessment. A restricted channel model* was employed that included only the distortion caused by multipath fading in the propagation channel. In the simplest case considered it is shown that the discriminator output $\nu(t)$ may be related to the frequency modulator input $x(t)$ by the approximate parameteric representation

*This model and its generalizations can also handle the measurement of channel distortion parameters caused by RF and IF filtering.

$$\nu(t) = P_0 x(t-\xi_0) + P_1 \dot{x}(t-\xi_0) + P_2 \ddot{x}(t-\xi_0) + P_3 x(t-\xi_0)\dot{x}(t-\xi_0) \quad (1.1)$$

which includes significant linear distortion terms up to second-order and first-order nonlinear terms. The quantity ξ_0 represents the average delay of the channel. Equation (1.1) is called the quadratic model because it involves use of a three-term power series expansion of the transfer function of the channel. A more involved input-output representation than (1.1) is also used in the study, based upon a four-term or "cubic" expansion of the transfer function.

The baseband modem assumed for analysis is the one being considered for the Phase I DCS upgrade — the so-called "duo-binary" modem [1.2]. To be consistent with DCS requirements, the modulation index of the baseband modem signal into the frequency modulator is adjusted so that the transmitted RF signal occupies a 99% power bandwidth of 14 MHz for a data rate of 12.6 Mb/s.

While the channel parameters $\{P_k\}$ can apply to the composite effect of multipath fading and any RF or IF filter distortion, attention was confined to performance evaluations for a multipath channel because much faster adaptation is required for multipath fading than equipment variations. The three-path multipath model used for representative calculations is taken from those developed by CNR in a previous study for RADC [1.3] assuming a typical DCS 30-mile link. This model involves a direct path and two equal strength multipath components. For the example chosen the multipath components were of amplitude 1.25 times the direct path and around 1.6 and 2.2 nanoseconds after the direct path.

It was shown in [1.3] that the degree of frequency selectivity increases with fade depth. Moreover, at a given fade depth, the degree of distortion produced varies according to the relative phases of the paths. In order to keep the effort within reasonable bounds, for comparative performance analysis, "good" and "bad" channels are defined at a given fading depth according to whether the channel phases have been adjusted roughly for minimum or maximum values of the channel parameters $\{P_k\}$, respectively.

Appendix B contains plots of the amplitude and group delay vs. frequency for the transfer functions of the "bad" and "good" channels at various fade depths. These may be regarded as "snapshots" of the time-variant transfer function exhibiting different degrees of distortion at a given fade depth. Figures 1.1 and 1.2

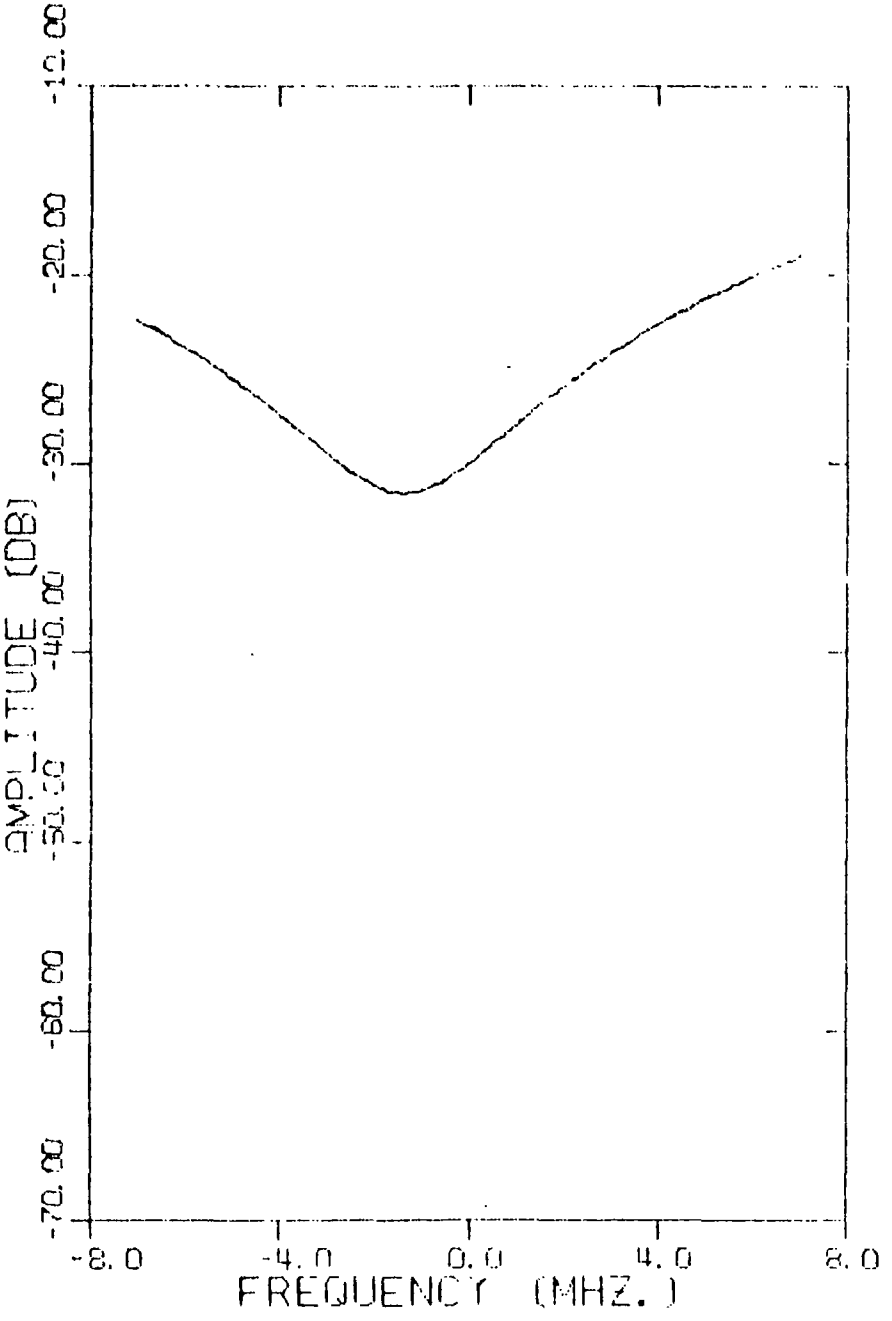

Figure 1.1 Amplitude Vs. Frequency for 30 dB Fade ("Bad" Channel)

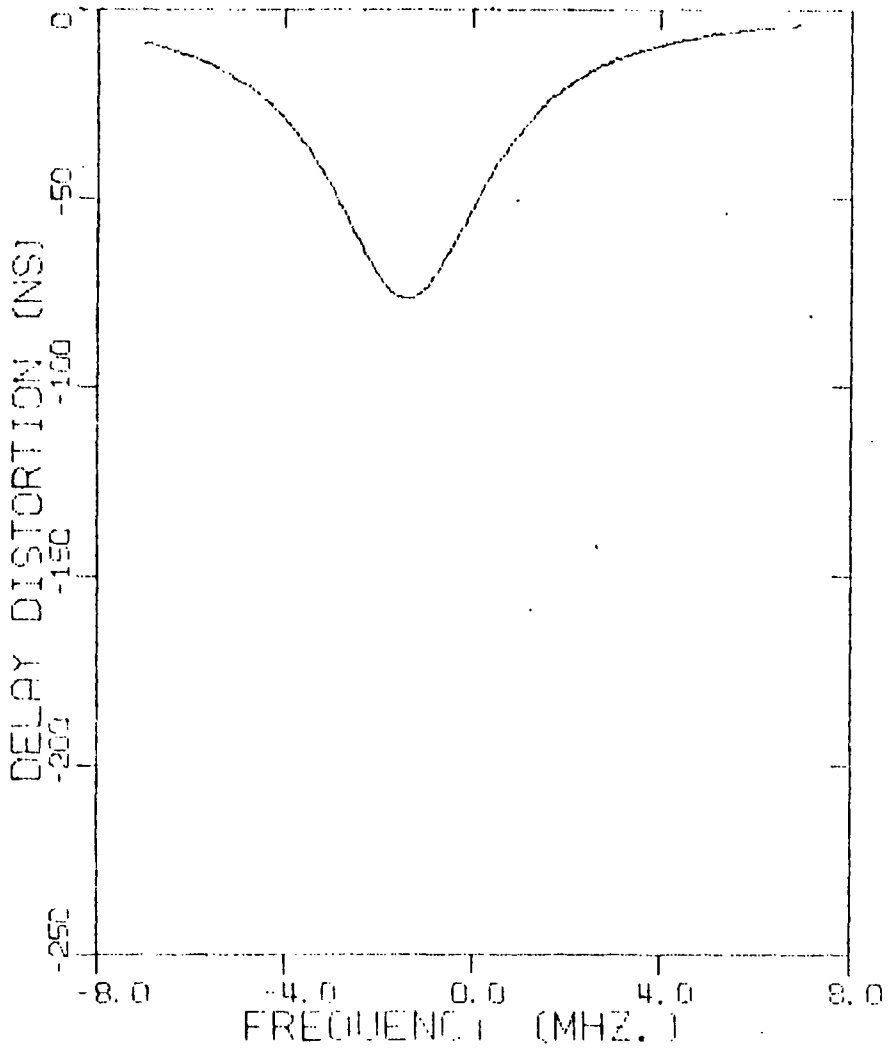

Figure 1.2 Group Delay Vs. Frequency for 30 dB Fade ("Bad" Channel)

show the transfer function amplitude and group delay vs. frequency for a 30 dB fade, while Figs. 1.3 and 1.4 show them for a 32 dB fade, both assuming the "bad" channels. The fade depth is defined at the center of the band, f=0 in these figures. While the group delay is negative in Figs. 1.2 and 1.4 there are equally "bad" channels for which the group delay vs. frequency is the opposite sign. The three-term power series expansion of the complex transfer function produces amplitude and group delay plots which differ so little from the actual plots that this difference was not observable in plots such as shown in Figs. 1.1 to 1.4.

The "bad" channel is defined as the condition wherein the multipath components are phased to produce a high degree of signal distortion at a given fade depth. This state produces error rates considerably higher than those for flat fading. Figure 1.5 shows a plot of the "three-level" error rate of the duobinary modem* vs. fade depth for the three-path "bad" channel. It is assumed that the bit synchronizer exactly tracks the changing group delay to minimize bit error probability. The noise level is adjusted so that at a 40-dB flat fade the three-level error probability will be 5×10^{-9}. For the "bad" channel, this error rate is reached at a fade depth of 29.5 dB — a 10.5-dB penalty in SNR performance. If the bit synchronizer does not carry out such good tracking, the error rate will be worse.

The increased error rate at a given fade depth is caused by selective fading which produces intersymbol interference. As the fade depth increases, the distortion parameters increase, resulting in a further increase in error rate. Figures 1.6 and 1.7 present plots of three-level error rate as a function of dimensionless parameters P_1/T and P_3/T^2, where T is the bit duration. Note the rapid increase in error rate with P_1 and P_3 which is quite similar to an increase in error rate with noise level for a distortionless system. A "threshold" effect may be observed with the error rate rising rapidly for values of P_1/T less than $-.7$ or P_3/T^2 exceeding .6. The parameter P_2 was found to have little effect on error rate.

Clearly performance assessment is possible via such relationships as produced the results in Figs. 1.6 and 1.7 when P_1 and P_3 can be determined with sufficient accuracy. The adaptive channel measurement technique for measurement of these parameters was examined with this possibility in mind. Extensive numbers of

---

*This error rate was easier to compute than the binary error rate which is about 50% higher than the former. This point is discussed in Appendix E.

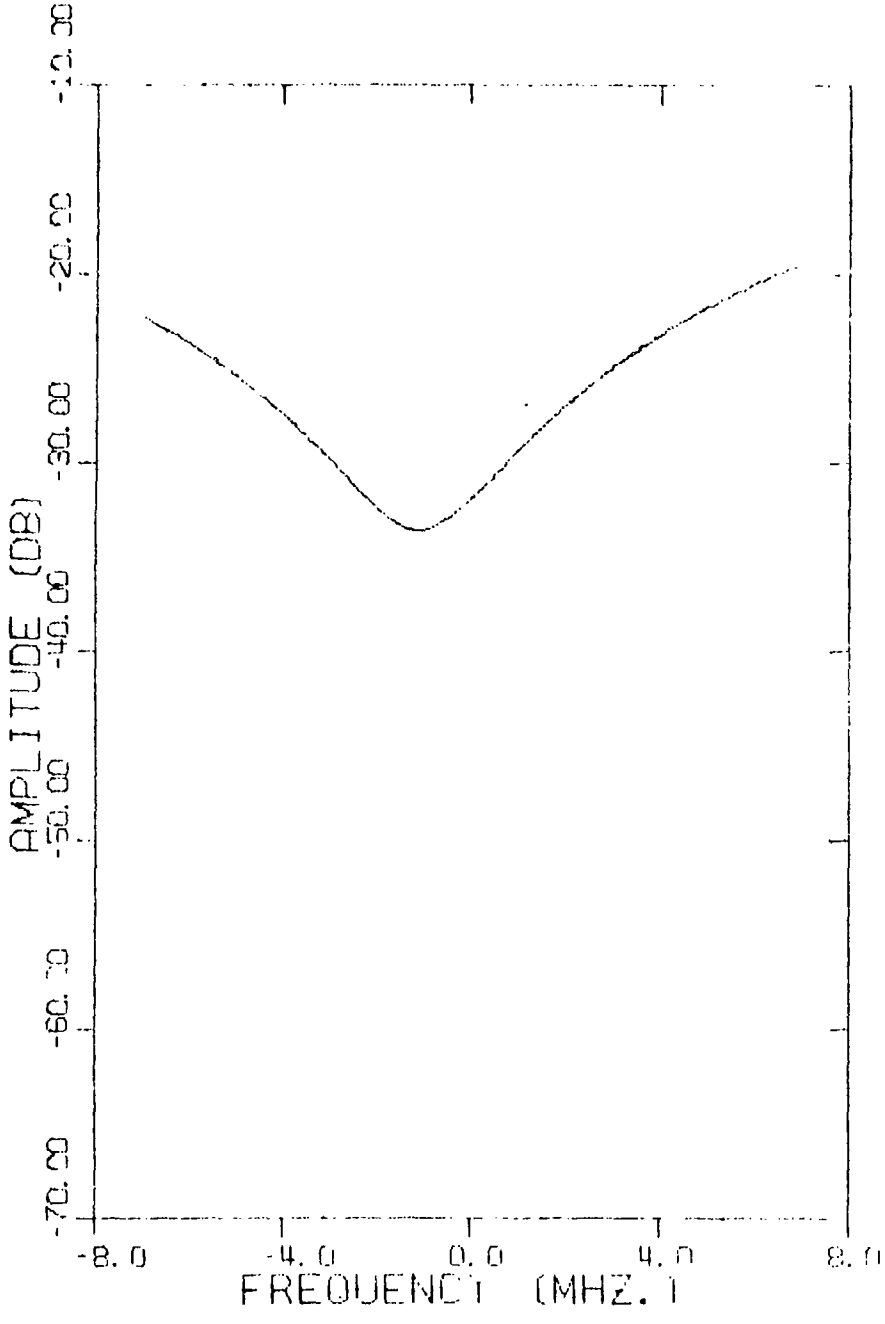

Figure 1.3 Amplitude Vs. Frequency for 32 dB Fade ("Bad" Channel)

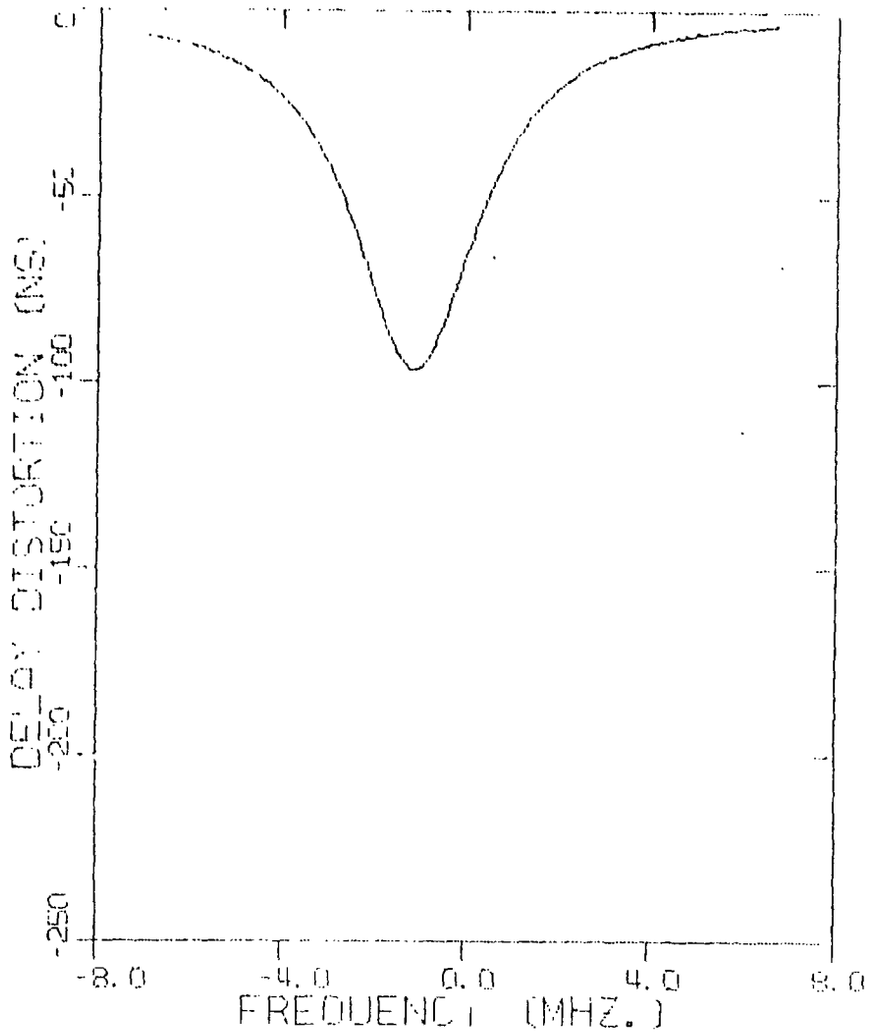

Figure 1.4 Group Delay Vs. Frequency for 32 dB Fade ("Bad" Channel)

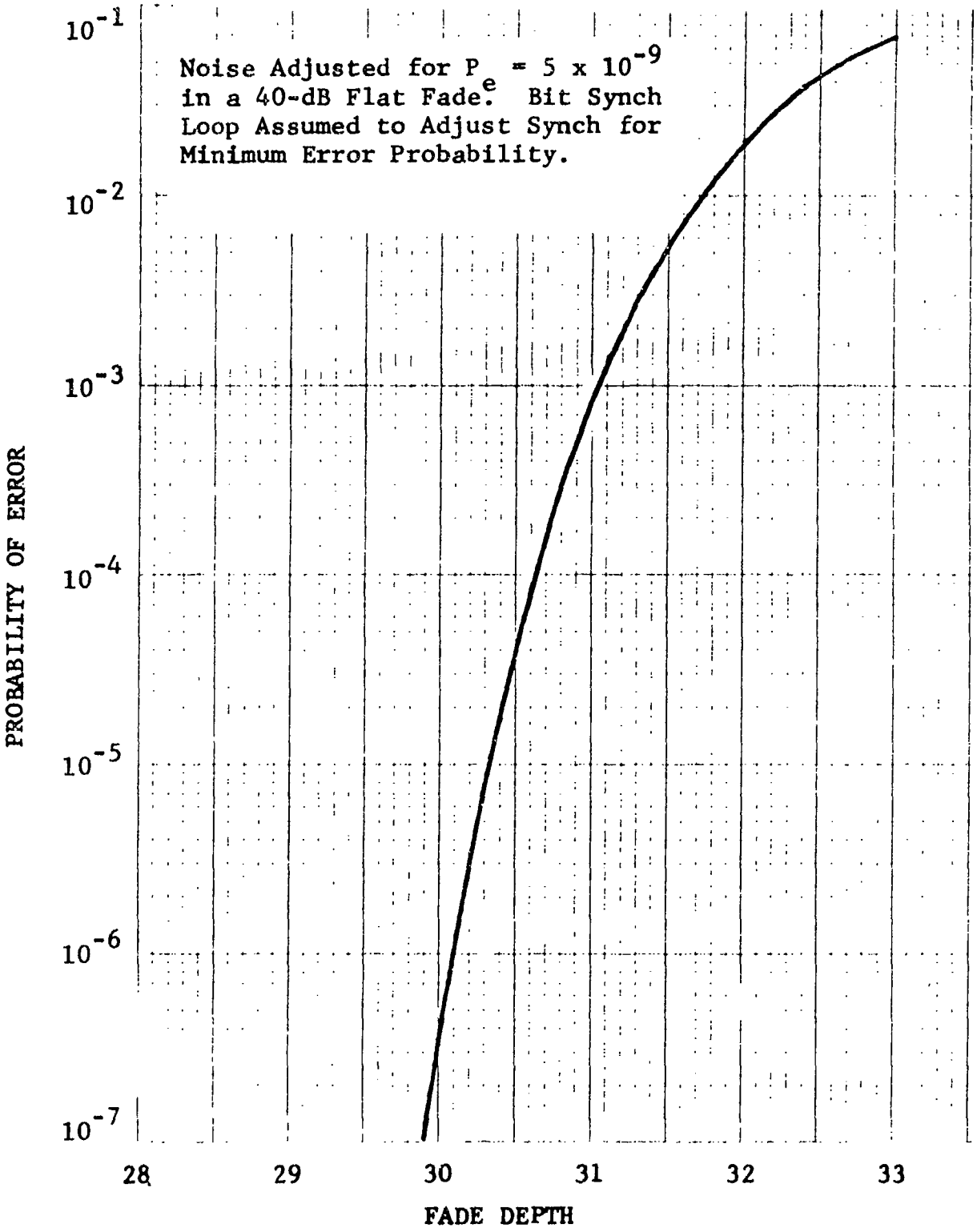

Figure 1.5 Three-Level Error Rate as a Function of Fade Depth for Duo-Binary Modem Used Over FM System With Three-Path "Bad" Channel

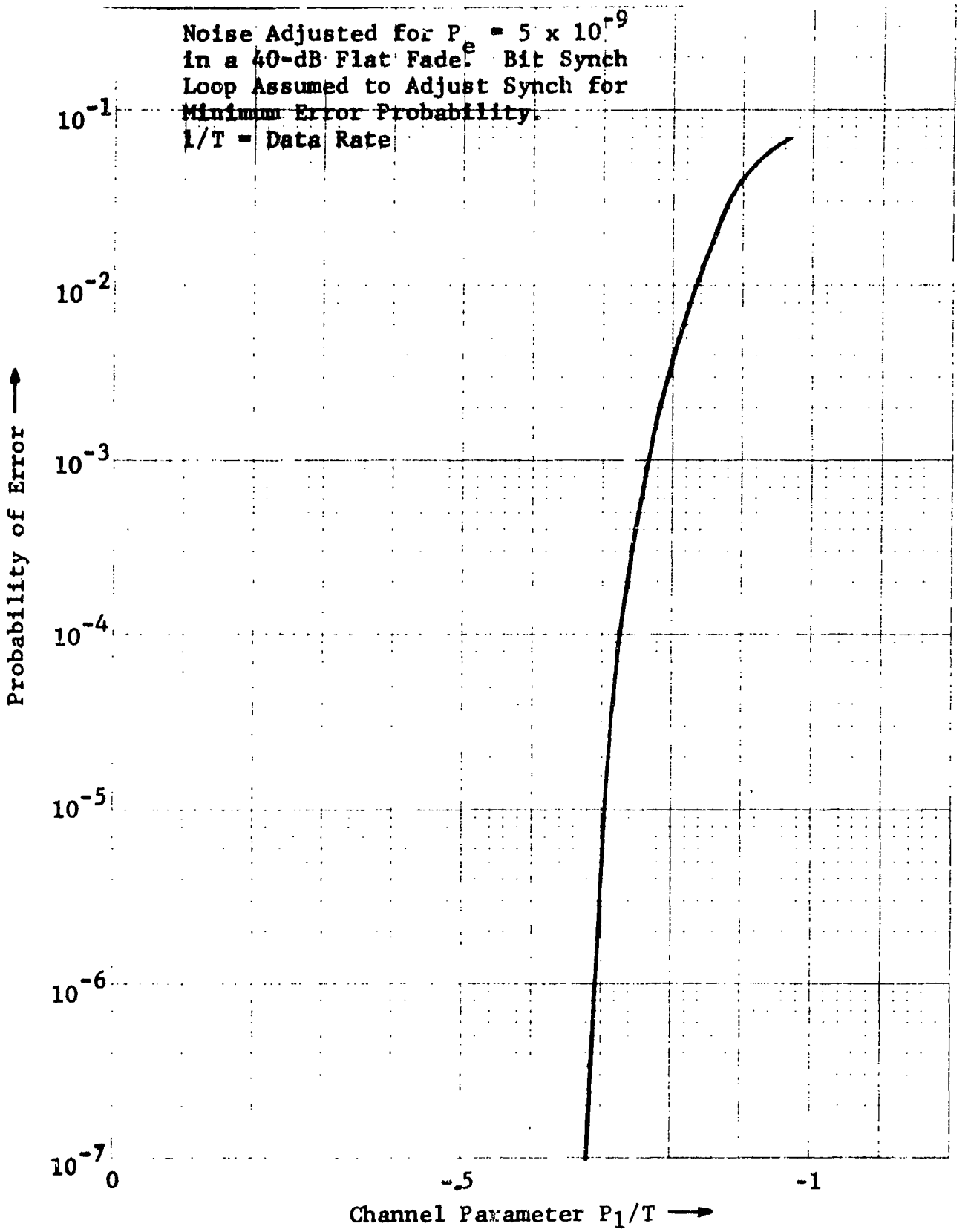

Figure 1.6 Three-Level Error Rate for Duo-Binary FM System as a Function of P_1 for Three-Path "Bad" Channel

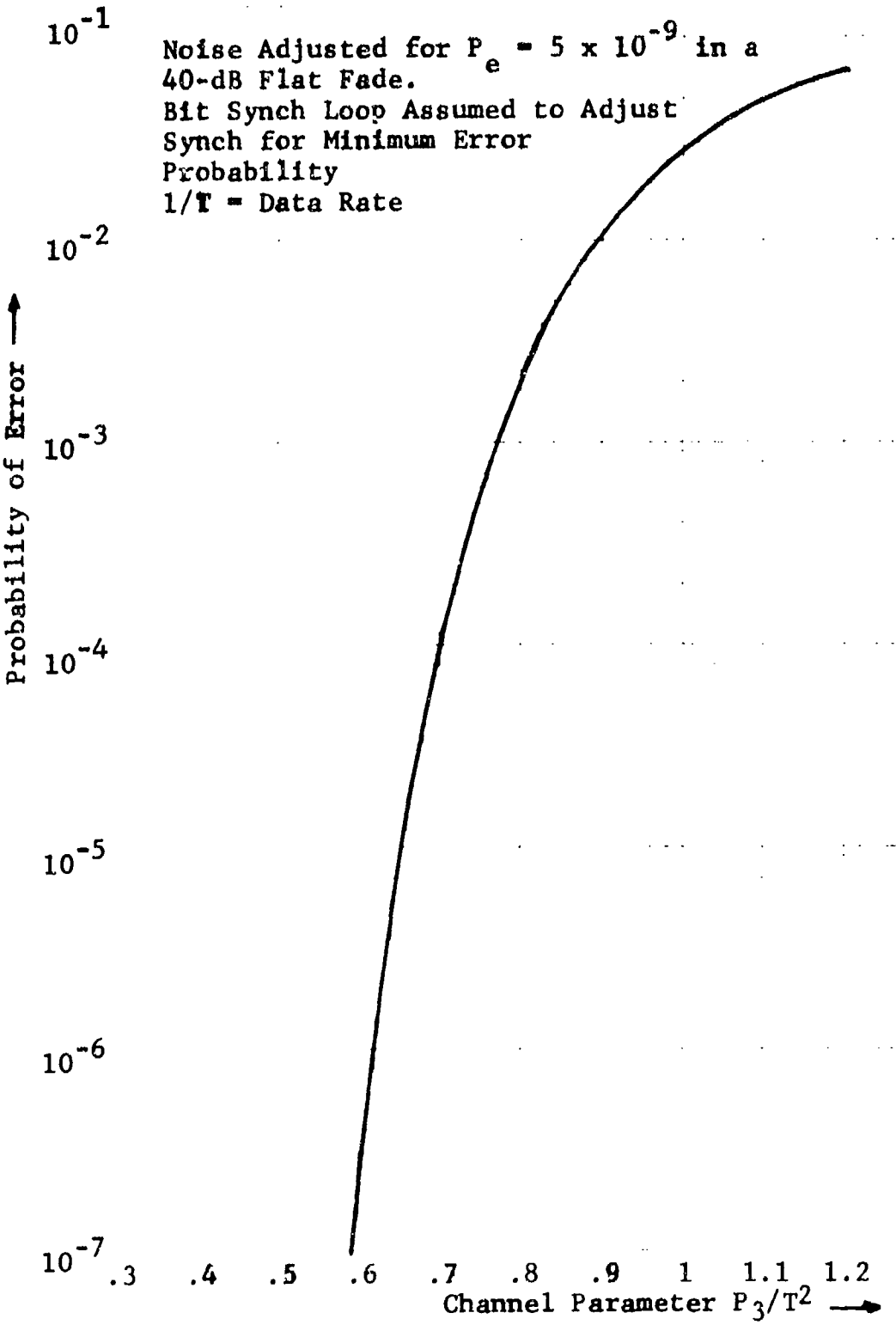

Figure 1.7 Three-Level Error Rate for Duo-Binary FM System as a Function of P_3 for Three-Path "Bad" Channel

computer simulation runs were required to determine the effectiveness of the approach. Unfortunately, there are a very large number of variables to consider and determination of an exhaustive set of performance trade-offs was not possible. However, enough calculations were made to obtain meaningful conclusions on the utility of the technique. Table 1-1 shows some of the combinations of variables considered in the simulations.

The step size δ is a dimensionless quantity controlling the maximum amount of parameter adjustment used in each step or iteration of the adaptation. The smaller δ, the longer the time it takes to converge to the correct parameter estimate but the more accurate the final result, at least within the limitations imposed by the accuracy of the channel model itself and the presence of noise.

The channel output for purposes of modeling was taken to be at one of two places — the discriminator output or the output of a filter following the discriminator. This filter is the receive filter of the duobinary modem. An advantage of using the receive filter output is the reduction of noise. However, the channel measurement implementation is more complex.

In using the demodulated data signal as an input signal for the adaptive parameter estimator, it must be recognized that the timing of the output digits are controlled by a bit sync tracking loop. In addition to the average channel delay ξ_0 in (1.1) there is a variable group delay inserted in the vicinity of the carrier frequency by the presence of channel distortion. For example, the quantity $[-P_1/P_0]$ is seen to be the group delay that is associated with the linear terms in (1.1). Since the group delay variations accompanying the channel disturbances are already inserted into the output digits by the bit sync loop, (assuming the bit synch loop capable of tracking) they should not be inserted again by the adaptive channel estimator. Thus, one must add to the adaptive channel estimator a means of compensating for any delay variations introduced by the bit synch loop. This may be done either adaptively or explicitly when it can be computed from the model. Three approaches are considered in 4.3.2 (see Figs. 4.5(a), (b), and (c)).

Two basic kinds of adaptation algorithms were studied — the LMS (least mean-squared error) and the BR (binary reinforcement) algorithms, in addition to a modification of these, called Variance Equalization, that reduces adaptation time. The variable bit synch delay associated with the channel distortion was adaptively eliminated in cases 6 and 7 in Table 1-1. All other cases (labeled no τ) assume exact measurement and compensation of bit

TABLE 1-1
LIST OF SOME COMBINATIONS OF VARIABLES IN SIMULATIONS

Adaptive Channel Estimator Configuration Number	Channel Model	Pickoff Point	Adaptation Algorithm	Normalized Step Size (δ)	Data Errors	Noise	Variance Equalization	Channel Type	Fade Level
1	Quadratic	Discriminator Output	LMS, no τ	0.002	WO	WO	W	B	25
2	Quadratic	Discriminator Output	LMS, no τ	0.01	WO	WO	W	B	20,25, 30,35
3	Cubic	Discriminator Output	LMS, no τ	0.002	WB/ WO	W/ WO	W/WO	B/G	20,25 30
4	Cubic	Discriminator Output	LMS, no τ	0.01	WB/ WO	W/ WO	W/WO	B/G	20,25 30,35
5	Cubic	Discriminator Output	BR , no τ	0.01	WO	WO	W/WO	B	25
6	Cubic	Discriminator Output	LMS for P_i BR for τ	0.002	WO	WO	W	B	25
7	Cubic	Discriminator Output	LMS for P_i BR for τ	0.01	WO	WO	W	B	25
8	Quadratic	Shaping Filter Output	LMS, no τ	0.002	D	W	W	B	25
9	Quadratic	Shaping Filter Output	LMS, no τ	0.01	D	W	W	B	25
10	Quadratic	Shaping Filter Output	BR , no τ	0.01	D	W	W	B	25
11	Quadratic	Discriminator Output	LMS, no τ	.1,.01,.001 .0005,.0001	WO	W/ WO	W	B	30
12	Quadratic Cubic	Discriminator Output	LMS, no τ	.01,.001	WR	W/ WO	W	B	32
13	Quadratic	Shaping Filter Output	LMS, no τ	.01	D	W	W	B	30,31 31.5,32

W - With
WO - Without
D - Actual Data Errors
B - Bad Channel
G - Good Channel
WB - With Burst Errors Introduced
WR - With Random Errors Introduced

synch delay variations. Such a procedure is possible, in principle, by use of sufficiently stable clocks which allow comparison of bit synch timing during fading and nonfading conditions.

In comparing various algorithms it was found that the LMS algorithm with variance equalization outperformed all other approaches in requiring fewer iterations to produce a given level of RMS error in parameter estimation. Adaptive removal of bit synch timing shift was only briefly studied and resulted in a considerable increase in the number of iterations to achieve a given measurement performance objective. Time limitations prevented optimization of this adaptive timing shift removal procedure so any conclusions concerning its effectiveness must be regarded as tentative.

Focusing on the LMS algorithm with Variance Equalization and assuming direct elimination of bit synch timing shift, simulations were carried out to determine the effect of step size and number of iterations on the rms error in estimating the important parameters P_1 and P_3. These calculations were carried out at a fade level of 30 dB for the case of the "bad" channel both with and without noise added. The level of noise added was such as to produce an error rate of 5×10^{-9} for a 40 dB flat fade. For the "bad" channel we see from Figs. 1.5 to 1.7 that a 30 dB fade is approximately the "threshold" of operation, the error rate rising rapidly to between 10^{-2} and 10^{-1} for a 2 dB increase in fade depth. The values of the normalized parameters P_1/T and P_3/T^2 are given by -.695 and .605, respectively for the 30 dB faded "bad" channel.

Table 1-2 presents examples of the fractional estimation error found from the simulations for parameters P_1 and P_3 for values of normalized step size δ = .1, .01, .001 and iteration numbers of 6000 and 9000, considering both noise absent and noise present in the amount defined above. The presence of noise sets a floor on the accuracy of parameter measurement. Decreasing the step-size and simultaneously increasing the number of iterations reduces this floor. From this table we see that 2% rms measurement errors can be achieved for 6000 iterations and an order of magnitude reduction in rms measurement error achieved by increasing the number of iterations to 9000. A bias error amounting to around 3% was found to exist in the case of parameter P_3. This is due to the inherent error of the parameterization model (1.1). However, even with the bias error it is clear that sufficient accuracy exists to estimate error rates.

TABLE 1-2

FRACTIONAL PARAMETER ESTIMATION ERRORS FOR PARAMETER P_1 AND P_3 AS A FUNCTION OF NORMALIZED STEP SIZE AND NUMBER OF ITERATIONS FOR A 30 dB FADE OF THE "BAD" CHANNEL LMS ALGORITHM WITH VARIANCE EQUALIZATION AND EXACT BIT SYNCH DELAY COMPENSATION

Number of Iterations N	Noise Added*	Parameter	Normalized Step Size δ	Fractional RMS Error†
6000	No	P_1	.1	.018
6000	Yes	P_1	.1	.034
6000	No	P_1	.01	.018
6000	Yes	P_1	.01	.019
6000	No	P_1	.001	.018
6000	Yes	P_1	.001	.018
9000	No	P_1	.1	.003
9000	Yes	P_1	.1	.023
9000	No	P_1	.01	.0005
9000	Yes	P_1	.01	.0049
9000	No	P_1	.001	.00016
9000	Yes	P_1	.001	.0013
6000	No	P_3	.1	.022
6000	Yes	P_3	.1	.114
6000	No	P_3	.01	.018
6000	Yes	P_3	.01	.03
6000	No	P_3	.001	.018
6000	Yes	P_3	.001	.018
9000	No	P_3	.1	.014
9000	Yes	P_3	.1	.107
9000	No	P_3	.01	.0012
9000	Yes	P_3	.01	.021
9000	No	P_3	.001	.00019
9000	Yes	P_3	.001	.003

*The noise added was at a level to produce 5×10^{-9} error rate in a 40 dB flat fade.

†In the case of parameter P_3 there was also a fractional bias error of approximately .03 for all cases.

The degree to which the simple model of Eq. (1.1) together with the adaptation process is able to reconstruct the actual discriminator output is shown in Table 1-3. The rms error in reconstruction is presented normalized to the same reference noise level used in Table 1-2, namely that which would produce an error rate of 5×10^{-9} in a 40 dB flat fade. We note that for step-sizes $\delta = .01, .001$ and $N = 6000, 9000$ the rms reconstruction error is dominated by the output additive noise level. Note also that increasing the number of iterations from 6000 to 9000 or the step-size from .01 to .001 does not improve the reconstruction. Evidently for $\delta \geq .01$, $N \geq 6000$ the residual inaccuracies are not due to the adaptation process but to the parameterization error in the simple model of Eq. (1.1). However it is clear that this simple model is still quite satisfactory for performance estimation.

We consider now the important question as to the effect of output data errors. The adaptive channel estimator utilizes the output data as if it were an error-free replica of the transmitted data signal. An analysis presented in Appendix G on the assumption of random errors shows that as the error rate increases the parameters P_0, P_1, and P_2 will become multiplied by approximately $(1-2p)$, while P_3 will become multiplied by $(1-2p)^2 - p^2$. Simulations carried out so far have supported this type of dependence up to error rates of 6×10^{-2}. On this basis alone error rates $\leq 10^{-2}$ should not affect the desired parameter measurements. However the data errors act like an increase in noise level in the sense of increasing the variance of the parameter estimates. Thus as the error rate increased the accuracy of parameter measurement degrades. For error rates less than 10^{-3} little degradation takes place.

Consideration was given in Section 4.6 to methods and complexity of implementation of several adaptive channel parameter estimators and of an error rate estimator utilizing the channel parameters. All the adaptive channel parameter/error rate estimators can readily be implemented with digital hardware preprocessors carrying out iterative operations in conjunction with a small mini-computer for the relatively complex but low-speed calculations. Utilization of 6000 - 9000 iterations per estimate, as are required for the LMS algorithm to yield parameter estimates sufficiently accurate for error rate estimation in the "threshold" region, allows the use of serial processing, modestly priced multipliers, and inexpensive A/D converters because these iterations may be spaced over a time interval equal to a sizeable fraction of a second due to the slowness of fading on LOS links. While the BR algorithm reduces the number of

TABLE 1-3

ERROR IN RECONSTRUCTING DISCRIMINATOR OUTPUT FOR PARAMETERIZED MODEL OF EQUATION (1.1)

Number of Iterations	Noise Added	Normalized Step Size δ	RMS Error Normalized To Reference RMS Noise*
6000	No	.1	.13
6000	Yes	.1	1.31
6000	No	.01	.11
6000	Yes	.01	1.00
6000	No	.001	.11
6000	Yes	.001	.98
9000	No	.1	.14
9000	Yes	.1	1.31
9000	No	.01	.10
9000	Yes	.01	1.01
9000	No	.001	.10
9000	Yes	.001	.99

*The reference RMS noise corresponds to the discriminator output RMS noise level which would produce 5×10^{-9} error rate in a 40 dB flat fade.

multiplies per iteration (in the ratio of 9/13), the number of iterations required/second to achieve a desired rms accuracy in parameter measurement is larger. On the basis of limited simulations (Section 4.4.2) it appears that the number of iterations required for the BR algorithm is at least 50% greater than the number required in the case of the LMS algorithm for the same rms parameter measurement accuracy. Thus the number of required multiplies/second is not clearly different for the two algorithms. A trial hardware design was blocked out in Section 4.6.4 (see Fig. 4.28).

To carry out the error rate estimation a modern mini-computer, such as the Data General Nova Series or the PDP-11 with hardware multiply/divide provide a reasonable safety factor in computation speed, based upon timing estimates in Section 4.6.3.

With a valid adaptive channel parameter measurement approach it is possible to consider the application of degradation trending and fault location. The following hierarchy of fault location levels are introduced for the system:

- Topological
- Subsystem
- Functional Unit
- Component

Each level represents a partition of the previous level. It is shown that fault location to the topological level, i.e., to a particular transmitter channel, propagation channel, receiver channel, or node in the network, is particularly appropriate to the spectrum of immediate corrective actions available in the DCS at the present time.

Three types of channel parameter measurement units are defined to combine parameter measurement with fault location. These have been given the abbreviations:

- TQU (Transmitter Quality Unit)
- MQU (Media Quality Unit)
- RQU (Receiver Quality Unit)

Fault location to the topological level is obtained by establishing performance assessment based upon measured channel parameters at interfaces located at increasingly distant points from the transmitter node toward the receiver node. The PMU (performance monitor unit), which has previously been introduced [1.4] as a means of direct estimation of link error rate performance, can be applied within the node at the digital modem, multiplexer, or other interfaces for fault location within the node.

As a result of the study, the following conclusions have been reached:

(1) For digital transmission by PCM-TDM-FM over the DCS microwave radio relay communication network, performance assessment that will lead to meaningful degradation trending and effective fault location requires the use of the proposed parametric approach to performance assessment. This involves the identification and measurement of parameters that quantify channel disturbances in the analog portions of the system.

(2) To allow ready fault location to the transmitter section, propagation medium, and receiver section of a link, it is necessary that three basic parameter measurement units be employed, called the TQU, MQU, and RQU. These are located, respectively, at the transmitter output, receiver input, and receiver output. Use of the service channel allows a central processor to utilize the TQU, MQU, and RQU outputs to perform the fault isolation that is required by the DCA.

(3) Parameterization of the input-output behavior of the analog processing portions of a link to quantify linear and nonlinear distortions appears feasible. The number of required parameters is not known at the present time. For the case of a single link it is found that two critical parameters (P_1 and P_3) define the linear and nonlinear distortions caused by the propagation medium undergoing multipath fading. A "quadratic" frequency selective fading model is found

adequate to characterize the propagation medium for the purposes of performance assessment. With the quadratic model and frequency discriminator output expansion leading to Eq. (1.1) the parameterization error at the discriminator output can be made well below expected noise levels at the output (see Table 1-3).

(4) A sharp "threshold" effect is exhibited by the error rate of the system as a function of the parameters P_1 and P_3. For a representative link with a typical three-path multipath model this threshold can occur at a fade level of 30 dB resulting in a 10 dB loss in fade margin for such links as computed on a flat fading basis.

(5) Selective fading causes the group-delay at the center of the band to vary and to shift the "eye" pattern at the baseband output. The bit synch loop will track this variation in group delay (unless it loses synch). In order to carry out an effective adaptive channel parameter measurement it is necessary to continually estimate this shift in bit synch relative to the non-selective fading case.

(6) The LMS algorithm with 6000 to 9000 iterations provides sufficient accuracy in parameter measurement to allow error rate estimation beyond the threshold region up to high error rates (10^{-3} to 10^{-2}). In the sharp threshold region percentage errors in estimation of P_1 and P_3 can be less than a percent, yielding error rate estimates well within a decade of the correct values.

(7) Limited simulation results indicate that the BR algorithm requires well in excess of twice the number of iterations as the LMS algorithm to achieve the same parameter measurement accuracy.

(8) As the error rate exceeds 10^{-3} the variance of the parameter estimators increases and a bias error is introduced (see Figs. 4.21 and 4.22).

(9) With 6000 - 9000 iterations spanning a time interval short compared to the fading time constant of the LOS channel, the signal processing operations required to measure P_0, P_1, P_2, and P_3 are occurring at a slow enough rate to allow digital signal processing implementation with serial processing employing modestly priced multipliers and inexpensive A/D converters.

(10) While the BR algorithm reduces the number of multiplies per iteration in comparison to the LMS algorithm, the total number of multiplies/second appears to be roughly the the same because of the greater number of iterations required to achieve a given parameter measurement accuracy.

(11) The error rate estimation from parameters can be implemented with a modern minicomputer such as the Data General Nova or PDP-11 series with hardware multiply/divide.

1.2 Recommendations

As a result of the study, the following recommendations are made:

(1) Various levels of fault location were defined in Section 2.1.2. The impact of the availability of various levels of fault location capability upon system technical control effectiveness should be investigated. As a result of this investigation, the need for additional requirements on fault location for effective technical control will be determined.

(2) The necessity of a parametric approach to performance assessment for digital communications has been pointed out in Section 2.1.3. It is important to establish by measurement the number of parameters and the parametric models most suitable for use on the DCS links. The parameters and models assumed in the present study for detailed calculations apply to the effect of multipath fading for a single link which is known to cause performance impairment. By parameter measurements on actual links at the transmitter outputs, receiver inputs, and receiver outputs, a firm data base can be established for the design of performance assessment, degradation trending, and fault location techniques based upon the parametric approach.

(3) As has been pointed out in Section 1.1 (page 1-13) and will be discussed in Section 4.3.2 (see Figs. 4.5(a), (b), and (c)) the changing output bit timing, caused by the bit synch loop tracking changes in group delay, must be continually estimated in order to apply the adaptive channel parameter estimator. Because of its importance and the limited investigation of the problem presented in this report, it is recommended that additional study of the three approaches outlined in Section 4.3.2 be pursued. As a result of this study the trade-off in complexity and performance will be exhibited, allowing an optimum choice for the system designer.

(4) The adaptive channel parameter estimator based upon Eq. (1.1) which utilizes a quadratic frequency selective model was found to be adequate for performance assessment in the case of propagation medium distortions; that is to say, a sufficiently good parameterization (Table 1-3) and sufficiently accurate parameter measurement (Table 1-2) would be obtained so that error rate could be estimated to within a fraction of a decade at the sharp "threshold" region of operation. A more general model was employed also, involving a cubic frequency

a cubic frequency selective model, but the additional accuracy was not needed in the case of the propagation medium distortions. It is recommended that the software for the two described parameterized models be applied to the case of linear distortions in IF and RF amplifiers. This study could also include the effect of incorrect apriori knowledge of the duo-binary transmit and receive filter characteristics. As a result of the study the effectiveness of parameterization, parameter measurement, and performance assessment will be determined for distortions in the RF and IF and duo-binary filters by utilizing the same quadratic and cubic models found applicable to the propagation medium distortions.

(5) It is recommended that the simulation study be expanded to include additional distortion parameters, such as those caused by AM/PM conversion, nonlinear modulators and demodulators, and amplifier nonlinearities. As in the present program, the questions to be addressed are the effectiveness of performance assessment based upon adaptive parameter measurement and the complexity of implementation. Expanding the simulation/analysis study to include these additional channel disturbances will provide a more complete view of the effectiveness of the parametric approach to performance assessment.

(6) The study focused on digital transmission by PCM-TDM-FM wherein the existing DCS frequency modulators and demodulators would be retained and used with baseband modems, as in the Phase I DCS upgrade. It is necessary to extend the study to alternate modulation techniques in order to evaluate adaptive parameter measurement techniques that may be applied in the Phase II DCS upgrade. Here one must consider complex (i.e., in-phase and quadrature) processing instead of the real baseband processing of the present study.

(7) Due to the positive results obtained on adaptive channel parameter measurements, it is recommended that implementation of an adaptive channel parameter device be carried out for the quadratic model. The performance should be checked first with laboratory simulation of the LOS channel so that measured parameters may be compared with actual channel parameters. Field tests should then be conducted. The implementation and test will provide verification of the effectiveness of the technique.

1.3 Outline of Report

The rationale for the parametric approach to performance assessment is developed in Section 2. The system of interest is first defined and a system topology introduced subdividing the network into transmitter channels, propagation channels, receiver channels, and nodes. Within the context of this topology, a hierarchy of fault locations is introduced for the system, each level representing a partition of the previous level. Sources and locations of performance impairments on microwave LOS links and their relation to channel parameters are discussed. Various techniques of channel parameter measurement are defined and their utility compared. Performance assessment and trending alternatives are discussed and compared, including those previously discussed and the more general parameter measurement approaches. The TQU (transmitter quality unit), MQU (media quality unit), RQU (receiver quality unit), and PMU (performance monitor unit) are defined and their application to fault location, performance assessment, and degradation trending delineated.

Since the foundations of the fault location, performance assessment, and degradation trending techniques proposed here are based upon the concepts of channel modeling and the parametric representation of input-output channel behavior, Section 2.2 is introduced to sketch out the basic mathematical framework involved. First, mathematical models are given for the signal processing associated with the various modulation, demodulation, and filtering functions in the transmitter and receiver, in addition to models of the signal processing associated with the propagation media. Following this, parametric representations of input-output behavior are introduced.

Section 3 is devoted to an examination of the use of adaptive processing to acquire channel measurement information. The discussion includes both nonlinear and linear modulation techniques. Particular attention is given to adaptive processors which have a linear structure as a function of assumed channel parameters. Consideration is given to convergence time constants and measurement accuracy. Application to adaptive channel parameter measurement in the receiver and transmitter is sketched out.

The parametric approach to channel quality performance monitoring of digital communications systems was introduced in Section 2 as a general tool for performance assessment, degradation trending, and fault location. A particular approach to channel parameter measurement, called adaptive channel parameter measurement, was introduced in Section 3 as a means of implementing the parametric approach. In Section 4, detailed calculations are carried out for the performance of an adaptive channel parameter estimator that operates at the receiver output of a PCM-TDM-FM LOS digital communications system. To keep the analyses and simulations within bounds, a mathematical model of the LOS link was used that included only distortions introduced by the propagation medium. Digital signal processing implementation for the parameter and error rate estimation is considered.

Section 5 briefly considers the application of adaptive channel measurement to troposcatter links.

Appendixes A to G are provided to support the detailed analyses and simulations of Section 4.

REFERENCES FOR SECTION 1

[1.1] P. A. Bello, L. E. Jankauskas, and L. W. Pickering, "Equivalence Measurement Studies," CNR, Inc., Final Report, on RADC Contract No. F30602-73-C-0267 , RADC-TR-75-95, Vol I (AD010004), Vol II (AD010005).

[1.2] A. Lender, "The Duobinary Technique for High Speed Data Transmission," IEEE Trans. on Comm. and Elect., May 1963, pp. 214 - 218.

[1.3] P. A. Bello, C. J. Boardman, D. Chase, and J. K. DeRosa, "Line-of-Sight Techniques Investigation," CNR, Inc., Final Report on RADC Contract No. F30602-73-C-0244, January 1975 , RADC-TR-74-330, (AD006104).

[1.4] D. R. Smith, "Performance Assessment of Digital Transmission Systems," 1973 National Telecommunications Conference.

SECTION 2

A CHANNEL PARAMETER MEASUREMENT APPROACH TO FAULT LOCATION, PERFORMANCE ASSESSMENT, AND DEGRADATION TRENDING

The main emphasis of this study is on the application of adaptive channel measurement techniques to fault location, performance assessment, and degradation trending in PCM-TDM LOS microwave relay communication systems. This section is concerned with developing a rationale for the use of channel parameter measurements to carry out fault isolation, performance assessment, and degradation trending.

From the point of view of system theory, a communications link or channel consists of a cascade of linear and nonlinear signal processing operations which transform the "input" signal into the "output" signal, where suitable interfaces at baseband, intermediate frequency (IF), or radio frequency (RF), have been defined to make the terms "input signal" and "output signal" explicit.

It is clear that the effective design of a radio link for either analog or digital communications requires the modeling and parameterization of these signal processing operations so that the effects of linear and nonlinear distortion on the communications reliability may be determined. It should be equally clear, although it is perhaps less well appreciated, that these linear and nonlinear signal processing parameters can provide the basis for performance assessment, degradation trending, and fault isolation in both PCM-TDM data transmission and analog communications. The rationale is simply the following: changes in key channel parameters from their design values imply changes in distortion and/or noise levels and thus (usually) deterioration in communications systems performance. By measuring these channel parameters, relating them to estimated communications performance, and establishing trends, the technical controller may reduce outages through early alerting of maintenance functions. To the extent that particular parameters may be identified with location in the link, channel parameter measurement will allow some degree of physical isolation of faults or impending faults.

In Section 2.1, we first define the system of interest and pertinent interpretations for the word "channel". A hierarchy of fault location levels are introduced for the system, each level

representing a partition of the previous level. Sources and locations of performance impairments on microwave LOS links and their relation to channel parameters are discussed. Various techniques of channel parameter measurement are defined and their utility compared. Performance assessment and trending alternatives are discussed and compared, including those previously discussed and the more general parameter measurement approaches. The TQU (transmitter quality unit), MQU (media quality unit), RQU (receiver quality unit), and PMU (performance monitor unit) are defined and their application to fault location, performance assessment, and degradation trending delineated.

Since the foundations of the fault location, performance assessment, and degradation trending techniques proposed here are based upon the concepts of channel modeling and the parametric representation of input-output channel behavior, Section 2.2 is introduced to sketch out the basic mathematical framework involved. First, mathematical models are given for the signal processing associated with the various modulation, demodulation, and filtering functions in the transmitter and receiver, in addition to models of the signal processing associated with the propagation media. Following this, parametric representations of input-output behavior are introduced.

2.1 Fault Location, Performance Assessment, and Degradation Trending Alternatives

In this section, we examine the problem of performance assessment, degradation trending, and fault location for a microwave LOS digital communications system representative of those in the DCS. A basic approach, called the parametric approach, is proposed to handle the difficulties caused by the "threshold behavior" of digital communications systems. Particular attention is given to system configurations representative of presently conceived DCS digital communication system upgrades.

2.1.1 System of Interest and Channel Definitions

This study is concerned with channel quality monitoring for digital transmission over microwave line-of-sight radio relay systems. Of primary interest are such digital transmission systems being planned and implemented for the DCS (Defense Communications System). The present microwave LOS DCS uses conventional analog transmission by frequency modulation of frequency-division-multiplexed voice channels (FDM-FM). Plans for changing from

the analog FDM-FM to PCM-TDM-FM or PM have been set forth by the DCA.

The first stage of this change involves the use of PCM-TDM equipment in place of FDM equipment for a selected portion of the DCS. A baseband partial response modem (same as duobinary) would be used with the PCM-TDM equipment. The FM radios per se would be unaffected. Projected further changes in the system would involve replacing the baseband partial response modem and FM radio with more sophisticated modems having higher data rate packing and performance. Our major attention in this study is with the initial system modification using the FM radios (called the Phase I upgrade) although the general philosophy and approach are clearly applicable to future upgrades using more advanced modems.

Figure 2.1 shows a possible digital transmission system configuration in the DCS. The partial response modem is not specifically indicated and may be incorporated into the MUX. From the point of view of fault location and channel measurement, as outlined in succeeding sections, it is convenient to redraw a system such as in Figure 2.1 by a topological "channelized" representation as shown in Figure 2.2.

Three types of "channels" may be identified in Figure 2.2,

- Transmitter channels
- Propagation channels
- Receiver channels

in addition to nodes. This type of topological breakdown is into major signal processing operations of each link: a transmitter channel includes those signal processing operations from the FM transmitter radio baseband input to the transmitting antenna input; a propagation channel includes the signal processing from transmitting antenna input to receiving antenna output; a receiver channel includes the signal processing from the receiver antenna output to the FM radio receiver discriminator baseband output. All other signal processing operations are assumed included within the node, e.g., the PCM equipment, multiplexers, and baseband partial response modems. Note that, apart from the nodes, the signal processing shown in Figure 2.2 is identical for the PCM-TDM-FM and the standard analog systems. The FDM of the latter system has been replaced by the PCM-TDM and baseband modem.

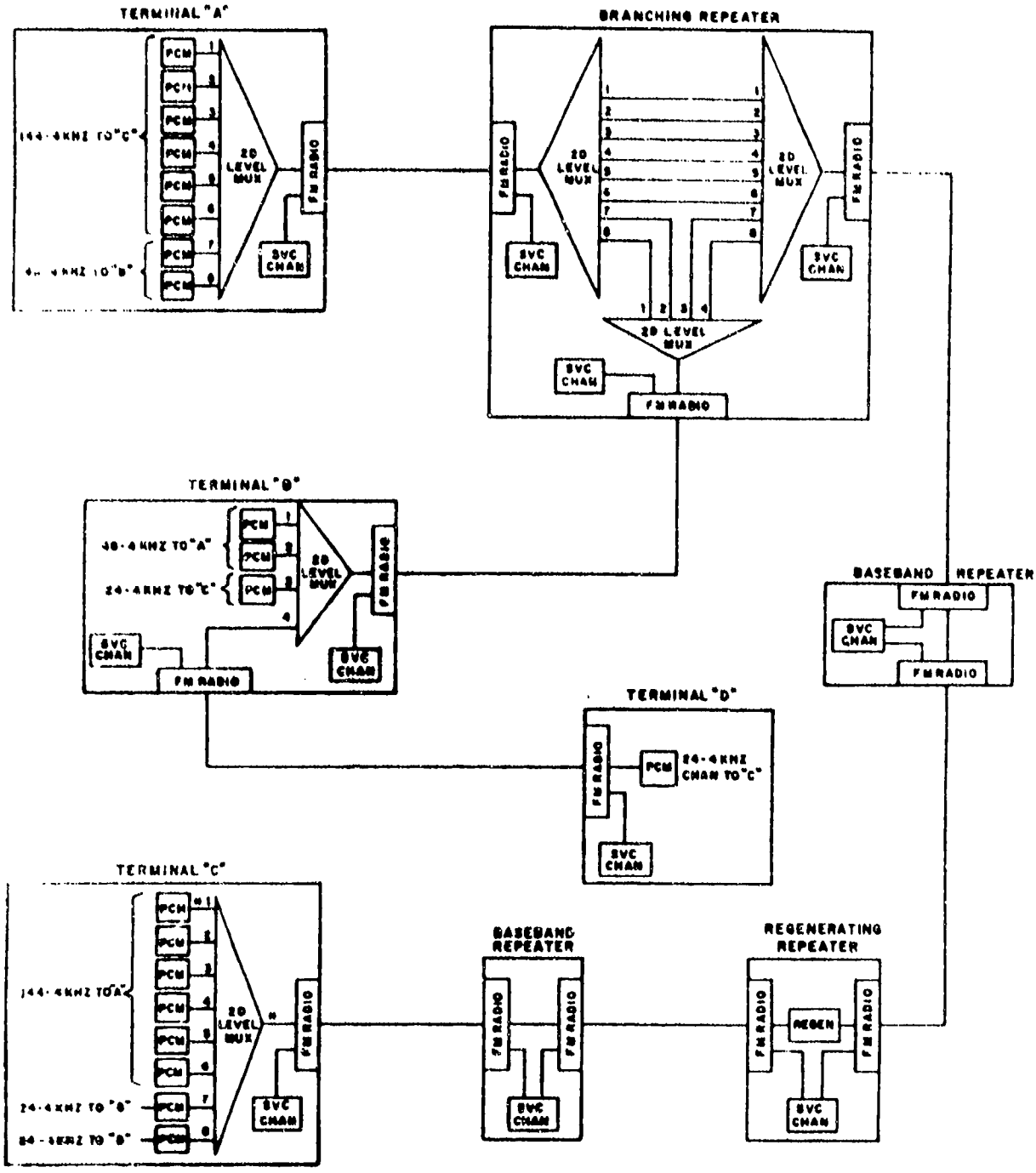

Figure 2.1 A Possible DCS Digital Transmission System Configuration

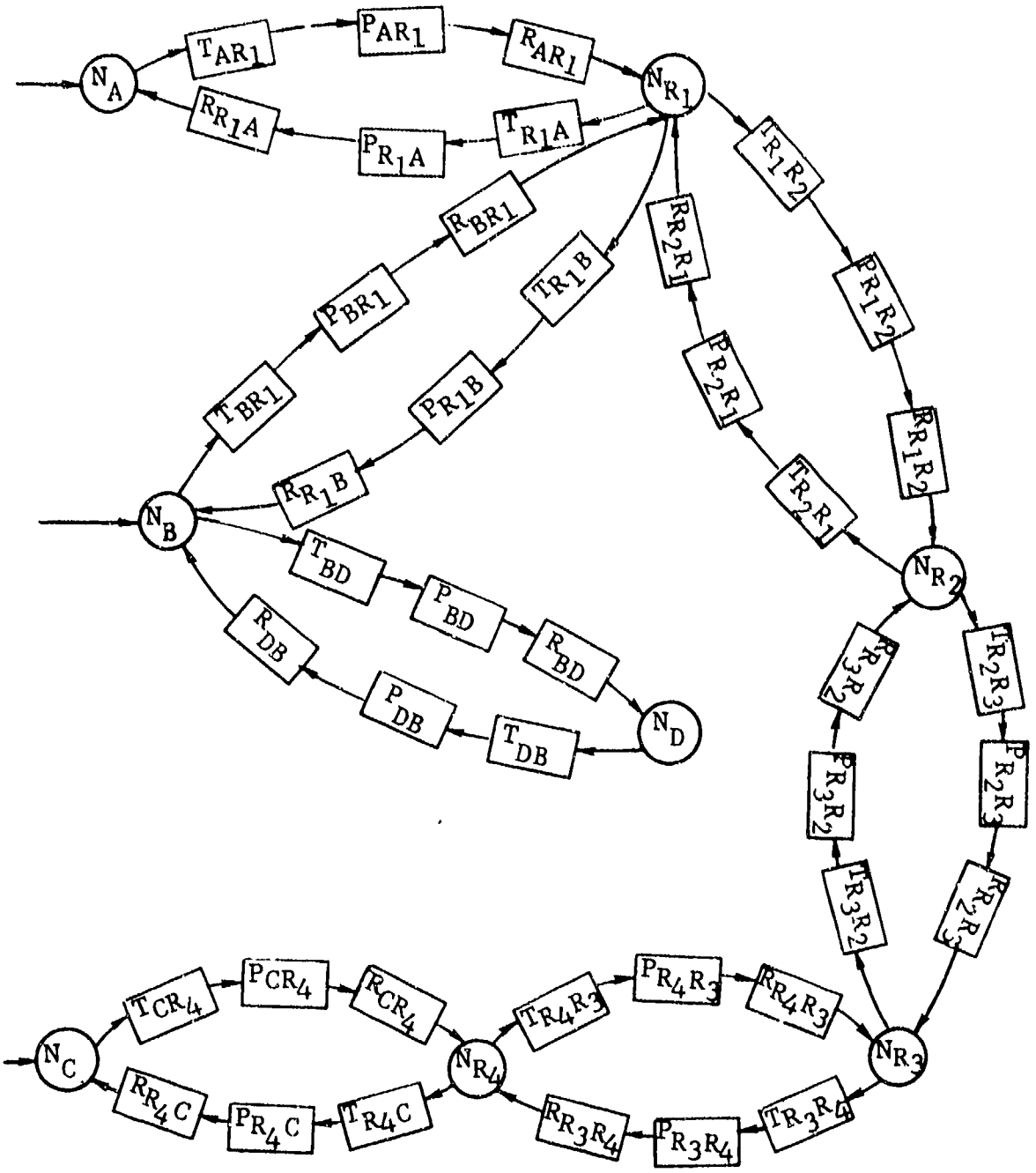

Figure 2.2 Topological Representation of System Configuration of Figure 2.1 in terms of Three Types of Channels Plus Signal Processing Nodes

2.1.2 Levels of Fault Location

The location of faults in a communications network is necessary as a prelude to carrying out corrective action. The degree to which the fault needs to be isolated depends upon the spectrum of corrective actions available and the desired MTTR (mean time to repair) upon isolation of the fault. We may identify the following four levels of increasingly finer fault isolation:

- Topological
- Subsystem
- Functional units
- Component level

We call the first level of fault location the topological level because a simple topological map (see Figure 2.2) of the communications network can be constructed to identify the transmitter channel, propagation channel, receiver channel, and the node which, by our definition, includes switches, multiplexers, and baseband digital modems. At the present operational level of corrective actions, it appears* that fault isolation to the topological level is of most utility in the DCS. Thus, in the event that a present or impeding fault is identified in the transmitter channel, the hot standby transmitter can be switched in and the nearest maintenance team alerted to repair the faulty transmitter channel. In the event that the receiver channel is in fault, a diversity (or protection) channel may be switched in to replace the faulty receiver channel. Identification of the problem as being in the node would probably involve automatic replacement of some subystems (e.g., multiplexers, crypto boxes, etc.) and manual replacement of others, also followed by an alert to the maintenance department. The prime utility of tracing a fault to the propagation channel is probably in the avoidance of false corrective action in other parts of the link, although rerouting of a high priority message might be called for.

Fault location to the next finer level, the subsystem level, identifies faults in subsystems of the four basic units of the topological level. Such subsystems are: multiplexers, digital modems, power supply, frequency modulator, etc. Automatic fault

*Personal communication from Mr. D. Iram of RADC.

isolation to the subsystem level can accelerate restoration of service, particularly if spares are available and modular construction has made replacement simple.

Fault location to functional units, such as amplifiers, filters, cards, etc., is frequently done in modern telecommunications equipment and digital modems in particular. With the availability of spare parts, such fault location can minimize the time lag involved in utilizing the maintenance crew. Fault isolation to the component level (transistors, resistors, etc.) does not appear likely to play a role in optimizing the technical control of a communications system.

2.1.3 Performance Impairments and Their Effects on Analog and Digital Systems

Performance impairments in an LOS link can range from outages to a modest increase in error rate with a variety of possible sources for the impairment. Table 2-1 lists possible sources of impairments located in the transmitter, propagation, and receiver channels. As indicated in this table, the impairments can fall into one or more of the following categories:

- Signal reduction or loss
- Increased noise level
- Linear signal distortion
- Nonlinear signal distortion

These disturbing effects apply whether TDM-PCM digital signals or FDM analog signals are being processed by these channels. However, the actual degree to which service is degraded by these disturbances need not be the same in the two cases, as is discussed in Section 2.2.1.

Ultimately, it is the impact on the end user that we must determine in order to evaluate the effect of a channel disturbance. In the case of voice transmission, the end user requires sufficient speaker intelligibility and speaker recognition. No simple formulas relate these measures of performance to channel conditions for digital and analog communications systems. However, some general comments are appropriate comparing the two systems.

TABLE 2-1

SOME SOURCES OF PERFORMANCE IMPAIRMENT IN TRANSMITTER, PROPAGATION, AND RECEIVER CHANNELS OF A MICROWAVE LOS LINK

Transmitter Channel	Propagation Channel	Receiver Channel
• Transmitted power loss due to TWT aging • Excessive AM/PM conversion caused by TWT • Excessive distortion in RF or IF filtering • Excessive nonlinear distortion in frequency modulator • Excessive linear distortion produced by echoes on line between TWT and antenna • Signal reduction or loss due to reduced amplifier gains and poor connections • Power supply failure • Local oscillator degradation and failure	• Decreased received signal due to antenna misalignment • Decreased received signal due to flat fading • Distortion due to multipath fading • Interference	• Increased noise figure due to RF preamplifier and mixer degradations • Excessive linear distortion in RF or IF filtering • Excessive nonlinear distortion in frequency discriminator • Local oscillator degradation and failure • Power supply failure • Signal reduction or loss due to reduced amplifier gains and poor connections

First, as has been pointed out frequently, the digital system exhibits a sharp threshold phenomenon in performance as a function of SNR (signal-to-noise ratio), the performance being excellent somewhat above the "threshold" and degrading to unacceptable somewhat below this SNR threshold. On the other hand, the analog systems shows a gradual deterioration in performance with increasing SNR.

The effects of signal reduction or loss and/or increased noise level, which are characterized simply in terms of an appropriate SNR, are perhaps the most common causes of performance impairment. However, the other categories of linear disturbances and nonlinear signal distortion are equally important. Unfortunately, it is much more difficult to make simple comparative statements as were made for SNR because distortion is not so easily parameterized and related to performance. However, it still appears likely that a threshold effect will occur for the digital system when system performance degradation is plotted against suitably selected channel distortion parameters.

The reasoning behind this statement is that signal distortion produces intersymbol interference which acts somewhat like the usual receiver noise in producing errors. Since it is the rapid change in error rate vs. noise level (for fixed signal strength) that produces the basic threshold effect noted previously, one may generally expect digital system performance degradation to have a sharp threshold, at least for channel distortion that produces intersymbol interference. This threshold has been observed in the calculations of Section 4 as indicated in Figure 1. .

In the case of analog systems, again, a gradual performance deterioration with increasing distortion occurs. The major distorting effect of interest in the FDM-FM systems is nonlinear or intermodulation distortion which results in broadband unintelligible crosstalk between voice channels that has characteristics similar to receiver noise when viewed from a particular voice channel. In this connection, it should be noted (see Section 2.2) that the linear distortion of RF and IF filters and the propagation channel become converted into both linear and nonlinear (intermodulation) distortion at the output of the FM discriminator.

Because of the described threshold behavior of the digital communications systems with channel disturbances, in contrast to the analog systems, channel quality monitoring at the voice channel output is unlikely to provide advance indication of impending problems. Even direct raw error rate measurement at the modem

or MUX output is not very useful in this regard because the threshold behavior is basically on the error rate vs. channel parameter characteristic, leading to a situation in which the error rate is either too small to be reliably measured or, if measurable, too large and thus too close to (or beyond) the threshold.

In addition to producing short-term error rates on digital streams, channel and equipment nonidealities can cause observable timing jitter, error pattern structure, and loss of bit sync integrity. However, the operation of regenerating the digital data which was transmitted at the far end is such a massively nonlinear operation that it appears unlikely that one may extract from measurements of timing jitter, error patterns, or loss of bit sync integrity any information as to whether the source of the channel disturbance is at the transmitter, propagation, or receiver channels.

As a result of these considerations, it is proposed that the only effective approach to performance assessement as a tool in trending performance degradation and in location of faults (or impending) faults is a parametric approach in which appropriate channel parameters are defined and measured for the transmitter, propagation, and receiver channels of every link. (For example, see the channels of Figure 2.2.) For these parameters to be useful, their measurement must lead to link performance estimation. In addition, each of these parameters should not exhibit a sharp threshold behavior as a function of the four basic channel disturbances listed above.

In the preceding discussion we have concentrated on performance impairments associated with the transmitter, propagation, and receiver channels of links because (apart from any analog processing involved in the digital modem) these channels constitute the analog processing portion of the network. Modern digital telecommunications practices involve the use of built-in test equipment and fault isolation hardware in digital equipment and digital modems. It is assumed that the outputs of these test equipments and fault indicators are available to aid in the general task of system channel quality monitoring and fault isolation. No attempt is made to apply the parametric approach to the primarily digital signal processing in the nodes, both because it is felt that adequate built-in performance monitors will be available and because threshold behavior is typical for any parameters that would be found in this section.

2.1.4 The Parametric Approach to Fault Location, Performance Assessment, and Degradation Trending

The parametric approach to channel quality monitoring is illustrated in Figure 2.3. It is assumed that the input-output signal-processing relationships of the transmitter, propagation, and receiver channels are each characterizable by means of a finite set of parameters, say, $\{T_1,T_2,\ldots,T_M\}$, $\{P_1,P_2,\ldots,P_N\}$, and $\{R_1,R_2,\ldots,R_L\}$, respectively, for which formulas have been developed relating parameter values to link performance (e.g., error rate). Performance assessment would involve the measurement of channel parameters and utilization of these formulas. Degradation trending would be accomplished by extrapolating transmitter and receiver channel parameters vs. time and continually determining the margin separating current values from the "threshold" values.

The boxes labeled TQU (transmitter quality unit), MQU (media quality unit), and RQU (receiver quality unit) carry out channel parameter measurements at portions of the link which allow maximum opportunity to obtain information about the transmitter, propagation, and receiver channels. The TQU output is shown fed to the service channel, labeled SVC, for transmission over the link. Note that the baseband modem output, i.e., FM radio input, is fed into the TQU. This procedure is consistent with adaptive channel measurement procedures and others described in Section 2.1.5. In effect, the radio input is regarded as a channel probing signal while the place(s) at which the TQU takes measurements are channel outputs. Ideally, the TQU input should be as near to the antenna input as possible.

The MQU* input is located as close as possible to the receiving antenna output. This unit can obtain channel parameter information but, due to its location, these parameters are for a composite channel — the cascade of the transmitter and propagation channels. With the aid of the TQU information transmitted over the service channel, however, it is possible to isolate the parameters of the propagation channel alone in the Channel Quality Monitor.

Similarly, the RQU obtains channel parameter information for the composite transmitter-propagation-receiver channels. With the aid of the TQU and MQU outputs, it is possible to extract parameters of the receiver channel alone. By the above means

*This unit was introduced by CNR, Inc., in [2.1].

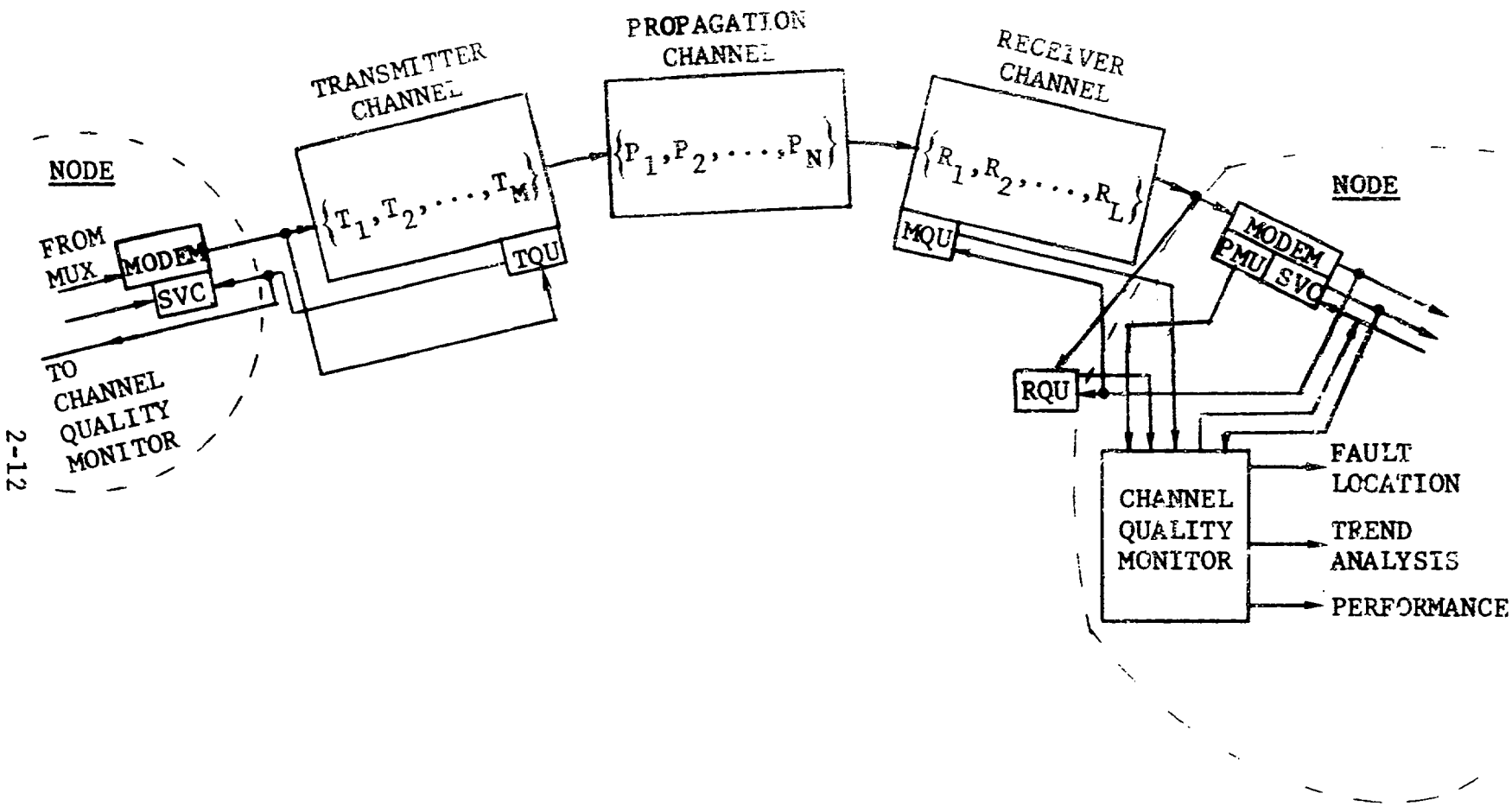

Figure 2.3 Illustration of Fault Location, Trend Analysis, and Performance Assessment Using the Parametric Approach

one may obtain a link performance assessment based upon the parameters of the transmitter, propagation, and receiver channels, to perform trend analysis, and to isolate faults at the topological level at least. Fault isolation to subsystems and lower levels from channel parameters may be possible but is an unexplored area.

Figure 2.3 also shows the existence of a PMU (performance monitor unit) whose objective is to obtain a direct estimate of actual link error rate at the baseband digital modem output. Smith [2.2] discusses several approaches for obtaining such an estimate. The PMU can be used to isolate faults to the baseband digital modem by comparing actual error rates with estimated error rates from the TQU, MQU, and RQU.

A final point is worth mentioning for LOS microwave relay links. Such links are basically two-state channels, in the sense of being nonfading most of the time with occasional digressions into flat fading and frequency-selective (multipath) fading modes. Thus, channel parameter measurements during the nonfading periods (identified by the MQU) can yield information of transmitter/receiver parameters alone, which simplifies the untangling process.

2.1.5 Channel Measurement Procedures

Basic to the parametric approach of performance assessment, degradation trending, and fault isolation is the process of channel parameter measurement. Figure 2.4 presents a breakdown of channel parameter measurement techniques that may be employed for channel quality monitoring. A first major subdivision is according to whether special probing signals, such as pseudo-noise sequences or tones [2.3], are used for the channel measurements or whether the information-bearing signal itself is regarded as the probing signal.

If the information-bearing signal is used, two choices are possible: the output digital NRZ signal can be regarded as a true replica of the transmitted signal, i.e., as the probing signal; or the received signal somewhere prior to digital demodulation can be used as the source of channel information. The former case is used extensively in the ubiquitous adaptive equalizer, while the latter has been analyzed and proposed in the case of MQU implementation [2.1].

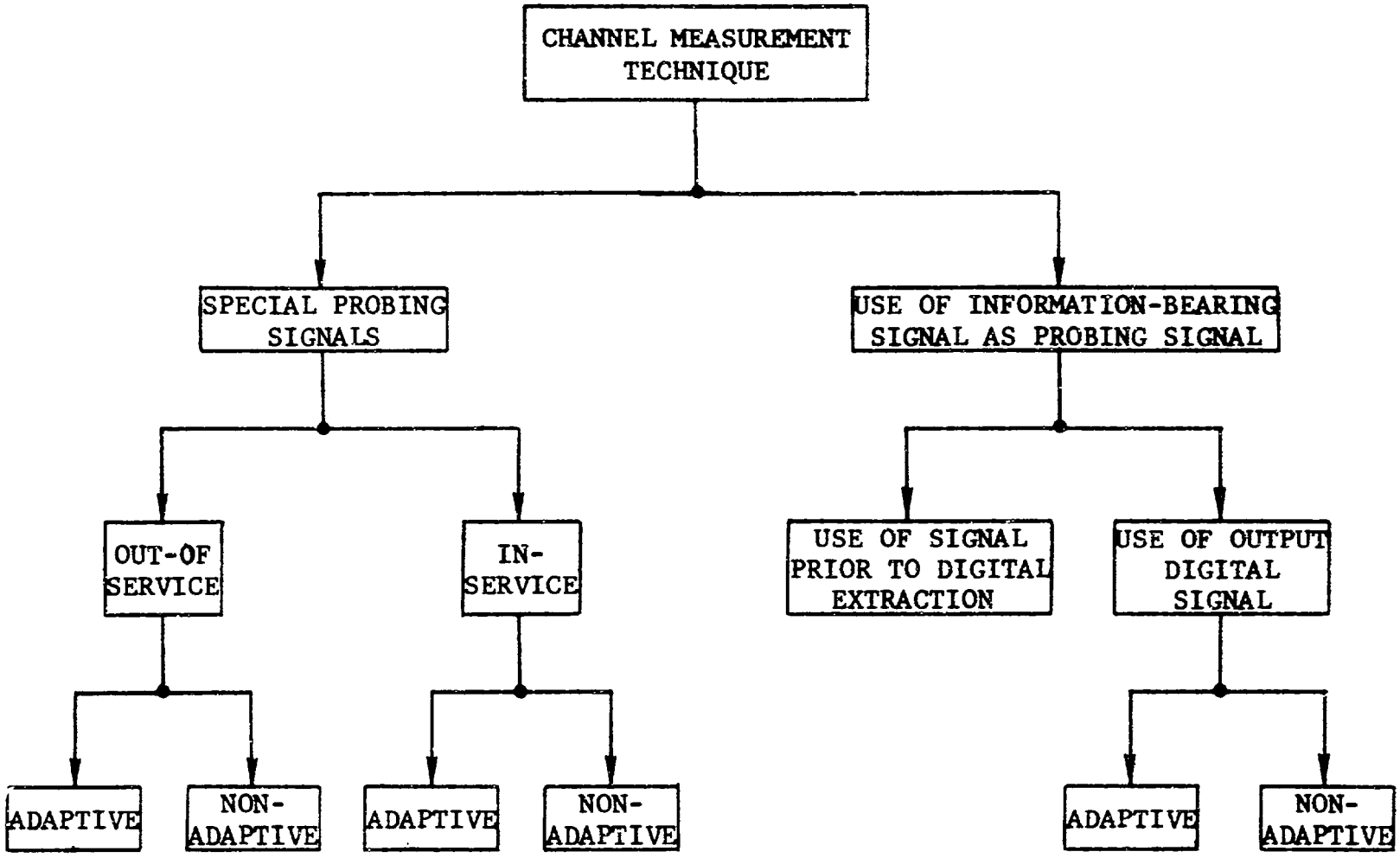

Figure 2.4 A Classification of Channel Parameter Measurement Techniques

When the output digital signal is regarded as a delayed replica of the transmitted signal, channel measurement may proceed in two ways: adaptive or nonadaptive. Processing in the nonadaptive case is exemplified in linear systems by the operation of cross correlation [2.3]. Adaptive processing is exemplified by the adaptive filter work of Widrow [2.4] and is the subject of this study.

In the case of special probing signals, we may distinguish between out-of-service measurement, when the digital signal is disconnected, and in-service measurement, wherein the probing signal is multiplexed with the information-bearing signal. In either case, channel measurement may proceed by adaptive or nonadaptive means.

The prime attention of this final report is on the signal distorting parameters of the link, rather than signal and noise level measurements. The latter already exist in the FDM equipment due to AGC voltages and baseband out-of-band noise measurements. Additional approaches to these measurements have been covered in CNR's prior study on the MQU [2.1].

2.2 Channel Modeling

A general philosophy of fault location, performance assessment, and degradation trending, called the parametric approach, was introduced in Section 2.1. This approach is based upon the representation of the input-output behavior of subsystems in terms of signal processing operations of specified form containing a finite number of parameters. The purpose of the present section is to justify this parametric representation on a general basis. First, nonparameterized mathematical models are given for the signal processing associated with the various modulation, demodulation, and filtering functions in the transmitter, receiver channels, and propagation channel. Following this, general parametric representations of input-output behavior are developed.

Primary attention is given to the characterization of the distortion-producing character of the signal processing operations involved, since adquate methods of determining signal level and noise level are available.

2.2.1 Signal Processing Operations in a Single Link

Figure 2.5 presents a simplified block diagram of a single microwave link in which digital transmission is effected by adding a baseband partial-response [2.5] modem to the existing FM radio, as in the Phase I DCS upgrade [2.6]. We consider the signal processing operations taking place in this link and their ideal and nonideal characteristics. Note, however, that in the case of radio relay operation, some of the operations in Figure 2.5 may be missing, as, for example, in the case of a baseband relay, where the partial response receive filter and bit synchronizer would be absent.

The signal processing operations have been grouped into a cascade of three "channels": the transmitter channel, the propagation channel, and the receiver channel. The interfaces defining the transmitter channel are the input to the frequency modulator and the input to the transmit antenna. Similarly, the receiver channel consists of all signal processing operations between the output of the receive antenna and the input to the baseband modem demodulator. The propagation channel includes all operations from the input of the transmit antenna to the output of the receive antenna.

We consider the individual signal processing operations in each of the three channels. To simplify the notation, we use complex envelope signal representations throughout, discussing both the ideal and nonideal behavior of the signal processing operations. As a general comment, it should be noted that from transmitter channel input to receiver channel output the ideal input-output behavior is distortionless, i.e., this behavior consists of at most a delay and a gain change. Perturbations from this ideal behavior may be classed roughly into two categories: multiplicative and additive. The distinction between the two is that the former disappears when the input signal is removed, while the latter does not (although it may change). These perturbations cause degradation in the quality of communications when they become sufficiently large.

It should be noted that a complete characterization of the signal processing functions allows a determination of the multiplicative and additive disturbances on the output signal, given the input signals and additive disturbances, whether the input signal arose from a PCM-TDM digital modem input or an FDM set of analog voice channels. However, as will be pointed out, the

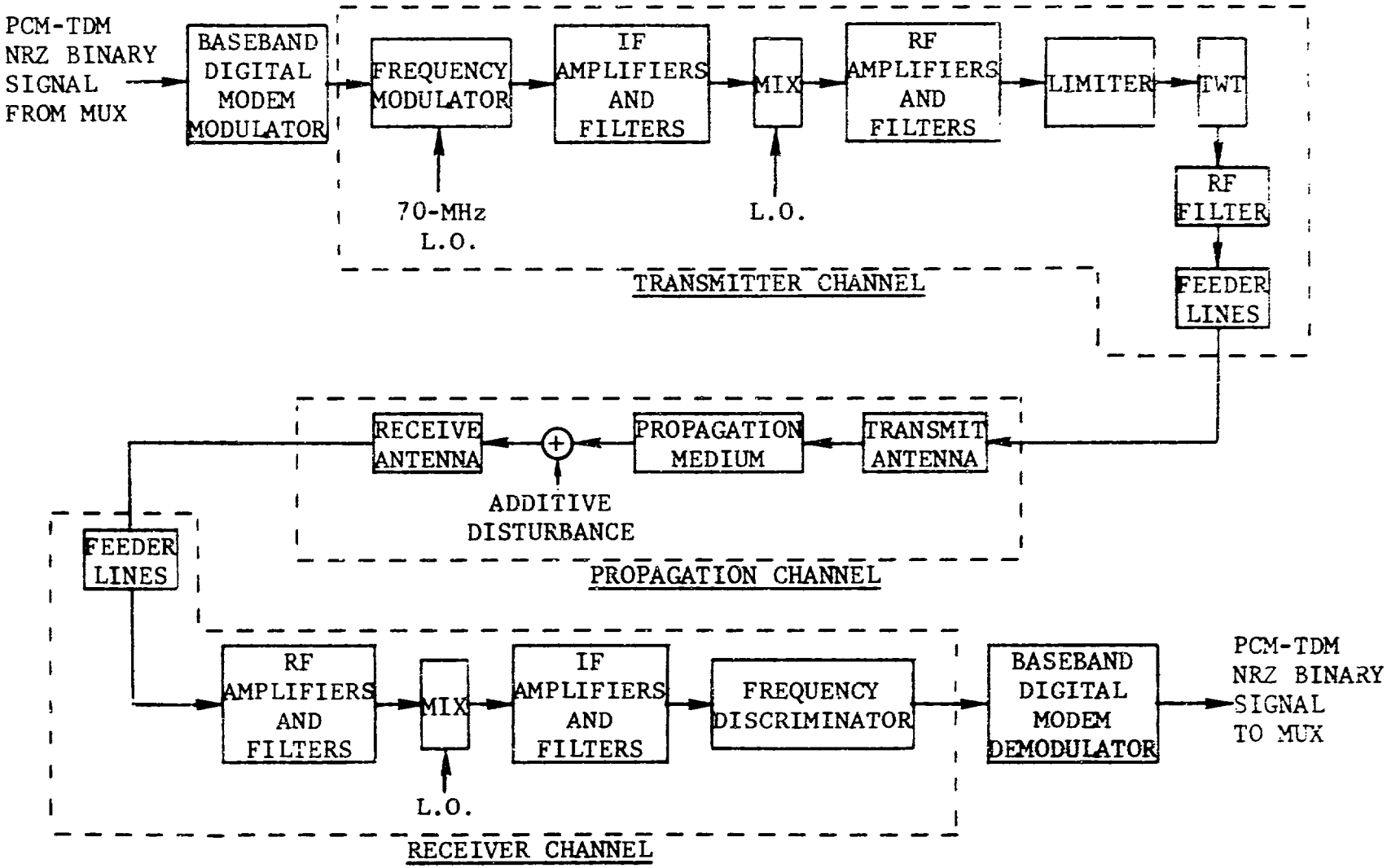

Figure 2.5 Block Diagram for Single Link PCM-TDM Transmission Using Existing Frequency Modulators and Discriminators Plus Baseband Digital Modem

relative importance of these disturbances on communications performance can be quite different for the analog and digital communications.

2.2.1.1 The Transmitter Channel

We denote the input to the transmitter channel by the signal x(t). This signal is fed to a frequency modulator whose complex output under ideal conditions is given by

$$z_1(t) = e^{j\psi(t)} \tag{2.1}$$

where $\psi(t)$ is the phase of the FM modulator output with reference to the carrier frequency,

$$\psi(t) = 2\pi M \int x(t)\, dt \ , \tag{2.2}$$

and M is a proportionality constant determining the modulation index. The instantaneous frequency of the output is given by

$$\frac{\dot{\psi}(t)}{2\pi} = M x(t) \tag{2.3}$$

which, in accordance with the ideal behavior of the frequency modulator, is proportional to the input baseband signal.

In practice, due to modulator nonlinearity, the instantaneous frequency must be represented as

$$\frac{\dot{\psi}(t)}{2\pi} = M x(t) + F\left(x(t)\right) \tag{2.4}$$

where $F(\cdot)$ is a nonlinear function defining the perturbing nonlinearity of the modulator. The size of $F(\cdot)$ in relation to $M x(t)$ is designed to be small for the FDM/FM radios, say 1% of full scale. Such stringent linearity requirements are necessary for FDM/FM transmission because nonlinearities create intermodulation distortion in such systems. Thus, an increase in the nonlinearity of the frequency modulator characteristics can be

quite harmful for the conventional analog system. On the other hand, a stringent linearity requirement for the frequency modulator does not appear justified for the PCM-TDM-FM system of Figure 2.5, although detailed analysis of the effects of modulator nonlinearity on performance is not available.

Another nonideality associated with the frequency modulator is local oscillator noise. This adds a low-level spurious low-frequency modulation term to the instantaneous frequency at the modulator output

$$\frac{\psi(t)}{2\pi} = M\,x(t) + F\big(x(t)\big) + \nu_{\ell o}(t) \tag{2.5}$$

Normally, the low frequencies are cut off with a high-pass filter to eliminate oscillator noise and possible biases due to frequency offsets.

Finally, the frequency modulator output may be expected to have some small amount of signal-dependent amplitude modulation at its output, yielding the modulator output representation

$$z_1(t) = \Big[1 + G\big(x(t)\big)\Big] \exp\Big\{j\,2\pi\,M \int x(t)dt\Big\} \exp\Big\{j\,2\pi \int \Big[F\big(x(t)\big) + \nu_{\ell o}(t)\Big]dt\Big\} \tag{2.6}$$

where $G\big(x(t)\big)$ characterizes the signal-dependent amplitude modulation. Figure 2.6 diagrams the signal processing involved.

While it may seem that amplitude modulation should be unimportant in an FM system, it turns out, as we shall discuss, that limiting or saturating amplifiers, in particular the TWT, will convert amplitude fluctuations into phase fluctuations. This AM/PM conversion will produce a phase-modulation term proportional to $G\big(x(t)\big)$ which, due to the nonlinearity of $G(\cdot)$, will produce intermodulation distortion.

We consider now the filtering operations at IF and RF which are provided to eliminate noise and unwanted signals. The mixing operation, which translates the IF signal to the desired RF carrier frequency, is broadband and distorts the signal negligibly. At the transmitter, these filters can generally be broader and thus less distorting than those at the receiver because of the much stronger SNR's in the former case. However, they still distort the signal producing linear and nonlinear distortion of the FM signal in addition to causing some amplitude modulation.

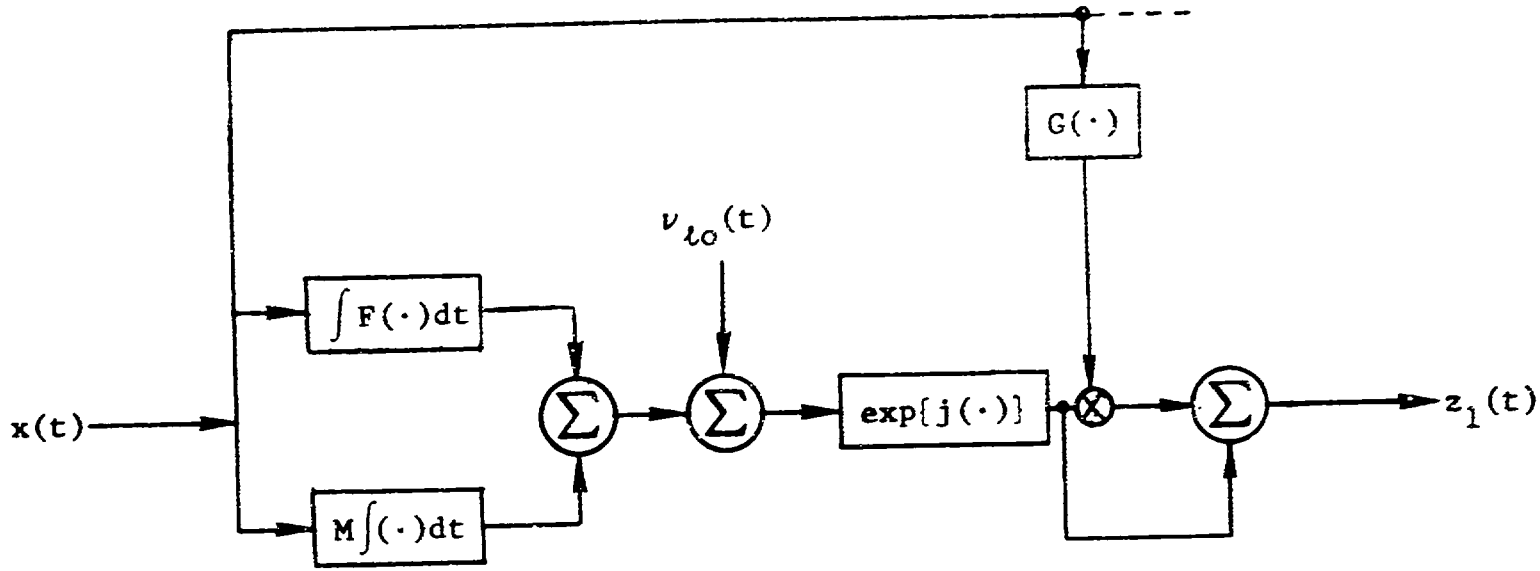

Figure 2.6 Signal Processing Model of Frequency Modulator

The analysis of the FM distortion caused by linear filtering has been the preoccupation of numerous investigators (e.g., [2.7] - [2.18]) up to the very recent past.

The most general results have been obtained by Mircea [2.15] and these results have been placed in an elegant form by Bedrosian and Rice [2.18]. The latter authors express the ideal phase detector output as a Volterra functional series expansion [2.19] in the input phase modulation, with general formulas given for the kernels of the functionals in terms of the distorting filter. This phase-input phase-output expansion is readily converted into a frequency-input frequency-output expansion by differentiation. In addition to presenting the functional expansion, Bedrosian and Rice [2.18] give expressions for the power spectrum of the detector output when the input is Gaussian.

We will present the basic expansion in the time domain without reference to Volterra functionals. The filter is assumed to have an impulse response $\gamma(t)$, an input signal $\exp\{j\psi(t)\}$, and an output $w(t) = \exp\{\alpha(t) + j\theta(t)\}$ so that

$$w(t) = e^{\alpha(t)}\, e^{j\theta(t)} = \int \gamma(\mu)\, e^{j\psi(t-\mu)}\, d\mu \tag{2.7}$$

The output phase modulation is $\theta(t)$ and the output envelope $e^{\alpha(t)}$ ($\alpha(t)$ may be called the output attenuation). For notational convenience, the filter is assumed normalized to unit amplitude transmission at the carrier frequency, or in complex notation

$$\int \gamma(\mu)\, d\mu = \Gamma(0) = 1 \tag{2.8}$$

where

$$\Gamma(f) = \int \gamma(t)\, e^{-j2\pi ft}\, df \tag{2.9}$$

is the filter transfer function.

The time-variant attenuation and phase may be expressed explicitly as

$$\theta(t) = \mathrm{Im}\{y(t)\} \tag{2.10}$$

$$\alpha(t) = \mathrm{Re}\{y(t)\} \tag{2.11}$$

where

$$y(t) = \ell n \left[\int \gamma(\mu)\ e^{j\psi(t-\mu)}\, d\mu\right] \tag{2.12}$$

The desired expansion is obtained by expanding the exponential in (2.12) in a power series and then expanding the logarithm in a power series. Defining

$$y_n(t) = \gamma(t) \otimes \psi^n(t) \tag{2.13}$$

where $\otimes$ denotes convolution, we see that

$$\begin{aligned} y(t) &= \ell n\left[1 + \sum_1^\infty \frac{(j)^n}{n!}\, y_n(t)\right] \\ &= \Sigma - \frac{1}{2}(\Sigma)^2 + \frac{1}{3}(\Sigma)^3 - \frac{1}{4}(\Sigma)^4 + \ldots \end{aligned} \tag{2.14}$$

Collecting terms of the same order, it is readily found that

$$\begin{aligned} y(t) &= jy_1(t) + \frac{1}{2}\left[y_1^2(t) - y_2(t)\right] \\ &\quad - \frac{j}{6}\left[2y_1^3(t) - 3y_1(t)y_2(t) + y_3(t)\right] + \ldots \end{aligned} \tag{2.15}$$

which is a time domain expression identical to the involved-looking Volterra expansion derived in [2.18].

The imaginary part of the first term in (2.15) is the "exact" linear term of the output phase modulation $\theta_1(t)$,

$$\theta_1(t) = \mathrm{Re}\left\{\int \gamma(\mu)\ \psi(t-\mu)\,d\mu\right\}$$

$$= \int \mathrm{Re}\{\gamma(\mu)\}\ \psi(t-\mu)\,d\mu \qquad (2.16)$$

By taking the derivative of the phase modulation, we obtain the frequency modulation output which will contain a linear term and nonlinear distortion terms. Thus, the linear FM output is just

$$\frac{\dot{\theta}_1(t)}{2\pi} = \int \mathrm{Re}\{\gamma(\mu)\}\ \dot{\psi}(t-\mu)\,d\mu$$

$$= M\int \mathrm{Re}\{\gamma(\mu)\}\ x(t-\mu)\,d\mu \qquad (2.17)$$

where we have used Eq. (2.3) relating the PM and FM inputs.

The real part of the first term in (2.15) contains the term in the output attenuation expansion that is linearly related to the input signal

$$\alpha_1(t) = -\ \mathrm{Im}\left\{\int \gamma(\mu)\ \psi(t-\mu)\,d\mu\right\}$$

$$= -\int \mathrm{Im}\{\gamma(\mu)\}\ \psi(t-\mu)\,d\mu \qquad (2.18)$$

All other terms are nonlinearly related to $\psi(t)$. When the filter is strictly symmetrical with respect to the carrier frequency, it is readily seen that $\gamma(t)$ will be real, $\alpha_1(t)$ will vanish, and the linear term $\theta_1(t)$ is a filtered version of the input signal with a filter identical to the lowpass equivalent of the actual bandpass filter.

When the filter is distortionless

$$\gamma(t) = \delta(t-\tau) \qquad (2.19)$$

where τ is some delay. (Recall that, due to normalization, the area under $\gamma(t)$ is unity.) Using (2.19) in (2.13), we see that

$$y_n(t) = \psi^n(t-\tau) = y_1^n(t) \tag{2.20}$$

Using (2.20) in (2.15), we see that, indeed, all distortion terms vanish.

In general, we can express the filter output w(t) in the form

$$w(t) = \exp\left\{\alpha_1(t) + \sum_{n=2}^{\infty} \alpha_n(t)\right\} \exp\left\{j\,\beta_1(t) + \sum_{n=2}^{\infty} \beta_n(t)\right\} \tag{2.21}$$

where the subscript n denotes the "order" of the distortion term. The first two nonlinear distortion terms are, from (2.15),

$$\alpha_2(t) = \frac{1}{2}\,\mathrm{Re}\left\{y_1^2(t) - y_2(t)\right\} \tag{2.22}$$

$$\beta_2(t) = \frac{1}{2}\,\mathrm{Im}\left\{y_1^2(t) - y_2(t)\right\} \tag{2.23}$$

$$\alpha_3(t) = \frac{1}{6}\,\mathrm{Im}\left\{2y_1^3(t) - 3y_1(t)y_2(t) + y_3(t)\right\} \tag{2.24}$$

$$\beta_3(t) = -\frac{1}{6}\,\mathrm{Re}\left\{2y_1^3(t) - 3y_1(t)y_2(t) + y_3(t)\right\} \tag{2.25}$$

Figure 2.7 depicts the signal processing operations relating the input phase modulation $\psi(t)$ and the output attenuation and phase modulations. The above expansion can be readily generalized to include both input attenuation and phase modulation by defining the exponential in (2.12) to be complex. This is done in Section 2.2.2.2.

In the case of FDM-FM analog transmission, little attention is given to any linear distortion contained in $\theta_1(t)$ because the filter $\gamma(t)$ is very much wider than that of a particular voice channel and the linear distortion in a voice channel is completely negligible. On the other hand, in PCM-TDM-FM transmission the

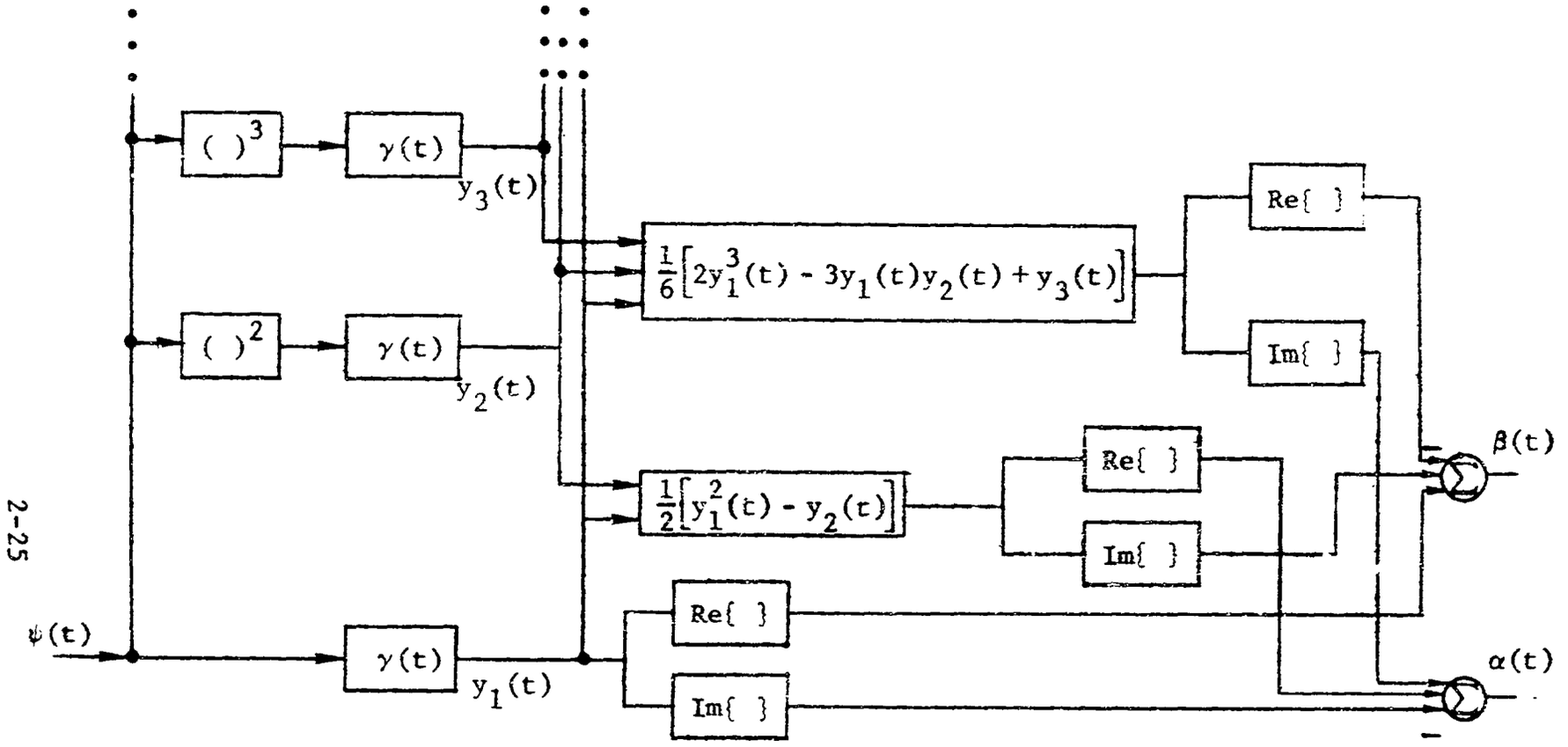

Figure 2.7 Signal Processing Operations Relating Output Attenuation and Phase Modulation to Input Phase Modulation for a Distorting Filter

linear operation forming $\theta_1(t)$ can introduce intersymbol interference, since the signaling element bandwidths are likely to be comparable to the filter bandwidth.

The nonlinear phase modulation terms are particularly harmful in FDM-FM analog transmission because they introduce intermodulation distortion as did the nonlinearities in the frequency modulator characteristic. Only small amounts of nonlinear distortion are allowable in meeting transmission performance objectives of these analog systems. For PCM-TDM-FM systems, the nonlinear distortion terms in the output phase modulation may be regarded as a form of nonlinear intersymbol interference. However, because the size of distortion terms usually decrease as the order of distortion increases, for a mildly distorting situation, it is likely that the linear intersymbol interference will dominate in its effect on performance. Thus, the relative importance of filter distortion terms is likely to be quite different for the analog FDM-FM and the digital TDM-PCM-FM systems.

In the preceding discussion, we have lumped together the RF and IF filtering as a composite linear filter. It is conceivable, however, that nonlinearities may develop in some IF and RF amplifiers. These nonlinearities, acting on the bandpass signal, produce harmonics of the IF or RF signal, which are eliminated by the bandpass filter. Their effect on the desired signal is then only to cause some nonlinear operations on the envelope of the input signal. Since the system is FM, any envelope fluctuations are spurious anyway, and their clipping or saturation is not harmful per se.

The amplitude modulation at the filter output is harmful to the extent that succeeding signal processing operations involve sufficient AM/PM conversion. Then linear and nonlinear distortions on the attenuation will become converted into linear and nonlinear signal-dependent phase modulation terms.

The major source of AM/PM conversion in the transmitter channel is the TWT (traveling wave tube) power amplifier and, for this reason, a limiter may be introduced prior to the TWT. Although the limiter itself produces AM/PM conversion, its conversion coefficient can be made less than that of the TWT. The measurement of AM/PM conversion and the effect of this conversion on FDM-FM systems has received considerable attention [2.20] - [2.29].

In the case of the TWT, which is a broadband device, the AM/PM conversion is not frequency-dependent. Thus, the resulting PM may be represented as

$$\theta_2(t) = K[\alpha(t)] \tag{2.26}$$

where $\alpha(t)$ is the input attenuation modulation. According to Cross [2.21], the TWT's "when driven at moderate, essentially constant input power level and biased from well controlled sources, are adequately characterized for small envelope fluctuations by a constant K degrees/dB". Under such conditions, (2.21) simplifies to

$$\theta_2(t) = C\,\alpha(t) \tag{2.27}$$

where C is a constant. Conversion constants of a few degrees (usually under 10^o) per dB of amplitude modulation may be expected, although some manufacturers claim less.

For AM/PM conversion to be a problem in an FM system, there must be a source of FM/AM conversion, such as a distorting linear filter. The signal processing for such a cascade is indicated in Figure 2.8 where the composite IF and RF filtering is shown in cascade with a TWT operated at saturation. For simplicity, the TWT is regarded as removing amplitude fluctuations at its output.

The effect of the AM/PM conversion on PCM-TDM-FM systems is to introduce linear and nonlinear intersymbol interference. Provided the maximum value of the intersymbol interference is small compared with the desired signal, little loss in performance will occur. It is not known whether the level of combined AM and AM/PM conversion that would make an FDM-FM system unacceptable due to intermodulation would also appreciably degrade a PCM-TDM-FM system. Considerable additional work would be required to resolve this question.

Due to mismatch of the feeder lines between the TWT and transmitting antennas, echoes can occur. These echoes constitute a form of linear distortion and will produce the linear and nonlinear AM and PM distortions discussed above for the RF and IF filters. For the FDM-FM system, the intermodulation distortion is known to be the effect of major importance. One may infer this to be true for the PCM-TDM-FM systems if one is willing to generalize from calculations of a performance degradation for discrete multipath channels reported in Section 4. It was found

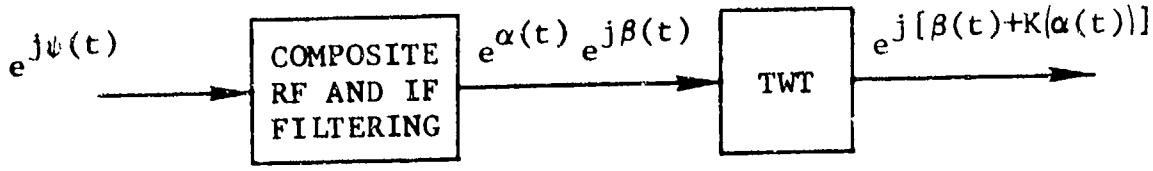

Figure 2.8 Example of Output Phase Modulation due to AM/PM Conversion of TWT Acting on AM Introduced by IF and RF Filtering

that the nonlinear intersymbol interference caused by the intermodulation distortion was the dominant effect on performance degradation.

2.2.1.2 The Propagation Channel

A detailed modeling of the LOS microwave relay propagation channel from both the system function and propagation points of view has been carried out by Bello and DeRosa in [2.30]. We present a brief summary here. The various modes of propagation are shown in Figure 2.9. A block diagram of the LOS propagation model showing the various component channels is shown in Figure 2.10. It is seen that the overall link model consists of the parallel combination of three component channels:

(1) The direct path channel

(2) The tropospheric refraction channel

(3) The surface scatter channel

In addition, each of these is connected in cascade with:

(4) The volume scatter channel

(5) The atmospheric filter channel

The direct path channel is defined as that which models the normal signal transmission from transmitter to receiver in the absence of any atmospheric anomalies, inhomogeneities, or selectivity. The effects of tropospheric layers, volume scattering, and atmospheric filtering on normal signal transmission are accounted for by the other component channels. The direct path signal may experience earth bulge fading due to the intercession of the earth's surface in the direct propagation path. This type of fading is, of course, flat across the frequency band and can be avoided by proper location of the terminals.

The tropospheric refraction channel allows several paths to reach the receiver which are delayed and amplitude-scaled with respect to the direct path. These multiple paths are caused by the focusing effects of steep negative gradients of refractive index sometimes present in the atmosphere. It is shown in [2.30] that several nanoseconds of delay spread are to be expected for extreme conditions. This results in relatively flat fading in a 14-MHz bandwidth for fades which are not too deep. It is demonstrated theoretically in [2.30], in agreement with Babler's

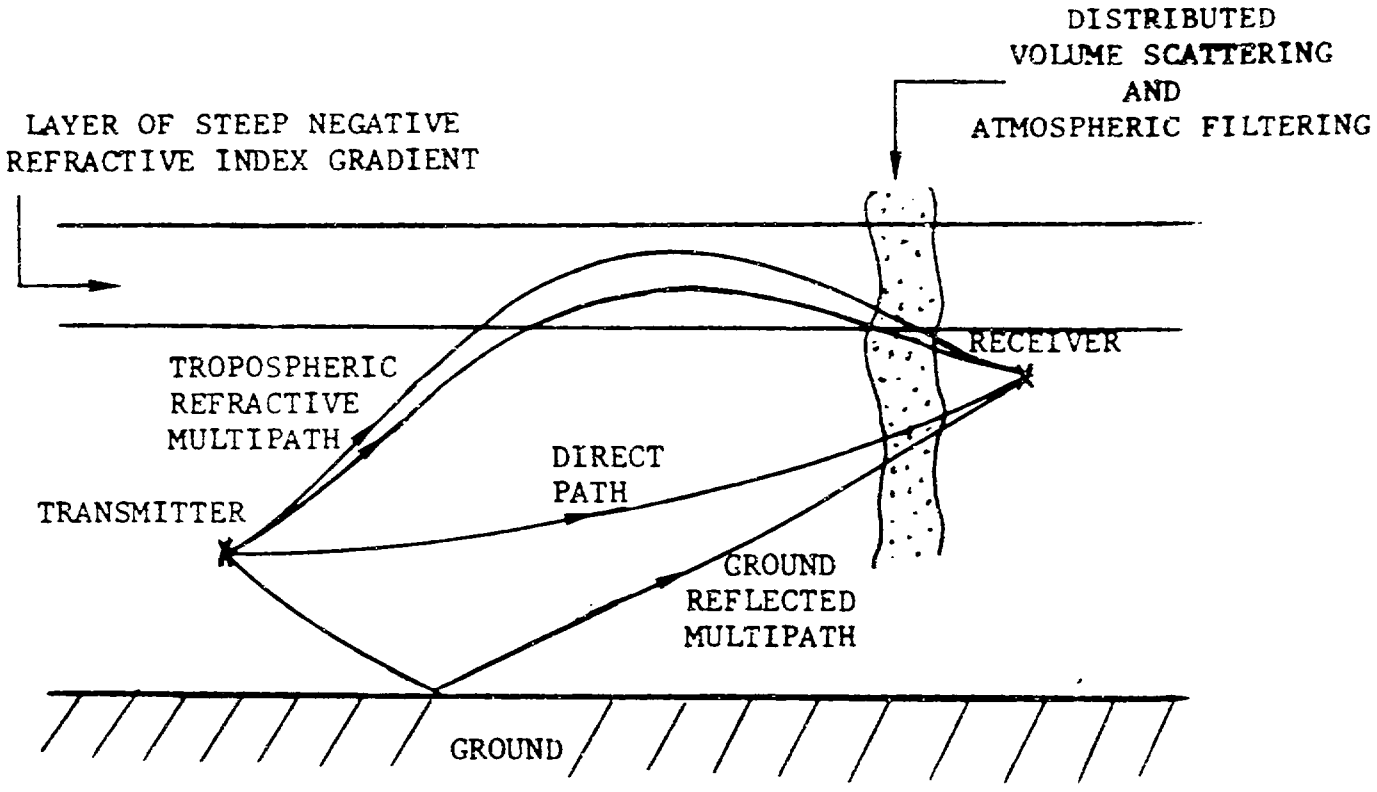

Figure 2.9 Propagation on a Microwave LOS Link

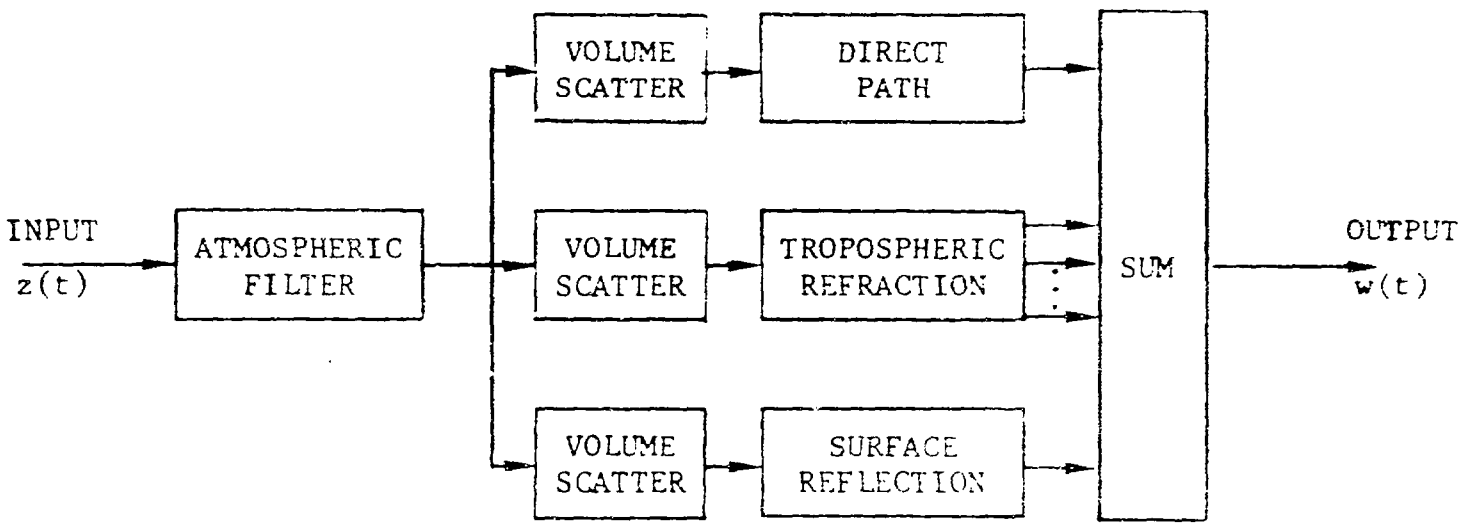

Figure 2.10 Block Diagram of Microwave LOS Link

experiment [2.31],[2.32], that deep fades are considerably more frequency-selective than shallow fades.

When surface scatter multipath occurs on microwave relay LOS links, it is usually scattered at such low grazing angles that the surface appears smooth to the incident radiation. Thus, the multipath is predominantly specular and can sometimes be avoided by screening or raising antennas high enough while using sufficiently narrow beamwidths. When there is a ground return signal, the typical delay of this signal is of the order of several nanoseconds, which again results in predominantly flat fading in a 14-MHz bandwidth except for some deep fades.

It is shown in Section 2.1.4 of [2.30] that the usual effect of the volume scatter channel is to introduce small random phase and amplitude modulation on the direct path and multipath signals. This random modulation, which is caused by atmospheric turbulence, is highly correlated across a 14-MHz band. The effect of volume scattering by hydrometeors is negligible.

The atmospheric filter channel is discussed in Section 2.1.5 of [2.30]. The frequency dependence of the complex permittivity of the atmosphere causes some frequency distortion in each signal propagating through the atmosphere. However, this is negligibly small in the 1- to 12-GHz range.

The propagation channel is a time-variant linear system. In complex notation, the input-output relationships are frequently presented with the aid of the time-variant impulse response $g(t,\xi)$ or the time-variant transfer function $T(f,t)$, as follows:

$$w(t) = \int Z(f)\, T(f,t)\, e^{j2\pi ft}\, df \qquad (2.28)$$

$$w(t) = \int z(t-\xi)\, g(t,\xi)\, d\xi \qquad (2.29)$$

where $w(t)$ is the output; $z(t)$,$Z(f)$ are the input process and its spectrum; and $T(f,t)$. $g(t,\xi)$ are related by Fourier transformation

$$T(f,t) = \int g(t,\xi)\, e^{-j2\pi f\xi}\, d\xi \qquad (2.30)$$

$$g(t,\xi) = \int T(f,t)\, e^{j2\pi ft}\, df \qquad (2.31)$$

It is shown in [2.30] that the LOS link has an impulse response whose complex envelope referenced to the carrier frequency f_0 is given by

$$g(t,\xi) = \sum_{k=1}^{N} a_k(t)\left[1+h_k(t)\right] e^{-j2\pi f_0 \tau_k(t)} \delta\left[\xi - \tau_k(t)\right] \quad (2.32)$$

where $a_k(t)$ and $\tau_k(t)$ are the slowly varying amplitude and delay of the k^{th} path signal in the absence of volume scattering. Volume scattering is accounted for by the more rapidly varying complex gain $h_k(t)$, where it is shown in [2.30] that, usually, $|h_k(t)|^2 \ll 1$.

Fourier transforming (2.32) with respect to ξ gives the time-variant transfer function

$$T(f,t) = \sum_{k=1}^{N} a_k\left[1+h_k(t)\right] e^{-j2\pi(f_0+f)\tau_k} \quad (2.33)$$

The complex envelope of the output signal is then given by:

$$w(t) = \sum_{k=1}^{N} a_k\left[1+h_k(t)\right] e^{-j2\pi f_0 \tau_k(t)} z(t-\tau_k) \quad (2.34)$$

where z(t) is the complex envelope of the input signal. Bullington [2.33] has noted that the relative phase variations of the individual paths are much more rapid than the relative amplitude variations in agreements with the model presented here.

For concreteness, we define the contribution of k=1 as the direct path and the contribution for k=2 as the surface reflection path. The contributions for larger values of k (k = 3,4,....) are due to the multipath components produced by refractive anomalies, i.e., layers of steep negative gradient in refractive index. For the usual case of a single refractive layer, Section 2.1 of [2.30] shows that usually two such components exist. Neglecting volume scattering, the delay and amplitude time variations of the paths $[a_k(t),\tau_k(t)]$ are slow. For the direct and reflected paths (k = 1,2), time variations on the scale of hours with small percentage changes may be expected. For the refractive multipath, however, the time variations are on the scale of minutes because they depend upon local movement of the refractive layer. The

scintillation due to volume scattering is more rapid with $g_k(t)$ having fluctuations with time scale of the order of of a second. In general, $g_k(t)$ is small compared with unity producing on each path usually a fraction to one dB of amplitude fluctuation and a fraction of a radian phase fluctuation, depending upon atmospheric turbulence.

Note that in (2.33) and (2.34) we have expressed a_k without a time argument and τ_k sometimes with and without a time argument depending upon whether it occurs in the product $2\pi f_0 \tau_k(t)$. Although τ_k is slowly changing, f_0 is a very large number (1 to 12 GHz for this study) so that even very small changes in τ_k (fractions of a nanosecond and greater) can cause radians of phase shift and even several complete rotations of $\exp\{-j2\pi f_0 \tau_k(t)\}$. On the other hand, for bandwidths of interest, f in $\exp\{-j2\pi f \tau_k\}$ is of the order of 7 MHz, so that the same variations that make $\exp\{-j2\pi f_0 \tau_k(t)\}$ rotate many times will cause only a few degrees change in $\exp\{-j2\pi f \tau_k\}$. If the delay separations between the refractive paths and the carrier frequencies are large enough, as the refractive layer moves the various factors, $\exp\{-j2\pi f_0 \tau_k(t)\}$ will appear like a set of phasors of incommensurate frequencies rotating relative to one another several cycles. In such a case, one may model these factors as random independent uniform phase modulators $\exp\{-j\varphi_k(t)\}$ and express (2.32) and (2.33) in the form

$$g(t,\xi) = a_1\left[1 + h_1(t)\right] e^{-j2\pi f_0 \tau_1}\, \delta(\xi - \tau_1) + a_2\left[1 + h_2(t)\right] e^{-j2\pi f_0 \tau_2}\, \delta(\xi - \tau_2) + \sum_{k=3}^{K} a_k\left[1 + h_k(t)\right] e^{-j\varphi_k(t)}\, \delta(\xi - \tau_k) \qquad (2.35)$$

$$T(f,t) = a_1\left[1 + h_1(t)\right] e^{-j2\pi f_0 \tau_1}\, e^{-j2\pi f \tau_1} + a_2\left[1 + h_2(t)\right] e^{-j2\pi f_0 \tau_2}\, e^{-j2\pi f \tau_2} + \sum_{k=3}^{K} a_k\left[1 + h_k(t)\right] e^{-j\varphi_k(t)}\, e^{-j2\pi f \tau_k} \qquad (2.36)$$

Such a characterization with random phase is a worst-case modeling which should, nonetheless, be valid often at the higher frequencies in the range (1 to 12 GHz). Consequently, we use this formulation to model worst-case frequency selectivity recognizing that at lower frequencies or sufficiently small multipath spreads, the phases $2\pi f_0 \tau_k(t)$ may not vary sufficiently to use a random independent uniform phase distribution $(0,2\pi)$.

Except for overwater transmission, which is a special case, the reflected path does not constitute a significant interference problem on a well-designed link and we ignore it in the subsequent discussion. In addition, to simplify the notation, we use the direct path arrival as a time reference and normalize amplitude to the strength of the direct path in the absence of scintillation. A final simplification is to ignore the scintillation term, yielding

$$T(f,t) = 1 + \sum_{k=3}^{K} a_k \, e^{-j\varphi_k(t)} \, e^{-j2\pi f \tau_k} \tag{2.37}$$

$$g(t,\xi) = \delta(\xi) + \sum_{k=3}^{K} a_k \, e^{-j\varphi_k(t)} \, \delta(\xi - \tau_k) \tag{2.38}$$

where now τ_k is to be interpreted as the delay of the k^{th} path relative to the direct path, a_k as the amplitude of the k^{th} path relative to the direct path (in the absence of volume scattering), and the $\varphi_k(t)$ are assumed independent and uniformly distributed over $(0,2\pi)$.

Deep fading will be caused at the frequency f_0+f whenever the first term on the right side of (2.37) is approximately cancelled by the remaining terms. Lin [2.34] shows that, under rather general conditions (including those pertaining in the present instance)

$$\Pr\left\{[T(f,t)] \le \alpha\right\} \sim \alpha^2 \tag{2.39}$$

for small α, where α is the fade level. This result is in accordance with extensive measured results for overland paths.

The selective fading introduced by the multipath will cause output linear and nonlinear phase and attenuation distortion modulation terms just as for the RF and IF filters, and feeder line echoes of the transmitter channel. Analytic expressions for these distortion terms have been presented in Section 2.2.1.1 and the corresponding signal processing illustrated in Figure 2.7.

2.2.1.3 The Receiver Channel

Signal processing operations in the receiver channel have largely been covered in the discussion of the transmitter channel except for the frequency discriminator and the presence of additive disturbances. The RF and IF filtering of the receiver will generally cause more distortion than in the transmitter because the need to eliminate receiver noise will generally require narrower bandwidth filtering. As in the transmitter channel, a composite RF/IF linear filter representation will usually be valid, but significant nonlinear operation of an amplifier within the RF and IF sections will obviate this simple model. In such a case, the nonlinear amplifier (or amplifiers) must be separately treated and composite linear filters may be employed external to the nonlinearly functioning element. Aside from the possible existence of a strong interfering signal or the failure of the AGC to reduce gain for a strong desired signal, a linear modeling of the RF/IF sections should be appropriate.

The receiver processing differs from that at the transmitter in having an AGC (automatic gain control) which adjusts the average signal level out of the final IF amplifier to be very nearly a fixed volage level for very large variations in input signal. The discriminator is normally unaffected by the operation of this AGC.

Ideally, the frequency discriminator output signal is (apart from a delay) directly proportional to the instantaneous frequency (phase derivative) of the input signal complex envelope. Thus, if the input to the discriminator is given by

$$z(t) = e^{\alpha(t)}\, e^{j\beta(t)} \tag{2.40}$$

the output of an ideal discriminator is just (apart from a proportionality constant and delay)

$$\nu(t) = \frac{\dot{\beta}(t)}{2\pi} \tag{2.41}$$

In actuality, the output will differ in three ways from this ideal:

- Linear distortion
- Nonlinear distortion
- AM/FM conversion

The linear distortion is generally regarded as unimportant in the conventional FDM-FM systems and, for this reason, little may be found in the literature characterizing the linear distortion imposed by the discriminator. In the case of PCM-TDM-FM digital transmission, where intersymbol interference produced by linear distortion is a factor of major concern, it is not clear that the linear distortion of the discriminator may be neglected.

Nonlinear distortion for the FM discriminator is usually characterized by means of a no-memory nonlinear function $H(\cdot)$, say

$$\nu(t) = \frac{\dot{\beta}(t)}{2\pi} + H[\dot{\beta}(t)] \tag{2.42}$$

Because the intermodulation distortion introduced by this nonlinear distortion causes rapid degradation of FDM-FM systems beyond allowable levels, the discriminators are designed to be quite linear[say, $H(\cdot)$ is within 1% of $(\dot{\beta}/2\pi)$]. This degree of linearity is not likely to be needed for proper performance of PCM-TDM-FM digital transmission.

The discriminator incorporates a hard limiter to remove amplitude fluctuations at its input. However, the limiter is not perfect and some AM/FM conversion will take place and result in possible intermodulation components at the discriminator output. Thus, including nonlinear distortion and AM/FM conversion, the output may be presented as

$$\nu(t) = \frac{\dot{\beta}(t)}{2\pi} + H[\dot{\beta}(t)] + K[\alpha(t)] \tag{2.43}$$

Only when large amplitude fluctuations occur, approaching and going below the limiter thresholds, will AM/FM conversion pose a performance limitation for PCM-TDM-FM systems.

The effect of an additive interfering signal at the receiver input is to produce undesired amplitude and phase modulation on an otherwise distortion-free FM signal. Provided the AM/FM conversion of the discriminator is small enough, the net effect of the interference will be to produce a spurious FM at the discriminator output, which will generally be nonlinearly related to both the desired FM and the AM and FM of the interfering signal. When the additive disturbance is small compared to the desired signal, some simplification in the representation of the output is possible because it is primarily only the disturbance component in quadrature to the desired signal that produces FM on the resulting signal and a spurious output of the discriminator.

In the case of the usual receiver noise, Rice [2.35] has developed expressions for the discriminator output noise for the full range of SNR's. However, for LOS links, the SNR's are so large that even in a deep fade the simple quadrature approximation to the phase noise is applicable, yielding an output FM noise

$$r(t) = x(t) + \frac{1}{2\pi}\frac{d}{dt}\,\mathrm{Im}\left\{\eta(t)e^{-j\psi(t)}\right\} \tag{2.44}$$

where the complex envelope of the input to the discriminator is given by

$$z(t) = e^{j\psi(t)} + \eta(t) \tag{2.45}$$

and the signal FM

$$x(t) = \frac{\dot{\psi}(t)}{2\pi} \tag{2.46}$$

Generally, the term $\exp\{-j\psi\}$ in (2.44) is neglected in characterizing the output noise, because the phase of the receiver noise term $\eta(t)$ is uniformly distributed and of wider bandwidth than $\psi(t)$, resulting in a very weak dependence of output noise statistics on $\psi(t)$. When $\eta(t)$ is a more general type of interference, it becomes necessary to reexamine this dependence when using the quadrature approximation.

2.2.1.4 IF Modem

In the case of IF modems (such as are being considered in the Phase II upgrade [2.6]), the digital signal output occurs at the 70-MHz IF frequency and the transmitter channel of Figure 2.5 would be modified to start at IF. The [illegible] of the signal processing operations could also show some [illegible]rations. The local oscillators may be further stabilized fo[illegible]rent operation. Those IF modems involving both amplitude and phase modulation would require linear power amplification. The receiver channel would be modified by removal of the discriminator since the IF modem demodulator accepts the IF signal directly. In addition to the AGC, some form of AFC (automatic frequency control) may be used. No additional signal processing models would be needed beyond those discussed in Sections 2.2.1.1 - 2.2.1.3 for defining input-output behavior.

2.2.2 Parameterization

If the relationship between the input and output signals of a communications link can be described in terms of a finite number of parameters, the performance of the communications link should be directly relatable to these parameters. This reasoning provides the rationale for a basic method of performance assessment consisting of two sequences of operations: parameter measurement followed by performance estimation based upon utilization of the measured parameters in formulas relating performance to parameter values.

The formulation of signal processing operations in the transmitter, propagation, and receiver channels in Section 2.2.1 was not presented in terms of sets of parameters. In this section we shall discuss the parameterization of these signal processing operations as a step toward evaluating the utility of performance assessment based upon channel parameter measurement.

As a result of the discussions in Section 2.2.1, we see that various signal processing operations in the link may be combined to produce the simplified link model of Figure 2.11, when IF and RF amplifier nonlinearities are unimportant. We consider first the parameterization of the linear signal processing operations shown in this figure, and then the nonlinear operations.

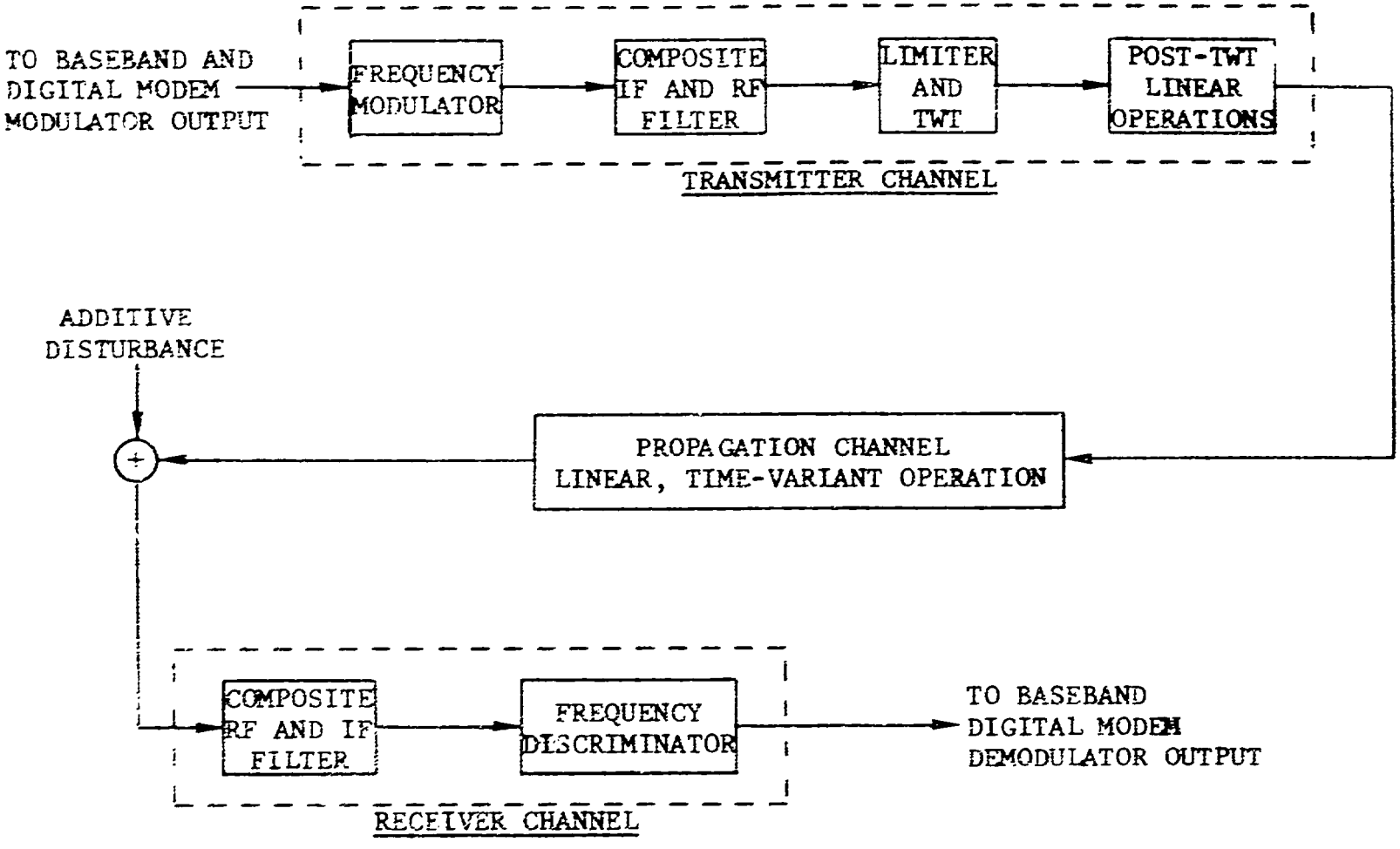

Figure 2.11 Composite Signal Processing Operations in Single LOS Link

2.2.2.1 Propagation Channel: Cartesian Representation

All real-life channels and signals have an essentially finite number of degrees of freedom due to restrictions on time duration, bandwidth, and dynamic range. These limitations have been used by Bello to derive canonical model representations of linear [2.38] and nonlinear [2.36] systems. In these representations, the signal processing of the channel is completely determined by a set of discrete channel-dependent parameters plus known channel-independent signal processing operations. The reader is referred to [2.36] and [2.38] for complete details. Here we wish to discuss only two of the many canonic model representations discussed in [2.38] – the "tapped delay line" and the "chain differentiator" models.* With these representations, the output complex signal is linearly related to the channel parameters. We call this a "cartesian" representation in order to distinguish it from the complex exponential representation discussed in Section 2.2.2.2 in which the attenuation and phase modulation of the output signal are related to channel parameters.

2.2.2.1.1 Tapped Delay Line Model

The tapped delay line model of a time-variant random channel has been studied extensively by Bello [2.38] with particular attention to its properties for time-variant random channels. It is useful in modeling when the product of the impulse duration times the signal bandwidth is not small. The derivation of this model is based upon the assumption that the spectrum of the input signal complex envelope $Z(f)$ is confined to a finite bandwidth, say $-W/2 < f < W/2$. Then the time-variant transfer function outside this interval clearly does not affect the output signal since only the product $Z(f)T(f,t)$ occurs in (2.28).

One may then replace $T(f,t)$ by a periodic function in f, $\hat{T}(f,t)$, which is identical to $T(f,t)$ within $-\hat{W}/2 < f < \hat{W}/2$, where $\hat{W} > W$, without changing the output complex envelope $w(t)$. However, since this modified time-variant transfer function is periodic, it has a Fourier series expansion and its Fourier transform on the frequency variable, $\hat{g}(t,\xi)$ has the discrete representation

*The terminology "f-power series" model was used in [2.38] instead of "chain differentiator" model.

$$\hat{g}(t,\xi) = \sum_{-\infty}^{\infty} g_k(t)\,\delta\left(\xi - \frac{k}{W}\right) \tag{2.47}$$

where $g_k(t)$ are the (time-variable) Fourier coefficients in the expansion of $\hat{T}(f,t)$. In [2.38], $\hat{W}$ was chosen equal to W which leads to the two equivalent expressions for the k^{th} tap complex gain

$$g_k(t) = \int \operatorname{sinc}\left[W\left(\xi - \frac{k}{W}\right)\right] g(t,\xi)\,d\xi \tag{2.48}$$

$$g_k(t) = \frac{1}{W} \int_{-\frac{W}{2}}^{\frac{W}{2}} T(f,t)\, e^{j2\pi\frac{fk}{W}}\,df \tag{2.49}$$

where

$$\operatorname{sinc} W\xi = \frac{\sin \pi W\xi}{\pi W\xi} \tag{2.50}$$

Equation (2.47) leads to the input-output representation

$$w(t) = \sum_{-\infty}^{\infty} g_k(t)\, z\left(t - \frac{k}{W}\right) \tag{2.51}$$

which, we see from Figure 2.12, is identical to the output of a uniformly tapped delay line with taps spaced 1/W seconds apart and with time-variable complex tap "gain" $g_k(t)$ applied to the tap providing delay k/W. Equation (2.51) represents a parameterized input-output relationship with the time-variant parameters $g_k(t)$.

Strictly speaking, the number of parameters (tap gains) is infinite; however, practically speaking, an adequate approximation may be achieved with a finite number. From (2.48) we see that, for $\hat{W} = W$, the k^{th} tap gain is given by samples at delays 1/W apart of the convolution of the channel impulse response with the function sinc $W\xi$. Let the width of the former, the "multipath spread", be L. The width of the latter is infinite, strictly speaking. However, one may choose a value of α such that, for $|\xi| > \alpha/W$, sinc $W\xi$ will be as small as desired. Because

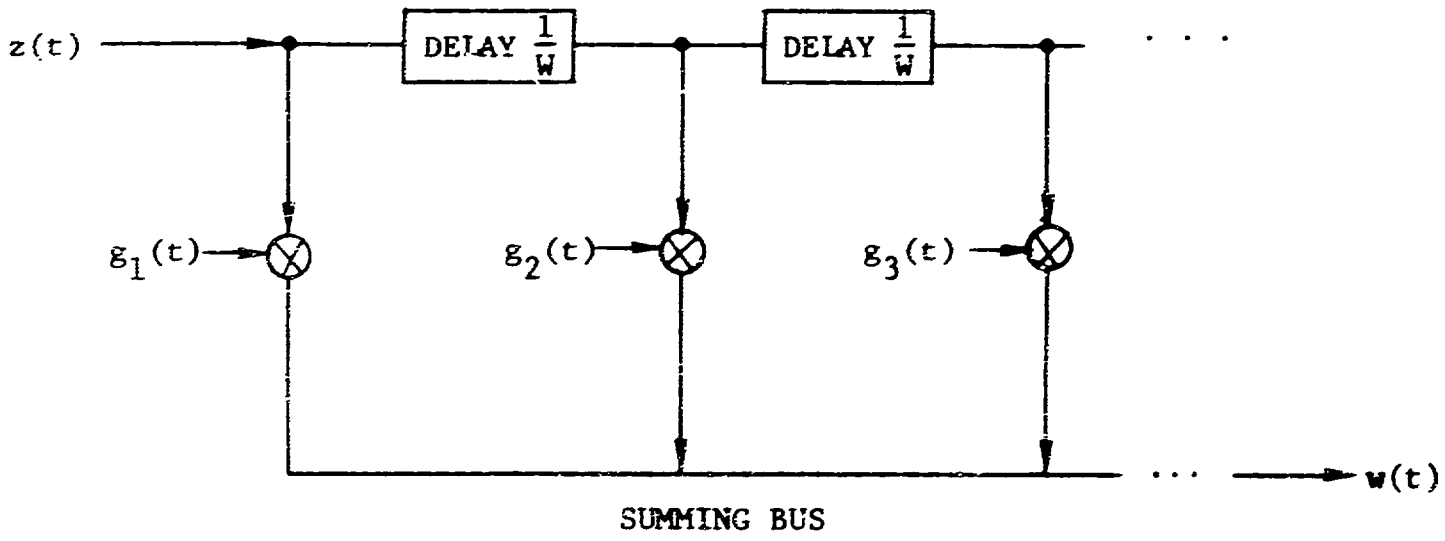

Figure 2.12 Tapped Delay Line Representation of Propagation Channel

sinc $W\xi$ decreases so slowly with ξ, α can be a large number for any reasonable definition of width. The convolution of sinc $W\xi$ and $g(t,\xi)$ will be effectively nonzero for values of ξ in an interval of duration $L+\alpha/W$. Since the taps are spaced $1/W$ apart, the number of taps needed is

$$N_W = WL + \alpha \tag{2.51}$$

Although choosing $\hat{W} = W$ spaces the taps farthest apart, it does not necessarily minimize the number of taps required to represent the channel. By choosing $\hat{W} > W$, it is possible to form a periodic time-variant transfer function which is essentially identical to the true $T(f,t)$ within $|f| < W/2$ but drops to zero sufficiently smoothly by $|f| = \hat{W}/2$ to considerably reduce the "edge" effect α/W. This is, of course, the familiar "window" function approach used in the spectral analysis of a finite record to reduce the number of Fourier components. For $\hat{W} > W$, the expressions (2.48) and (2.49) must be generalized to

$$g_k(t) = \int \frac{1}{\hat{W}} h\left(\xi - \frac{k}{\hat{W}}\right) g(t,\xi)\, d\xi \tag{2.52}$$

$$g_k(t) = \frac{1}{\hat{W}} \int_{-\frac{\hat{W}}{2}}^{\frac{\hat{W}}{2}} H(f)\, T(f,t)\, e^{j2\pi \frac{k}{\hat{W}} t}\, df \tag{2.53}$$

where $H(f)$ is the "window" function which is satisfactorily close to unity over $|f| < W/2$ and drops to zero smoothly by $|f| = \hat{W}/2$. Its transform

$$h(\xi) = \int H(f)\, e^{j2\pi f \xi}\, df \tag{2.54}$$

has tails which drop to zero much faster than sinc $W\xi$.

Given any channel impulse response structure, as in (2.35) or (2.38), one may compute the parameters of the tapped delay line model. Thus corresponding to (2.38) we have, from (2.52) that

$$g_k(t) = \frac{1}{W}\left[h\left(\frac{k}{W}\right) + \sum_{k=3}^{K} a_k\, e^{-j\varphi_k(t)}\, h\left(\tau_k - \frac{k}{W}\right)\right] \qquad (2.55)$$

When the impulse response duration is small compared to the duration of $h(\cdot)$, the parameters will be highly dependent.

2.2.2.1.2 Chain Differentiator Model

Our present concern is with the degree of selective fading in a bandwidth W and its effect upon a transmitted data signal. For the bandwidths of interest, say 14 MHz and the expected range of path delay spreads, a few nanoseconds, the degree of frequency selectivity to be expected within W will be small. Consequently, the few few, and frequently only the first three, terms in a power series expansion of the transfer function suffice to characterize the frequency selectivity. The utility of such a power series to model a time-variant dispersive channel by a chain of differentiations has been studied by Bello [2.38]. Formally,

$$T(f,t) = \sum_{n=0}^{\infty} T_n(t)\,(2\pi j f)^n \qquad (2.56)$$

which represents the channel by a sum of the outputs of successively higher orders of (bandpass) differentiators, with the n^{th}-order differentiator being multiplied by the complex function

$$T_n(t) = \begin{cases} \dfrac{1}{n!\,(2\pi j)^n}\left[\dfrac{\partial^n T(f,t)}{\partial f^n}\right]_{f=0} \\ \dfrac{1}{n!}\displaystyle\int (-\xi)^n\, g(t,\xi)\, d\xi \end{cases} \qquad (2.57)$$

Bello [2.38] has shown that the power series representation (2.56) will be most rapidly convergent when the expansion is taken for a channel in which a "mean" path delay has been removed. Assuming this mean path delay is ξ_0, the input-output representation corresponding to (2.56) (including the mean path delay) is given by*

*See Section 4.1 of Appendix B for further discussion.

$$w(t) = \sum_{n=0}^{\infty} T_n(t) \frac{d^n z(t - \xi_0)}{dt^n} \tag{2.58}$$

This parametric model is shown in Figure 2.13. (This chain-differentiator model is called the f-power series model in [2.38].

When the frequency-selective fading in the channel is sufficiently small, only the first term in the series (2.56) will be sufficient to characterize the channel output, i.e.,

$$w(t) = T_0(t)\, z(t - \xi_0) \tag{2.59}$$

where z(t), w(t), are the complex envelopes of the channel input and output, respectively. Equation (2.59) may be recognized as a "flat fading" or nonfrequency-selective channel model. If the first two terms are used,

$$w(t) = T_0(t)\, z(t - \xi_0) + T_1(t)\, \dot{z}(t - \xi_0) \tag{2.60}$$

which is called a "linearly frequency-selective fading" channel [2.38] since it corresponds to approximating T(f,t) by a complex linear term in the frequency variable. One may continue and define a "quadratically frequency-selective fading" channel, "cubically frequency-selective fading" channel, etc.

Given any channel impulse response structure, as in (2.35) or (2.38), one may compute the parameters $\{T_n(t)\}$ of the chain-differentiator model. For example, using (2.38) in (2.57), we see that

$$T_0(t) = 1 + \sum_{k=3}^{K} a_k\, e^{-j\varphi_k(t)} \tag{2.61}$$

$$T_n(t) = \sum_{k=3}^{K} \left(-\tau_k\right)^n a_k\, e^{-j\varphi_k(t)} \tag{2.62}$$

When the path delay separations are small compared to the reciprocal signal bandwidth (i.e., $WL \ll 1$) and the mean path delay has

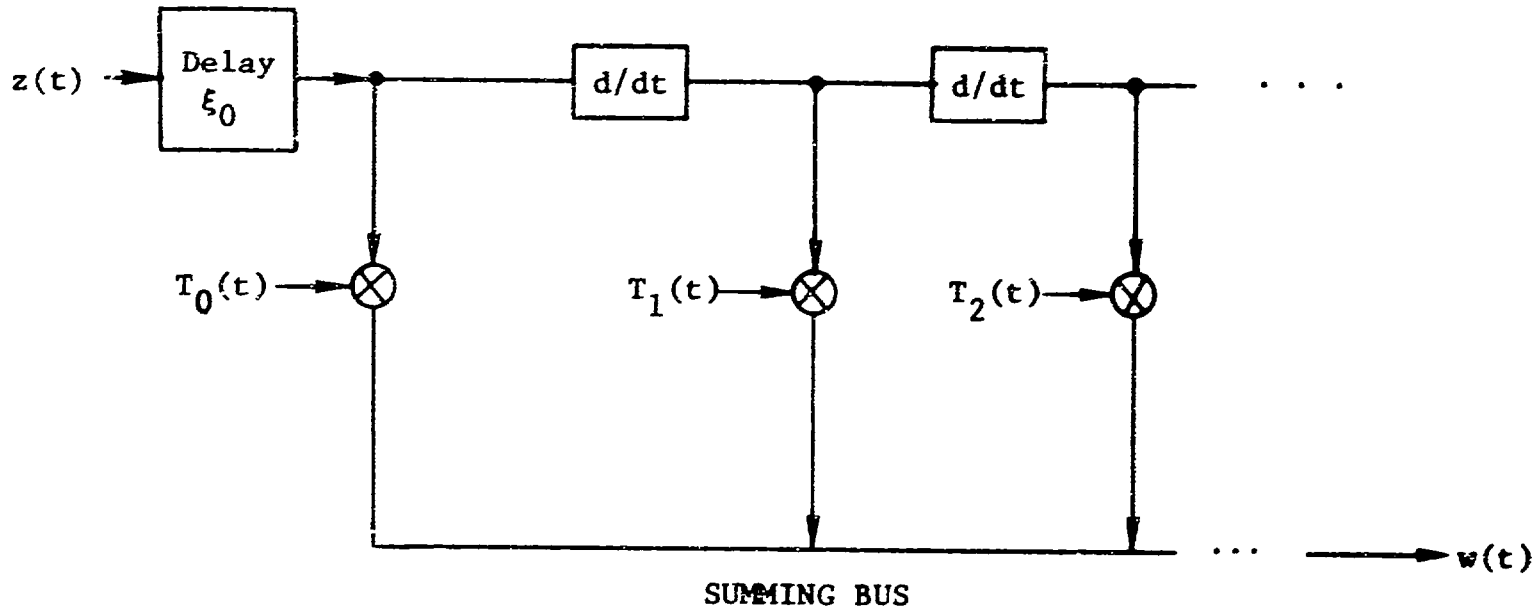

Figure 2.13 Chain-Differentiator Model of Propagation Channel

been removed in forming the model, the parameter $T_n(t)$ will decrease rapidly with increasing n. This model is particularly appropriate for the refractive multipath on DCS LOS links in which the bandwidth occupancy is 14 MHz and maximum impulse response duration is less than 10 ns, i.e., (14 MHz)(10 ns) = 0.140 << 1.

2.2.2.2 Propagation Channel: Complex Exponential Representation

In the case of FM systems and for the cascading of distortion effects, it is particularly useful to be able to represent the distorted signal in a form that relates the input and output attenuations and phase modulations. To obtain such an exponential parametric representation, we may use a generalization of the signal processing model of Figure 2.7 in conjunction with the Cartesian expansions in Section 2.2.2.1 to obtain parametric series expressions for the output attenuation and phase modulation in terms of the input.

For notational simplicity, we normalize the channels to have a transfer function of unity at the carrier frequency, so that the normalized transfer function and impulse responses are given in terms of the unnormalized by

$$\Gamma(f,t) = \frac{T(f,t)}{T_0(t)} \tag{2.63}$$

$$\gamma(t,\xi) = \frac{g(t,\xi)}{T_0(t)} \tag{2.64}$$

where

$$T(0,t) = \int g(t,\xi)\, d\xi = T_0(t) \tag{2.65}$$

is the time-varying complex gain of the channel at the carrier frequency.

With this normalization, the input and output signals are related by

$$w(t) = T_0(t) \int z(t-\xi)\, \gamma(t,\xi)\, d\xi \tag{2.66}$$

The input and output signals are represented in the exponential forms

$$z(t) = e^{\rho(t)}\, e^{j\psi(t)} \tag{2.67}$$

$$w(t) = e^{\alpha(t)}\, e^{j\beta(t)} \cdot T_0(t) \tag{2.68}$$

where $\rho(t),\psi(t)$ are the input attenuation and phase modulation and $\alpha(t),\beta(t)$ are the output attenuation and phase modulation relative to the attenuation and phase modulation imparted at the center of the band.

From (2.66) and (2.68) we see that

$$\alpha(t) + j\beta(t) = \ell n\left|\int \gamma(t,\xi)\; e^{[\rho(t-\xi)+j\psi(t-\xi)]}\, d\xi\right| \tag{2.69}$$

The desired expansion is obtained by expanding the exponential in (2.69) in a power series and then expanding the logarithm in a power series. Defining

$$u_n(t) = \gamma(t,\xi) \otimes [\rho(t) + j\psi(t)]^n$$

$$= \sum_{p=0}^{n} C_p^n\, \gamma(t,\xi) \otimes \left\{[\rho(t)]^{n-p}[j\psi(t)]^p\right\} \tag{2.70}$$

where $\otimes$ denotes convolution, we see that

$$\alpha(t) + j\beta(t) = \ell n\left[1 + \sum_{1}^{\infty} \frac{u_n(t)}{n!}\right]$$

$$= \Sigma - \frac{1}{2}(\Sigma)^2 + \frac{1}{3}(\Sigma)^3 - \frac{1}{4}(\Sigma)^4 \ldots \tag{2.71}$$

Collecting terms of the same order

$$\alpha(t) + j\beta(t) = u_1(t) - \frac{1}{2}\left[u_1^2(t) - u_2(t)\right] + \frac{1}{6}\left[2u_1^3(t) - 3u_1(t)u_2(t) + u_3(t)\right] + \ldots \tag{2.72}$$

we see that $\alpha(t),\beta(t)$ may be expressed as the series

$$\alpha(t) = \sum \alpha_n(t) \tag{2.73}$$

$$\beta(t) = \sum \beta_n(t) \tag{2.74}$$

where successive terms are of higher order in the sense that changing $\rho(t)$ and $\psi(t)$ by a factor C changes $\alpha_n(t),\beta_n(t)$ by a factor C^n.

The first terms are given by

$$\alpha_1(t) = \mathrm{Re}\{\gamma \otimes \rho\} - \mathrm{Im}\{\gamma \otimes \psi\} \tag{2.75}$$

$$\beta_1(t) = \mathrm{Im}\{\gamma \otimes \rho\} + \mathrm{Re}\{\gamma \otimes \psi\} \tag{2.76}$$

in which we have used the simplified notation,

$$\gamma \otimes h = \int h(t - \xi)\,\gamma(t,\xi)\,d\xi \tag{2.77}$$

The second terms are given by

$$\alpha_2(t) = \frac{1}{2}\,\mathrm{Re}\left|\gamma \otimes \left(\rho^2 - \psi^2\right)\right| - \mathrm{Im}\left|\gamma \otimes \rho\psi\right| - \frac{1}{2}\,\mathrm{Re}\left|(\gamma \otimes \rho)^2 - (\gamma \otimes \psi)^2\right| + \mathrm{Im}\left|(\gamma \otimes \rho)(\gamma \otimes \psi)\right| \tag{2.78}$$

$$R_2(t) = \frac{1}{2}\left|\text{Im } \gamma \otimes (\rho^2 - \psi^2)\right| + \text{Re}\left|\gamma \otimes \rho\psi\right|$$

$$- \frac{1}{2}\left|\text{Im } (\gamma \otimes \rho)^2 - (\gamma \otimes \psi)^2\right| - \text{Re}\left|(\gamma \otimes \rho)(\gamma \otimes \psi)\right| \tag{2.79}$$

Higher-order terms may be readily formulated.

For an FM system, the desired signal is contained in the second term of (2.76), i.e., $\text{Re}\{\gamma \otimes \psi\}$. All other terms are distortion terms. Parameterization of the terms $\{\alpha_n(t), \beta_n(t)\}$ can be carried out by representing $\gamma(t,\xi)$ in parameterized form. In particular, the tapped delay line and cascade differentiator canonic models may be applied to the normalized impulse response $\gamma(t,\xi)$.

Using the definitions of the previous subsection and Eqs. (2.63) and (2.64), we see that the appropriate expansion to use for the cascade differentiator normalized transfer function is

$$\Gamma(f,t) = 1 + (j2\pi f)\frac{T_1(t)}{T_0(t)} + (j2\pi f)^2 \frac{T_2(t)}{T_0(t)} + \ldots \tag{2.80}$$

in terms of which (ignoring the mean path delay for simplicity)

$$u_n(t) = [\rho(t) + j\psi(t)]^n + \frac{T_1(t)}{T_0(t)} \frac{d}{dt}[\rho(t) + j\psi(t)]^n$$

$$+ \frac{T_2(t)}{T_0(t)} \frac{d^2}{dt^2}[\rho(t) + j\psi(t)]^n + \ldots \tag{2.81}$$

It follows that $\alpha_n(t), \beta_n(t)$ can be expressed in terms of the parameters $\{T_m(t)/T_0(t)\}$ and the input attenuation and phase modulation by use of (2.81) in (2.72). For the case wherein the input $z(t)$ is purely phase-modulated and the channel is time-invariant, Liou [2.11] has carried out the representation $\alpha_n(t), \beta_n(t)$ for up to third-order terms in a fashion essentially identical to that described above. Bello [2.37] has also used such an expansion for the time-variant channel to compute error rates in FDM-FM transmission of data over troposcatter channels.

Application of the tapped delay line model proceeds in a similar fashion. In this case, the normalized impulse response has the expansion

$$\gamma(t,\xi) = \sum_k \frac{g_k(t)}{T_0(t)}\,\delta\left(\xi - \frac{k}{W}\right) \tag{2.82}$$

which leads to the representation of $u_n(t)$ in the form

$$u_n(t) = \sum_k \frac{g_k(t)}{T_0(t)}\left[\rho\left(t - \frac{k}{W}\right) + j\psi\left(t - \frac{k}{W}\right)\right]^n \tag{2.83}$$

Use of (2.83) in (2.72) will allow $\alpha_n(t), \beta_n(t)$ to be expressed in terms of the parameters $g_k(t)/T_0(t)$ and the input modulation. This type of representation has apparently not been used previously.

2.2.2.3 Other Signal Processing Functions

To the extent that the RF and IF sections are essentially linear operations, the parameterization procedures discussed in Sections 2.2.2.1 and 2.2.2.2 may, of course, be applied, since a time-invariant linear operation is a special case of the time-variant channel discussed there. If nonlinear amplification exists within these stages and may be isolated as an operation essentially in cascade and noninteracting with the linear filtering, one may separately parameterize the linear portions of the RF and IF sections and the nonlinear amplification. The nonlinear amplifier characteristic can be parameterized by power series or Fourier series expansions of the nonlinearity.

If the nonlinear amplification cannot be so isolated but interacts with the energy storage elements of the filters, considerably more sophisticated parameterization techniques, such as developed by Bello [2.36], must be used.

The nonlinearities in the frequency modulator and demodulator are frequently parameterized by means of the coefficients in power series expansions. Thus, in Figure 2.6 the nonlinear function $F(x(t))$ characterizing the nonlinearity of the frequency modulator can be expanded in the series

$$F[x(t)] = a_2x^2 + a_3x^3 + \ldots \tag{2.84}$$

where the linear term is absent and x(t) is the input frequency modulation.

Similarly, the function $H[\dot{\beta}(t)]$ in Eq. (2.42), defining the nonlinearity of the frequency discriminator, may be expanded in a Taylor series

$$H[\dot{\beta}(t)] = b_2[\dot{\beta}(t)]^2 + b_3[\dot{\beta}(t)]^3 + \ldots \tag{2.85}$$

where $\dot{\beta}(t)$ is the FM input to the discriminator. Power series expansions are suitable for gradual nonlinearities. For small ripples, a Fourier series expansion converges more rapidly.

The broadband AM/FM and AM/PM conversion characteristics of the signal processing elements are expressed in terms of nonlinear operations on input envelopes such as $K[\alpha(t)]$ in Figure 2.8 and Eq. (2.43). The same power series or Fourier series may be used for parameterization.

REFERENCES FOR SECTION 2

[2.1] P. A. Bello, L. E. Jankauskas, and L. W. Pickering, "Equivalence Measurement Studies," CNR, Inc., Final Report on RADC Contract No. F30602-73-C-0267, RADC-TR-75-95, Vol I (AD010004), Vol II (AD010005).

[2.2] P. R. Smith, "Performance Assessment of Digital Transmission Systems," 1973 National Telecommunications Conf.

[2.3] P. A. Bello and R. Esposito, "Measurement Techniques for Time-Varying Dispersive Channels," Alta Frequenza, No. 11, Vol. XXXIX, 1970, pp. 980 - 996.

[2.4] B. Widrow, "Adaptive Filters I: Fundamentals," Stanford Electronics Labs., Stanford, Calif., Report No. SEL-66-126, December 1966.

[2.5] A. Lender, "The Duobinary Technique for High Speed Data Transmission," IEEE Trans. on Comm. and Elect., May 1963, pp. 214 - 218.

[2.6] "Digital Transmission System Design," Defense Communications Engineering Center Technical Report No. 3-74, March 1974.

[2.7] R. G. Medhurst and G. F. Small, "An Extended Analysis of Echo Distortion in the FM Transmission of Frequency-Division Multiplex," Proc. Inst. Elec. Eng. (London), Vol. 103, Part B, March 1956, pp. 190 - 198.

[2.8] J. V. Murphy, "Intermodulation Distortion Due to an Echo in FM F.D.M. Radio Systems," Alta Frequenza, Vol. 38, 1969, pp. 570-164E - 577-172E.

[2.9] F. M. Clayton and J. M. Bacon, "Intermodulation Distortion in FM F.D.M. Trunk-Radio Systems in 2-Path Fading Situations," Proc. Inst. Elec. Eng. (London), Vol. 117, February 1970, pp. 359 - 368.

[2.10] E. Bedrosian and S. O. Rice, "Distortion and Crosstalk of Linearly Filtered, Angle-Modulated Signals," Proc. IEEE, Vol. 56, January 1968, pp. 2 - 13.

[2.11] M. L. Liou, "Noise in an FM System Due to an Imperfect Linear Transducer, BSTJ, Vol. 45, November 1966, pp. 1537 - 1561.

[2.12] W. R. Bennett, H. E. Curtis, and S. O. Rice, "Interchannel Interference in FM and PM Systems Under Noise Loading Conditions," BSTJ, Vol. 34, May 1955, pp. 601 - 636.

[2.13] C. L. Ruthroff, "Computation of FM Distortion in Linear Networks for Band Limited Periodic Signals," BSTJ, Vol. 47, July-August 1968, pp. 1043 - 1063.

[2.14] R. G. Medhurst and J. H. Roberts, "Evaluation of Distortion in FM Trunk Radio Systems by a Monte Carlo Method," Proc. Inst. Elec. Eng. (London), Vol. 113, April 1966, pp. 570 - 580.

[2.15] A. Mircea, "Harmonic Distortion and Intermodulation Noise in Linear FM Transmission Systems," Rev. Electrotech. Energet. (Romania), Vol. 12, No. 3, 1967, pp. 359 - 371. Also see, Proc. IEEE (Correspondence), Vol. 54, April 1966, pp. 705 - 706, and Vol. 54, October 1966, pp. 1463 - 1466.

[2.16] S. O. Rice, "Second and Third Order Modulation Terms in the Distortion Produced when Noise Modulated FM Waves Are Filtered," BSTJ, Vol. 48, No. 1, January 1969, pp. 87 - 141.

[2.17] A. Anuff and M. L. Liou, "A Time-Domain Approach to Computing Distortion of Linearly Filtered FM Signals," IEEE Trans. on Comm. Tech., Vol. COM-19, No. 2, April 1971, pp. 218 - 221.

[2.18] E. Bedrosian and S. O. Rice, "The Output Properties of Volterra Systems (Nonlinear Systems With Memory) Driven by Harmonic and Gaussian Inputs," Proc. IEEE, Vol. 59 December 1971, pp. 1688 - 1707.

[2.19] V. Volterra, Theory of Functions of Integral and Integro-Differential Equations, Blackie & Sons, Ltd., London, 1930.

[2.20] J. P. Laico, H. L. McDowell, and L. R. Moster, "Minimum-Power Traveling-Wave Tube for 6000 Mc Radio Relay," BSTJ, November 1956, pp. 1285 - 1346.

[2.21] T. G. Cross, "Intermodulation Noise in FM Systems Due To Transmission Deviations and AM/PM Conversion," BSTJ, December 1966, pp. 1749 - 1773.

[2.22] O. Shimbo, "Complete Analysis of the Combined Effects of Intermodulation, AM-PM Conversion and Additive Noise in Multi-Carrier TWT Systems," COMSAT Laboratories, Clarksburg, Md., Technical Memorandum CL-61-69, December 1969.

[2.23] A. L. Berman and C. E. Mahle, "Nonlinear Phase Shift in Traveling-Wave Tubes as Applied to Multiple Access Communications Satellites," IEEE Trans. on Comm. Tech., Vol. 18, February 1970, pp. 37 - 47.

[2.24] A. Berman, "Experimental Determination of Intermodulation Distortion Produced in a Wideband Communications Repeater," Communications Satellite Corp. Technical Memo ED-16-66, August 1966.

[2.25] O. Shimbo, "Effects of Intermodulation, AM-PM Conversion, and Additive Noise in Multicarrier TWT Systems," Proc. IEEE, February 1971, pp. 230 - 235.

[2.26] G. J. Garrison, "Intermodulation Distortion in Frequency-Division-Multiplex FM Systems - A Tutorial Summary," IEEE Trans. on Comm. Tech., April 1968, pp. 289 - 303.

[2.27] J. A. Hall and A. J. Fuller, "Use of Differential Phase and Gain to Predict Performance of FM Radio Relay Systems," IEEE Trans. on Comm. Tech., June 1970, pp. 234 - 241.

[2.28] D. Chakrakorty and D. Geden, "Measurements of AM-PM Conversion in Low-Noise TWT's, TDA's, and Parametric Amplifiers," Proc. IEEE, November 1968, pp. 2059 - 2060.

[2.29] R. F. Pawula, "The Effects of Quadratic AM-PM Conversion in Frequency-Division-Multiplexed Multiple Access Communication Satellite Systems," IEEE Trans. on Comm. Tech., June 1971, pp. 345 - 349.

[2.30] P. A. Bello, C. J. Boardman, D. Chase, and J. K. DeRosa, "Line-of-Sight Techniques Investigation," CNR, Inc., Final Report on RADC Contract No. F30602-73-C-0244, January 1975, RADC-TR-74-330, (AD006104).

[2.31] G. M. Babler, "A Study of Frequency-Selective Fading for a Microwave Line-of-Sight Narrowband Radio Channel," BSTJ, Vol. 51, No. 3, March 1972.

[2.32] G. M. Babler, "Selectivity Faded Nondiversity and Space Diversity Narrowband Microwave Radio Channels," BSTJ, Vol. 52, No. 2, February 1973.

[2.33] K. Bullington, "Phase and Amplitude Variations in Multipath Fading of Microwave Signals," BSTJ, Vol. 50, No. 6, July-August 1971, pp. 2039 - 2053.

[2.34] S. H. Lin, "Statistical Behavior of a Fading Signal," BSTJ, December 1971, pp. 3211 - 3270.

[2.35] S. O. Rice, "Noise in FM Receivers," Time Series Anaylsis, (M. Rosenblatt, ed.), John Wiley & Sons, 1963, Chap. 25.

[2.36] P. A. Bello, "Nonlinear Canonic Models of Receivers," IEEE Int. Conf. on Comm. Conv. Record, June 1972, pp. 30-1 - 30-9.

[2.37] P. A. Bello and B. D. Nelin, "The Effect of Frequency-Selective Fading on Intermodulation Distortion and Sub-Carrier Phase Stability in FM Systems," IEEE Trans. on Comm. Systems, Vol. CS-12, No. 1, March 1964, pp. 87 - 101.

[2.38] P. A. Bello, "Characterization of Randomly Time-Variant Linear Channels," IEEE Trans. on Comm. Systems, Vol. CS-11, No. 4, December 1963, pp. 360 - 393.

SECTION 3

ADAPTIVE CHANNEL MEASUREMENTS

This section is devoted to an examination of the use of adaptive processing to acquire channel measurement information. The discussion includes both nonlinear and linear modulation techniques. Particular attention is given to adaptive processors which have a linear structure as a function of assumed channel parameters. Consideration is given to convergence time constants and measurement accuracy. Application to adaptive channel parameter measurement in the receiver and transmitter is sketched out.

3.1 The Adaptive Processor

3.1.1 Nonlinear Processor

To appreciate the utility of adaptive processing techniques for channel parameter measurement, it is necessary to define the structure of the adaptive processor, its inputs, its outputs, and exactly what the adaptation consists of. We consider the general nonlinear structure of Figure 3.1 as a start because of the possible utility of nonlinear processors in the case of nonlinear modulation techniques. This structure includes as special cases all the adaptive processors previously discussed in the literature including those of Widrow [3.1] and, of course, those described in the many papers on adaptive linear transversal and feedback equalizers.

We note from Figure 3.1 that the adaptive processor consists of two basic structures – a linear or nonlinear signal processor containing a finite number of adjustable parameters and the "adaptor" which implements the algorithm for adaptive variation of the signal processor parameters. The input to the signal processor consists of n processes having complex envelopes $w_1(t)$, $w_2(t),\ldots,w_N(t)$ and a single output having complex envelope $u(t)$. In the formulation of the adaptive processor concept, there is always a "desired" signal $d(t)$, either explicitly given or implied, which is the desired output of the signal processor. The complex error signal

$$e(t) = d(t) - u(t) \quad , \tag{3.1}$$

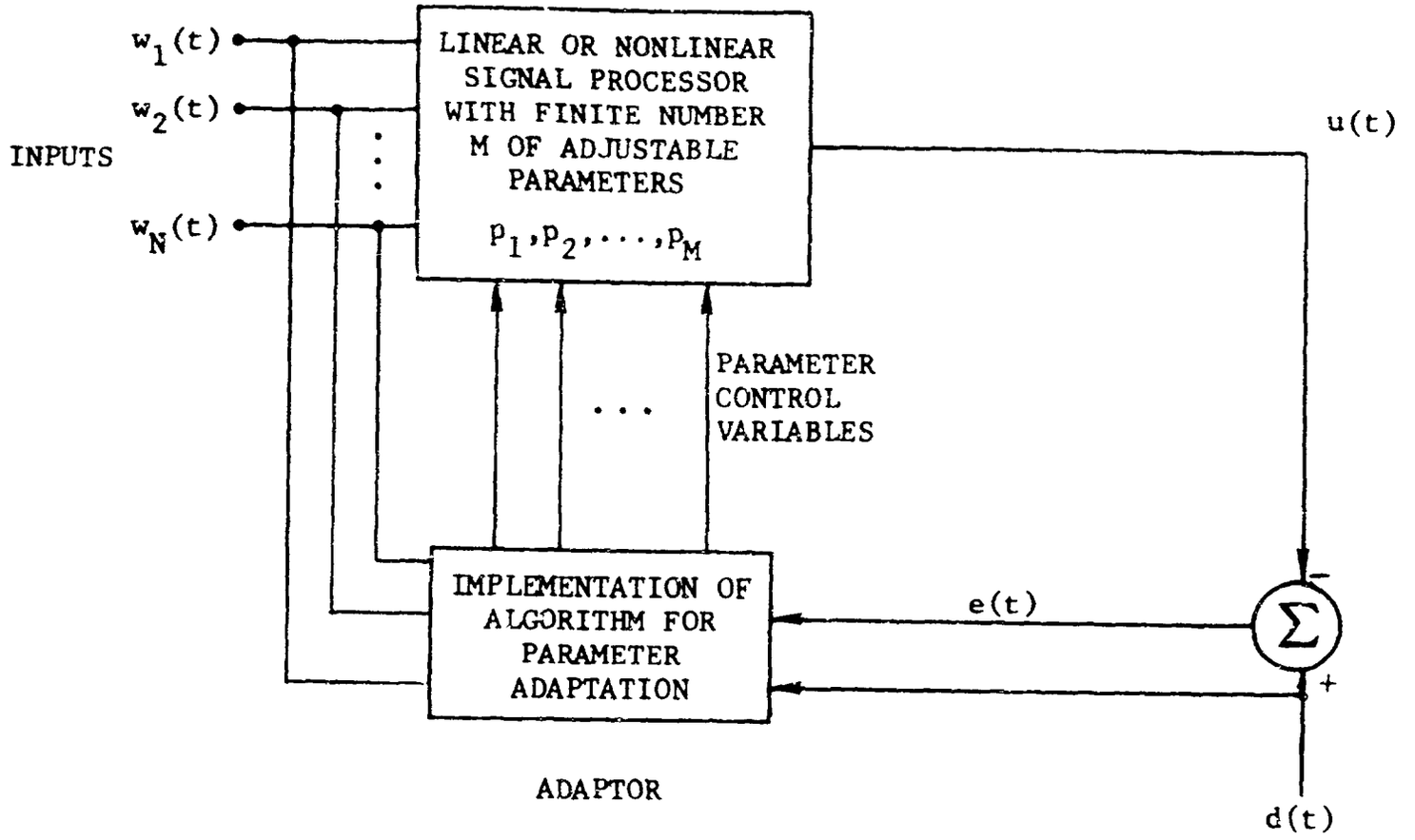

Figure 3.1 General Single-Output Adaptive Processor

the desired signal, and the inputs $\{w_n(t);\ n = 1,2,\ldots,N\}$ are fed to the adaptor which adjusts the M complex parameters $p_1, p_2, \ldots, p_M$ to minimize some positive measure of the complex error signal e.

Consider the minimization of the mean-squared error. We define the output to be a functional of the N inputs and M parameters

$$u(t) = F\left[w_1(t), \ldots, w_N(t);\ p_1, \ldots, p_M\right] \tag{3.2}$$

If a unique minimum of $\overline{|e|^2}$ exists, it may be found as a set of parameter values $\{p_m^0;\ 1,2,\ldots,M\}$ for which $\overline{|e|^2}$ has a stationary point. This is equivalent to saying that the set of partial derivatives of $\overline{|e|^2}$ vanish,*

$$\frac{\partial \overline{|e|^2}}{\partial R_m} = 0$$

$$; \quad m = 1,2,\ldots,M \quad p_m = p_m^0 \tag{3.3}$$

$$\frac{\partial \overline{|e|^2}}{\partial I_m} = 0$$

where we have defined R_m, I_m as the real and imaginary parts of p_m, i.e.,

$$p_m = R_m + j\, I_m \tag{3.4}$$

Noting that for any parameter y

$$\frac{\partial \overline{|e|^2}}{\partial y} = 2\,\mathrm{Re}\left\{\overline{e^* \frac{\partial e}{\partial y}}\right\} \tag{3.5}$$

*With appropriate restrictions on the second derivative to ensure a minimum.

$$\frac{\partial e}{\partial y} = - \frac{\partial F\left[w_1(t),\ldots,w_N(t);\ p_1,\ldots,p_M\right]}{\partial y} \tag{3.6}$$

we see that

$$\frac{\partial \overline{|e|^2}}{\partial y} = -2\,\mathrm{Re}\left\{\overline{e^*(t)\ \frac{\partial F(\cdot)}{\partial y}}\right\}\ ;\ p_m = p_m^0;\ m = 1,2,\ldots,M \tag{3.7}$$

A number of parameter-adjustment algorithms exist which minimize the mean-squared error. For many cases, minimization is usually accomplished by gradient-search techniques. Typically, theoretical presentations start with algorithms called the "method of steepest descent". Changes in each parameter are made in the direction of the gradient or derivative

$$p_m(k+1) = p_m(k) - \Delta\left(\frac{\partial \overline{|e|^2}}{R_m} + j\ \frac{\partial \overline{|e|^2}}{\partial I_m}\right) \tag{3.8}$$

where

$p_m(k)$ = m^{th} parameter before adaptation (at k^{th} time instant)

$p_m(k+1)$ = m^{th} parameter after adaptation (at $k+1^{th}$ time instant)

Δ = scalar constant controlling rate of convergence and stability*

and we have assumed a discrete time model.

In all practical cases, the quantity $\overline{|e|^2}$ cannot be determined apriori because its computation involves unknown statistics. Thus, although much to-do is made about this technique in theoretical analyses, in instrumenting adaptation only an approximation, sometimes a very crude approximation, is used. Surprisingly, only a crude approximation is satisfactory in some cases. The approximations are based upon Eq. (3.7), where the average in (3.7) is approximately determined. The simplest case involves no averaging at all, i.e.,

*The quantity Δ is taken as a positive number here.

$$p_m(k+1) = p_m(k) + 2\Delta \mathrm{Re}\left\{ e^*(k) \frac{\partial F\left[w_1(k),\ldots,w_N(k);\ p_1(k),\ldots,p_M(k)\right]}{\partial R_m} \right\}$$
$$+ j\,2\Delta \mathrm{Re}\left\{ e^*(k) \frac{\partial F\left[w_1(k),\ldots,w_N(k);\ p_1(k),\ldots,p_M(k)\right]}{\partial I_m} \right\} \tag{3.9}$$

The structure of the signal processing box is usually simple enough that the partial derivative is a known function of the inputs and parameter values. Since e(t) is known also, the parameter adjustment may be computed in a conceptually straightforward fashion.

3.1.2 Linear Processor

We now make a further simplification which is assumed in most applications of adaptive processing (in particular, in adaptive equalization) that the signal processor has the linear structure shown in Figure 3.2. This is the case studied by Widrow [3.1]. Specializations of this case yield the transversal and feedback equalizers. For this processor.

$$u(t) = \sum_{n=1}^{N} p_n w_n(t) \tag{3.10}$$

and

$$\frac{\partial F}{\partial R_n} = w_n(t); \quad \frac{\partial F}{\partial I_n} = j\, w_n(t) \tag{3.11}$$

yielding the (complex form) LMS algorithm popularized by Widrow [3.1]

$$p_m(k+1) = p_m(k) + 2\Delta\, e(k)\, w_m^*(k) \tag{3.12}$$

which involves adjusting the value of the m^{th} parameter at k+1 by an amount proportional to the product of the error signal and the conjugate of the m^{th} input at the k^{th} instant. From (3.12) we

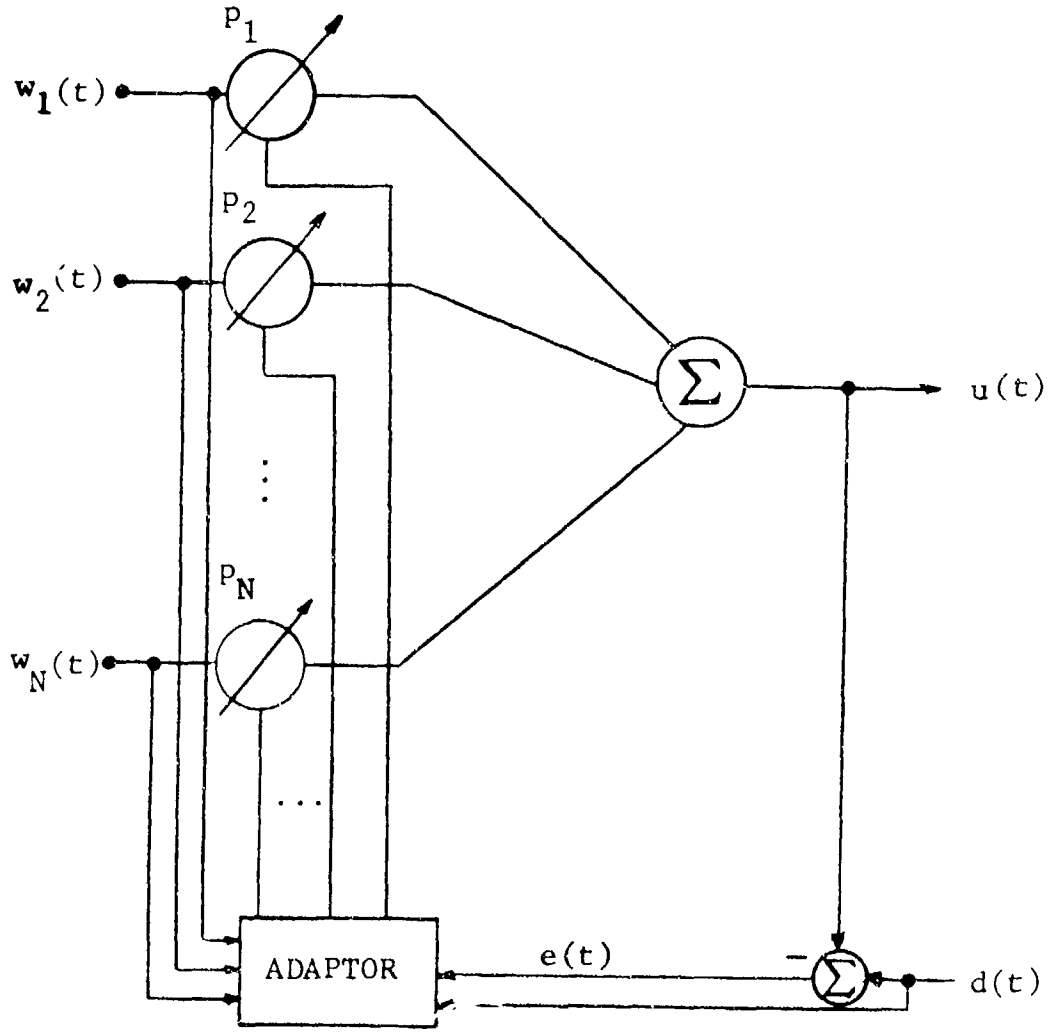

Figure 3.2 Simple Linear Adaptive Processor

arrive at the simple adaptive structure shown in Figure 3.3. Aside from summers and accumulators, the basic operations involved in Figure 3.3, in complex notation, are multiplies and complex-conjugate multiplies (where one input port is conjugated).

The LMS algorithm is a stochastic approximation [3.2] - [3.4] technique. For stationary input processes, Widrow shows that the mean value of the parameter p_m converges to the value p_m^0 yielding minimum mean-squared error (the Weiner solution) when the step size Δ is not too large. The minimum mean-squared error solution for the parameters occurs when (3.3) is satisfied. From (3.7) and (3.11), we see that this is equivalent to

$$\overline{e(k)\, w_m^*(k)} = 0; \quad m = 0,1,\ldots,N \tag{3.13}$$

which, from the definition of e and (3.10) becomes

$$\overline{dw_m^*} = \sum_1^N p_n^0 \, \overline{w_n \, w_m^*}; \quad m = 1,2,\ldots,N \tag{3.14}$$

We define the matrix

$$C = \left\{ \overline{w_n \, w_m^*} \right\} \tag{3.15}$$

as the cross-correlation matrix of the input waveforms, and the column matrices

$$D = \begin{bmatrix} dw_1^* \\ dw_2 \\ \vdots \\ dw_N^* \end{bmatrix} \tag{3.16}$$

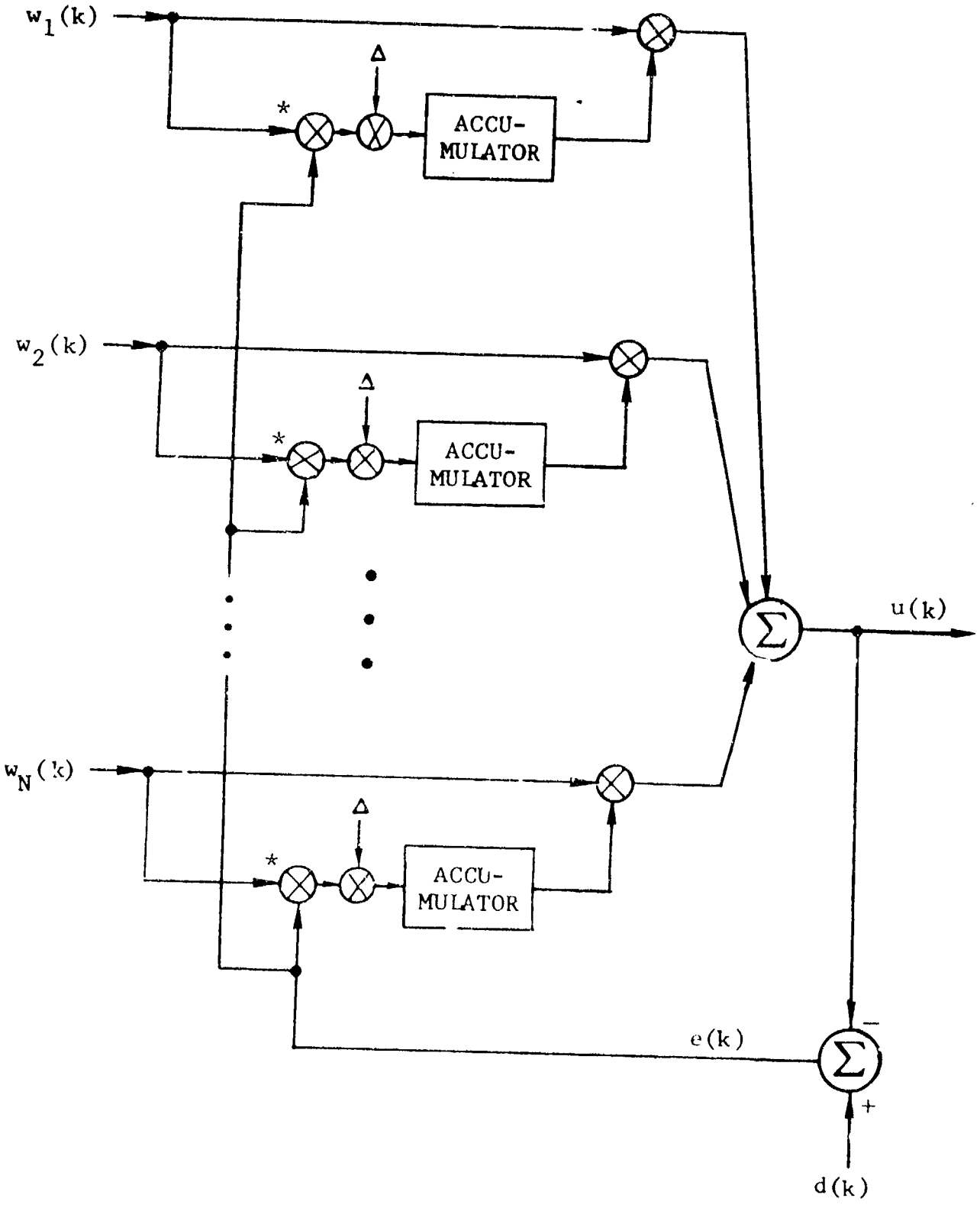

Figure 3.3 Application of LMS Algorithm to Linear Adaptive Processor (Complex Notation)

$$P^0 = \begin{bmatrix} p_1^0 \\ p_2^0 \\ \vdots \\ p_N^0 \end{bmatrix} \tag{3.17}$$

of cross correlation between the desired output and the inputs, D, and of the parameters P^0. Using this notation, we see that (3.14) becomes

$$CP^0 = D \tag{3.18}$$

whose solution is

$$P^0 = C^{-1} D \tag{3.19}$$

The value of the minimum mean-squared error is readily found to be

$$\overline{|e(t)^2|} = \overline{|d(t)|^2} - D_T^* C^{-1} D \tag{3.20}$$

Widrow shows that if the step size is bounded by

$$0 < \Delta < \frac{1}{\lambda_{max}} \tag{3.21}$$

where λ_{max} is the maximum eigenvalue of C, then the LMS algorithm will cause the mean values of the parameter values to converge to the parameters which produce the minimum mean-squared error. This does not mean that the parameters actually converge to the values p_m^0 because the stochastic approximation with nonzero step size Δ will yield parameters which are random variables or rather

random processes as a function of the discrete time. Only the mean of these random parameters are the true values p_m^0.

All adaptive or learning systems experience losses in performance because their system adjustments are based upon statistical averages taken with limited sample sizes. The faster a system adapts, in general, the poorer will be its expected performance.

State-variable methods, which are widely used in modern control theory, have been applied by Widrow [3.1] and Koford and Groner [3.5] to the analysis of stability and time constants (related to rate of convergence) of the LMS algorithm. As shown by Widrow, the parameters undergo transients during adaptation. The average transients consist of sums of exponentials with time constants (in units of the discrete time increment)

$$\tau_n = \frac{1}{2\Delta\lambda_n} \; ; \quad n = 1,2,\ldots,M \tag{3.22}$$

where λ_n is the n^{th} eigenvalue of the correlation matrix C. Thus, as the step size Δ is lowered, the time constants increase. When actual experimental adaptation curves are plotted, they are generally in the form of noisy exponentials because of the noise in the adaptation process. The slower the adaptation, the smaller will be the amplitude of the noise apparent in the learning curve.

When the LMS algorithm is used, the expected level of mean-square error will be greater than that of the Wiener optimum system. A measure of the extent to which the adaptive system is misadjusted as compared to the Wiener system is the ratio of the excess mean-square error to the minimum mean-square error. This dimensionless measure of the loss in performance has been defined as the "misadjustment" M. Thus, it may be shown [3.1] that, for the LMS algorithm

$$M \approx \Delta \sum_{m=1}^{N} \lambda_m = \Delta \text{ Trace } C = \Delta \sum_{n=1}^{N} \overline{|w_n|^2} \tag{3.23}$$

Note that for a given misadjustment M, the time constant τ_n, Eq. (3.22)

$$\tau_n = \frac{1}{2M} \sum_{m=1}^{N} \frac{\lambda_m}{\lambda_n} \tag{3.24}$$

As

$$\frac{\lambda_{max}}{\lambda_{min}} = \xi \tag{3.25}$$

increases, the longest time constant gets increasingly longer. Thus, the ratio of the largest to smallest eigenvalue of the correlation matrix would appear to be an important consideration in the estimation of the adaptation time. However, the recent interesting paper by Ungerboeck [3.6] shows that this ratio may not be as important as previously thought. He has shown that the longer transients in adaptation have smaller amplitude. In addition, he has studied the convergence properties of the mean-squared estimation error and found that convergence requires that the step size satisfy the inequality

$$0 < \Delta < \frac{1}{\sum_{n=1}^{N} \lambda_n} = \frac{1}{\sum_{1}^{N} \overline{w_n^2}} \tag{3.26}$$

which is a more stringent requirement than (3.21). The results of his paper lead us to conclude that the previous adaptive equalizer work on optimum fixed and variable step sizes based upon mean parameter values, such as the work of Richman [3.7], Shonfeld and Schwartz [3.8],[3.9], and Gersho [3.10], to mention a few, may be misleading.

Other algorithms than the LMS algorithm may be used. A particularly simple one from the implementation point of view is called the binary reinforcement algorithm (BRA) [3.11]. This involves replacing the real and imaginary parts of the error signal in the LMS algorithm by 1-bit quantized values. A somewhat longer adaptation time is then necessary to achieve the same performance. In the case of LOS microwave channels, this lengthened adaptation time is hardly a problem since the channel parameter variations are extremely slow compared to the data rate. As a result, the misadjustment error will be small and the rms error will be essentially equal to the minimum value given by (3.20).

3.2 Application to Channel Parameter Measurement

The previous discussion of optimal (minimum mean-squared error) adaptive filtering was sufficiently general to cover many physical situations. In this section we consider its application to channel parameter measurement in LOS PCM-TDM digital transmission links. This discussion is somewhat general. Section 4 presents a detailed examination of a situation of interest, the RQU of a PCM-TDM-FM digital system.

Figure 3.4 shows a receiver channel and four possible pickoff locations for the desired signal d(t). The probing signal is assumed to be the transmitted signal which is taken as the digital output of the system. For ranges of error rates of interest, this assumption is reasonable. By passing the output digital signal through a parameterized model of the channel, one may construct an approximation to the desired signal. Adaptive adjustment of the parameters according to an algorithm for minimizing the difference between the desired signal and the reconstructed signal will lead to an estimate of the channel parameters.

Depending upon the pickoff point for the desired signal, one may obtain parameter estimates ranging from those suitable for the MQU to those suitable for the RQU. Aside from the output of the discriminator, the desired signals in Figure 3.4 are narrowband processes, at either RF or IF. The corresponding reconstruction processor must then produce a narrowband signal at RF or IF, unless the narrowband signals are mixed down to video with quadrature carriers and complex signal processing is used. Note that in all cases a compensating delay must be used to account for the processing delays between the desired signal pickoff and the digital output.

A similar set of possible desired signals may be identified in the case of applying the adaptive channel measurement to the transmitter. In this case the actual data signal is directly available for use as the probing signal. Using the RF signal at the TWT output as the desired signal would be consistent with the definition of the TQU in Section 2.1.

We examine here only the general structure of the adaptive channel parameter measurement procedure for the case of the desired signal identified as the discriminator output. In addition, we consider only the case wherein the chain-differentiator model may be used to parameterize linear filtering operations and power

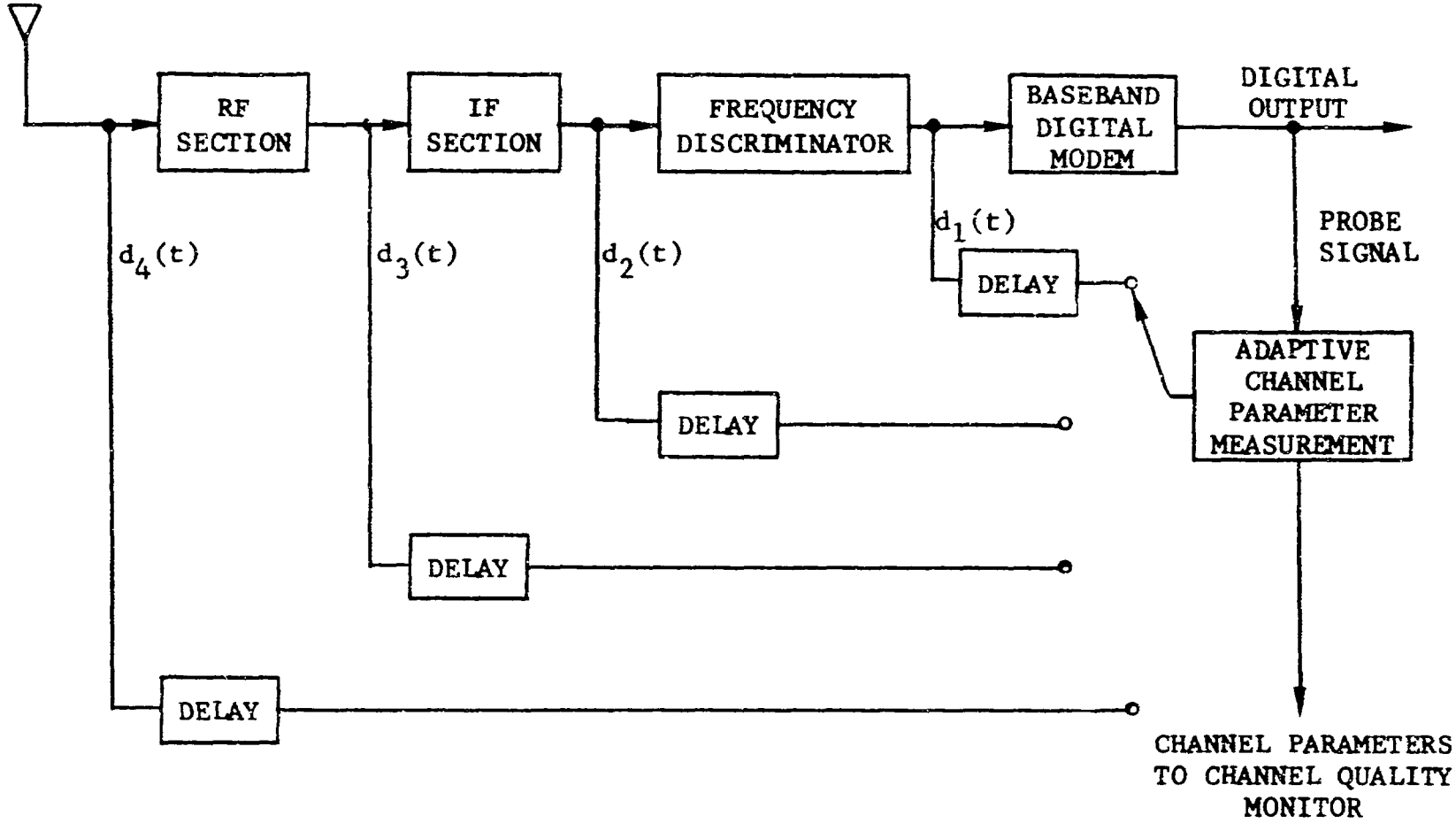

Figure 3.4 Possible Locations in Receiver for Obtaining Desired Signal Adaptive Channel Measurements. Output digits used as probing signal.

series expansions may be used to parameterize the frequency modulator, frequency discriminator, and amplifier nonlinearities. These assumptions are not necessary but they appear to be valid for most cases of interest. More complex cases may be handled with the aid of the tapped delay line model or, if necessary, Volterra functionals, as in [3.12].

From the results in Section 2.2, one may deduce that with the channel distortion assumptions above, the frequency discriminator output may be expressed as a series involving the undistorted frequency modulator input signal plus linear and nonlinear distortion terms. Thus, if x(t) is the modulator input, we can represent the discriminator output as

$$\begin{aligned}\nu(t) = {} & a_0 x(t-\xi_0) + z_1 \dot{x}(t-\xi_0) + a_2 \ddot{x}(t-\xi_0) + \ldots \\ & + b_1 x^2(t-\xi_0) + b_2 x(t-\xi_0)\dot{x}(t-\xi_0) + b_3 \dot{x}^2(t-\xi_0) + b_4 x(t-\xi_0)\ddot{x}(t-\xi_0) \\ & + \ldots + c_1 x^3(t-\xi_0) + c_2 x^2(t-\xi_0)\dot{x}(t-\xi_0) + c_3 x(t-\xi_0)\dot{x}^2(t-\xi_0) \\ & + c_4 \dot{x}^3(t-\xi_0) + c_5 x^2(t-\xi_0)\ddot{x}(t-\xi_0) + \ldots \\ & + n(t) \end{aligned} \tag{3.27}$$

where n(t) is the output noise. The a coefficients represent the linear distortion parameters, the b coefficients the first-order nonlinear parameters, the c coefficients the second-order nonlinear parameters, etc.

Note that $\nu(t)$ is represented as a linear function of the channel parameters. By use of the output digital signal, one may form an estimate of x(t) and thus an estimate of $\nu(t)$, assuming a finite number of parameters. The basic adaptive channel measurement structure then becomes that applicable to the linear model discussed above. The fact that here the functions multiplying the parameters are nonlinear functions of the data signal does not prevent applicability of the results discussed above for the linear adaptive filter, because in the latter case "linearity" referred to dependence upon parameters only.

When the linear distortion in the RF and IF filters and propagation channel are the dominant sources of distortion, (3.27) simplifies to the expression

$$\nu(t) \approx a_0 x(t-\xi_0) + a_1 \dot{x}(t-\xi_0) + a_2 \ddot{x}(t-\xi_0)$$

$$+ b_2 x(t-\xi_0)\dot{x}(t-\xi_0) + n(t) \qquad (3.28)$$

including only significant terms up to second-order linear and first-order nonlinear distortion. Much of the adaptive channel measurement analysis and simulation of Section 4 is based upon this model. However some calculations used the more involved model

$$\nu(t) \approx a_0 x(t-\xi_0) + a_1 \dot{x}(t-\xi_0) + a_2 \ddot{x}(t-\xi_0) + a_3 \dddot{x}(t-\xi_0)$$

$$+ b_2 x(t-\xi_0)\dot{x}(t-\xi_0) + b_3 \dot{x}^2(t-\xi_0) + b_4 x(t-\xi_0)\ddot{x}(t-\xi_0)$$

$$+ c_5 x^2(t-\xi_0)\dot{x}(t-\xi_0) + n(t) \qquad (3.29)$$

which includes a second-order nonlinear term plus additional first-order nonlinear and linear terms of comparable size.

REFERENCES FOR SECTION 3

[3.1] B. Widrow, "Adaptive Filters I: Fundamentals," Stanford Electronics Labs., Stanford, Calif., Report SEL-66-1126, December 1966.

[3.2] H. Robbins and S. Monro, "A Stochastic Approximation Method," Ann. Math. Stat., Vol. 22, March 1951, pp. 400 - 407.

[3.3] J. Kiefer and J. Wolfowitz, "Stochastic Estimation of the Maximum of a Regression Function," Ann. Math. Stat., Vol. 23, March 1952, pp. 462 - 466.

[3.4] A. Drovetsky, "On Stochastic Approximation," Proc. Third Berkeley Symposium on Math. Stat. and Prob. (J. Neyman, ed.), University of California Press, Berkeley, Calif., 1956, pp. 39 - 55.

[3.5] J. S. Koford and G. F. Grover, "The Use of an Adaptive Threshold to Design a Linear Optimal Pattern Classifier," IEEE Trans. on Inform. Theory, Vol. IT-2, January 1966, pp. 42-50.

[3.6] G. Ungerboeck, "A Theory on the Convergence Process in Adaptive Equalizers," Proc. ICC, June 1972, pp. 22-6 - 22-11.

[3.7] S. H. Richman, "Dynamic Equalization in Adaptive Equalization of Digital Communication Channels," (Doctoral Dissertation), Polytechnic Institute of Brooklyn, Brooklyn, N.Y., June 1971.

[3.8] T. J. Schonfeld and M. Schwartz, "A Rapidly Converging First Order Training Algorithm for an Adaptive Equalizer," IEEE Trans. on Inform. Theory, Vol. IT-17, No. 4, July 1971, pp. 431 - 439.

[3.9] T. J. Schonfeld and M. Schwartz, "Rapidly Converging Second-Order Tracking Algorithms for Adaptive Equalization," IEEE Trans. on Inform. Theory, Vol. IT-17, No. 5, September 1971.

[3.10] A. Gersho, "Adaptive Equalization of Highly Dispersive Channels for Data Transmission, BSTJ, January 1969, pp. 55 - 69.

[3.11] A. Gersho, "Adaptive Filtering with Binary Reinforcement," Proc. IEEE Int. Symp. on Information Theory, Asilomar, Calif., February 1972, pp. 94 - 95.

[3.12] P. A. Bello, "Nonlinear Canonic Models of Receivers," IEEE Int. Conf. on Comm. Conv. Record, June 1972, pp. 30-1 - 30-9.

SECTION 4

EVALUATION OF AN ADAPTIVE CHANNEL ESTIMATOR

4.1 Introduction

The parametric approach to channel quality performance monitoring of digital communications systems was introduced in Section 2 as a general tool for performance assessment, degradation trending, and fault location. A particular method of channel parameter measurement, called adaptive channel parameter measurement, was introduced in Section 3 as a means of implementing the parametric approach. In this section we carry out detailed calculations of the performance of an adaptive channel parameter estimator that operates in the receiver at the output of the discriminator of a PCM-TDM-FM LOS digital communications system. To keep the analyses and simulations within the available budget, a simplified mathematical model of the LOS link was used that was capable of including distortions introduced by RF and IF filtering and by the propagation medium, although calculations were carried out only for distortions introduced by the propagation medium. Subsequent investigations should include all the distortion mechanisms discussed in Section 2.

The proposed channel estimation technique uses the system function and parameterization concepts discussed in Section 2. This technique takes advantage of some work [4.1] - [4.10] in the area of calculating distortion in angle-modulated systems. The mathematical basis for the technique can be found in [4.2]; however, similar results can be obtained using many alternate distortion analyses.

In Section 4.2 we present the system to be analyzed. This is an FM LOS system employing a duobinary baseband modem. The proposed adaptive channel estimation techniques for monitoring this system are presented in Section 4.3. In that section we describe the methodology of the technique, the adaptation algorithms used to update the channel parameter estimates, and normalization of the channel parameters. The simulations used to evaluate the adaptive channel estimation techniques are also described.

The results of the simulations indicating the performance of the adaptive channel estimator are presented in Section 4.4. These include convergence time constant, measurement accuracies,

and the effect of errors on the output data stream. In Section 4.5 the error rate of the duobinary FM system is found as a function of the channel parameters to be estimated. The sensitivity of the error rate estimate to parameter measurement error is investigated by examples. Examples illustrating possible multipath-induced degradations are also presented. Implementation considerations of the adaptive channel estimator are discussed in Section 4.6.

4.2 System Description and Constraints

In Section 4.3 an adaptive channel estimator that estimates parameters of interest is presented. The performance of this estimator is considered in Section 4.4. To evaluate the performance of the estimator, it is necessary to specify the form of baseband modulation being employed. Several baseband modulations have been considered [4.11] to transmit digital data over the Defense Communications System (DCS). Currently, duobinary FM is likely to be used for the proposed upgrades discussed in Section 2 and is the system that will be used to evaluate the performance of the adaptive channel estimator being proposed.

Duobinary techniques [4.12] - [4.15] allow a controlled amount of intersymbol interference, which can be compensated for during detection. The advantage of this technique is that the bandwidth is reduced. This bandwidth reduction is at the expense of an effective reduction in noise immunity. However, for LOS links the SNR's (even during most fades) are very high.

Figure 4.1 is a functional block diagram of the duobinary FM system to be considered. For analysis purposes, we assume that a binary data sequence $\{a_n\}$ is used to modulate a train of impulses which are filtered to perform some duobinary pulse shaping prior to transmission. The output of the transmit filter is frequency-modulated and transmitted over a LOS link. At the receiver, the signal is frequency-demodulated and filtered. The receiver filter completes the duobinary pulse shaping and reduces the noise in the detector.

The receive filter output is sampled and sliced to generate a three-level sequence $\{\hat{b}_n\}$. This three-level sequence is used to detect the two-level NRZ sequence by compensating for the controlled intersymbol interference introduced by the duobinary pulse shaping.

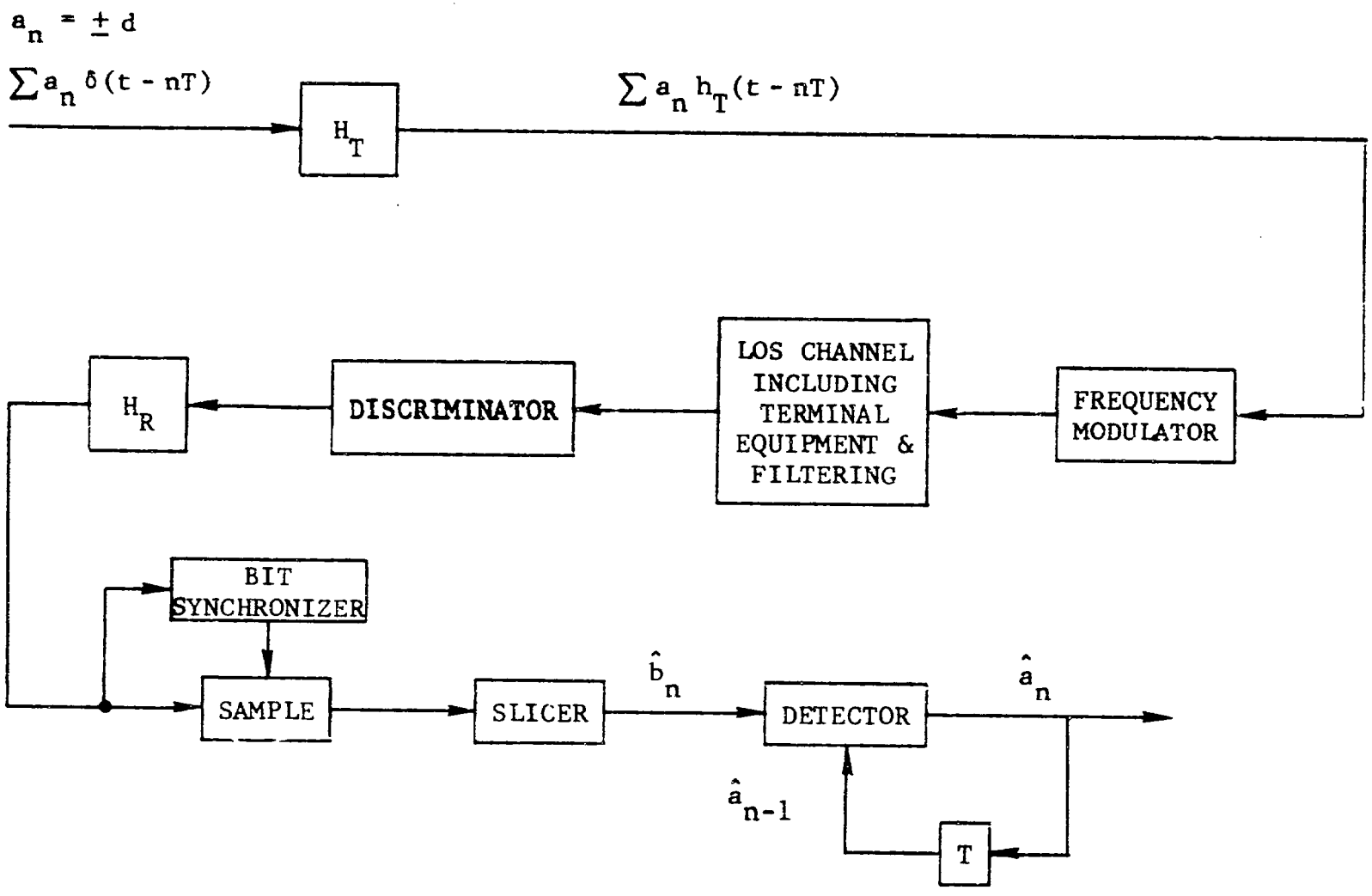

Figure 4.1 Functional Block Diagram of Duobinary FM Modem

For the duobinary technique used over a white Gaussian noise channel, minimum error probability in the transmit and receive filters have transfer functions given by [4.14].

$$H_T(f) = H_R(f) = \begin{cases} [T \cos(\pi f t)]^{\frac{1}{2}} , & |f| \le \frac{1}{2T} \\ 0 , & \text{otherwise} \end{cases} \tag{4.1}$$

Although the above filters cannot be exactly constructed, it is possible to find filters which are reasonable approximations to (4.1). The transmit and receive filters are discussed in greater detail in Appendix F, where the pulse shape information required to evaluate the performance of the adaptive channel estimator is presented.

With the transmit and receive filters having transfer functions given by (4.1), the intersymbol interference (at the correct sampling time and in the absence of noise or channel-induced distortions) comes only from the preceding symbol. That is, the desired three-level sequence is related to the two-level sequence by [4.14]

$$b_k = a_k + a_{k-1} \tag{4.2}$$

where the a_k can assume either $\pm d$ and the b_k can take on the three values $\pm 2d$ and 0. The data $\{a_k\}$ can be decoded from the detected three-level sequence by using the previously decoded data bit and eliminating its effect on b_k by subtraction. In particular, a_k can be detected by using

$$a_k = \begin{cases} +d , & \text{if } b_k = +2d \\ -d , & \text{if } b_k = -2d \\ -a_{k-1} , & \text{if } b_k = 0 \end{cases} \tag{4.3}$$

One drawback to using this system is that if a_{k-1} was in error and $b_k = 0$, then a_k will also be in error, thus indicating that errors have a tendency to propagate. A means for avoiding

this error propagation was introduced by Lender [4.13]. Lender's scheme eliminates error propagation by precoding at the transmitter. Figure 4.2 presents a block diagram of a precoded duobinary system. The precoding operation converts the input sequence $\{a_k\}$ to another sequence $\{y_k\}$ before transmission. The purpose of this conversion is to produce a detected three-level sequence $\{z_k\}$ from which the data sequence can be detected using this rule:

$$a_k = \begin{cases} +d \quad , & \text{if } z_k = \pm 2d \\ \\ -d \quad , & \text{if } z_k = 0 \end{cases} \tag{4.4}$$

Since detection of a_k does not depend upon a_{k-1}, errors do not propagate. For the proposed adaptive channel estimator, either precoded or nonprecoded duobinary systems can be accommodated with some modifications. In Appendix E, we consider the relationship between errors in detecting the three-level sequence and those in detecting the two-level sequence.

It is well-known [4.1] - [4.10] that, for angle modulation, linear distortion in the channel can result in linear and nonlinear distortion at the output of the demodulator. In the following section, we will investigate techniques for adaptively estimating channel parameters that are indicative of the degree of linear and nonlinear distortion. These parameters can be used to assess performance, isolate faults, and perform trend analysis.

4.3 Adaptive Channel Estimator Description

4.3.1 Introduction

In this section we address the problem of estimating parameters used to model the nonlinear channel discussed in Section 4.2. The techniques studied use the detected data sequence to adaptively estimate these channel parameters. This channel monitor will have the potential of measuring both linear and nonlinear distortions. The system analyzed is the one discussed in Section 4.2 that does not use precoding; however, the channel monitoring technique can be extended to precoded systems with only minor modifications. These modifications are also discussed.

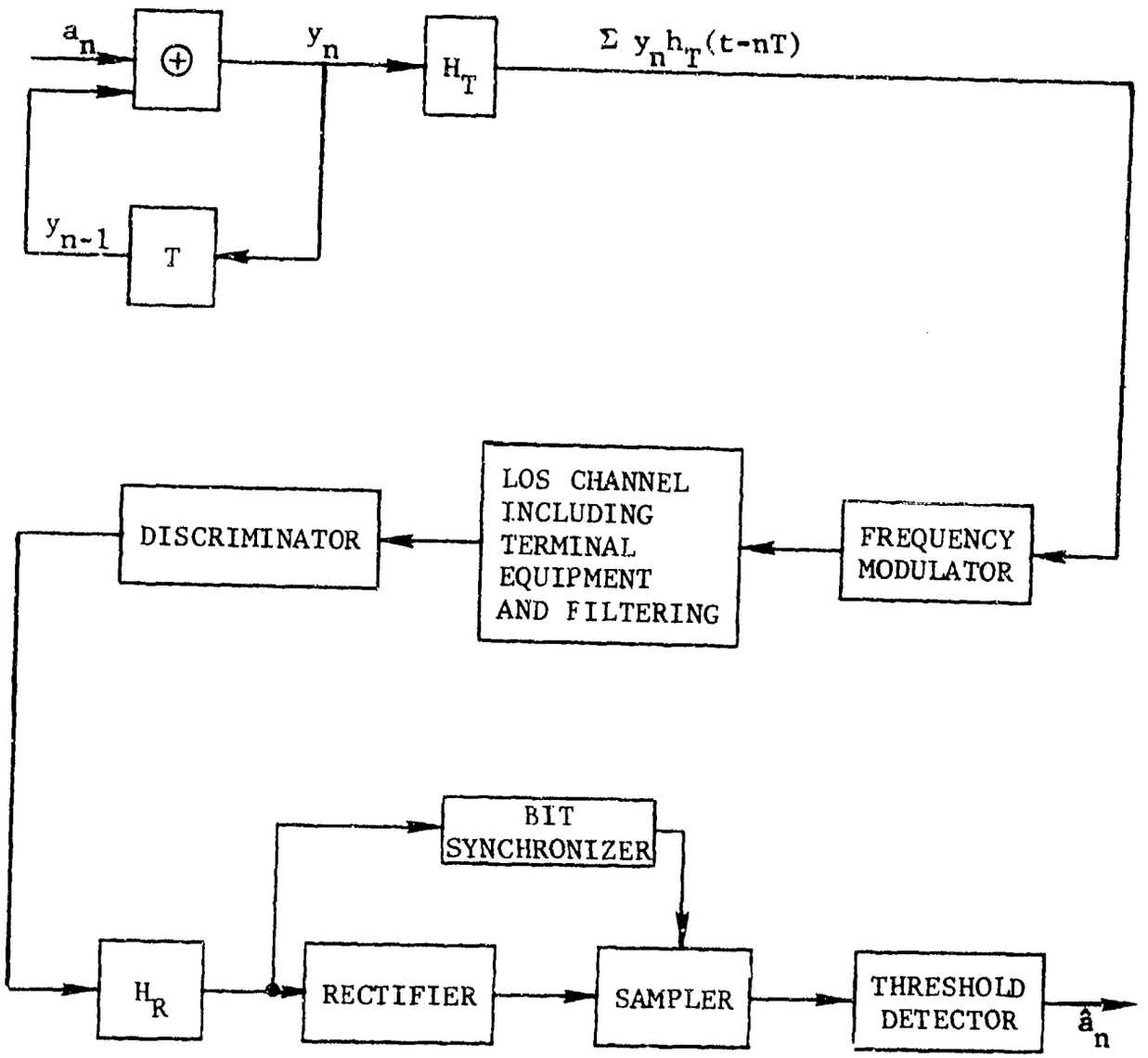

Figure 4.2 Functional Block Diagram of Duobinary System With Precoding

The channel monitor (or nonlinear adaptive channel estimator) is presented in Section 4.3.2. Some adaption algorithms are discussed in Section 4.3.3, while a simulation used to verify the technique, assess performance, and examine tradeoffs is detailed in Section 4.3.4.

4.3.2 Adaptive Channel Estimation

Adaptive techniques have been successfully used in digital data transmission to reduce intersymbol interference effects. Recently [4.16], they have been proposed as a means of estimating linear channels. The adaptive nonlinear channel estimator considered in this section is represented by Figure 4.3.

The estimator uses the detected data and parameters of a channel model to generate an estimate of the received baseband signal. The error in estimating the received baseband signal is used to update the channel model parameters. The channel model considered for detailed analysis is nonlinear with respect to the input signal but is linearly related to N parameters (P_i, $i = 0,\ldots,$ N-1). As the parameters in the channel model converge to their correct values, the error in estimating the received baseband signal will be small.

4.3.2.1 Without Precoding

Figure 4.4 illustrates the use of an adaptive channel estimator for a duobinary FM modem where the duobinary technique [4.17] does not precode the NRZ data sequence. In this figure, the data is filtered prior to transmission in order to perform some shaping of the baseband spectrum. H_T is the transmit shaping filter. The input to the frequency modulator is

$$x(t) = \sum a_n h_T(t - nT) \tag{4.5}$$

where a_n is the two-level ($\pm d$) NRZ data sequence and $h_T(\cdot)$ is the impulse response of the transmit filter.

Using the results from Section 2 of Appendix B for the quadratic channel model, we can represent the output of the frequency discriminator in terms of the input to the frequency modulator. This representation assumes a small amount of frequency selectivity in the baseband and uses the "f-power series"

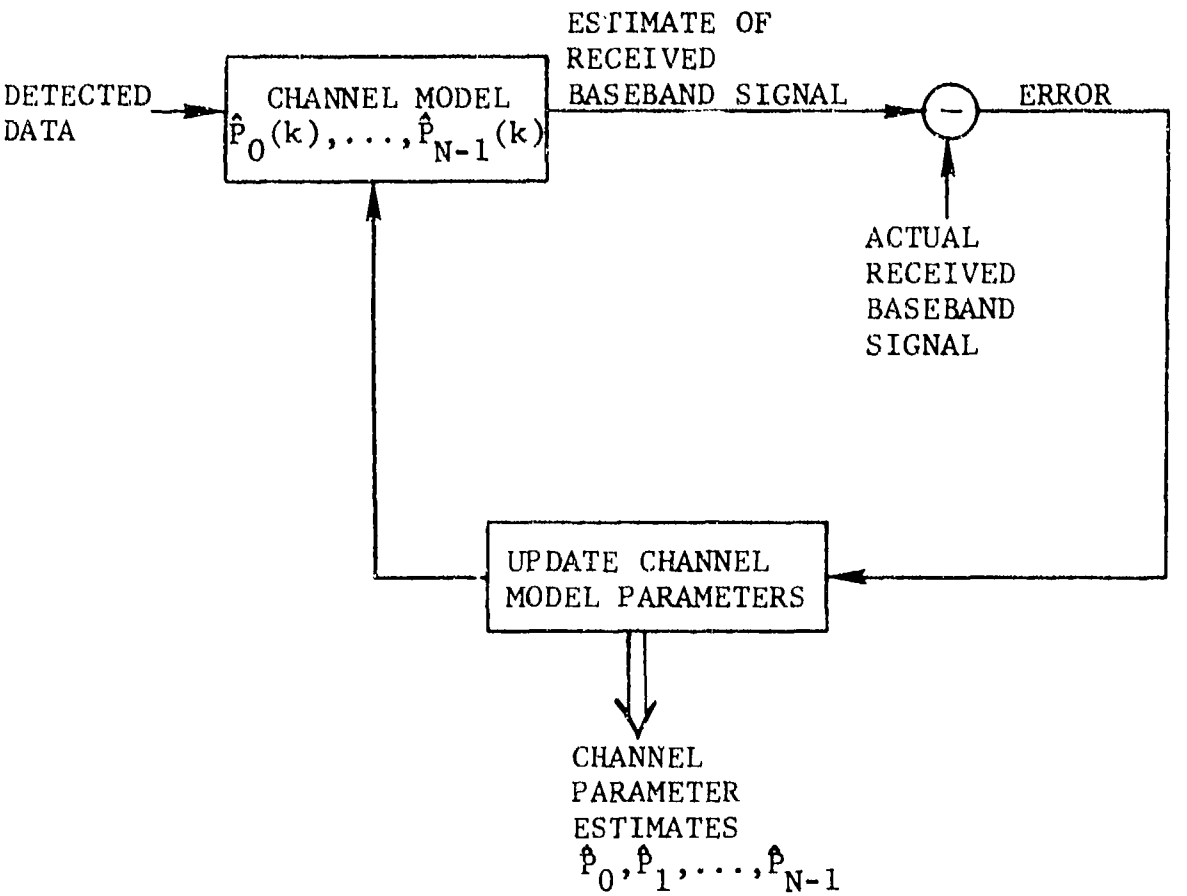

Figure 4.3 Adaptive Nonlinear Channel Estimator

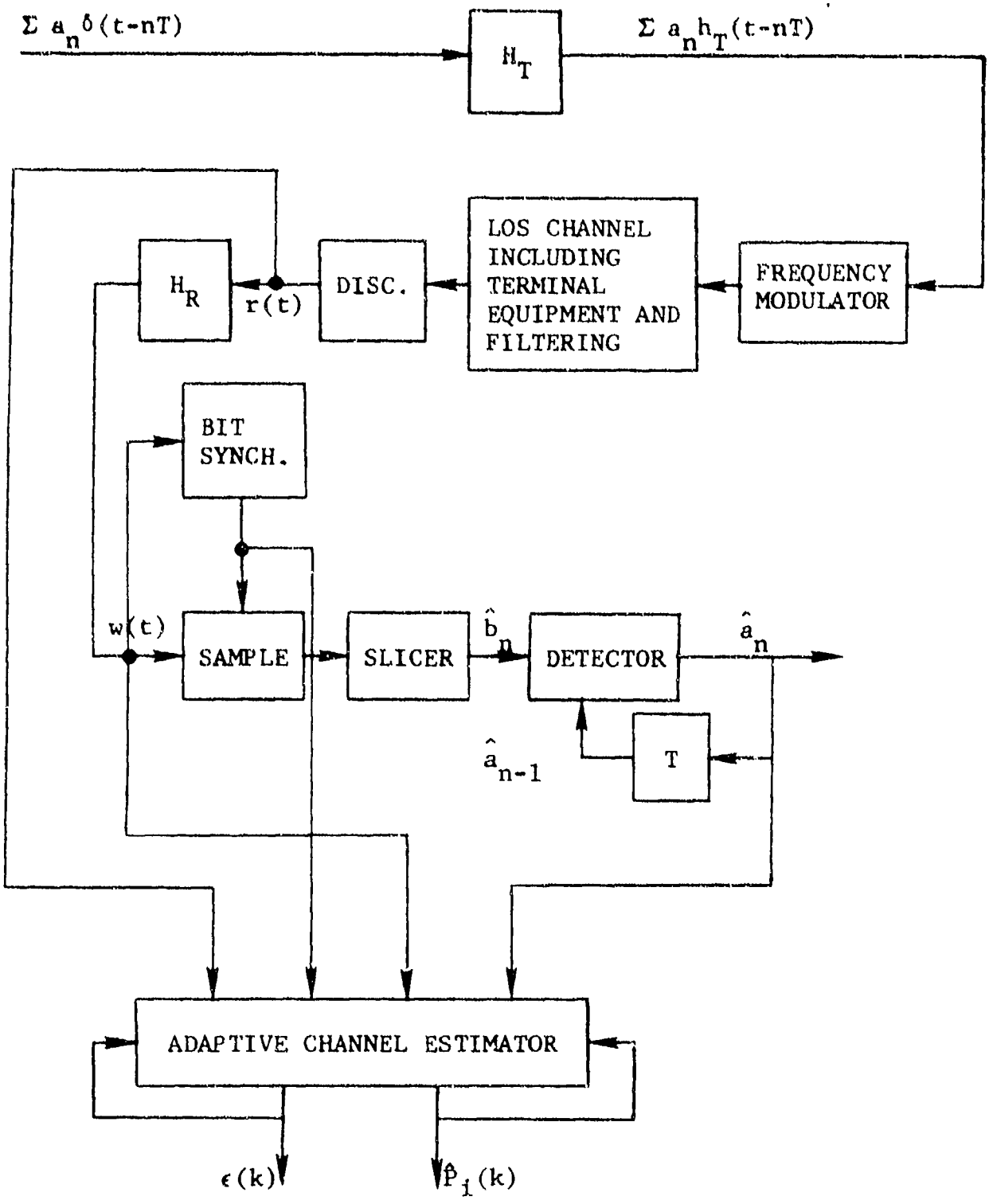

Figure 4.4 Use of Adaptive Channel Estimator for Duo-Binary FM Modem (Without Precoding)

model derived in [4.18]. From Section 4.2 of Appendix B, we can approximate the output of the discriminator r(t) (assuming the quadratic channel model approximation to be valid) by

$$r(t) \approx A\left[x(t-\xi_0) + x_{1D}(t) + x_{2D}(t)\right] \tag{4.6}$$

where A is a constant and x(t) is the input to the frequency modulator. The linear distortion $x_{1D}(t)$ is given by (see Section 4.2 of Appendix B)

$$x_{1D}(t) = \dot{x}(t-\xi_0)\ \mathrm{Re}\left\{\frac{T_1(t)T_0^*(t)}{|T_0(t)|^2}\right\} + \ddot{x}(t-\xi_0)\ \mathrm{Re}\left\{\frac{T_2(t)T_0^*(t)}{|T_0(t)|^2}\right\} \tag{4.7}$$

ξ_0 is the mean path delay of the propagation channel defined in an appropriate sense, and the factors $T_i(t)$ are the coefficients in the f-power series expansion of $T(f,t)$ (the time-varying transfer function). The quadratic distortion $x_{2D}(t)$ is given by

$$x_{2D}(t) = 2x(t-\xi_0)\dot{x}(t-\xi_0)\left[\mathrm{Re}\left\{\frac{T_1(t)T_0^*(t)}{|T_0(t)|^2}\right\}\ \mathrm{Im}\left\{\frac{T_1(t)T_0^*(t)}{|T_0(t)|^2}\right\} - \mathrm{Im}\left\{\frac{T_2(t)T_0^*(t)}{|T_0(t)|^2}\right\}\right] \tag{4.8}$$

In deriving (4.6), only $T_i(t)$, $i = 0,1,2$, were used. This is the quadratic channel model approximation to the f-power series channel model and is valid when the selectivity is small. Even with small selectivity, the degradation can be unacceptably high and, therefore, the quadratic channel model approximation should provide useful channel quality information. It should be noted that more coefficients can be used to obtain a channel model with greater detail. A cubic channel model was considered in Section 4.3 of Appendix B which involved four additional parameters.

From (4.6), for the quadratic channel model of the propagation channel, the parameters characterizing the channel to the discriminator output are given by:

$$P_0 = A$$

$$P_1 = A\ \mathrm{Re}\left\{\frac{T_1(t)T_0^*(t)}{|T_0(t)|^2}\right\}$$

$$P_2 = A\ \mathrm{Re}\left\{\frac{T_2(t)T_0^*(t)}{|T_0(t)|^2}\right\}$$

$$P_3 = A2\left[\mathrm{Re}\left\{\frac{T_1(t)T_0^*(t)}{|T_0(t)|^2}\right\}\ \mathrm{Im}\left\{\frac{T_1(t)T_0^*(t)}{|T_0(t)|^2}\right\} - \mathrm{Im}\left\{\frac{T_2(t)T_0^*(t)}{|T_0(t)|^2}\right\}\right] \qquad (4.9)$$

The adaptive channel parameter estimator utilizes the demodulated data sequence $\{\hat{a}_n\}$ as input to a parameterized channel model of the same general form as (4.6) but with initial guesses for the parameters. The parameters are changed by an appropriate algorithm to make the parameters of the model converge to the actual channel parameters. The demodulated data sequence $\{\hat{a}_n\}$ differs in two important respects from the transmitted data sequence $\{a_n\}$. First, there will generally be errors in the output data so that the sequences will not be identical. Second, the timing of the bits carrying $\{\hat{a}_n\}$ will vary with the time-variant group delay of the channel, while the timing of the transmitted bits will not. This time variation is caused by the bit sync loop as it attempts to track variations in receiver bit timing. The variations in bit timing introduced by the tracking loop must be removed if the output data sequence $\{\hat{a}_n\}$ is used to reconstruct an estimate of the discriminator output r(t).

From (4.6) we can express the estimate of r(t) by

$$\hat{r}(t) = \sum_{q=0}^{3} \hat{P}_q(t)\, S_q(t) \qquad (4.10)$$

where

$$S_0(t) = \hat{x}(t - \xi_0) = \sum_n \hat{a}_n h_T(t - \xi_0 + \tau_b(t) - nT)$$

$$S_1(t) = \dot{\hat{x}}(t - \xi_0) = \sum_n \hat{a}_n \dot{h}_T(t - \xi_0 + \tau_b(t) - nT)$$

$$S_2(t) = \ddot{\hat{x}}(t - \xi_0) = \sum_n \hat{a}_n \ddot{h}_T(t - \xi_0 + \tau_b(t) - nT)$$

$$S_3(t) = \hat{x}(t - \xi_0)\dot{\hat{x}}(t - \xi_0) = \sum_n \sum_m \hat{a}_n \hat{a}_m \dot{h}_T(t - \xi_0 + \tau_b(t) - nT) \cdot h_T(t - \xi_0 + \tau_b(t) - nT) \tag{4.11}$$

where an advance $\tau_b(t)$ has been inserted to counteract the delay of the bit sync loop.

If the cubic channel model as described in Section 4.3 of Appendix B was used, the estimate of r(t) would be given by

$$\hat{r}(t) = \sum_{q=0}^{7} \hat{P}_q(t) S_q(t) \tag{4.12}$$

where

$$S_4(t) = \dddot{\hat{x}}(t - \xi_0) = \sum_n \hat{a}_n \dddot{h}_T(t - \xi_0 + \tau_b(t) - nT)$$

$$S_5(t) = \hat{x}^2(t - \xi_0)\dot{\hat{x}}(t - \xi_0)$$

$$S_6(t) = \dot{\hat{x}}^2(t - \xi_0)$$

$$S_7(t) = x(t - \xi_0)\ddot{\hat{x}}(t - \xi_0) \tag{4.13}$$

Using (4.10) or (4.12), the discriminator output can be estimated using a quadratic or cubic channel model. In Section 4.3.3, algorithms for adaptively updating estimates of $P_q(t)$ will be introduced. These algorithms use the error signal generated by comparing $\hat{r}(t)$ with the actual discriminator output $r(t)$.

Figure 4.5 presents three adaptive channel estimator configurations obtained by using the quadratic channel model. The three configurations use the parametric approach to monitor a duobinary FM system and differ only in the manner in which timing information is extracted. In these estimators, the detected two-level NRZ sequence $\hat{a}_n$ and the transmit filter impulse response are required to form estimates of $x(t)$, $\dot{x}(t)$, and $\ddot{x}(t)$, which are used to estimate the discriminator output signal $r(t)$. The error in estimating $r(t)$ is needed to update the parameter estimates of the channel model.

In Figure 4.5(a), an adaptive channel estimator with a fixed timing reference is presented. The purpose of the fixed timing reference is to allow comparison of bit sync loop timing with fading multipath with sampling times for a channel in the absence of multipath. The fixed timing reference estimator is the easiest to simulate since knowledge concerning the performance of the bit synchronizer is not required. Furthermore, due to its relatively fast convergence [compared to adaptive delay elimination, Figure 4.5(c)], the simulation of the fixed timing reference can be used to assess the effect of degradations (noise, data errors, etc.) and to examine the system tradeoffs, thereby making efficient use of computer resources.

Figure 4.5(b) shows the adaptive channel estimator in which the bit synchronizer is used to sample the discriminator output. The estimates of channel parameters P_0 and P_1 are used to directly eliminate the group delay. For this configuration, the time-varying delay can be estimated by $-\hat{P}_1(k)/\hat{P}_0(k)$. This technique may be simpler to implement than the adaptive delay elimination technique discussed below, since no new parameters have to be estimated.

In Figure 4.5(c), an adaptive technique for estimating this time-varying delay is presented. $\hat{\tau}_b$ is the estimate of the time-varying delay. After convergence, the channel parameters estimated should be the same as those of the channel estimator with a fixed timing reference. The performance of the adaptive channel estimator with adaptive delay elimination has been evaluated using simulations. The results of these simulations are presented in Section 4.4.4.

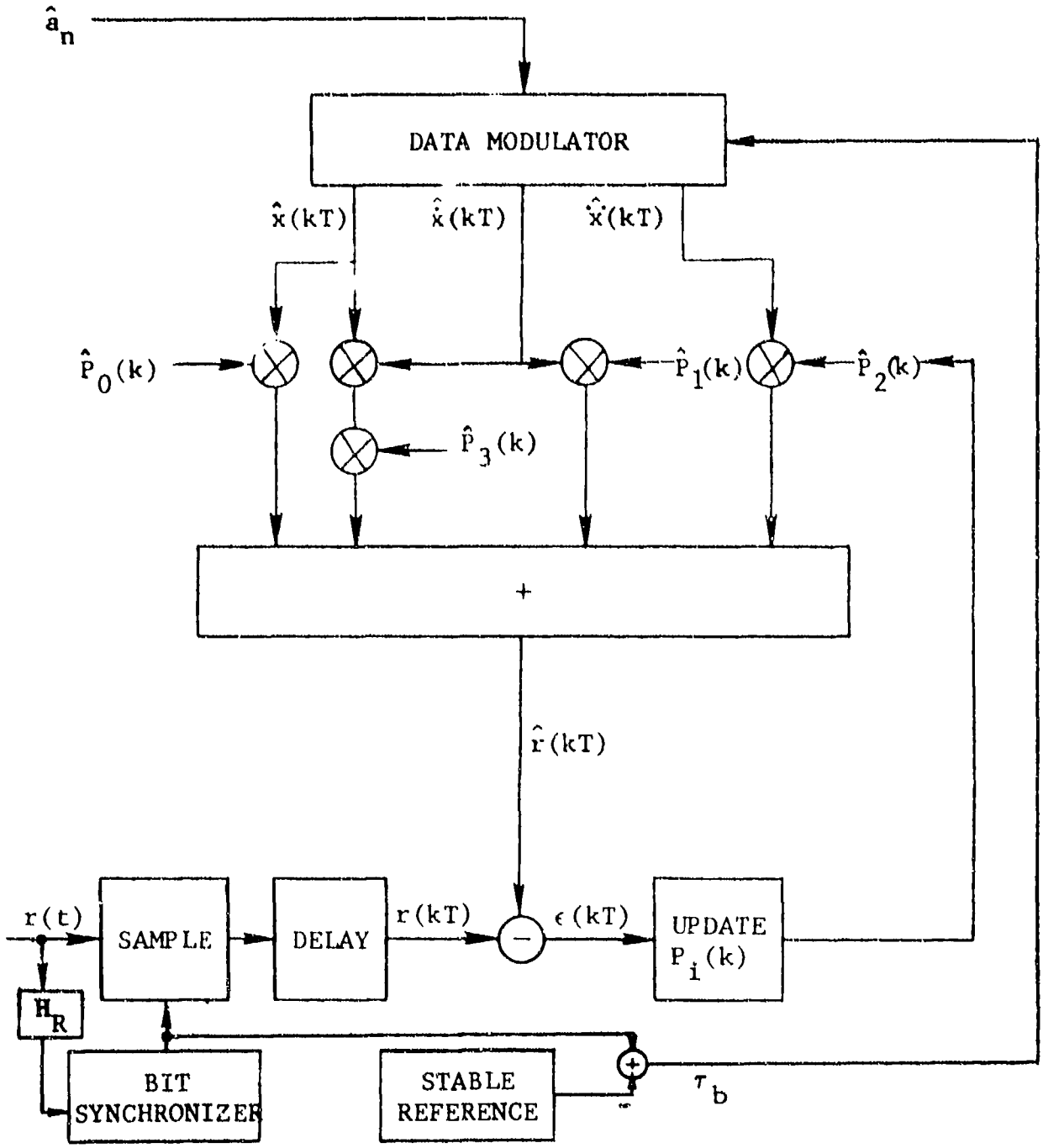

Figure 4.5(a) Adaptive Channel Estimator With Fixed Timing Reference

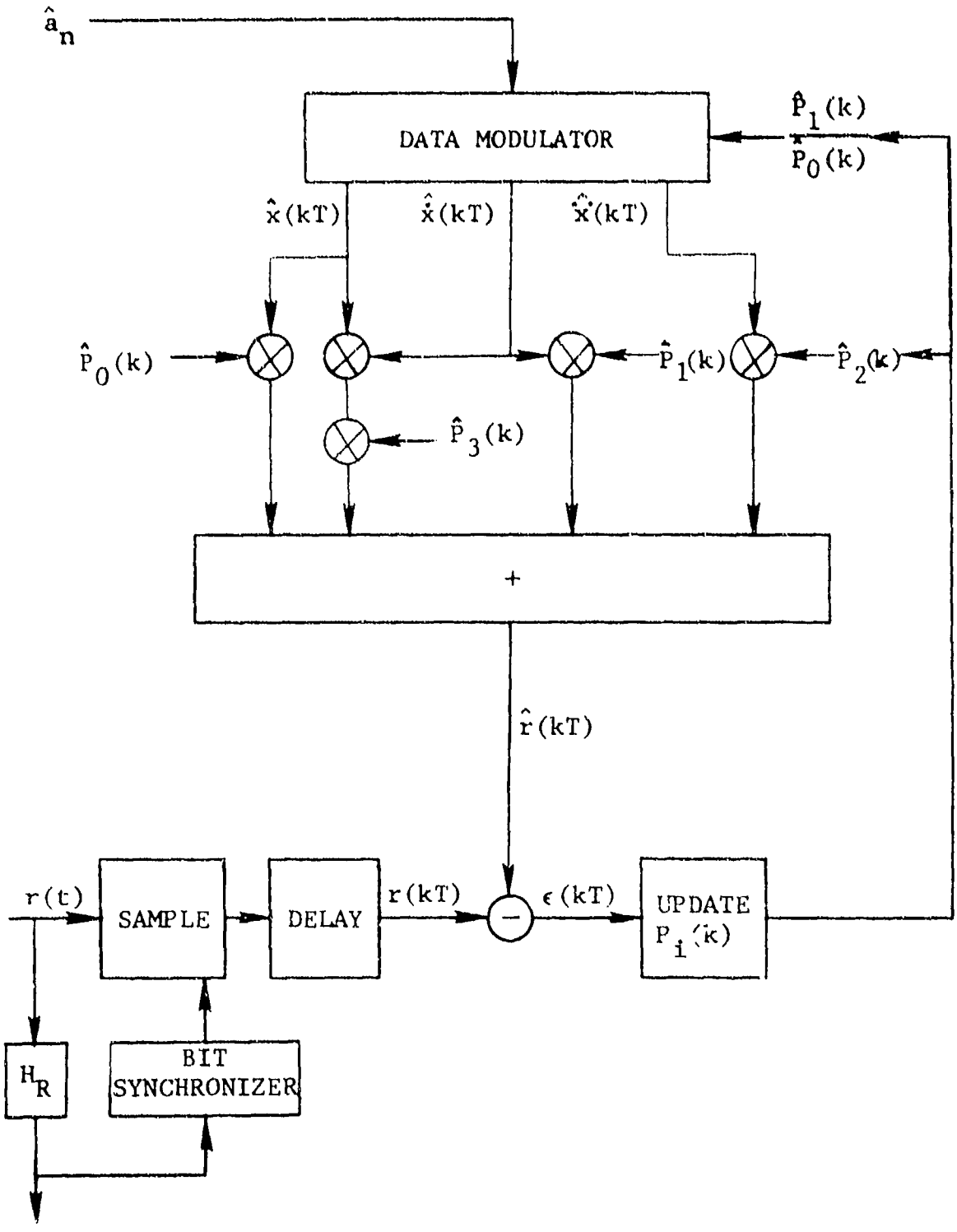

Figure 4.5(b) Adaptive Channel Estimator With Direct Group Delay Elimination

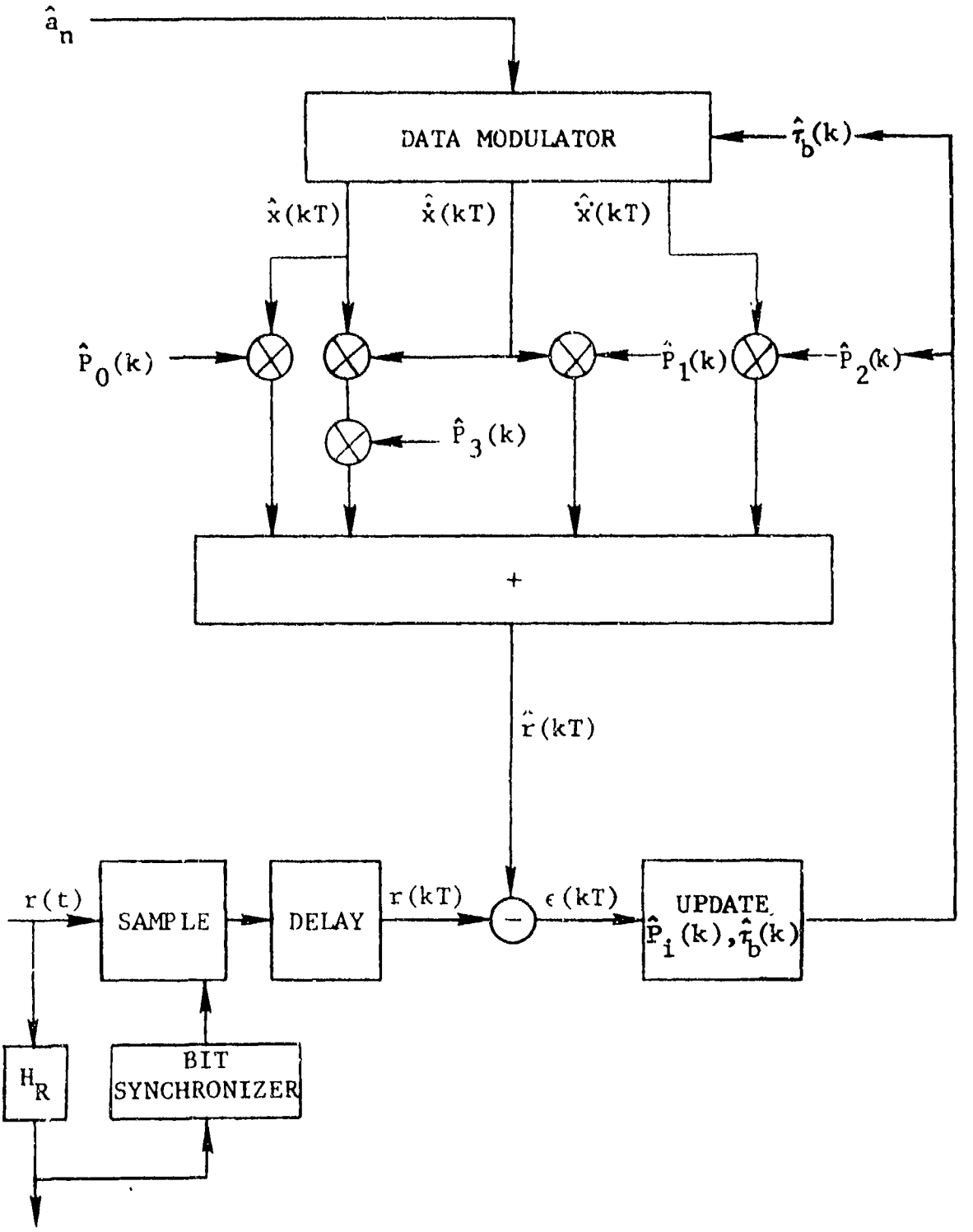

Figure 4.5(c) Adaptive Channel Estimator With Adaptive Group Delay Elimination

Returning to Figure 4.4, we note that an adaptive channel estimator can be developed to generate an estimate of w(t), the output of the receive filter H_R. One advantage to generating an estimate of w(t), as opposed to r(t), is that H_R is used to reduce the noise power. For this estimator we can define

$$y_0(t) = \sum_n \hat{a}_n \int_{-\infty}^{\infty} h_R(\nu)\, h_T(t - \xi_0 + \tau_b(t) - nT - \nu)\, d\nu$$

$$y_1(t) = \sum_n \hat{a}_n \int_{-\infty}^{\infty} h_R(\nu)\, \dot{h}_T(t - \xi_0 + \tau_b(t) - nT - \nu)\, d\nu$$

$$y_2(t) = \sum_n \hat{a}_n \int_{-\infty}^{\infty} h_R(\nu)\, \ddot{h}_T(t - \xi_0 + \tau_b(t) - nT - \nu)\, d\nu$$

$$y_3(t) = \sum_n \sum_m \hat{a}_n \hat{a}_m \int_{-\infty}^{\infty} h_R(\nu) h_T(t - \xi_0 + \tau_b(t) - nT - \nu)\, \dot{h}_T(t - \xi_0 - mT - \nu)\, d\nu \qquad (4.14)$$

Thus, the $Y_i(t)$ is output of H_R when $S_i(t)$ is input.

With $Y_i(t)$ varying much faster than the channel, the output of the receive filter can be estimated by

$$\hat{w}(t) = \sum_{q=0}^{3} \hat{p}_q(t)\, Y_q(t) \qquad (4.15)$$

A cubic channel model approximation for w(t) can also be found by filtering $S_q(t)$, $q = 0, \ldots, 7$. Thus, the receive filter output can be estimated by using a quadratic or cubic channel model and the channel parameters $P_i(t)$ can be adaptively updated using the algorithms discussed in Section 4.3.3. Channel estimator configurations analogous to Figure 4.5 can be used to estimate the output of the receive filter.

4.3.2.2 With Precoding

The duobinary FM system considered does not employ precoding; however, some duobinary systems use the precoding operation which allows the use of simple detection schemes and prevents error propagation. Figure 4.6 presents one possible precoded duobinary system. For this system, the detected two-level sequence is obtained from the three-level sequence by

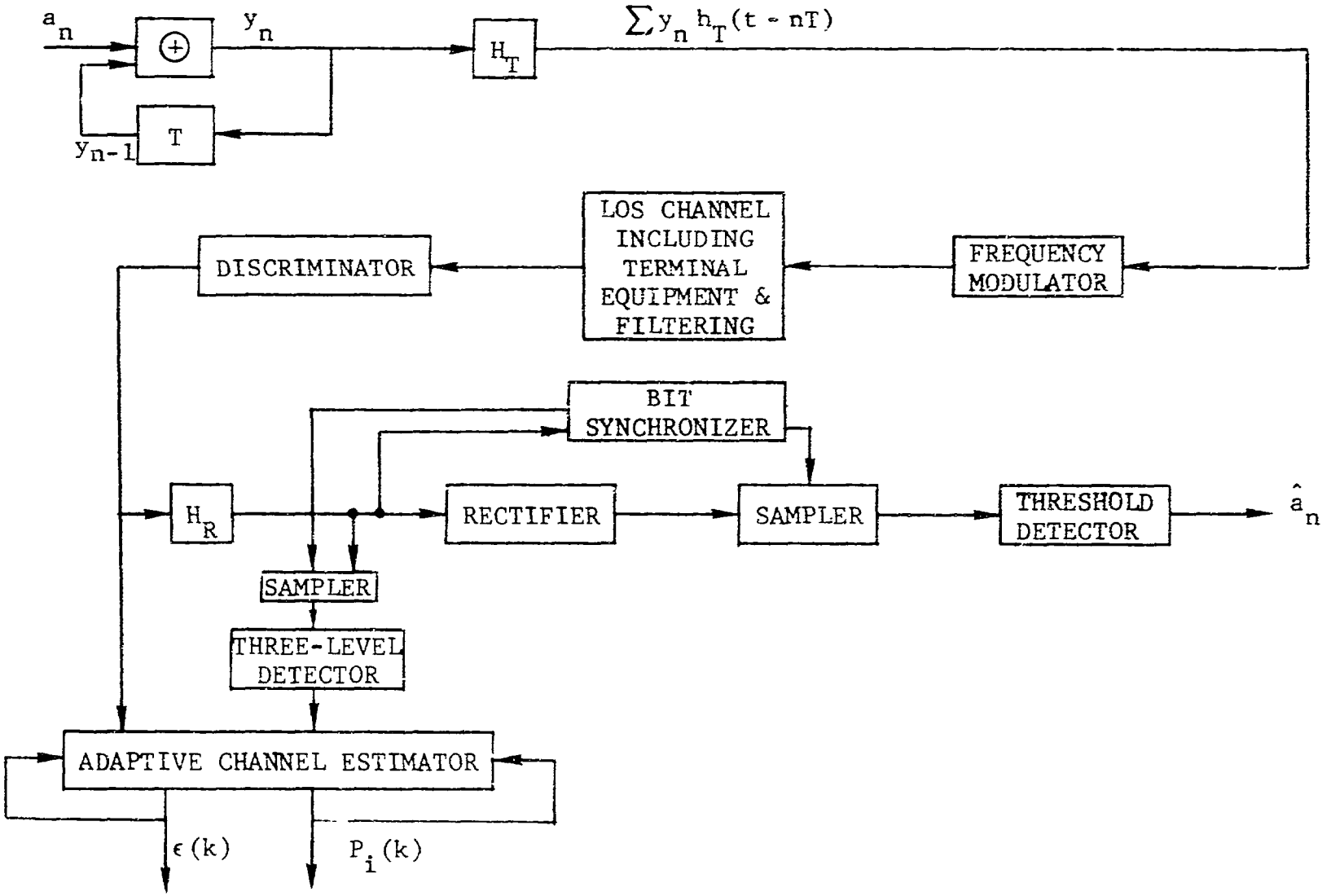

Figure 4.6 Use of Adaptive Channel Estimator for Duobinary System (With Precoding)

$$\hat{a}_n = \begin{cases} d \ , & \text{if } \hat{b}_n = \pm 2d \\ \\ 0 \ , & \text{if } \hat{b}_n = 0 \end{cases} \qquad (4.16)$$

Since the detection of $\hat{a}_n$ involves only $\hat{b}_n$ (note that in Figure 4.1 $\hat{a}_n$ depends upon $\hat{b}_n$ and $\hat{a}_{n-1}$), the detection is simpler. In fact, there may not be any need to detect b_n; instead, the output of the receive filter can be rectified and quantized to two levels. If b_n is not estimated in the detector, then either b_n must be estimated in the channel estimator or $\hat{a}_n$ should be used as input to the channel estimator. Due to the precoding operation, the effect of an error in detecting a_n will result in vastly different duobinary sequences $\{b_n\}$ and, thus, for precoded duobinary systems it is recommended that the adaptive channel estimator use the baseband signal to first estimate b_n and then proceed in a manner analogous to Figure 4.5.

4.3.3 Adaptation Algorithms

4.3.3.1 Introduction

For the adaptive channel estimator proposed in Section 4.3.2, the channel parameter estimates are updated from the previous estimate and the error signal. In this section we will discuss adaptation algorithms that were used in simulations to examine the feasibility of the proposed technique as well as to assess its performance. In Section 4.3.3.2, we will present two adaptation algorithms frequently employed in data transmission. The algorithms are called the Least Mean Squared (LMS) and the Binary Reinforcement (BR) algorithm. In Section 4.3.3.3, a technique with the potential for increasing the convergence rate of the adaptive channel estimator will be presented.

4.3.3.2 LMS and BR Adaptation Algorithms

The LMS adaptation algorithm is widely used [4.19] - [4.22] in theoretical analysis to examine performance of proposed equalizer techniques. This algorithm (which is discussed in Section 3) updates the channel parameter estimates by an amount proportional to the error in estimating the received baseband signal. In particular, for the LMS algorithm the channel parameters are updated by

$$\hat{P}_q(k+1) = \hat{P}_q(k) + 2\Delta\epsilon(kT)G_q(kT) \tag{4.17}$$

where $\epsilon(kT)$ is the error in estimating the received baseband signal, $G_q(\cdot)$ equals $S_q(\cdot)$ if the discriminator output is estimated or $Y_q(\cdot)$ if the receive filter output is estimated, and Δ is a step size parameter that affects the estimator convergence rate and its sensitivity to noise. With $d(kT)$ the desired baseband signal (in our case, the discriminator or receive filter output) and $\hat{d}(kT)$ its estimate as formed by the channel estimator, then $\epsilon(kT)$ is defined by

$$\epsilon(kT) = d(kT) - \hat{d}(kT) \tag{4.18}$$

In order to insure convergence of the estimator, Ungerboeck [4.22] recommended that Δ be selected according to the rule

$$\Delta \leq \left[\sum_{i=0}^{N} \sigma^2_{G_i(t)}\right]^{-1} \tag{4.19}$$

where $\sigma^2_{G_i(t)}$ is the variance of $S_i(t)$ or $Y_i(t)$ depending upon whether the discriminator or shaping filter outputs are used. Appendix F contains expressions for the variances of $S_i(t)$ and $Y_i(t)$ for the quadratic and cubic channel models, where a particular statistical description of the data was assumed.

Ungerboeck's recommendation given in [4.22] is for a linear equalizer. Due to the nature of our estimator, one might expect more stringent requirements upon Δ than those presented in (4.19). In practice, Δ is usually much less than the sum of the variances in order to reduce the tap gain fluctuations. The effects of Δ upon performance of the adaptive channel estimator have been determined by examples obtained via simulations. For the simulation examples presented in Section 4.4, a normalized step size δ is defined by

$$\delta = \frac{\Delta}{N+1} \sum_{i=0}^{N} \sigma^2_{G_i(t)} \tag{4.20}$$

The BR algorithm [4.23] updates the channel parameter estimates by using only the sign of the estimation error. For the BR adaptation algorithm, the channel parameters are updated by

$$\hat{P}_q(k+1) = \hat{P}_q(k) + \Delta_B \ \mathrm{sgn}[\epsilon(kT)]\ G_q(kT) \tag{4.21}$$

where

$$\mathrm{sgn}(x) = \begin{cases} 1 \ , & \text{if } x \geq 0 \\ -1 \ , & \text{if } x < 0 \end{cases} \tag{4.22}$$

and where Δ_B is the BR algorithm step size. A normalized BR step size can be defined by

$$\delta_B = \frac{1}{N+1} \ \frac{\Delta_B}{\sigma_\epsilon} \ \sum_{i=0}^{N} \sigma_{S_i}^2 \tag{4.23}$$

where σ_ϵ is the error standard deviation. For the examples presented in Section 4.4.2.1, the normalized step size was held constant and σ_ϵ periodically estimated. This resulted in the actual step size Δ_B being time-varying. The exact manner in which the changes in Δ_B were made are described in Section 4.4.2.1. One advantage of the BR (as opposed to the LMS) algorithm is that only the sign of the error is required; thus, updating the channel parameter estimates may be less costly to implement.

The above discussion on the adaptation algorithms has omitted several subtle points, one of which is that the channel parameters [and, hence, $S_i(t)$ and $Y_i(t)$] have different units; thus expressions like (4.20) and (4.23) must be used carefully. In Section 4.3.4 we will discuss the simulation and how the channel parameters and signals were normalized such that the discussion in this section is applicable. However, first a technique for increasing the convergence rate of the estimator will be introduced.

4.3.3.3 Variance Equalization

Since the variance of the taps [$S_i(kT)$ or $Y_i(t)$] are not all equal, errors in estimating the channel parameters result in unequal error statistics in estimating the received baseband signal. This can result in some channel parameter estimates converging much slower than others. As a means of increasing the convergence rate, an adaptation procedure, called variance equalization, was examined. The main feature of this procedure is to adaptively estimate pseudo-channel parameters, where these pseudo-channel parameters are related to the actual channel parameters by

$$\tilde{P}_q = \frac{P_q}{A_q} \tag{4.24}$$

where the A_q's are chosen such that $A_q G_q(kT)$ have equal variance for all q. Figure 4.7 presents nonlinear channel estimators for (for the quadratic channel model and estimating the discriminator output) with and without variance equalization. In this figure $\hat{P}_q(k)$ and $\tilde{P}_q(k)$ are the k^{th} estimates of P_q and $\tilde{P}_q(k)$, respectively.

Variance equalization can be employed with any adaptation algorithm. As an example, for the LMS algorithm (and variance equalization), the pseudo-channel parameters are updated according to the adaptation rule

$$\hat{\tilde{P}}_q(k+1) = \tilde{P}_q(k) + 2\Delta\epsilon(k)\, G_q(kT)\, A_q \tag{4.25}$$

In Section 4.4.2, simulation results illustrating convergence rate advantages obtained using variance equalization will be presented.

4.3.4 Channel Parameter Normalization

In order to relate the adaptation step size to the sum of the variances of the signal at each tap [see Eqs. (4.20) and (4.23)] and to make use of the variance equalization technique presented in the previous section, it is necessary to normalize the channel parameters. The purposes of this normalization are twofold: first, to choose a convenient time scale to express the pulse shape information; second, to express the received baseband signal in such a manner that all the channel parameters have the same units.

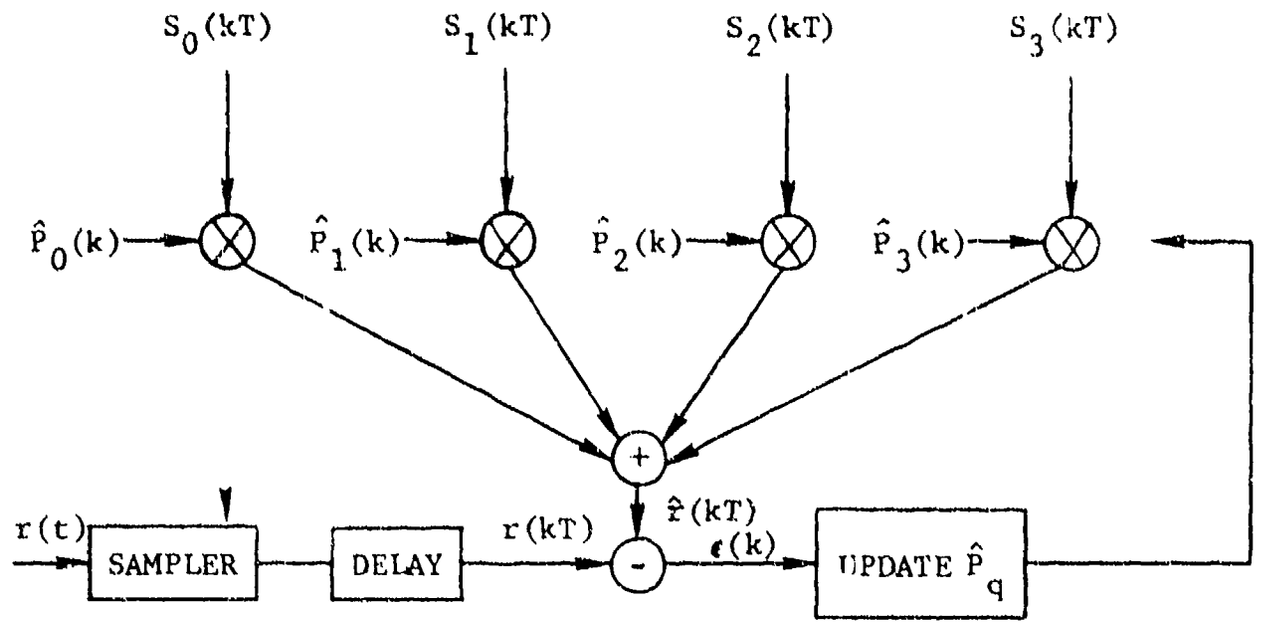

a) Without Variance Equalization

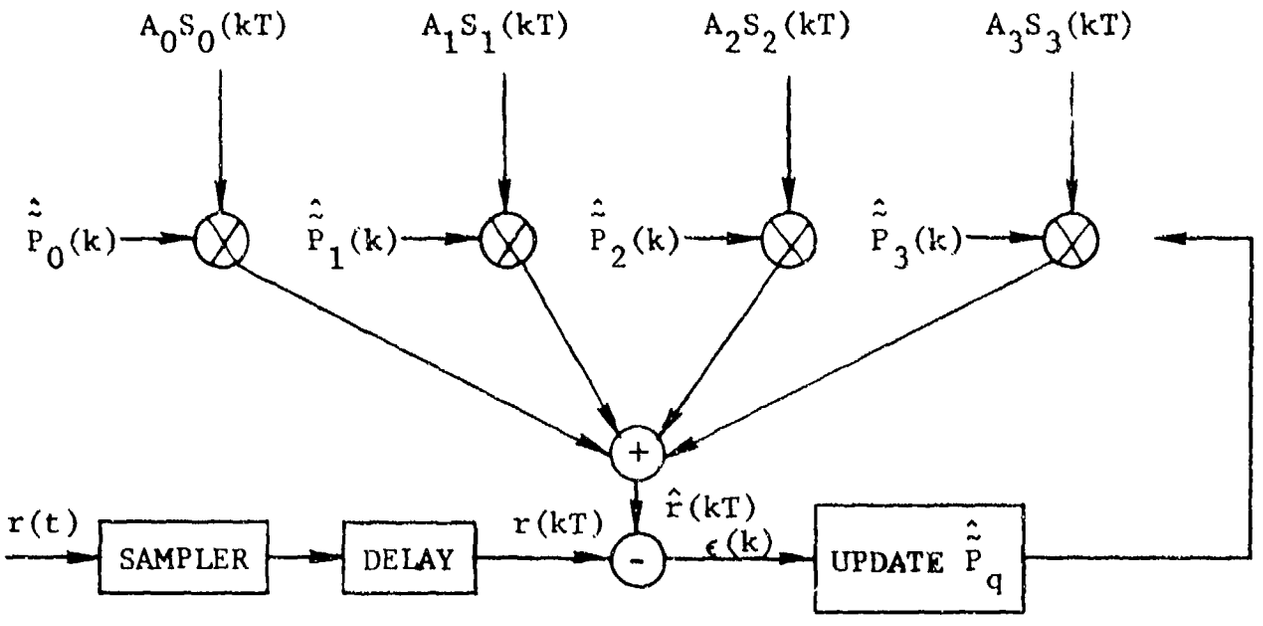

b) With Variance Equalization

Figure 4.7 Adaptive Nonlinear Channel Estimators

For an impulse response that is near its peak value for several pulse intervals T (where 1/T is the data rate), it is perhaps more meaningful to use T as a unit of time other than the "second". As an example, for a 12.6 Mb/s data rate and the two-path model considered in Appendix B, the 2-ns delay difference between the paths would be 0.0252 T.

In order to form the sum of variances as required by Eqs. (4.19), (4.20), and (4.23), all the $G_i(t)$ must be expressed in the same units. From Eq. (4.12), the discriminator output estimate can be expressed by

$$\hat{r}(t) = \sum_{q=0}^{N} \left(\frac{\hat{P}_q(t)}{T^{n_q}} \right) \left[T^{n_q} S_q(t) \right] \tag{4.26}$$

where n_q is the order of T in $\hat{P}_q(t)$. Therefore, $\hat{P}_q(t)/T^{n_q}$ is a dimensionless quantity and $T^{n_q}S_q(t)$ will have the same units for all q. For the computer simulations, these dimensionless channel parameters were estimated. Similar normalizations can be performed when the output of the receive shaping filter is estimated.

4.3.5 Simulation of Adaptive Channel Estimator

4.3.5.1 Introduction

This section describes the simulations used to verify the feasibility and assess the performance of the proposed adaptive channel estimator. Two simulations were written: the first estimates the output of the discriminator, while the second estimates the output of the receive filter. The results of these simulations are presented in Section 4.4.

4.3.5.2 Estimation of Discriminator Output

In this section we will describe the adaptive channel estimator simulation that estimates the baseband signal at the output of the discriminator. Figure 4.8 shows the flow diagram for this channel estimator simulation. The simulation can be subdivided into three main functions. They are: (1) generation of the discriminator output; (2) generation of the estimate of the discriminator output; and (3) updating the channel parameter estimates.

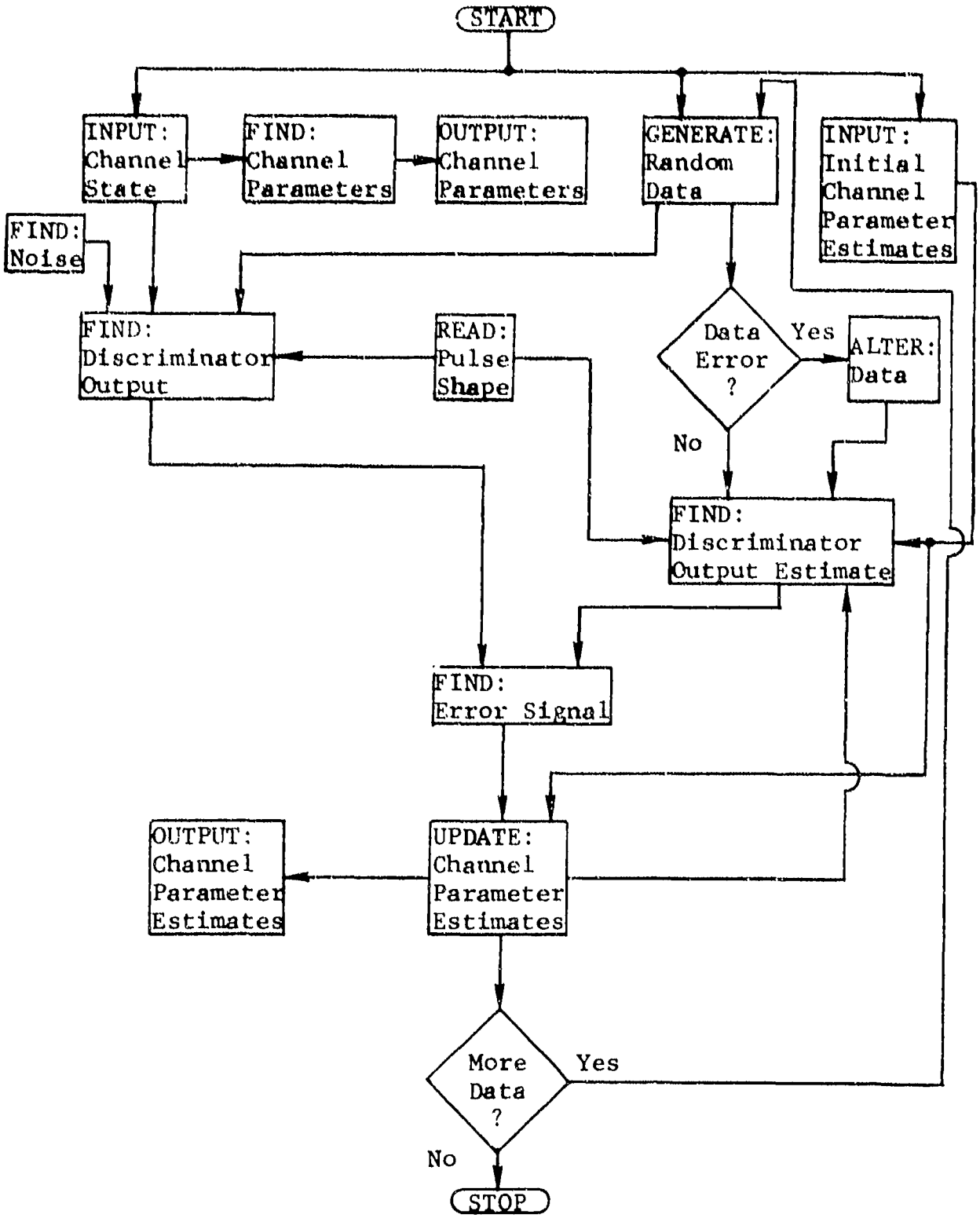

Figure 4.8 Flow Diagram of Channel Estimator Simulation That Estimates the Baseband Signal at the Discriminator Output

At the start of the simulation, information required to characterize the channel state is input. This information consists of the number of paths in the channel model as well as the amplitude and phase of each path (see Appendix B). From this information, the channel parameters to be estimated are evaluated using Eqs. (21) and (25) of Appendix B.

The two-level NRZ data is randomly generated to form an independent and identically distributed data sequence which takes on the values $\pm d$ with equal probability. The level d is chosen such that a 99% power bandwidth of 14 MHz is obtained. This data sequence, along with stored pulse shape information (Appendix F), is used to find the baseband signal at the discriminator output using the discrete path analysis of Appendix C. The discriminator output is found by adding Gaussian noise (see Appendix A) to this baseband signal.

To find the estimate of the discriminator output, either Eq. (4.10) or (4.12) of Section 4.3.2.1 was implemented. This implementation required that the generated data sequence (after alterations for data errors), the pulse shape information, and estimates of the channel parameters be used to form an estimate of the discriminator output.

In order to update the channel parameter estimates, an error signal must be found. From Eq. (4.18) the error signal required is

$$\epsilon(kT) = r(kT) - \hat{r}(kT) \tag{4.27}$$

where r(kT) is the baseband signal at the discriminator output and $\hat{r}(kT)$ is its estimate. In the simulation, either the LMS or BR adaptation algorithms presented in Section 4.3.3.2, as well as the Variance Equalization technique, can be used.

The salient features of the channel estimator simulation presented in Figure 4.8 are:

(1) Estimates discriminator output.

(2) Either a quadratic or cubic channel model (see Appendix C) can be used.

(3) Independent Gaussian noise samples are used.

(4) Data errors can be included.

(5) Any of the adaptation algorithms presented in Section 4.3.3 can be used to update the channel parameter estimates.

(6) The simulation can be modified to include the estimation of a timing parameter (see Section 4.4.4).

4.3.5.3 Estimation of Receive Filter Output

In the previous section, the channel estimator simulation that estimates the baseband signal at the discriminator output was discussed. In this section we will discuss the channel estimator simulation that was used to evaluate the performance of the channel estimator that estimates the baseband signal at the receive filter output. Figure 4.9 presents the flow diagram of the channel estimator simulation to be discussed. The simulation presented in this figure performs four main functions. They are: (1) generation of the receive filter output signal; (2) detection of the transmitted data sequence; (3) estimation of the receive filter output; and (4) updating the channel parameter estimates.

The primary differences between the two simulations occur in finding the receive filter output, finding the noise samples, and in detecting the data sequence. Since the receive filter output is obtained by passing the discriminator output through a filter with transfer function given by (4.1), it was necessary for the simulation to generate the discriminator output for the entire simulation and perform a fast convolution to obtain the entire receive filter output. The receive filter output was used (see Appendix D) to detect the transmitted data sequence. This was not done in the simulation described in Section 4.3.5.2 since the receive filter output is required for detection. To detect the data sequence and find the estimation error, correlated Gaussian noise samples were generated using Eqs. (18) and (48) of Appendix A (see Appendix E for the method used to generate correlated noise samples). The estimates of the receive filter output were found by using (4.15) of Section 4.3.2.1.

The salient features of the channel estimator simulation described in this section are:

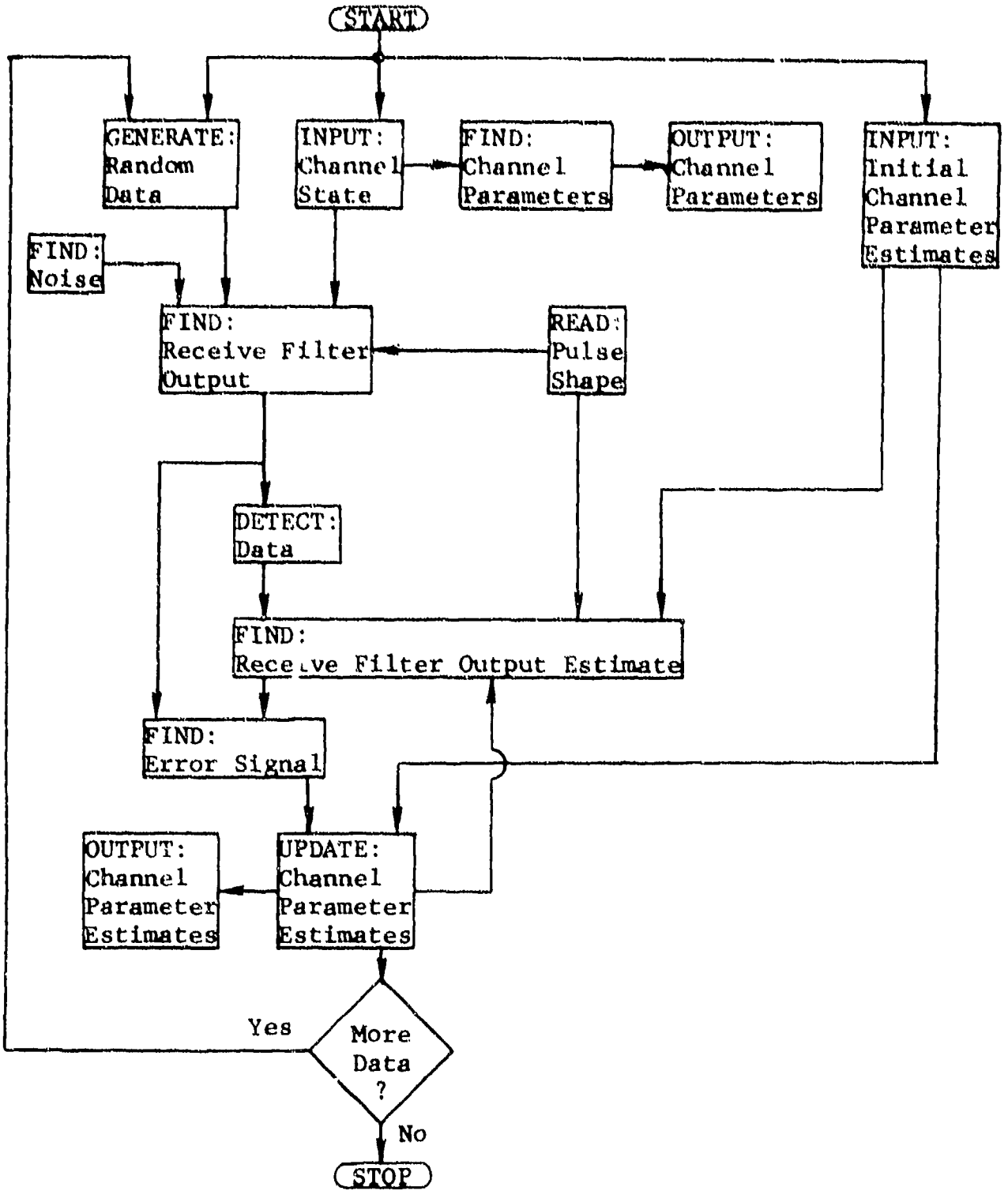

Figure 4.9 Flow Diagram of the Channel Estimator Simulation That Estimates the Baseband Signal at the Receive Filter Output

(1) Estimates receive filter output.

(2) Correlated Gaussian noise samples were used.

(3) Implementation of the detection algorithm is used to produce output binary data.

(4) Data errors occur by incorrect detections.

(5) Any of the adaptation algorithms presented in Section 4.3.3 can be used to update the channel parameter estimates.

Due to the longer time per simulation required to estimate the receive filter output (as opposed to estimating the discriminator output) only the quadratic channel model was implemented and the simulation was not modified to estimate a timing parameter (see Section 4.4.4).

4.4 Performance of Adaptive Channel Estimator

4.4.1 Introduction

In this section we will present simulation results which illustrate the performance of the examined adaptive channel estimators. The performance of the channel estimator which forms an estimate of the discriminator output is given in Section 4.4.2. The simulation results are used to compare the performance of the adaptation algorithms presented in Section 4.3.3. This comparison is given in Section 4.4.2.1. Degradations resulting from data errors and noise are shown in Sections 4.4.2.3 and 4.4.2.5. In Section 4.4.2.4, the adaptive channel estimator performance for the quadratic and cubic channel models is used to determine channel model applicability.

In Section 4.4.3, the performance of the channel estimator which forms an estimate of the receive filter output is presented. Section 4.4.4 addresses the problem of obtaining the required timing information and proposes solutions to this problem.

As is shown in Figure 4.35, system performance is relatively insensitive to variations of channel parameter P_2, indicating accurate estimates of this parameter are not required. Therefore, only estimation of channel parameters P_1 and P_3 will be illustrated in the examples.

Also, to conserve computer resources, the examples presented in Section 4.4.2 and 4.4.3 use the fixed timing reference configuration of the adaptive channel estimator. This configuration is

illustrated by Figure 4.5(a). Section 4.4.4 illustrates the performance of the adaptive channel estimator configuration as given by Figure 4.5(c), which adaptively estimates a timing parameter.

4.4.2 Performance of the Adaptive Channel Estimator That Estimates the Discriminator Output

Using the simulation described in Section 4.3.5.2, which simulates the adaptive channel estimator that estimates the baseband signal at the discriminator output, we were able to verify the feasibility of the proposed technique as well as to assess its performance. Results of this simulation have been used to evaluate the adaptation algorithms, assess the effects of noise and data errors, and to determine the range of applicability of the quadratic and cubic channel models. (See figures for details.)

4.4.2.1 Rate of Convergence of Adaptation Algorithms

Two adaptation algorithms for updating the channel parameter estimates were presented in Section 4.3.3. They were called the LMS and BR adaptation algorithms. Also in Section 4.3.3, a technique for increasing the rate of convergence of the adaptive channel estimated was proposed. This technique was called Variance Equalization and involved estimating scaled channel parameters.

The LMS algorithm updates the channel parameter estimates using Eq. (4.17), while the BR updates the channel parameter estimates using Eq. (4.21). For the BR, we selected for the error standard deviation required by Eq. (4.23), a short-term estimate obtained by summing error sample magnitudes from 100 previous estimates of the discriminator output. The error standard deviation was found from this sum, assuming that the errors were Gaussian-distributed and had zero mean. In particular, the error standard deviation used by the BR adaptation algorithm was found by

$$\hat{\sigma}_e(i) = \sqrt{\frac{\pi}{2}} \sum_{k=100i+1}^{100i+100} |\epsilon_k| \qquad (4.28)$$

Figures 4.10 and 4.11 present the convergence of channel parameters P_1 and P_3 using the LMS and BR adaptation algorithms with and without Variance Equalization. As shown in these figures, variance equalization greatly increases the convergence rate of the adaptive channel estimator. From Fig. 4.10 we see that the convergence of the BR algorithm is somewhat slower than the LMS algorithm. By simulations such as these we estimate that around a 50% greater number of iterations is required for the BR algorithm to achieve the same RMS parameter measurement error as for the LMS algorithm.

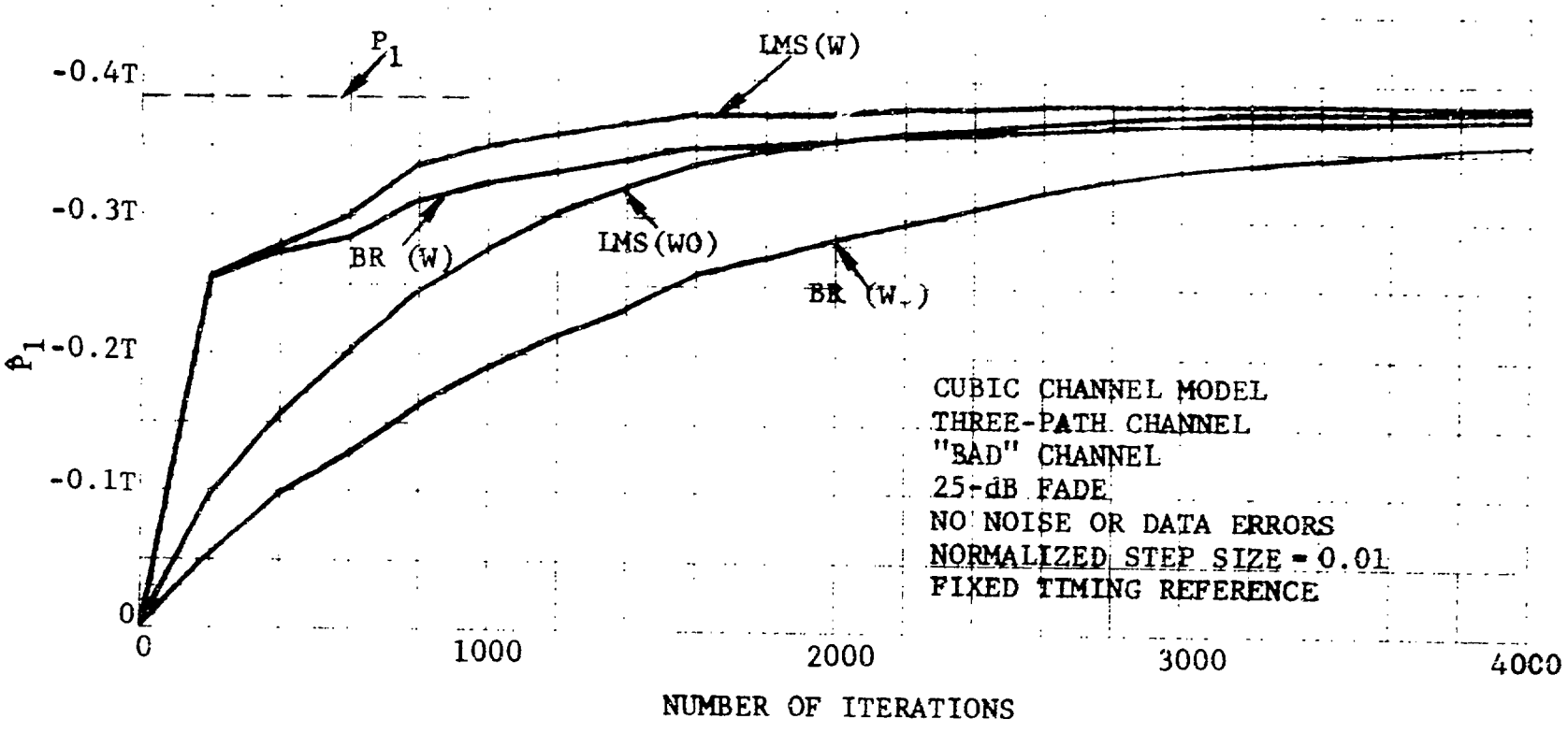

LMS - Least Mean Square Algorithm
BR - Binary Reinforcement Algorithm
With (W) or without (WO) Variance Equalization

Figure 4.10 Comparison of Adaptation Algorithms (P_1 Convergence)

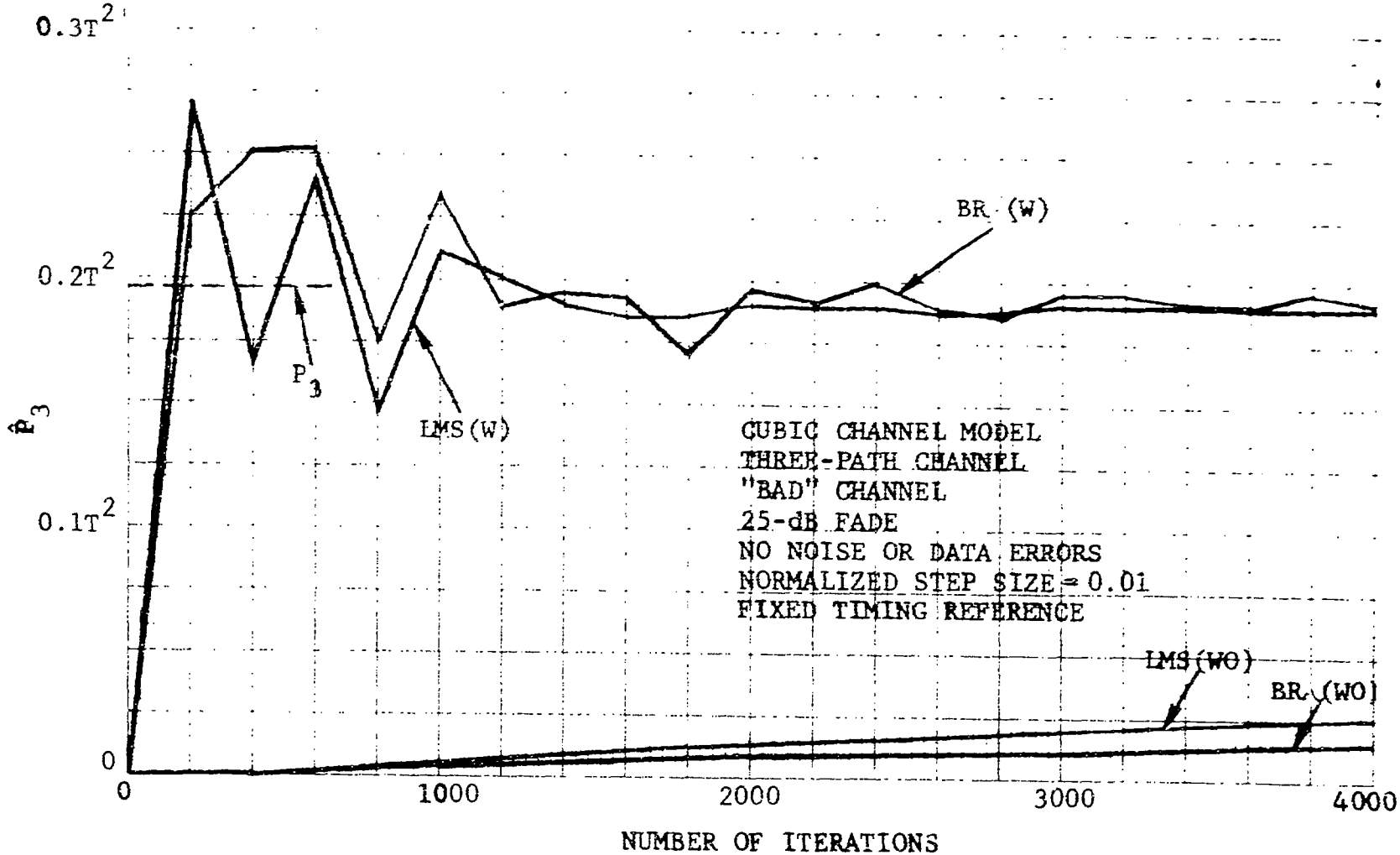

LMS - Least Mean Square Algorithm
BR - Binary Reinforcement Algorithm
With (W) or Without (WO) Variance Equalization

Figure 4.11 Comparison of Adaptation Algorithms (P_3 Convergenee)

Either a quadratic or cubic (see Appendix B) channel model can be used to describe the received baseband signal. The use of the cubic channel model for the adaptive channel estimator will require more complex hardware implementation than the quadratic channel model, but should be better able to model the channel over a wider range of channel conditions. The applicability of the quadratic and cubic channel models is addressed in Section 4.4.2.4.

Figures 4.12 and 4.13 present the convergence of channel parameters P_1 and P_3 using the quadratic and cubic channel models and two step sizes. For 25-dB simulation runs, the quadratic channel model parameter estimate converged more rapidly than the cubic channel model parameter estimate. A possible explanation for the superior convergence of the quadratic channel model may be that the Variance Equalization technique increases the convergence of the additional channel parameters [which are not necessary to model a 25-dB fade accurately (see Section 4.4.2.4)] at the expense of channel parameters P_i, $i = 0,1,2,3$.

Also shown in Figs. 4.12 and 4.13 is the dependence of convergence rate on step size. As shown in these figures, the larger step size provides more rapid convergence. In fact, as may be expected from Eq. (3.22) of Section 3, if the step size is decreased by a factor, then the convergence time is increased by the same factor. The effect of the step size upon channel estimator performance will be considered in the following Section.

Figures 4.14 and 4.15 illustrate that the convergence of parameters P_1 and P_3 does not change with fade level.

4.4.2.2 Effect of Step Size and Number of Iterations on Parameter Measurement Error

In order to evaluate the utility of the adaptive channel measurement technique for performance assessment it is necessary to determine the accuracy to which the parameters can be measured and the amount of time, or equivalently, the number of iterations, required to achieve a desired accuracy. The preceding section presented qualitative results showing the relative time-constants of convergence for the parameters P_1 and P_3 using the LMS and BR algorithms with and without variance equalization, using the quadratic and cubic parameterized models, and using different fade levels. Here we wish to present the results of some extensive simulations providing numerical results on the variation of parameter measurement error with step size δ and

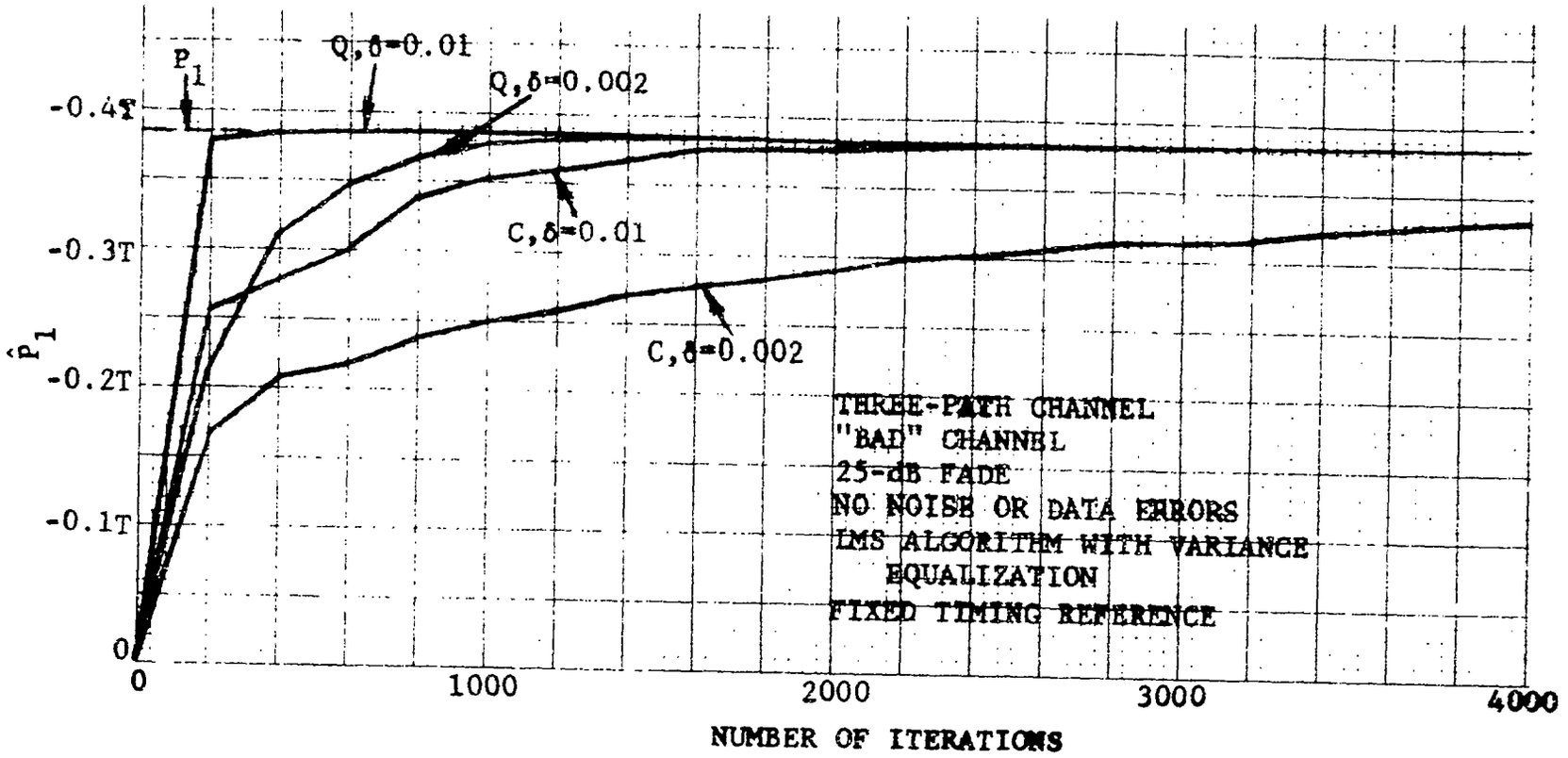

Quadratic (Q) or Cubic (C) Channel Model
δ - Normalized Step Size
$\frac{1}{T}$ - Data Rate

Figure 4.12 Dependence of P_1 Convergence on Step Size

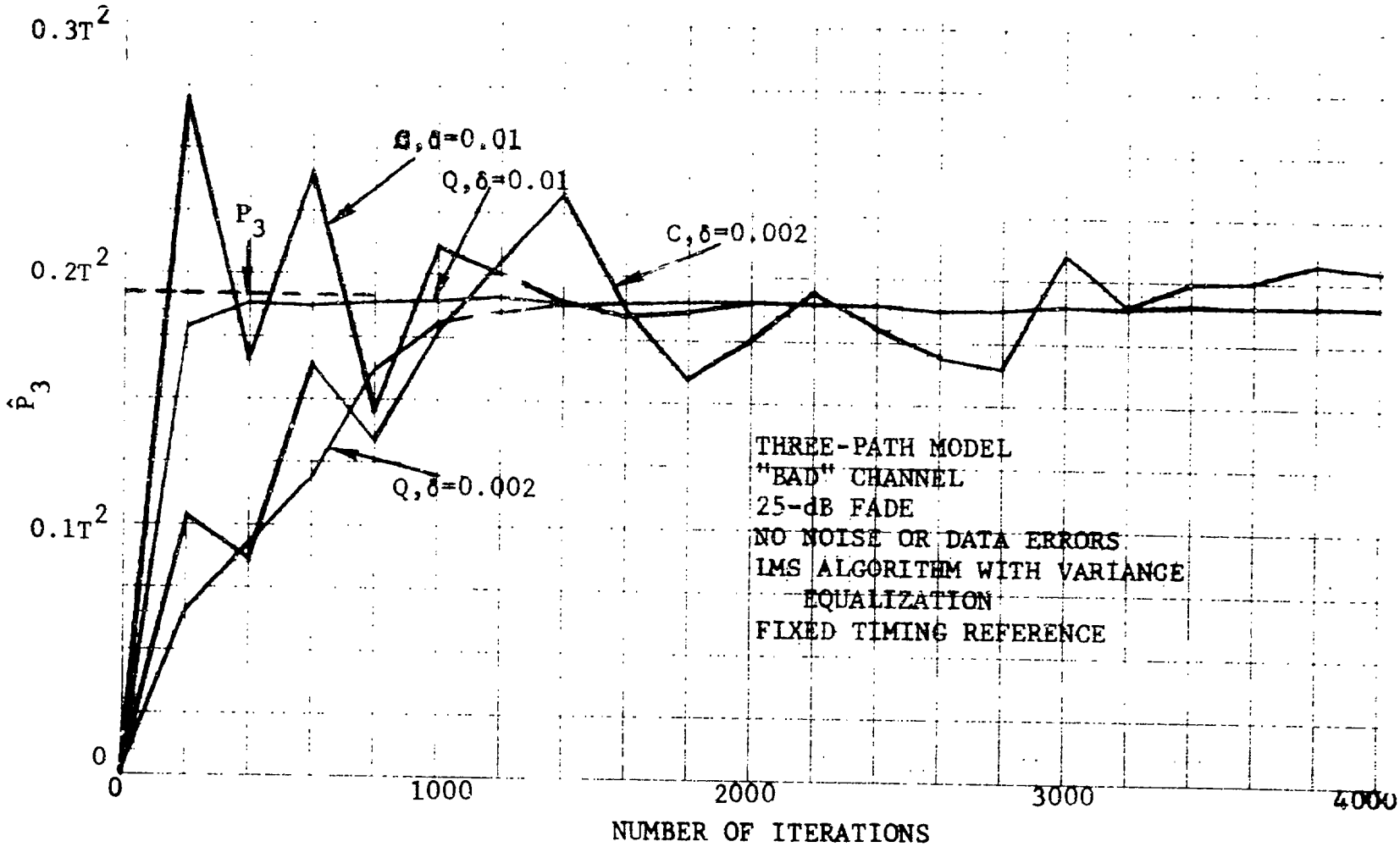

Quadratic (Q) or Cubic (C) Channel Model
δ - Normalized Step Size
$\frac{1}{T}$ - Data Rate

Figure 4.13 Dependence of P_3 Convergence on Step Size

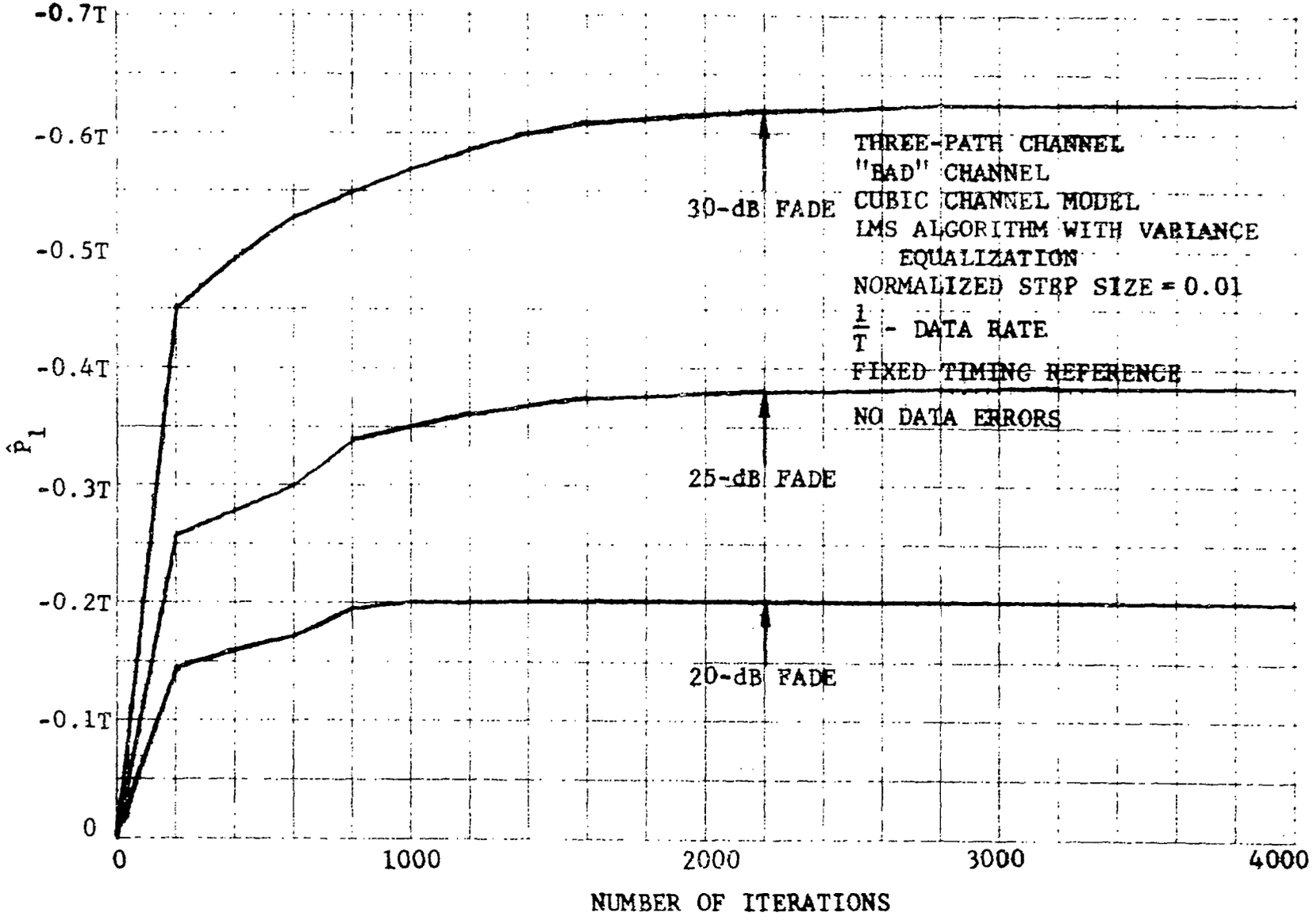

Figure 4.14 P_1 Convergence for Several Fade Levels

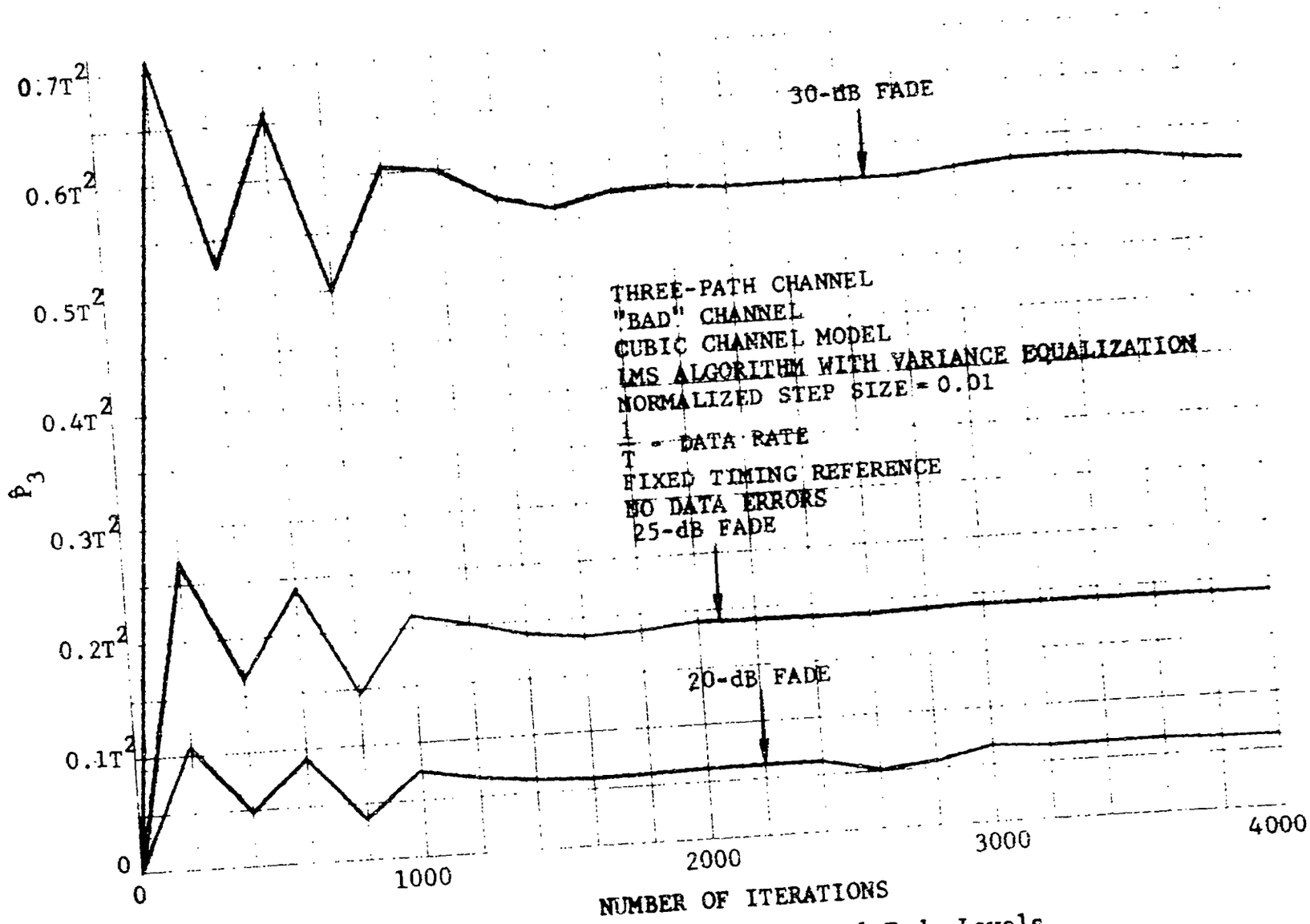

Figure 4.15 P_3 Convergence for Several Fade Levels

number of iterations N, with and without noise present. We have selected the LMS algorithm with variance equalization to illustrate these results because of its superior performance. In addition we have focused our attention on measurements at a 30 dB fade level for the "bad" channel because this represents the threshold of the system as far as nonlinear distortion is concerned. Increases of P_1 and P_3 beyond their values at this fade level results in rapid increase of error rate.

Figures 4.16 and 4.17 present plots of RMS error in estimation of P_3 and P_1, respectively, normalized to the true value of the parameters as a function of the number of iterations up to 30,000 for values of normalized step size δ of .1, .01, .001, .0005, and .0001, with and without noise. The noise level is adjusted so that at a flat fade of 40 dB an error rate of 5×10^{-9} will result. The mean-squared error is computed by averaging over the sample variances of the previous 3000 iterations. From these results we note that for values of $\delta \leq .0005$ steady state is reached by 9000 iterations.

One percent rms fluctuation error in measurement of P_3 may be achieved with values of $\delta = .001, .0005$ at 9000 iterations (with noise present). An order of magnitude lower error rate may be achieved for P_1 under the same conditions. For $\delta = .0001$ convergence is much slower, and has not been reached by 30,000 iterations. When the noise level is removed lower measurement errors occur indicating that the noise level is limiting measurement accuracies. However the noise level added is representative of that to be expected on typical DCS links. Fortunately the percentage measurement errors can be made quite small even in the presence of noise with a number of iterations/second small enough to lead to a reasonable complexity of implementation.

One interesting result which does not appear on the plots is that while the mean value of the estimated parameter P_1 converged to the true value, the mean value of the estimated parameter P_3 converged to a value which was 3% different from the true value. This is due to the approximate nature of the quadratic model in its attempt to model the three-path channel FM system in the adaptive channel estimator. However this 3% bias is small enough to allow performance assessment, and for the three-path channel it does not appear necessary to use more complicated models such as the cubic model.

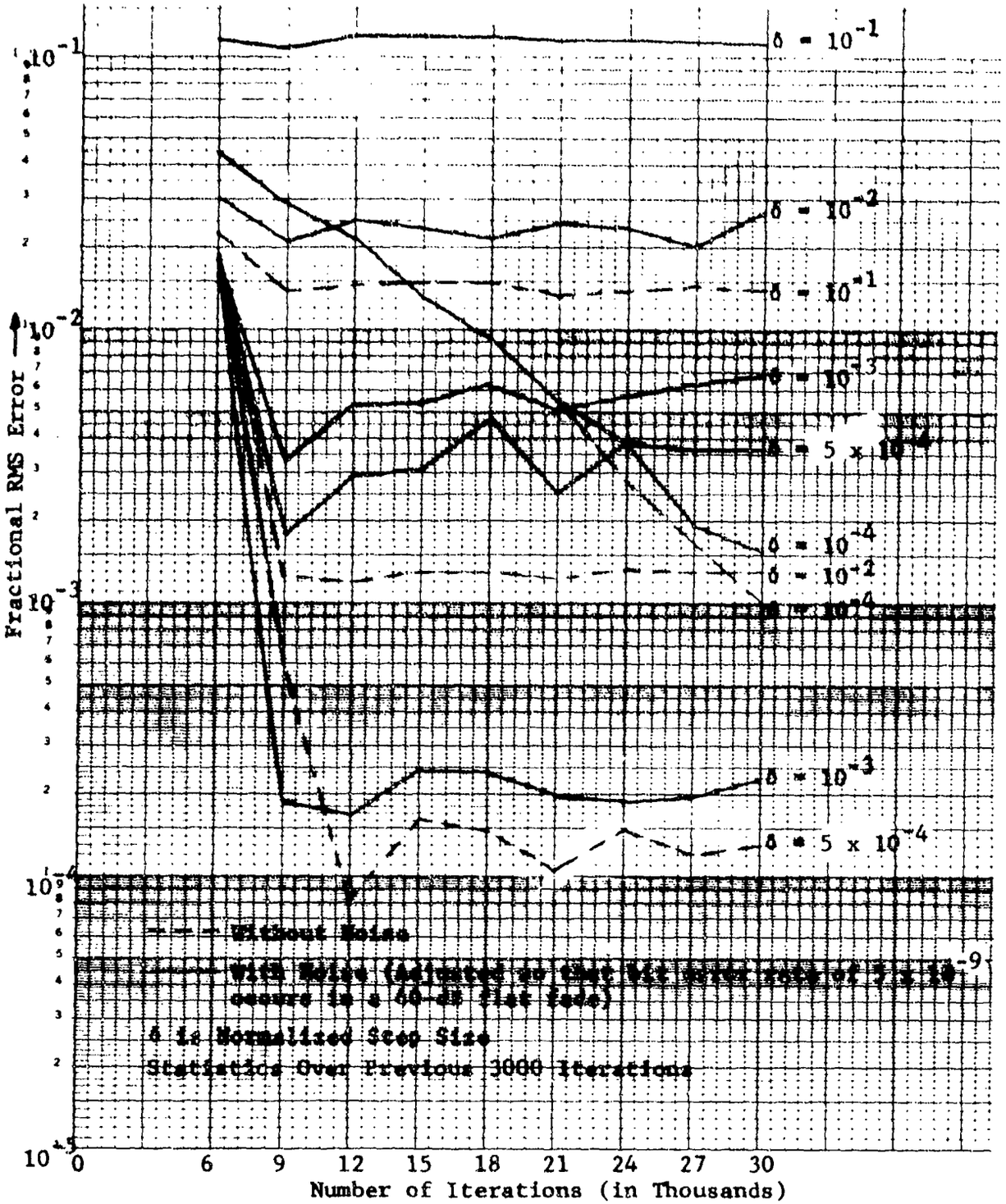

Figure 4.16 Fractional RMS Error in Estimate of P_3 as a Function of Step Size and Iteration Number With and Without Noise Using the LMS Algorithm and a Quadratic Model at a Fade Depth of 30 dB for the "Bad" 3-Path Channel

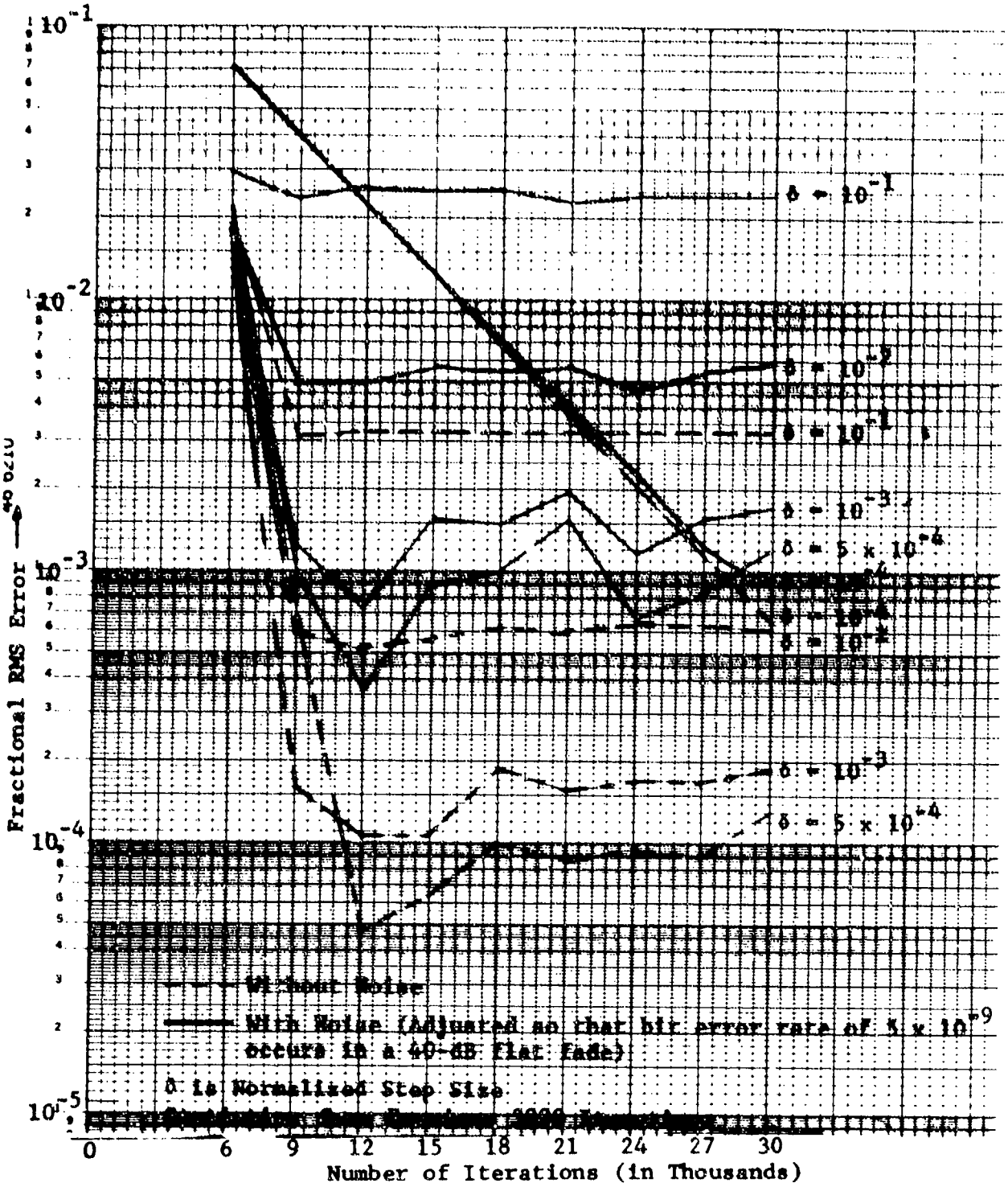

Figure 4.17 Fractional RMS Error in Estimate of P_1 as a Function of Step Size and Iteration Number With and Without Noise Using the LMS Algorithm and a Quadratic Model at a Fade Depth of 30 dB for the "Bad" 3-Path Channel

4.4.2.3 Parameterization Error in Reconstructing the Discriminator Output

In this section we present some simulation results to indicate the degree to which the simple quadratic model (Eqs. 4.6 to 4.9) can represent the discriminator output for the three-path propagation channel. Table 4-1 presents the rms error in estimating the discriminator output for the quadratic and cubic (Eq. 4.12) models assuming a "bad" three-path channel at fade depths of 20, 25, 30, and 35 dB. The cubic model achieves a lower error but as the fade depth increases this advantage decreases. At the "threshold" fade level of 30 dB the error is only 30% higher for the quadratic model, and at 35 dB the advantage vanishes.

Figure 4.18 presents the rms error in reconstructing the discriminator output as a function of step size δ and number of iterations when the parameters from the adaptive channel estimator are used, assuming the quadratic model. When noise is present we note that for $\delta = .01$ and smaller the rms error becomes identical to the additive noise level at the discriminator output, indicating that the actual distortion levels are much smaller. This supposition is verified by examination of the rms reconstruction error in the absence of noise. We note, as in Figs. 4.16 and 4.17, a value of $\delta = .0001$ leads to very slow convergence.

4.4.2.4 Data Errors

The proposed adaptive channel estimator uses the detected data sequence to form an estimate of the received baseband signal. The effect of incorrectly detected data bits upon the performance of the adaptive channel estimator was investigated. With regard to burst errors, two error patterns were examined to determine data error effects upon the performance of the adaptive channel estimator performance. One error pattern is a short error burst in which five bits in a row were in error (bits 500 - 504). The other burst error pattern was a long error burst in which five bits (250, 300, 500, 650, 775) were in error. Since LOS links have very low error rates, the cases considered are very severe during normal operating fault-free conditions.

Figures 4.19 and 4.20 show the convergence of channel parameters P_1 and P_3 when data bits are in error. From these figures we note that the convergence of P_1 is only temporarily affected

TABLE 4-1

PARAMETERIZATION ERROR FOR QUADRATIC AND CUBIC MODELS IN REPRESENTING THREE-PATH "BAD" CHANNEL

Fade Level	RMS Signal Level	RMS Nonlinear Distortion Level	Parameterization Error*	
			(Cubic)	(Quad)
20 dB	0.256	0.17×10^{-2}	0.73×10^{-5}	0.62×10^{-4}
25 dB	0.256	0.54×10^{-2}	0.63×10^{-4}	0.19×10^{-3}
30 dB	0.256	0.17×10^{-1}	0.59×10^{-3}	0.82×10^{-3}
35 dB	0.256	0.53×10^{-1}	0.58×10^{-2}	0.58×10^{-2}

*Parameterization error is the rms error in estimating the discriminator output.

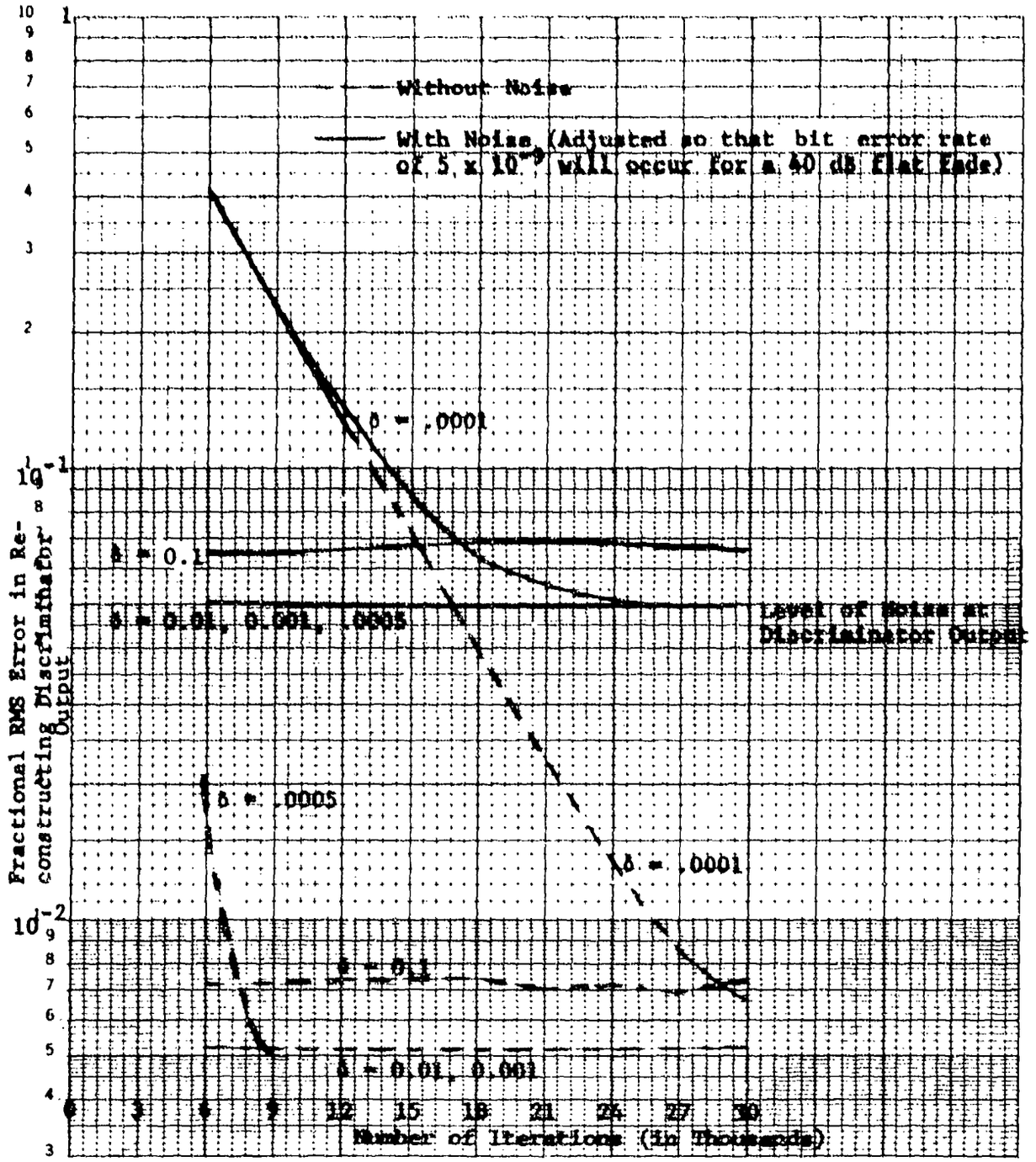

Figure 4.18 Fractional RMS Error in Reconstructing Discriminator Output as a Function of Step Size and Number of Iterations With and Without Additive Noise Using the LMS Algorithm With the Quadratic Channel Model at a Fade Depth of 30 dB for the "Bad" Three-Path Channel

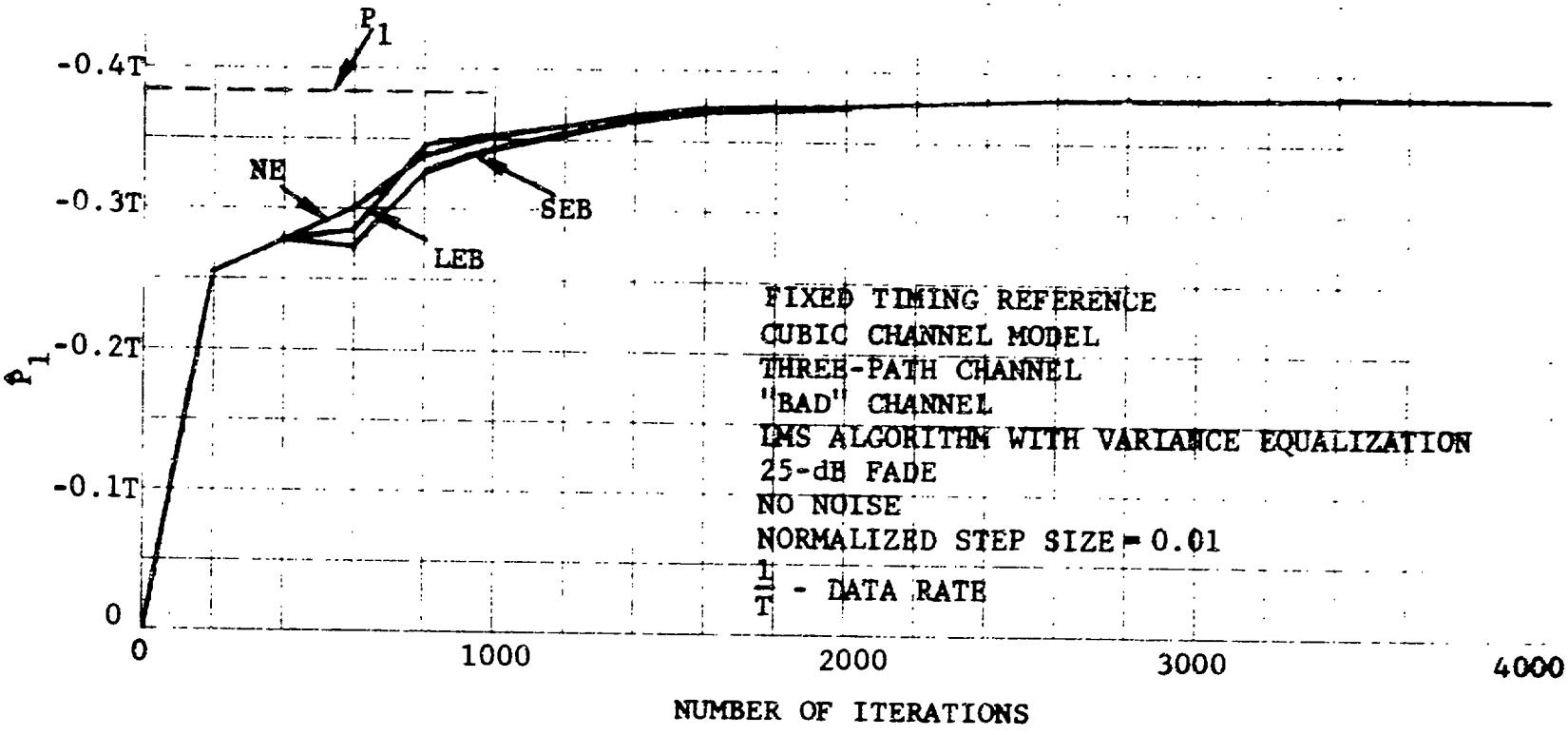

SEB - Short Error Burst (Errors at Bits 500 - 504)
LEB - Long Error Burst (Errors at Bits 250, 500, 650, 775)
NE - No Error

Figure 4.19 Effect of Data Errors (P_1 Convergence)

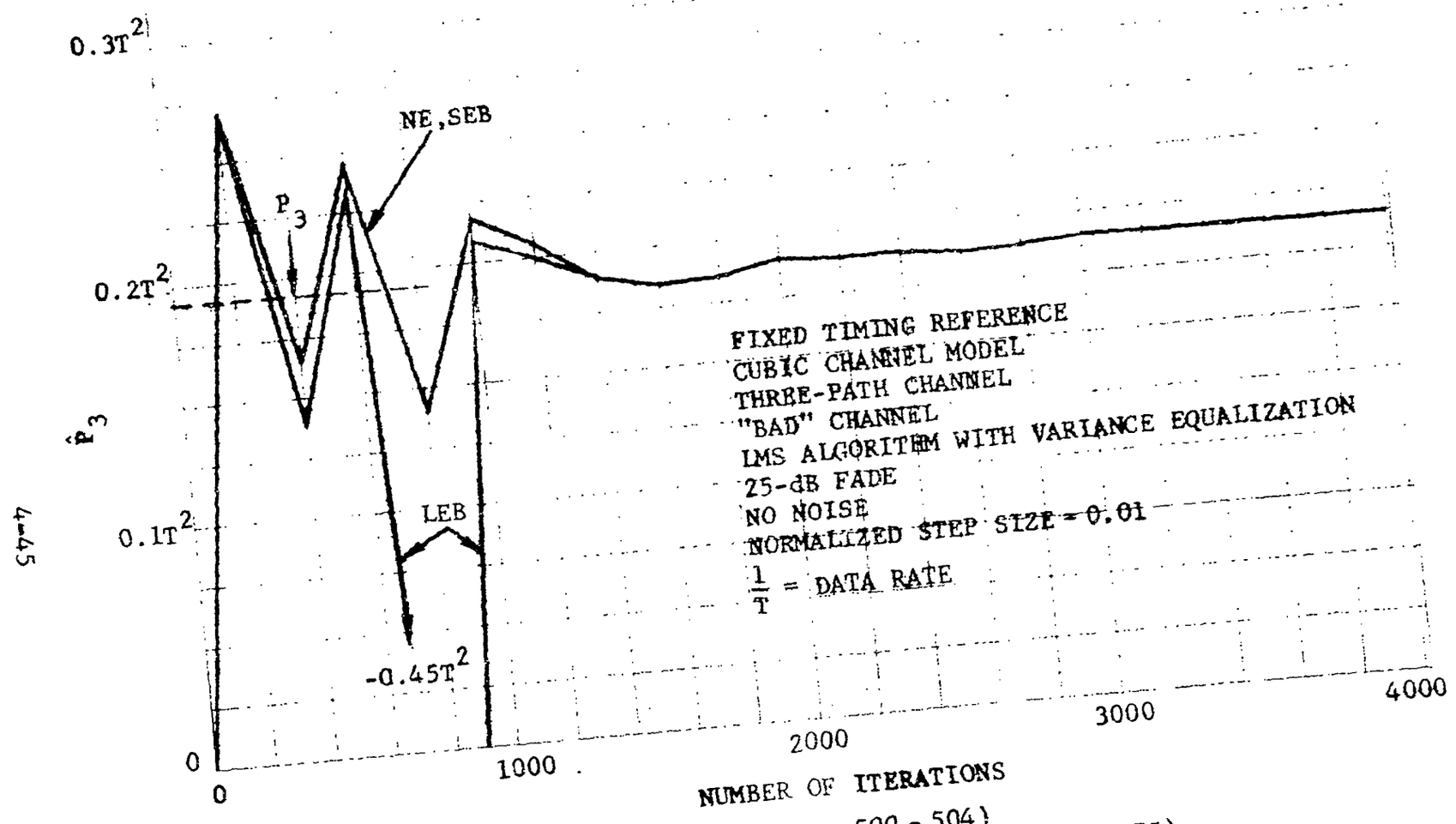

SEB - Short Error Burst (Errors at Bits 500 - 504)
LEB - Long Error Burst (Errors at Bits 250, 300, 500, 650, 775)
NE - No Error

Figure 4.20 Effect of Data Errors (P_3 Convergence)

and quickly recovers once the errors stop. The convergence of P_3 is more severely affected, but also quickly recovers once the errors stop. Due to the quick recovery of the adaptive channel estimator after the error bursts, the degradations resulting from data errors should have only a short-term degradation upon the performance of the adaptive channel estimator during an error burst.

The effect of high average error rate upon the performance of the adaptive channel estimator was investigated. For the channel estimator that estimates the discriminator output, it is shown in Appendix G that high average error rates with independent bit errors produce biased estimates of the channel parameters. Expressions for the bias are derived in Appendix G, where the theoretical results are shown to compare favorably with simulation results. From that appendix we conclude that error rates less than about 10^{-2} do not degrade the channel estimator performance significantly over the error-free case.

The simulation that adaptively estimates the output of the receive filter (see Section 4.3.5.3) was used to assess the channel estimator degradation during high error rate conditions. From Fig. 4.36 we note that fade levels ranging from less than 30 to greater than 32 dB define the transition from small error rates to large error rates. Figures 4.21 and 4.22 show the actual, predicted, and measured values of channel parameters P_1 and P_3. The predicted channel parameters use the analysis of Appendix G with the measured error rate of the particular simulation run. As shown in these figures, the channel estimator performance is good for 30 and 31 dB fades, where the measured mean is within one standard deviation of the predicted and actual values. For 31.5 dB the measured values are close to that predicted (which now varies considerably from the actual parameter value). At 32 dB the estimator performance has seriously degraded and channel parameters cannot be accurately measured at such a high error rate.

It should be mentioned that although the error rates measured in the above simulation runs are within an order of magnitude of those predicted by Fig. 4.36, the measured values are larger. The reason for this discrepancy is that Fig. 4.36 shows three-level error rates which are about 50% less than two-level error rates (see Appendix E). Furthermore, the sampling time used to generate Fig. 4.36 was chosen to minimize the three-level error rate, while the sampling time used in the simulation was not as optimally chosen due to the extensive computer simulations involved and time limitations.

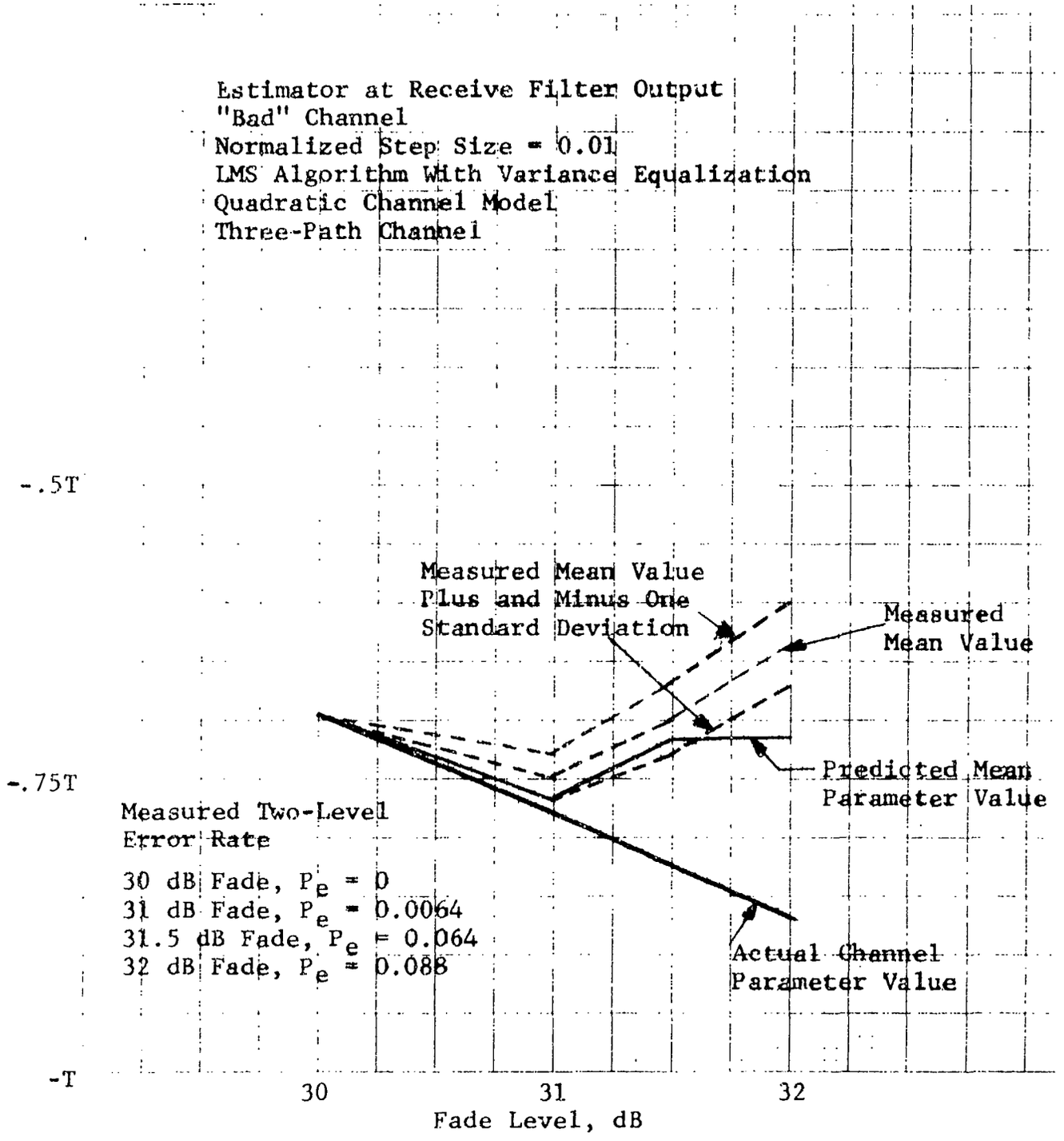

Figure 4.21 Performance of Channel Estimator With Data Errors (P_1 Convergence)

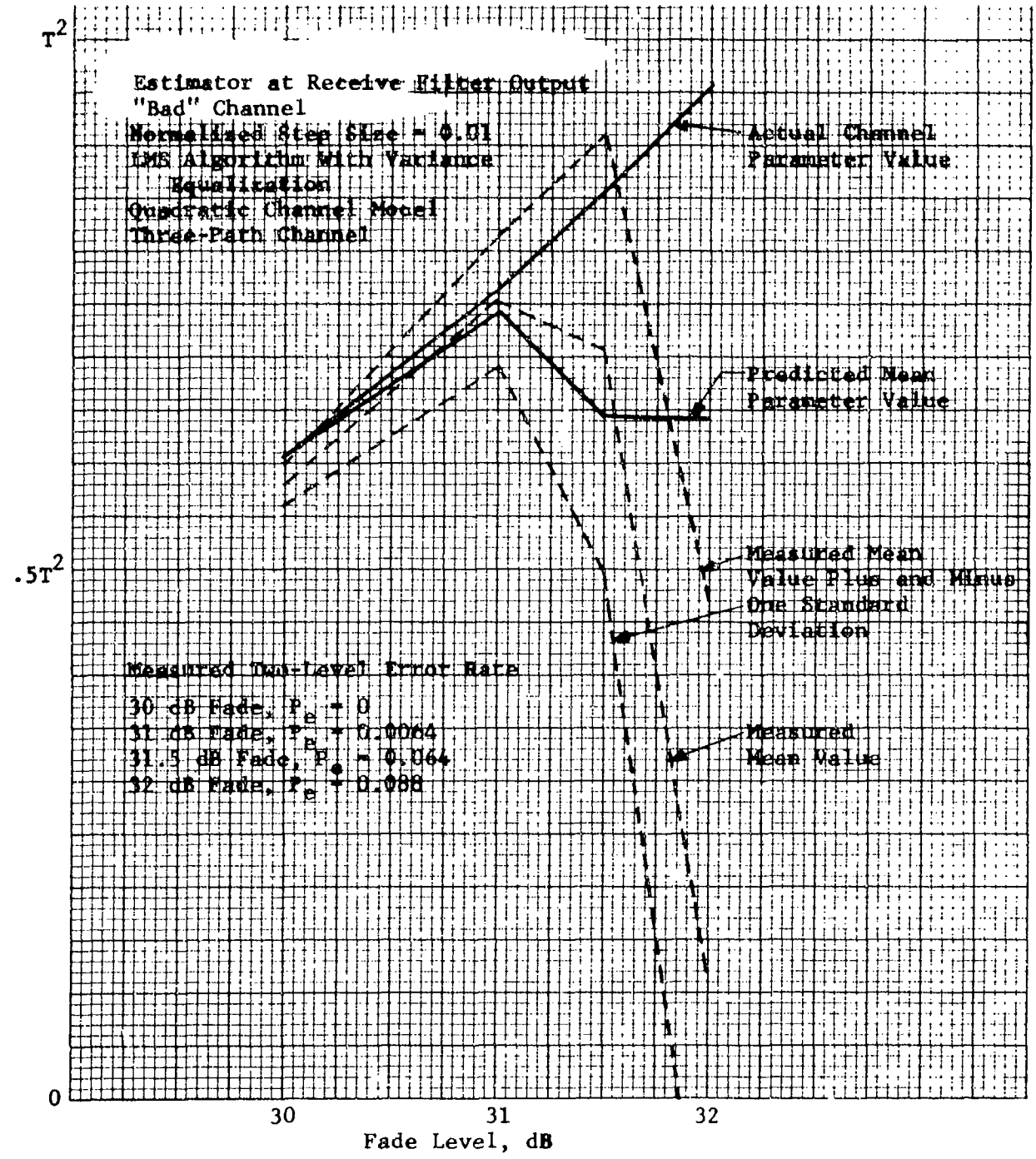

Figure 4.22 Performance of Channel Estimator With Data Errors (P_3 Convergence)

In Appendix G, the effect of high average error rate was examined under the assumption that the errors occur independently. Since the duobinary system considered does not precode the data prior to transmission, an error in the detection of a data bit can propagate and result in error bursts. From Figs. 4.21, 4.22, and Table 1 of Appendix G, we note that the estimation bias error resulting from dependent errors is more severe than that for the corresponding independent error case. As shown in Fig. 4.22, the measured mean is significantly different from the predicted mean beyond a fade level of 31.5 dB corresponding to an error rate of 6.4×10^{-2}. The measured standard deviation of the estimate of channel parameter P_3 for the independent error case (Table 1 of Appendix G) agrees quite favorably with the measured dependent error case of Figs. 4.21 and 4.22. This indicates that the independent error analysis and simulation results can be used to predict performance for the adaptive channel estimator corrupted by dependent errors. However, the effect of dependent errors upon the mean of the estimate of channel parameter P_3 indicates that further examination of the effect of data errors is necessary for very high error rates.

The degree to which an independent error analysis can be extended to the duobinary system of interest is still an open question for very high error rates. Due to the relatively few computer simulations that were run with very high error rates and dependent errors, any conclusions made concerning the performance of the adaptive channel estimator under these severe operating conditions are tentative.

4.4.3 Performance of Adaptive Channel Estimator That Estimates the Receive Filter Output

In Section 4.4.2, the performance of the adaptive channel estimator that estimates the discriminator output was presented. In this section, we will discuss the performance of the adaptive channel estimator that estimates the output of the receive filter. The main advantage for estimating the receive filter output (as opposed to the discriminator output) is that the noise is reduced by the receive filter.

A simulation (discussed in Section 4.3.5.3) was used to evaluate the performance of the adaptive channel estimator. Figures 4.23 and 4.24 show the convergence of the estimates of channel parameters P_1 and P_3. By comparing these figures with figures from Section 4.4.2, we can assess the relative performance of the two pickoff points. Using the receive filter output has reduced the fluctuations in the estimate of channel

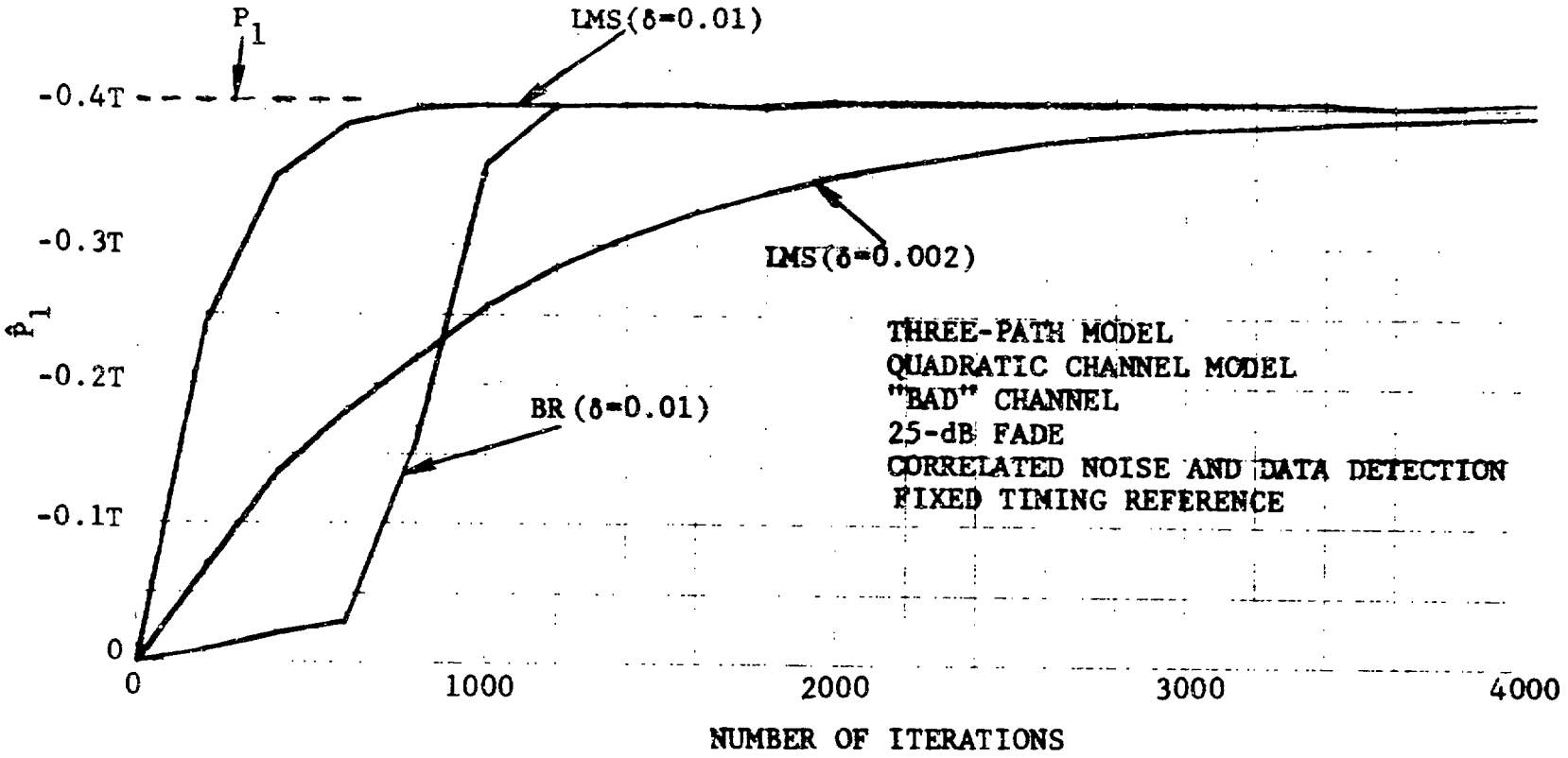

LMS - Least Mean Square Algorithm
BR - Binary Reinforcement Algorithm
δ - Normalized Step Size
$\frac{1}{T}$ - Data Rate

Figure 4.23 Convergence of P_1 for Channel Estimator Estimating the Receive Filter Output

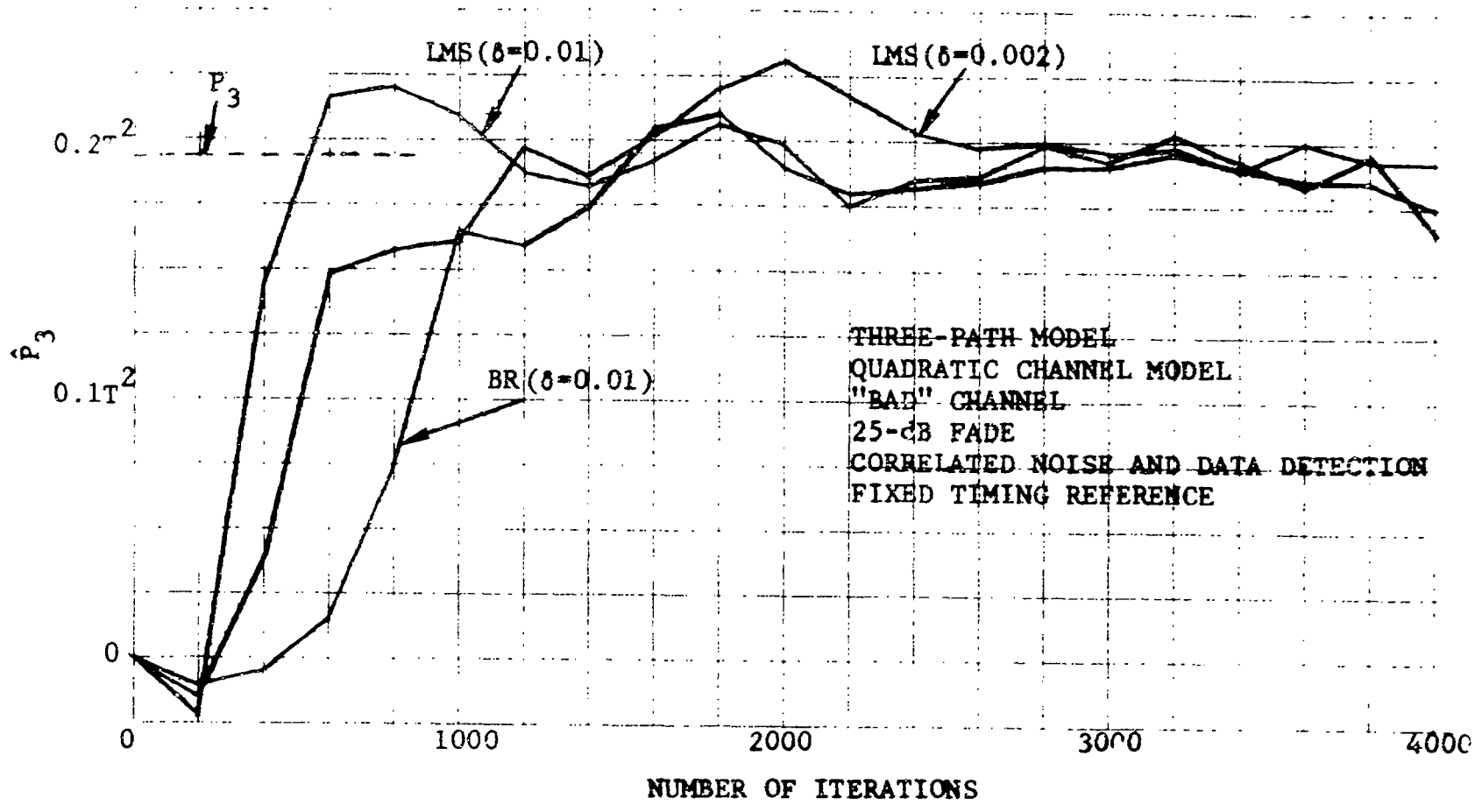

LMS - Least Mean Square Algorithm
BR - Binary Reinforcement Algorithm
δ - Normalized Step Size
$\frac{1}{T}$ - Data Rate

Figure 4.24 Convergence of P_3 for Channel Estimator Estimating the Receive Filter Output

parameter P_3. This is due to the noise reduction characteristics of the receive filter.

From Fig. 4.24 we note that the estimate of P_3 intially went in the negative direction. This may have been due to incorrectly detecting the first few data bits due to improper selection of the first data bit [see Eq. (4.3)]. Figure 4.15 indicates that data errors can produce this behavior.

Although only a few simulations were run to estimate the receive filter output, those that were run indicated that one might reasonably expect behavior similar to that observed in the estimation of the discriminator output. Therefore, we would expect the tradeoff involved in selecting a pickoff point to center around the noise fluctuations versus hardware implementation considerations.

4.4.4 Adaptive Delay Elimination

The adaptive channel estimator requires samples of the received baseband signal (either discriminator or shaping filter output) to estimate channel parameters. In order to improve the performance of the adaptive channel estimator, the time-variable delay (Section 4.5.3) introduced by the channel multipath must be tracked by the bit sync loop. One bit sync loop optimization criterion is to sample at the mean zero crossings. This would result in the bit sync loop sampling near the maximum "eye" opening of the mean "eye" patterns (see Section 4.5.4).

If this bit sync loop optimization criterion is used (and achieved) and if the channel estimator uses pulse shape information [Eqs. (2) - (5) of Appendix F] sampled at $\tau_s = nT + \frac{T}{2}$, (which are the nominal duobinary sampling times), then the channel parameters to be estimated will be adjusted such that $P_1 = 0$. In most cases, this will not result in the best estimate of distortion using the quadratic or cubic channel model (see Section 4.4 of Appendix B).

To achieve a better estimate of the baseband signal, the pulse shape information should be sampled near

$$\tau_s = \tau_b + nT + \frac{T}{2} \tag{4.30}$$

where τ_b is approximately given by the difference between the sampling time and the mean path arrival time.

Another solution to the bit timing compensation problem [presented in Fig. 4.5(c)] would be to adaptively estimate τ_b given in Eq. (4.30). For the estimation of the discriminator output, this would involve forming an estimate of r(t) analogous to Eq. (4.12) given by

$$\hat{r}(t) = \sum_{w=0}^{N} \hat{P}_q(t) S_q(t + \hat{\tau}_b) \tag{4.31}$$

The algorithms for updating the channel parameter estimates were discussed in Section 4.3.3. To update the timing parameter τ_b using the LMS algorithm, we would use

$$\hat{\tau}_b(k+1) = \hat{\tau}_b(k) + 2\Delta\epsilon(k) \sum_{q=0}^{N} P_q(k)\dot{S}_q[kT + \hat{\tau}_b(k)] \tag{4.32}$$

The adaptive channel estimator simulation which estimates the discriminator output was adjusted to include a timing parameter. Use of the LMS algorithm for updating $\hat{\tau}_b$ resulted in our not being able to select a step size Δ that would give a reasonable convergence time without traces of instability. To remedy this situation, a BR that updates the timing parameter estimate by

$$\hat{\tau}_b(k+1) = \hat{\tau}_b(k) + \Delta_B \operatorname{Sgn}\{\epsilon(k) \sum_{q=0}^{N} P_q(k)\dot{S}_q[kT + \hat{\tau}_b(k)]\} \tag{4.33}$$

was used.

Figures 4.25 and 4.26 show the convergence of the estimates of channel parameters P_1, P_3, and τ_b when Eq. (4.33) is used to update the timing parameter estimates. As shown in these figures, compared to the examples without estimating the timing parameter, a much longer time is required for convergence. This is due, in part, to our use of an example that must adjust for a large (0.35T) sampling time offset.

In conclusion, the proposed adaptive elimination technique is a feasible solution to the timing problem. The performance of this approach does not place overly severe implementation restrictions upon the adaptive channel estimator, as is shown in Section 4.6. However, an in-depth study of the timing problem is needed, and, in particular, the direct group delay elimination technique of Fig. 4.5(b) should be further examined.

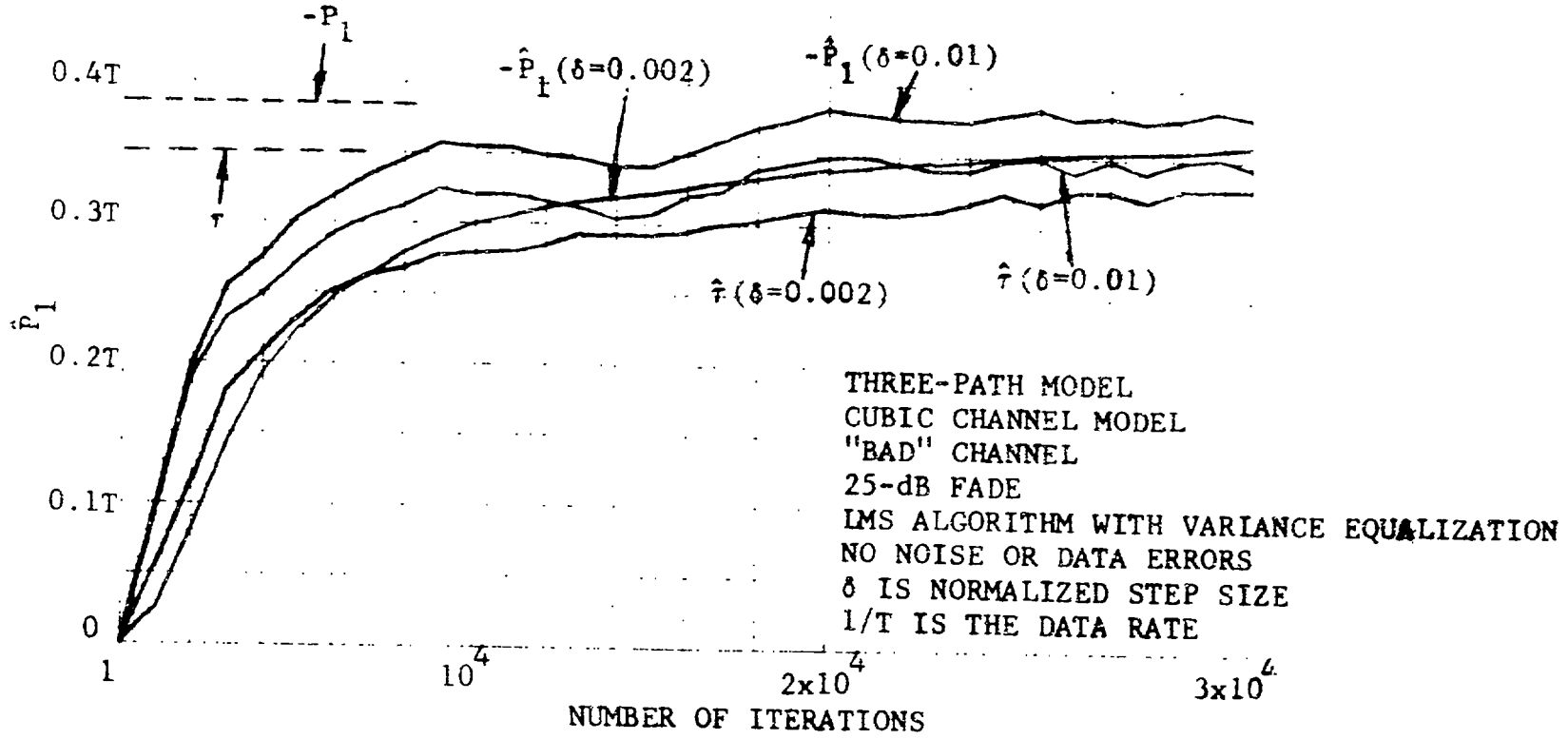

Timing Parameter Step Size Δ_B = 0,002T

Figure 4.25 Convergence of P_1 (Adaptive Delay Elimination)

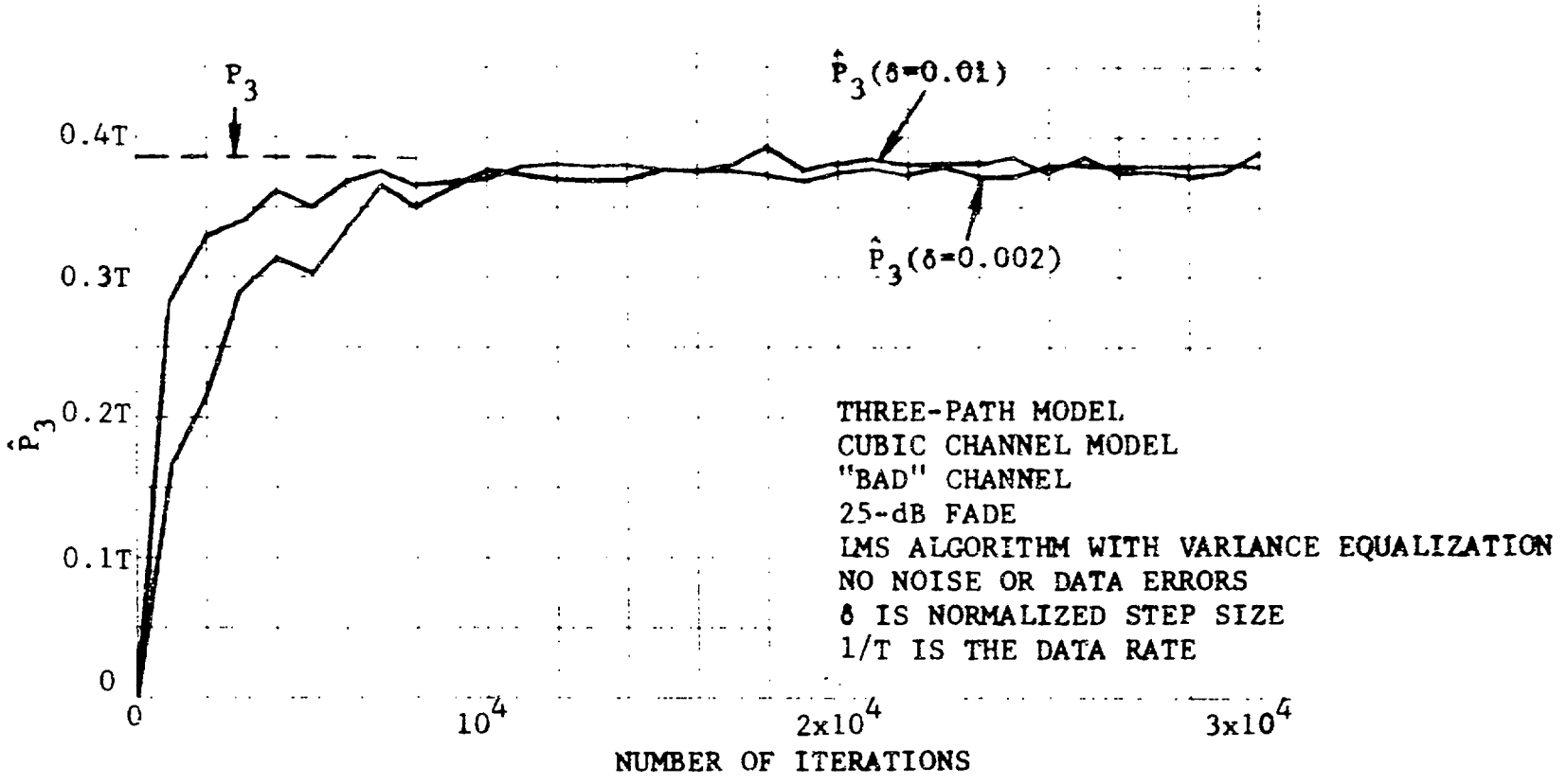

Timing Parameter Step Size $\Delta_B = 0.002T$

Figure 4.26 Convergence of P_3 (Adaptive Delay Elimination)

4.5 Error Rate Estimation from Channel Parameters

4.5.1 Introduction

In this section we address the problem of evaluating the error rate of a duobinary FM LOS system as a function of the quadratic channel model. The error rate that will be evaluated is the probability of incorrectly detecting the three-level duobinary sequence. The relationship between the three-level error rate and the probability of incorrectly detecting the two-level data sequence is examined in Appendix E.

The evaluation of the error rate will allow the determination of distortion-induced degradations for digital data transmission. Furthermore, the method of calculating error rates can be used in conjunction with the proposed adaptive channel estimator to perform real-time performance assessment.

4.5.2 Derivation of Error Rate Expressions

In this section the error rate expressions will be derived for the system presented in Figure 4.1. In this figure, the data is filtered in order to perform some shaping of the baseband spectrum prior to transmission, where H_T is the transmit shaping filter. The input to the frequency modulator is [repeating Eq. (4.5)]

$$x(t) = \sum a_n h_T(t - nT) \tag{4.34}$$

where a_n is the two-level ($\pm d$) NRZ data sequence and $h_T(\cdot)$ is the impulse response of the transmit filter.

Using the result from [4.1], we can represent the output of the frequency discriminator in terms of the input to the frequency modulator. This representation assumes a small amount of frequency selectivity and uses the f-power series model derived in [4.18]. Therefore, the signal at the output of the discriminator can be approximated by

$$r(t) = P_0 x(t - \xi_0) + P_1 \dot{x}(t - \xi_0) + P_2 \ddot{x}(t - \xi_\theta) + P_3 x(t - \xi_0)\dot{x}(t - \xi_0) \tag{4.35}$$

where the P_i are the quadratic channel model parameters which are discussed in detail in Appendix A. From (4.35) it immediately follows that

$$\dot{x}(t) = \sum a_n \dot{h}_T(t - nT)$$

$$\ddot{x}(t) = \sum a_n \ddot{h}_T(t - nT) \tag{4.36}$$

The output of the receive shaping filter can be expressed in terms of the discriminator output by

$$w(t) = \int_{-\infty}^{\infty} h_R(\tau)\, r(t - \tau)\, d\tau + n(t) \tag{4.37}$$

where n(t) is the noise at the filter output.

Using Eqs. (4.34) through (4.37), it follows that

$$w(t) = \sum_{q=0}^{3} P_q Y_q(t) + n(t) \tag{4.38}$$

where $Y_q(t)$ are given by [see Eq. (4.14)]

$$Y_0(t) = \sum_n a_n \int_{-\infty}^{\infty} h_R(\tau)\, h_T(t - \xi_0 - nT - \tau)\, d\tau$$

$$Y_1(t) = \sum_n a_n \int_{-\infty}^{\infty} h_R(\tau)\, \dot{h}_T(t - \xi_0 - nT - \tau)\, d\tau$$

$$Y_2(t) = \sum_n a_n \int_{-\infty}^{\infty} h_R(\tau)\, \ddot{h}_T(t - \xi_0 - nT - \tau)\, d\tau$$

$$Y_3(t) = \sum_n \sum_m a_n a_m \int_{-\infty}^{\infty} h_R(\tau) h_T(t - \xi_0 - nT - \tau) \dot{h}_T(t - \xi_0 - mT - \tau)\, d\tau \tag{4.39}$$

The shaping filter output is then sampled and the three-level detected sequence is generated according to the rule

$$\hat{b}_k = \begin{cases} +2d, & w(kT+\tau_0) \geq C_T \\ 0, & |w(kT+\tau_0)| < C_T \\ -2d, & w(kT+\tau_0) \leq -C_T \end{cases} \tag{4.40}$$

where C_T is the threshold level and τ_0 is the sampling offset. We will determine the probability of incorrectly detecting b_k.

For the present analysis, we will assume that $w(kT+\tau_0)$ conditioned upon a_k, a_{k-1}, can be found in terms of the pulse shape, channel parameters, noise, and other data bits. Expressions for this conditional signal are presented in Appendix B.

For notational purposes, we will define

$$w_k(m,n,\tau_0) \triangleq w(kT+\tau_0)|a_k = m,\ a_{k-1} = n \tag{4.41}$$

to be $w(kT+\tau_0)$ conditioned upon $a_k = m$, $a_{k-1} = n$. The correct three-level sequence is generated by [4.14]

$$b_k = a_k + a_{k-1} \tag{4.42}$$

Therefore, from Eqs. (4.40) and (4.42), a three-level data variable is incorrectly detected if one of the following four conditions is satisfied:

$$\begin{aligned} &w(kT+\tau_0) < C_T \quad \text{and} \quad a_k = a_{k-1} = d \\ &w(kT+\tau_0) > -C_T \quad \text{and} \quad a_k = a_{k-1} = -d \\ &|w(kT+\tau_0)| \geq C_T \quad \text{and} \quad a_k = -d,\ a_{k-1} = d \\ &|w(kT+\tau_0)| \geq C_T \quad \text{and} \quad a_k = d,\ a_{k-1} = -d \end{aligned} \tag{4.43}$$

Since the above four conditions are mutually exclusive, the probability of incorrectly detecting a three-level data variable is

$$P_e(b_k) = \text{Prob.}\left\{w(kT+\tau_0) < C_T,\ a_k = a_{k-1} = d\right\}$$

$$+ \text{Prob.}\left\{w(kT+\tau_0) > -C_T,\ a_k = a_{k-1} = -d\right\}$$

$$+ \text{Prob.}\left\{|w(kT+\tau_0)| \geq C_T,\ a_k = -d,\ a_{k-1} = d\right\}$$

$$+ \text{Prob.}\left\{|w(kT+\tau_0)| \geq C_T,\ a_k = d,\ a_{k-1} = -d\right\} \qquad (4.44)$$

The above can be expressed in terms of conditional probabilities to obtain

$$P_e(b_k) = \text{Prob.}\left\{w(kT+\tau_0) < C_T \mid a_k = a_{k-1} = d\right\} \cdot \text{Prob.}\left\{a_k = a_{k-1} = d\right\}$$

$$+ \text{Prob.}\left\{w(kT+\tau_0) > -C_T \mid a_k = a_{k-1} = -d\right\} \cdot \text{Prob.}\left\{a_k = a_{k-1} = -d\right\}$$

$$+ \text{Prob.}\left\{|w(kT+\tau_0) \geq C_T \mid a_k = -d, a_{k-1} = d\right\} \cdot \text{Prob.}\left\{a_k = -d, a_{k-1} = d\right\}$$

$$+ \text{Prob.}\left\{|w(kT+\tau_0) \geq C_T \mid a_k = d, a_{k-1} = -d\right\} \cdot \text{Prob.}\left\{a_k = d, a_{k-1} = -d\right\}$$

(4.45)

We will assume a data sequence $\{a_n\}$ that is independent, identically distributed, and taking on the values $\pm d$ with probability 1/2. With this assumption, it follows that

$$\text{Prob.}\left\{a_k = \pm d,\ a_{k-1} = \pm d\right\} = \frac{1}{4} \qquad (4.46)$$

Furthermore, using the notation defined in (4.41), we can write

$$P_e(b_k) = \frac{1}{4}\,\text{Prob.}\left\{ w_k(d,d,\tau_0) < C_T \right\} + \frac{1}{4}\,\text{Prob.}\left\{ w_k(-d,-d,\tau_0) > C_T \right\}$$

$$+ \frac{1}{4}\,\text{Prob.}\left\{ |w_k(-d,d,\tau_0)| > C_T \right\} + \frac{1}{4}\,\text{Prob.}\left\{ |w_k(d,-d,\tau_0)| > C_T \right\} \tag{4.47}$$

It is shown in Appendix D that we can express $w_k(m,n,\tau)$ by

$$w_k(m,n,\tau_0) = C_k(m,n,\tau_0) + \sum_{\ell \neq k,k-1} a_\ell\, D_{\ell k}(m,n,\tau_0)$$

$$+ \sum_{\substack{\ell \neq k,k-1 \\ p \neq k,k-1,\ell}} a_\ell\, a_p\, E_{\ell p}^{(k)}(\tau_0) + n(kT+\tau_0) \tag{4.48}$$

where $n(kT+\tau)$ is the sampled noise, and $C_k(\cdot,\cdot,\cdot)$, $D_{\ell k}(\cdot,\cdot,\cdot)$ and $E_{\ell p}^{(k)}(\cdot)$ can be expressed in terms of the pulse shape and the channel parameters. Explicit expressions for these functions are presented in Appendix D. In Eq. (4.48), $C_k(m,n,\tau_0)$ is the conditional signal level, $D_{\ell k}(m,n,\tau_0)$ is the conditional intersymbol interference, $E_{\ell p}^{(k)}(\tau_0)$ is the conditional nonlinear intersymbol interference, and $n(kT+\tau_0)$ is the noise.

With the aforementioned assumptions on the data sequence and assuming zero mean noise, the mean of $w_k(m,n,\tau_0)$ averaged over the noise and data (except for a_k, a_{k-1}) is $C_k(m,n,\tau_0)$. Evaluating $C_k(m,n,\tau_0)$ as a function of τ_0 will generate the mean "eye" patterns presented in Section 4.5.4.

To numerically evaluate the three-level probability, a truncated pulse train approximation was used in which the 14 largest intersymbol interference terms were retained. The remainder of the intersymbol interference terms were assumed to be Gaussian-distributed and were used to increase the noise variance.

4.5.3 Time-Varying Delay

The frequency selectivity of the channel not only introduces distortion at the output of the discriminator, but also introduces a time-varying delay. This can be seen by recalling (4.35)

$$r(t) = P_0 x(t - \xi_0) + P_1 \dot{x}(t - \xi_0) + P_2 \ddot{x}(t - \xi_0) + P_3 x(t - \xi_0)\dot{x}(t - \xi_0) \tag{4.49}$$

where the channel parameters P_1 are given by (4.9).

Rearranging the terms gives

$$r(t) = P_0\left[x(t - \xi_0) + \frac{P_1}{P_0}\dot{x}(t - \xi_0) + \frac{P_1^2}{2P_0^2}\ddot{x}(t - \xi_0)\right] + \left(P_2 - \frac{P_1^2}{2P_0}\right)\ddot{x}(t - \xi_0)$$

$$+ P_3 x(t - \xi_0)\dot{x}(t - \xi_0) \tag{4.50}$$

Noting that the first term consists of the first three terms in a Taylor series expansion of $x(t - \xi_0 + P_1/P_0)$, we can rewrite Eq. (4.42) as

$$r(t) = P_0 x\left(t - \xi_0 + \frac{P_1}{P_0}\right) + \left(P_2 - \frac{P_1^2}{2P_0}\right)\ddot{x}(t - \xi_0) + P_3 x(t - \xi_0)\dot{x}(t - \xi_0) \tag{4.51}$$

where higher-order terms have been neglected. Therefore, the channel has introduced an apparent time-varying delay given by $-P_1/P_0$. To illustrate the importance (and size) of this time-varying delay, consider the three-path channel model presented in Appendix B. From Section 3 of Appendix B, we note that the total delay spread of the three paths is 2.6 ns or about 3% of a bit interval for a 12.6 Mb/s system. From Figure 1 of Appendix B, it is seen that the time-varying delay can exceed 40% of a bit interval even for a 25-dB fade. Therefore, during fading conditions, very small delay spreads can result in large time-varying delays; hence, large performance degradation if this time-varying delay is not tracked. By adjusting the sampling time in the detector to track this time-varying delay, it is possible to improve system performance. This improvement will be illustrated by examples in the following section.

4.5.4 Examples of Error Rate

4.5.4.1 Introduction

In order to illustrate the degradations resulting from multipath fading for the duobinary FM LOS system of interest, examples will be presented. For these examples we will use the three-path channel model presented in Appendix B. At a given fade depth and for given relative amplitudes, the relative phases of the three paths can produce varying amounts of frequency-selective distortion. Two relative phase angle assignments will be used for illustrative purposes. These have been called the "good" channel and the "bad" channel in Appendix B. We refer the reader to Appendix B for a detailed channel model description.

The advantages obtainable by tracking the mean path delay will be shown, as will the sensitivity of error rate to parameter variations.

4.5.4.2 Error Rate Examples for the "Good" Channel

For the "good" channel (see Appendix B), the channel parameters P_1, P_2, and P_3 are all less than one-half of their maximum value at a given fade level. Small P_1, P_2, and P_3 imply that the fade is relatively flat; therefore, we would expect that the degradation due to the frequency selectivity would not be severe.

Figure 4.27 presents the three-level error rate as a function of fade level for several sampling offsets. As is shown in this figure, adjusting the sampling time can improve system performance. Also, the degradation due to channel selectivity is small (less than 2-dB SNR loss at 10^{-6} error rate) if the sampling time can be chosen correctly.

Figure 4.28 illustrates the performance improvement obtainable by tracking the mean delay. From this figure, the best sampling time for this 40-dB fade is ~0.2T (from the direct path), where an improvement of about three orders of magnitude can be realized compared to sampling without tracking the mean delay. For the 42-dB fade, a sampling offset of ~0.25T is optimum and an error rate improvement of two orders of magnitude can be obtained.

Figures 4.29 and 4.30 show mean "eye" patterns [plots of $C_k(m,n,\tau_0)$ versus τ_0 - see Eq. (12) of Appendix D] for 40- and 42-dB fades. Comparing Figures 4.28 to 4.30, we note that the maximum probability of error sampling offset (see Figure 4.28) is

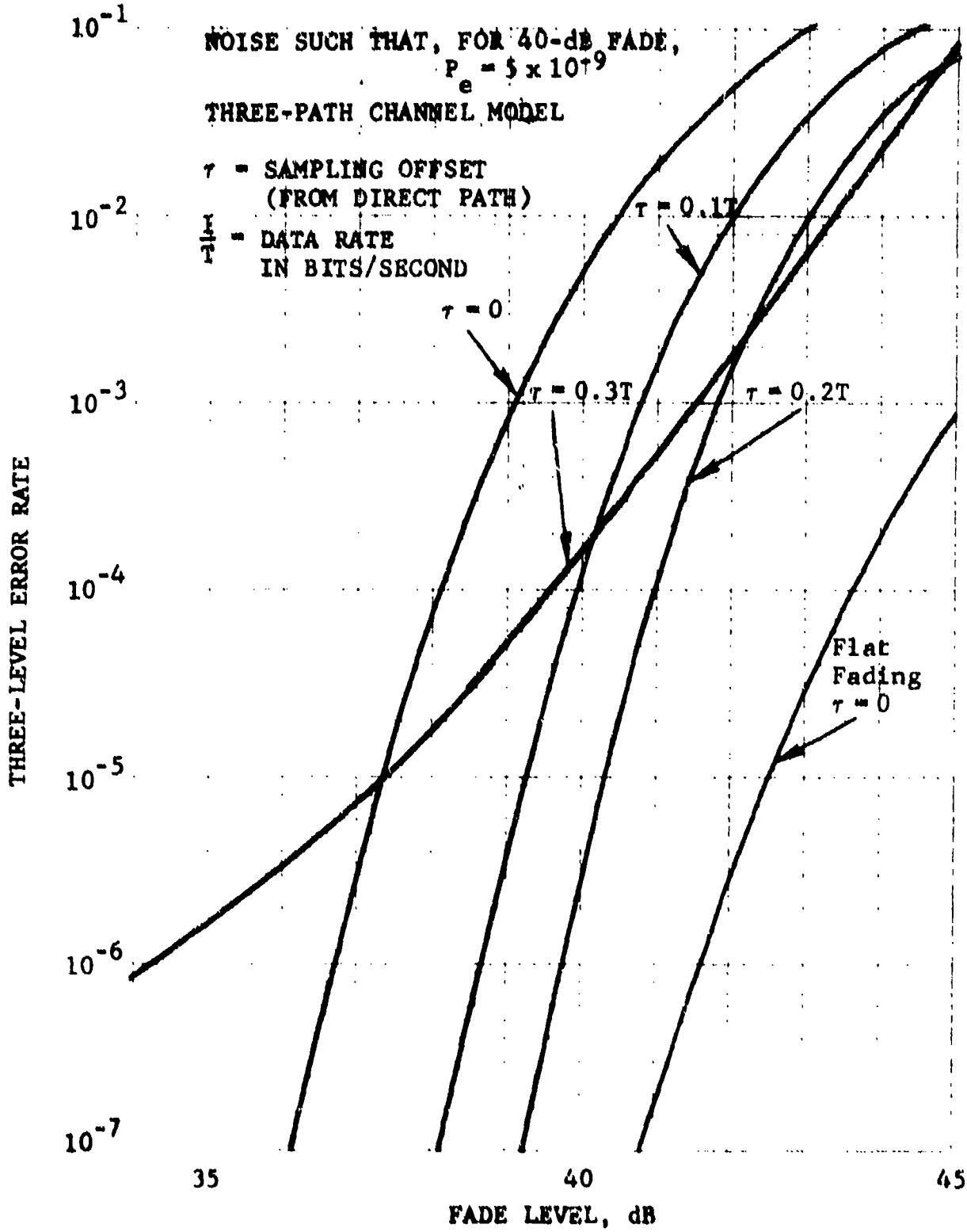

Figure 4.27 Three-Level Error Rate for "Good" Channel

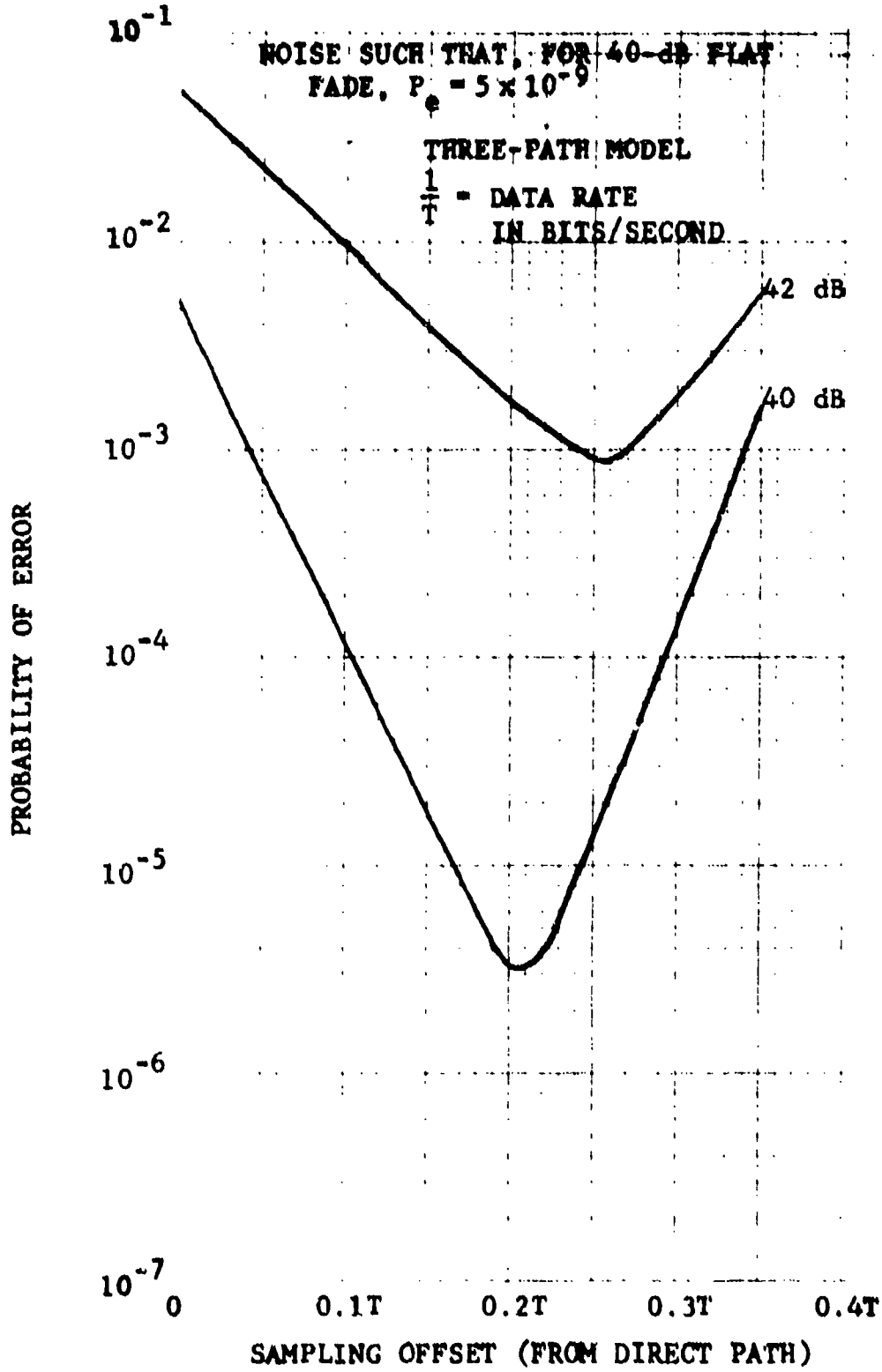

Figure 4.28 P_e vs. Sampling Offset("Good" Channel)

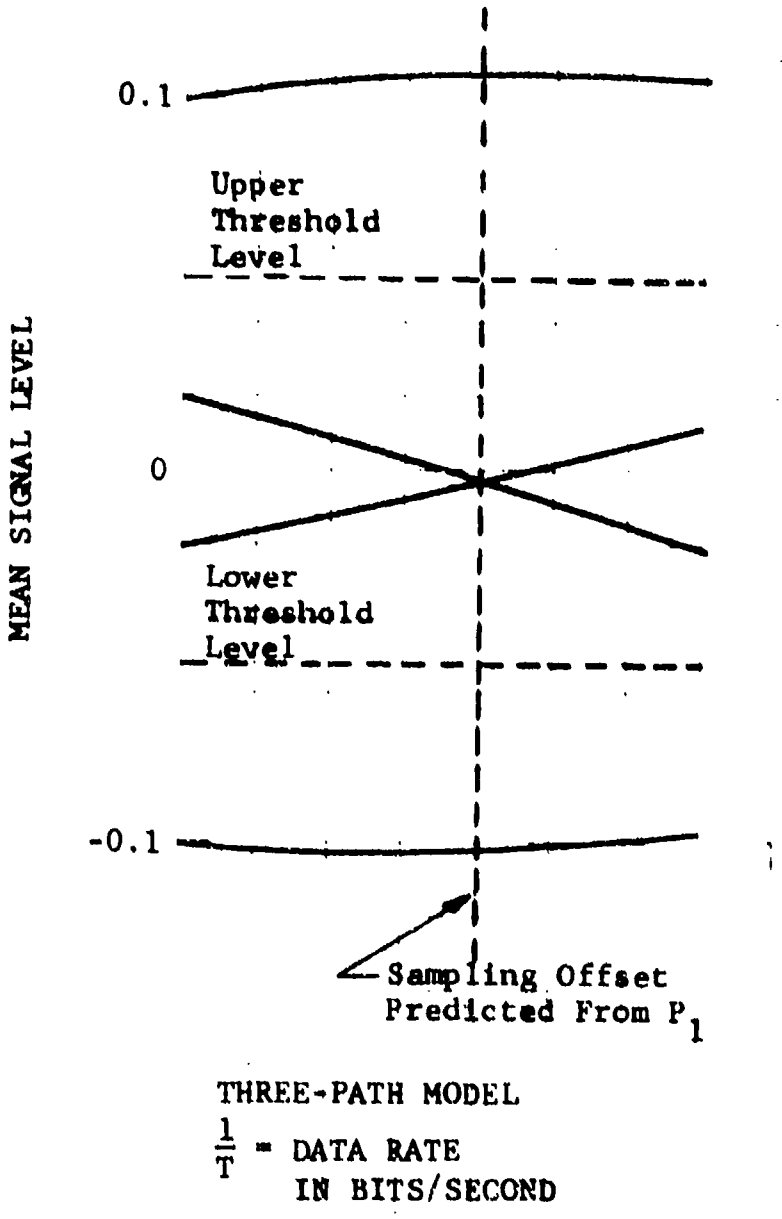

Figure 4.29 Mean "Eye" Pattern 40-dB Fade ("Good" Channel)

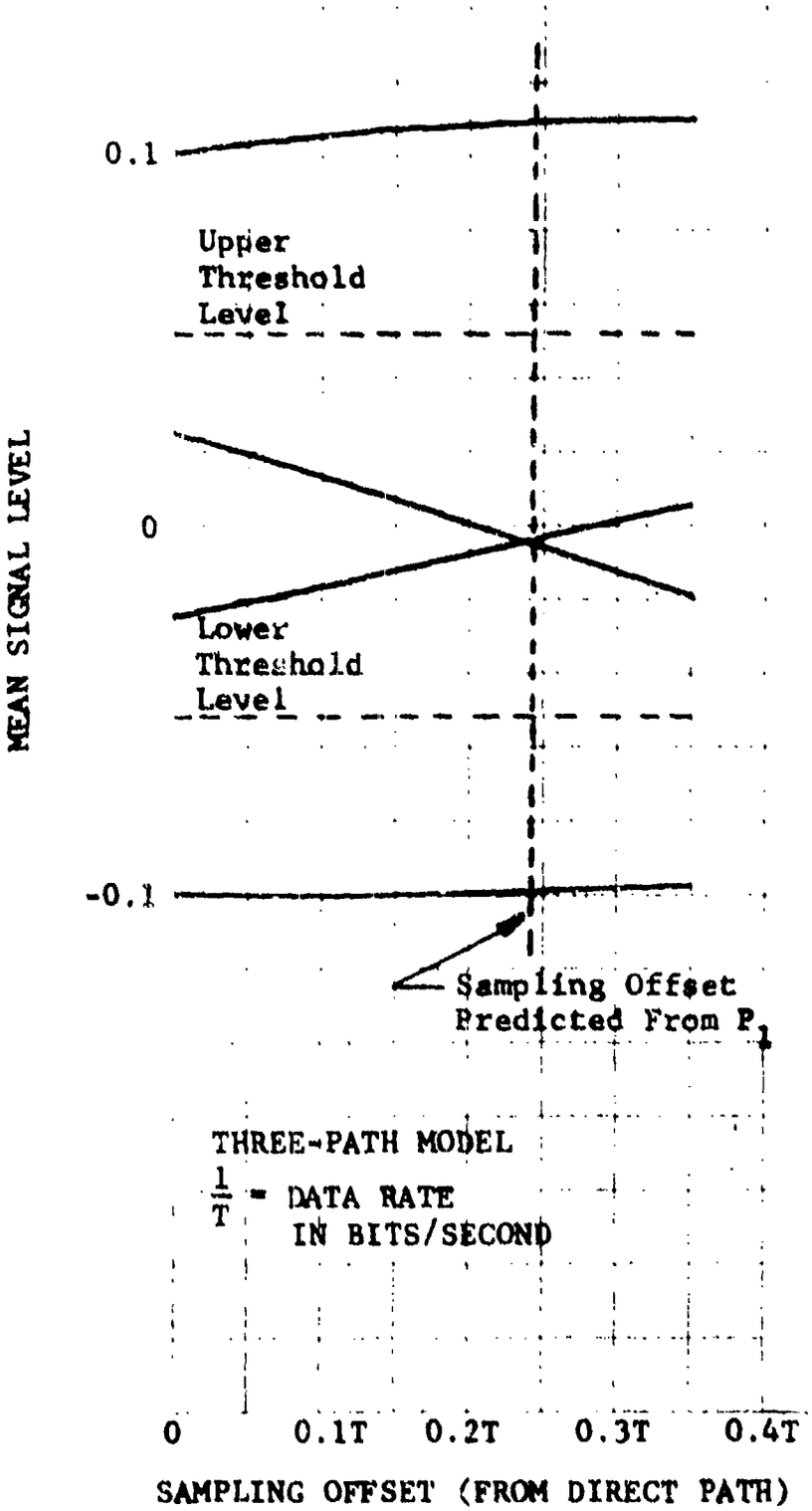

Figure 4.30 Mean "Eye" Pattern 42-dB Fade ("Good" Channel)

approximately equal to the offset at which the mean "eye" pattern has maximum "eye" opening. The maximum "eye" opening occurs at the intersection of $C_k(d,-d,\tau_0)$ with $C_k(-d,d,\tau_0)$. Furthermore, if channel parameter P_1 is used in Eq. (4.51) to predict the mean path delay, this mean path delay would closely predict the minimum error rate sampling offset. The sampling offset predicted by P_1 is indicated on Figures 4.29 and 4.30.

4.5.4.3 Error Rate Examples for the "Bad" Channel

For the "bad" channel (see Appendix B), the channel parameters P_1, P_2, and P_3 are all greater than one-half of their maximum value at a given fade level. Large P_1, P_2, P_3 channel parameter values would indicate a highly selective fade, and one would expect significant degradation due to the frequency selectivity.

Figure 4.31 presents the three-level error rate as a function of fade level for several sampling offsets. As shown in this figure, significant improvement can be obtained by proper selection of the sampling offset. This improvement is further illustrated in Figure 4.32, where the error rate is shown as a function of sampling offset for 26-, 30-, and 32-dB fades. As shown in Figure 4.32, for a 30-dB fade changing the sampling time by 0.05T from its optimum value results in the error rate increasing from $< 10^{-6}$ to about 10^{-3}. This indicates that for the error rates of primary interest ($\sim 10^{-7}$), performance is highly dependent on sampling time.

Figures 4.33 to 4.35 show the mean "eye" patterns for 26-, 30-, and 32-dB fades. By comparing these figures with Figure 4.82, it is seen that the mean "eye" pattern has maximum "eye" opening at approximately the minimum probability of error sampling offset. However, channel parameter P_1, as used in Eq. (4.51) is not as accurate in predicting the optimum sampling time as was the case for the "good" channnel. This is probably due to the "bad" channel being more distorted than the "good" channel.

Figure 4.32 shows how the error rate depends upon fade level when the sampling time is chosen to minimize the probability of error. Comparing Figure 4.36 with the flat fading portion of Figure 4.27, we note that: for flat fading, SNR changes of over 4 dB are required to increase the error rate from 10^{-7} to 10^{-3}; while for the severe selective fading of the "bad" channel, only a little over 1 dB is required. This indicates a threshold effect in which the system degrades quite rapidly once this threshold is reached.

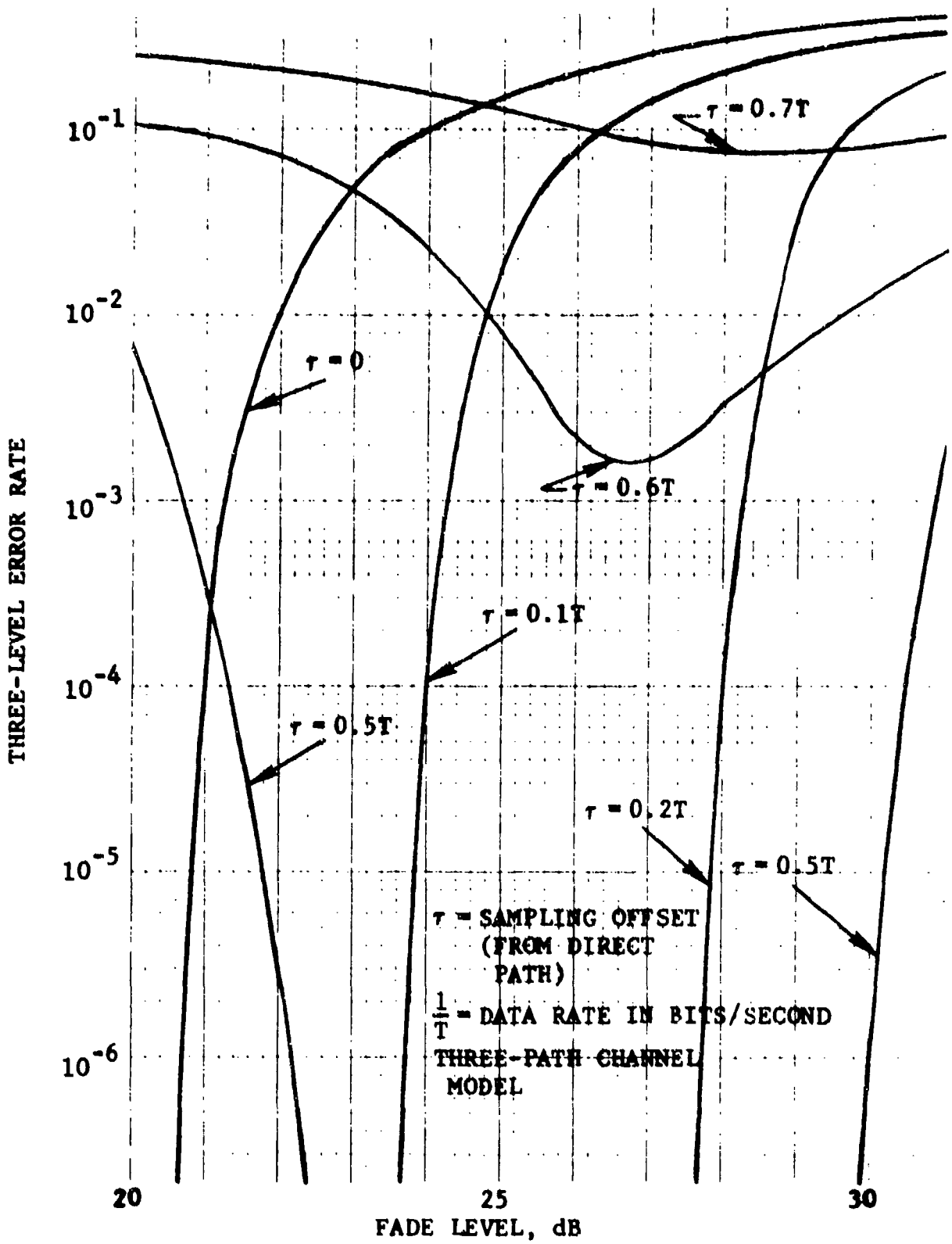

Figure 4.31 Three-Level Error Rate for "Bad" Channel (Noise such that for a 40-dB flat fade $P_e = 5 \times 10^{-9}$).

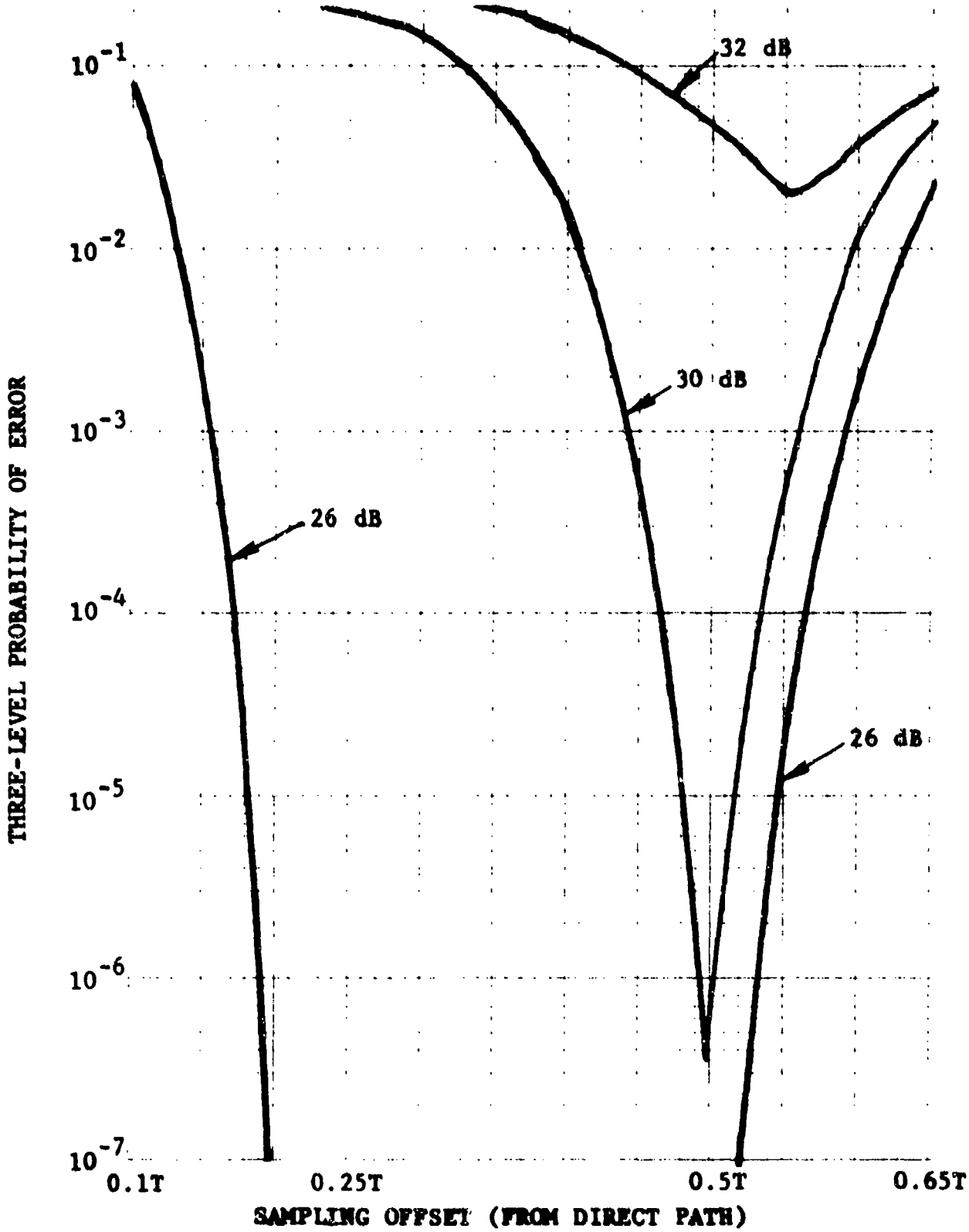

Figure 4.32 Three-Level Probability of Error as a Function of Sampling Offset (Noise such that for a 40-dB flat fade $P_e = 5 \times 10^{-9}$)

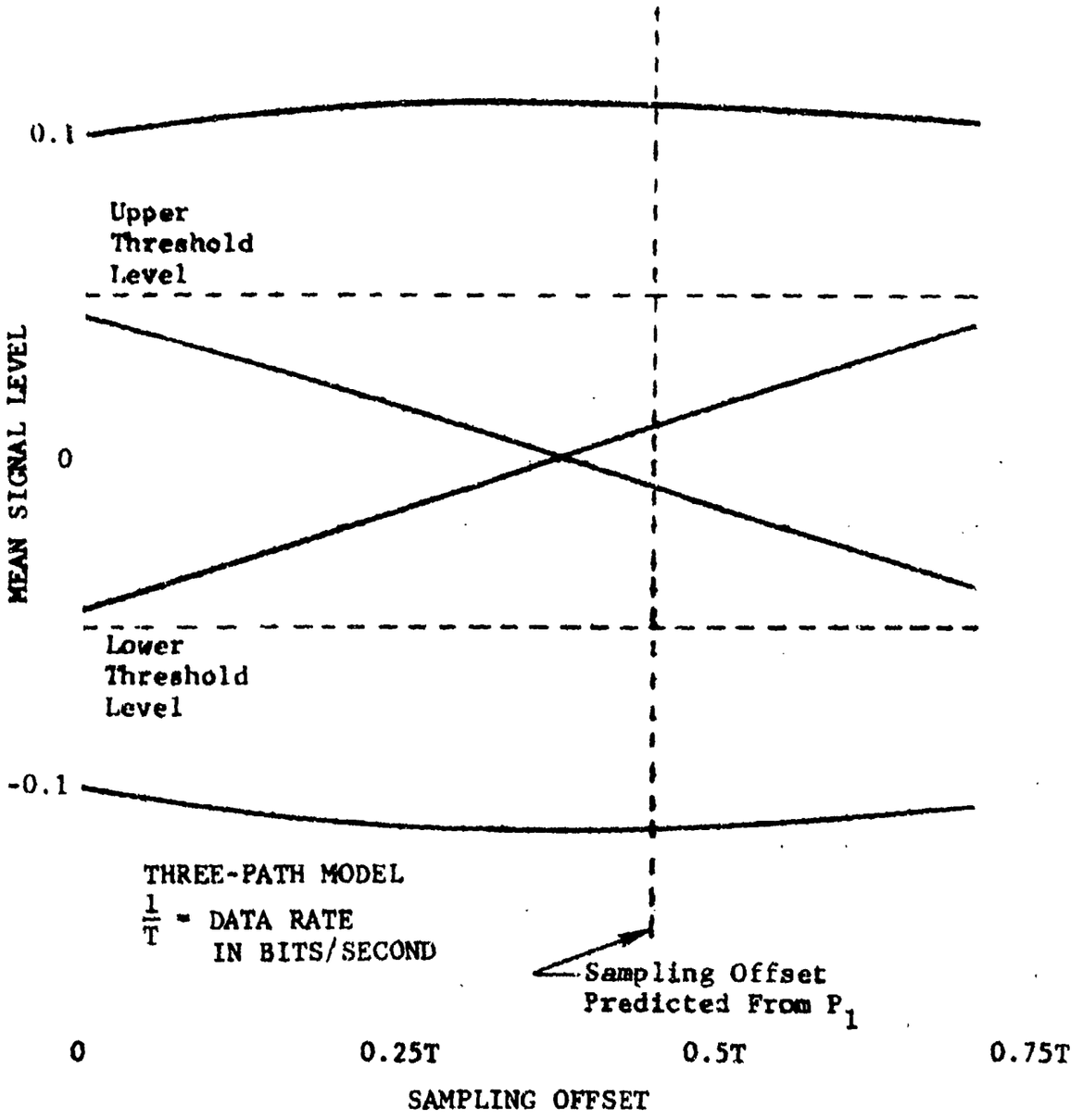

Figure 4.33 Mean "Eye" Pattern 26-dB Fade("Bad" Channel)

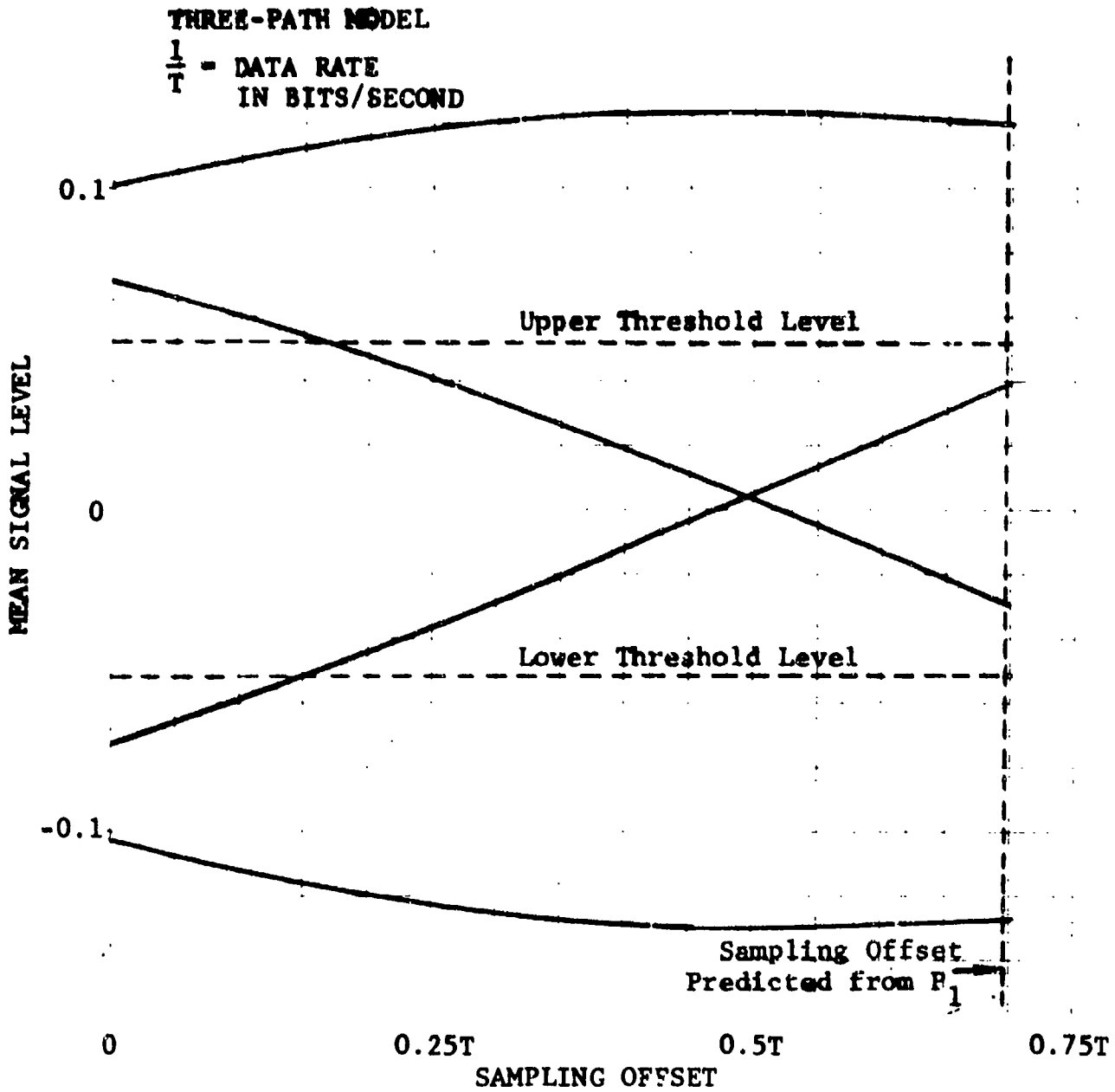

Figure 4.34 Mean "Eye" Pattern 30-dB Fade("Bad" Channel)

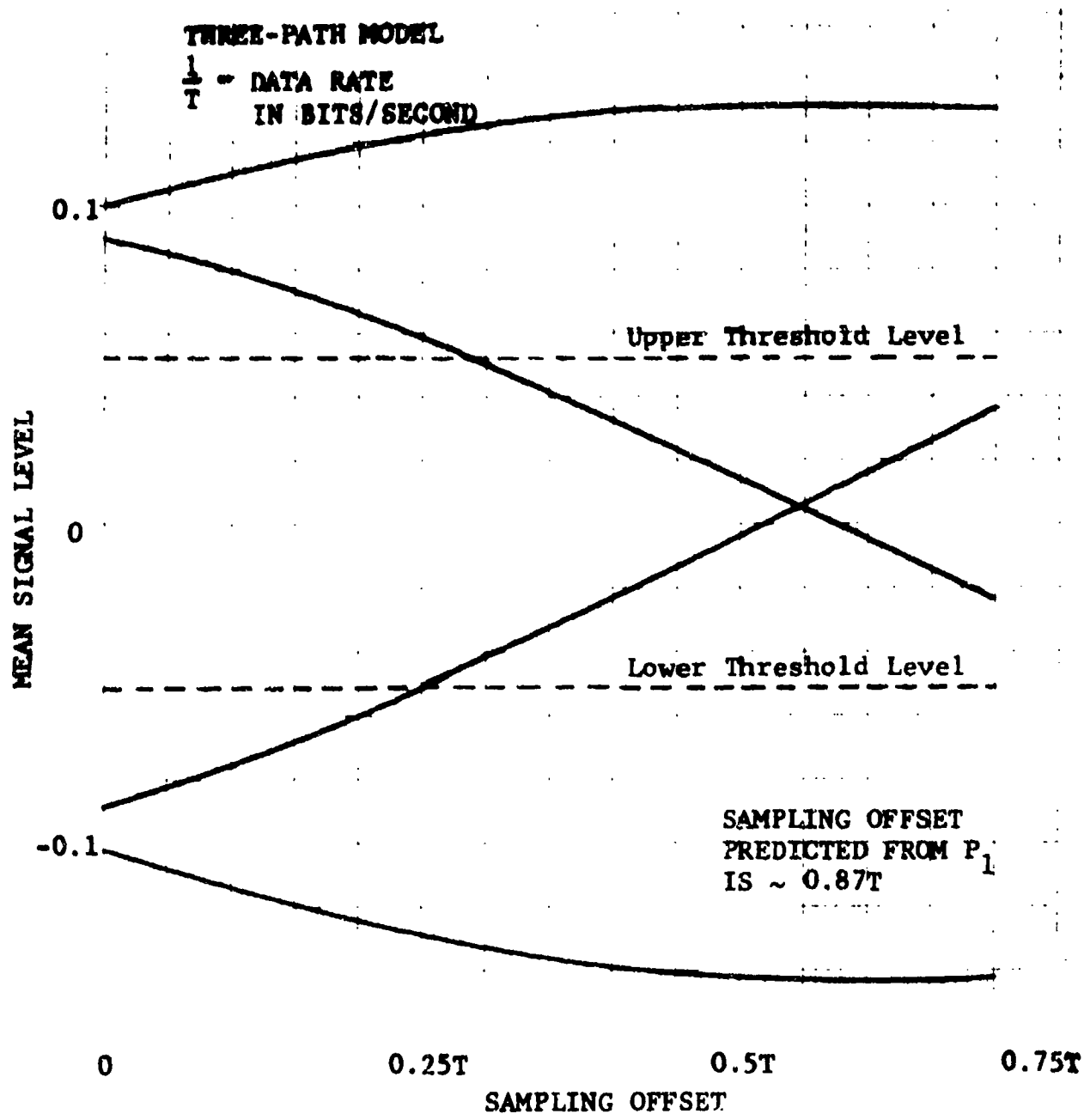

Figure 4.35 Mean "Eye" Pattern 32-dB Fade("Bad" Channel)

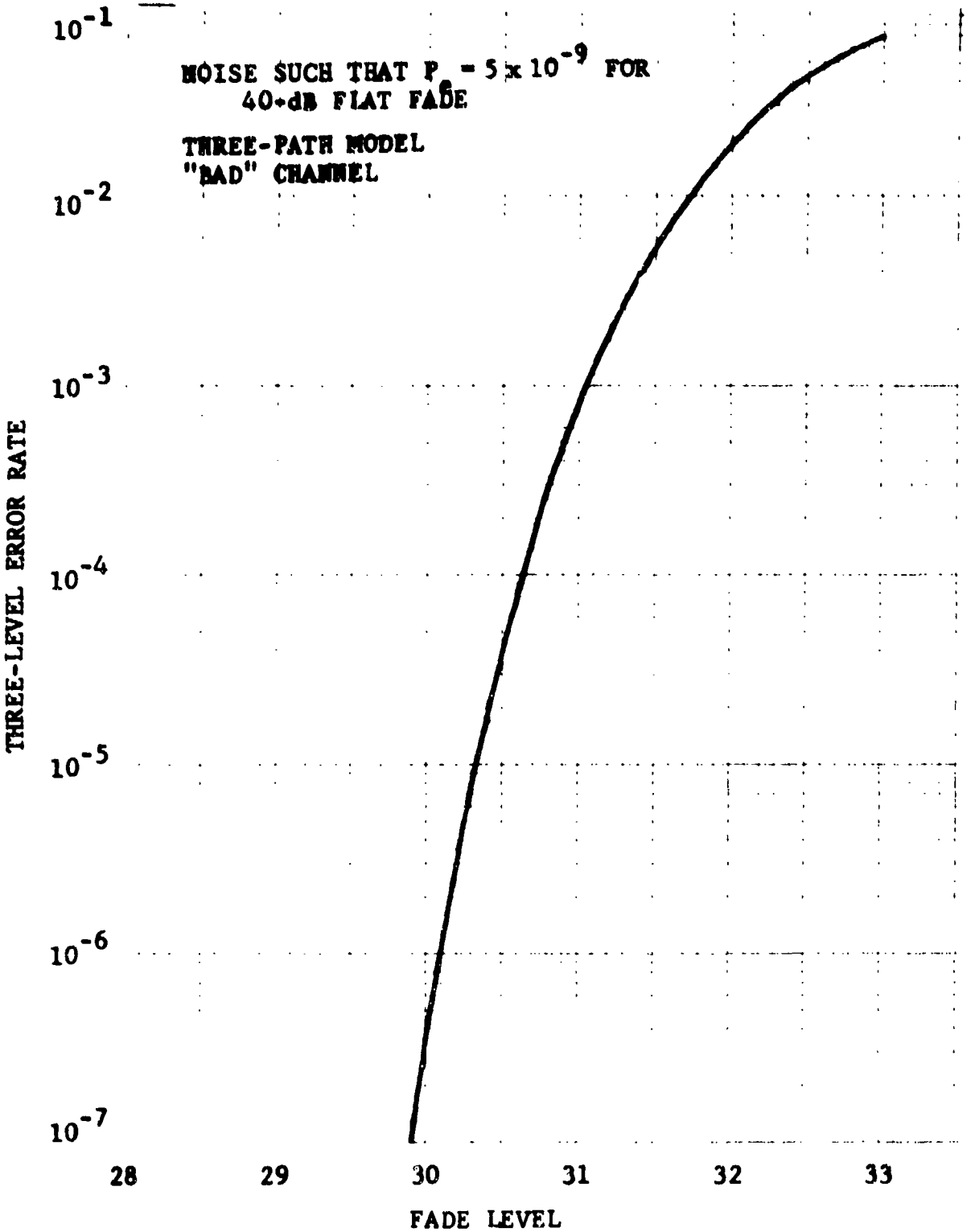

Figure 4.36 Three-Level Error Rate with Perfect Delay Tracking (Sampling Time Adjusted for Minimum P_e)

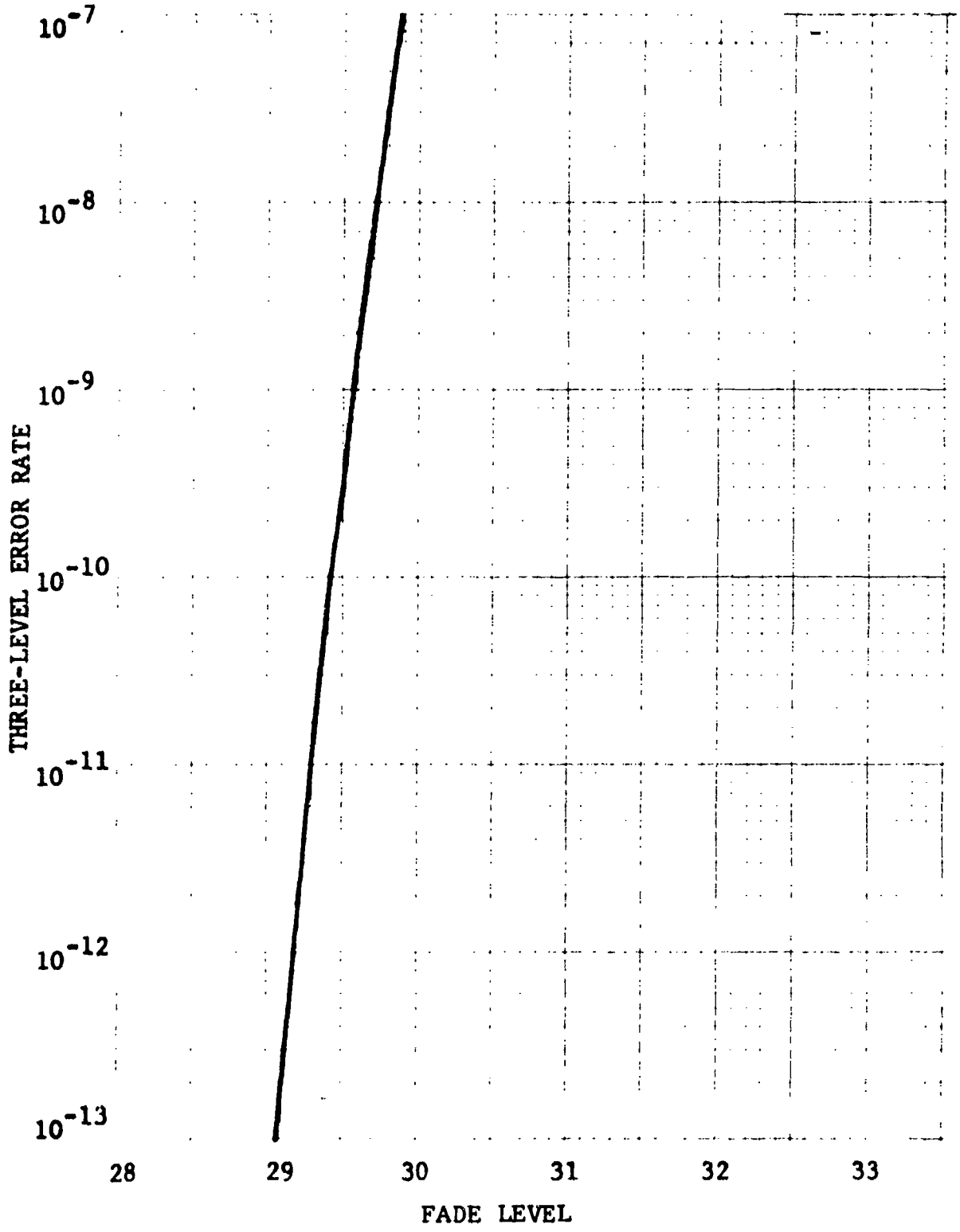

Figure 4.36 (Continued)

It should be mentioned that delay tracking algorithms do not always sample to minimize error rate, but might converge to the mean zero crossing or some other easily implementable criteria. Therefore, the degradation may be more severe than that indicated in Fig. 4.36.

4.5.4.4 Error Rate Sensitivity

In order to determine the accuracy with which the channel parameters and noise standard deviation must be estimated to assess performance, the sensitivity of error rate to parameter variations was investigated. Since error rate is dependent upon sampling offset and variations in channel parameters and noise change the minimum error rate sampling time, to investigate the sensitivity the parameters were varied one at a time and the sampling time was adjusted to minimize the error rate.

The sensitivity of error rate to parameter variations is shown in Fig. 4.37. As shown in this figure, for a 30-dB fade the error rate is very insensitive to variations in P_2, and variations of about $\pm$ 10% from nominal values in P_3 or σ_n are required to give a total excursion of an order of magnitude in error rate. However, variations of $\pm$ 1% in P_1 can produce an order of magnitude variation in error rate. These sensitivities are the worst because a 30-dB fade of the "bad" channel constitutes the "threshold" of operation for performance versus P_1 and P_3.

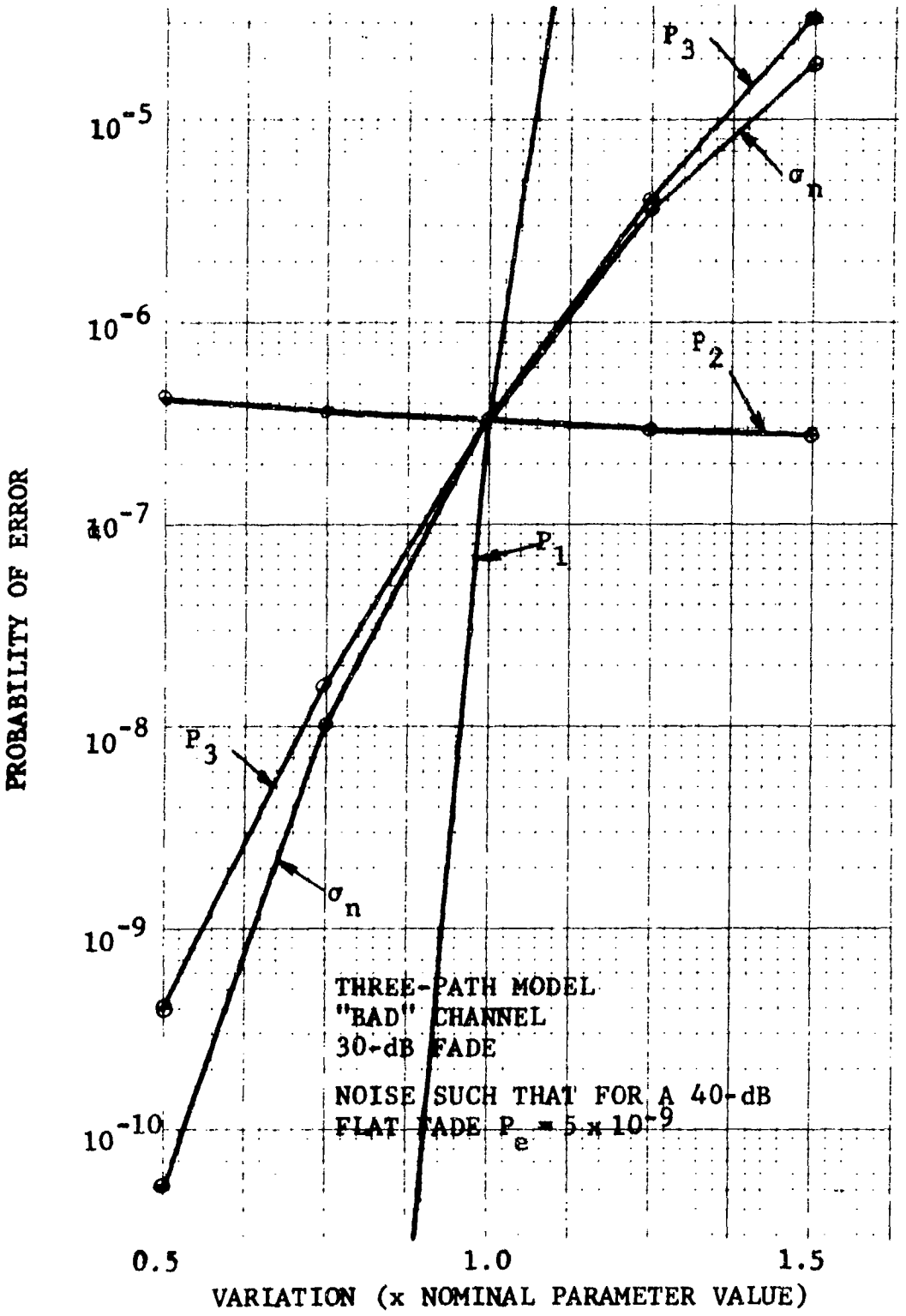

Figure 4.37 Error Rate Sensitivity (Sampling Time Adjusted for Minimum P_e)

4.6 Implementation Considerations

4.6.1 Introduction

This section discusses implementation of the adaptive channel estimator. The implementation requirements focus upon determining the number of multiplications per iteration and the total number of storage locations required to implement the adaptive channel estimator with the various tradeoffs previously mentioned.

Our goal in this section is to present the hardware requirements when the adaptive channel estimator assumes any one of the configurations used in the examples of Section 4.4. Also, the software required to assess system performance using the error rate calculation method outlined in Section 4.5 will be investigated.

4.6.2 Adaptive Channel Estimator Configurations

For the examples of Section 4.4, ten adaptive channel estimator configurations were used. Many of these differed only by varying the step size, while there were also major differences resulting from changing the channel model or pickoff point. The salient feasures of each of the ten configurations are summarized in Table 4-2.

In terms of implementation complexity, the number of multiplications per iteration required to estimate the received baseband signal can be found using Eqs. (4.10), (4.12), or (4.15) for the appropriate adaptive channel estimator configuration. For the quadratic channel model with the discriminator output being estimated, it follows from Eq. (4.10) that five multiplications per iteration are required (four to multiply $\hat{P}_q$ and S_q, and one to find S_3) to estimate the received baseband signal. With the cubic channel model being used to estimate the discriminator output, from Eq. (4.12) we note that 12 multiplications per iteration are required (eight to multiply $\hat{P}_q$ and S_q and one to find each of S_3, S_5, S_6, and S_7) to estimate the received baseband signal. To estimate the receive filter output using the quadratic channel model will require [from Eq. (4.15)] four multiplications per iteration (four to multiply $\hat{P}_q$ and τ_q). From Eq. (4.14), Y_3 will not require a multiplication (as was required to find S_3), but will require more storage. This storage increase will be discussed below. Finally, the multiplications per iteration required to find the estimate of the received baseband signal is also applicable if a timing parameter is being estimated.

Next, the number of multiplications per iteration required to update the channel parameter estimates will be determined. For the LMS adaptation algorithm, Eq. (4.17) is applicable, and two

TABLE 4-2

ADAPTIVE CHANNEL ESTIMATOR CONFIGURATIONS

Adaptive Channel Estimator Configuration Number	Channel Model	Pickoff Point	Adaptation Algorithm	Normalized Step Size (δ)	Timing Parameter Estimation
1	Quadratic	Discriminator Output	LMS	0.002	No
2	Quadratic	Discriminator Output	LMS	0.01	No
3	Cubic	Discriminator Output	LMS	0.002	No
4	Cubic	Discriminator Output	LMS	0.01	No
5	Cubic	Discriminator Output	BR	0.01	No
6	Cubic	Discriminator Output	LMS for P_i BR for τ	0.002	Yes
7	Cubic	Discriminator Output	LMS for P_i BR for τ	0.01	Yes
8	Quadratic	Shaping Filter Output	LMS	0.002	No
9	Quadratic	Shaping Filter Output	LMS	0.01	No
10	Quadratic	Shaping Filter Output	BR	0.01	No

multiplications are required per iteration for each channel parameter (2Δ times ϵ times G_q). Therefore, for the quadratic channel model and the LMS adaptation algorithm, eight (2×4 channel parameters) multiplications per iteration are required to update the channel parameter estimates. For the cubic channel model, 16 multiplications per iteration are required.

When the BR adaptation algorithm is used to update the channel parameter estimates, Eq. (4.21) is applicable. From this equation, one multiplication is required per iteration for each channel parameter [Δ_B times $\text{sgn}(\epsilon)G_q$]. Therefore, if the BR is used, four multiplications per iteration are required for the quadratic channel model, while the cubic channel model requires eight.

For adaptive channel estimator configurations 6 and 7 (see Table 4-2), the estimate of the timing parameter is updated using Eq. (4.33). To evaluate

$$\sum_{q=0}^{N} P_q(k)\, \dot{S}_q[kT + \hat{\tau}(k)] \tag{4.52}$$

for the cubic channel model ($N = 7$) requires evaluating $\dot{S}_q(t)$. From (4.11) and (4.13), we can write

$$\begin{aligned} S_3(t) &= S_0(t)\, S_1(t) \\ S_5(t) &= S_0^2(t)\, S_1(t) \\ S_6(t) &= S_1^2(t) \\ S_7(t) &= S_0(t)\, S_2(t) \end{aligned} \tag{4.53}$$

where the above can be found using four multiplications per iteration as was noted above. The $\dot{S}_q(t)$ that requires multiplications to be evaluated are:

$$\begin{aligned} \dot{S}_3(t) &= S_1^2(t) + S_0(t)\, S_2(t) \\ \dot{S}_5(t) &= 2S_0(t)\, S_1^2(t) + S_0^2(t)\, S_2(t) \\ \dot{S}_6(t) &= 2S_1(t)\, S_2(t) \\ \dot{S}_7(t) &= S_1(t)\, S_2(t) + S_0(t)\, S_4(t) \end{aligned} \tag{4.54}$$

From Eqs. (4.53) and (4.54), $\dot{S}_3(t)$ requires no additional multiplications, $\dot{S}_5(t)$ requires two additional multiplications $\{[2S_3(t) + S_7(t)]S_0(t)\}$, $\dot{S}_6(t)$ requires one additional multiplication [after $S_1(t)S_2(t)$ is found in evaluating $S_7(t)$], and $S_7(t)$ requires two additional multiplications. Therefore, to find $\dot{S}_q(t)$ requires five additional multiplications per iteration. To find the sign of the sum given in Eq. (4.52) requires eight more multiplications. Therefore, to update the timing parameter will require 13 additional multiplications per iteration (8 + 5). If this timing parameter is updated using only $\dot{S}_q(t)$ for q = 0,1,2,3, then only four multiplications per iteration will be required and a substantial implementation reduction will result with possibly only a small reduction in performance. Table 4-5 presents a summary of the required number of multiplications per iteration for each adaptive channel estimator configuration.

The storage requirements for each of the adaptive channel estimator configurations will now be found. For this computation we will assume that the pulse shape is essentially nonzero over M pulse intervals and, thus, the sums in Eqs. (4.11) and (4.13) are sums over M values of n. The stored pulse shape information will be found first. For the quadratic channel model, $h_T(\cdot)$, $\dot{h}_T(\cdot)$, and $\ddot{h}_T(\cdot)$ must be stored if the discriminator output is estimated. Therefore, if the timing parameter is not estimated, 3M storage locations are required. The cubic channel model also requires $\dddot{h}_T(\cdot)$, yielding a requirement for 4M storage locations.

If the timing parameter is to be estimated, the cubic channel model is used, and if Δ_B [see Eq. (4.33)] is expressed as a fraction of a pulse interval, then approximately $4M/\Delta_B$ storage locations are required if no interpolation between pulse shape entries is used. Interpolation can be used to reduce the storage requirements at the expense of increasing the processing burden.

Estimation of the receive filter output using the quadratic channel model requires finding $Y_q(t)$ as given by Eq. (4.14). Finding $Y_q(t)$ for q = 0, 1, 2 requires 3M storage locations, while $Y_3(t)$ requires $M^2/2$ storage locations. The total number of storage locations required is then $3M + (M^2/2)$.

Table 4-4 summarizes the storage requirements for the adaptive channel estimator configurations. Also presented in this table is the total number of multiplications per iteration required (from Table 4-3) as well as the approximate number of iterations required for convergence (from examples of Section 4.4).

TABLE 4-3

NUMBER OF MULTIPLICATIONS PER ITERATION REQUIRED BY ADAPTIVE CHANNEL ESTIMATOR CONFIGURATIONS

Adaptive Channel Estimator Configuration Number	Multiplication Per Iteration Required To Find Signal Estimate	Multiplication Per Iteration Required To Update Parameter Estimates	Total Number of Multiplications Per Iteration
1	5	8	13
2	5	8	13
3	12	16	28
4	12	16	28
5	12	8	20
6	12	29 (20*)	41 (32*)
7	12	29 (20*)	41 (32*)
8	4	8	12
9	4	8	12
10	4	4	8

*With timing parameter adaptation using only quadratic channel parameters.

For LOS links, significant channel variations usually do not occur over time frames of less than a sizable fraction of a second. To illustrate the speed of processing required, consider configuration 1 (quadratic channel model without timing estimation) and assume one second required for accurate tracking during fading conditions. Then, approximately $1.6 \times 10^3 \times 13 = 2.08 \times 10^4$ multiplications per second are required. This should not present a severe implementation burden. In fact, the only severe implementation requirement would occur by implementing the adaptive channel estimator with timing parameter estimation. This would require (for configuration 7) approximately 6.4×10^5 multiplies per second which implies that the channel estimator may have to use parallel processing in order to implement this configuration. It should be noted that, due to the severe implementation restriction inflicted by timing estimation and the limited effort expended upon the problem, more study of this problem is recommended.

In order to implement the adaptive channel estimator, the received baseband signal (either the discriminator or receive filter outputs) must be A/D-converted to generate the error signal necessary to update the channel parameter estimates. Assuming about one second is necessary for convergence, and noting that one sample of the received baseband signal is required for each iteration, then from Table 4-4 the range of sampling rates required for the ten estimator configurations fall in the range of 400 to 60,000 samples per second. Except for the 60,000 samples per second rate, the sampling rate is well within the range of today's inexpensive 12-bit A/D converters.

4.6.3 Error Rate Computation

Expressions for computing the three-level error rate for a duobinary FM system were derived in Section 4.5 in terms of the quadratic channel model parameters. The proposed adaptive channel estimator will assess performance by programming these expressions. The procedure for evaluating the error rate involves a truncated pulse train approximation in which the largest N_p intersymbol interference terms are used to find four probabilities [see Eq. (4.47)]. This involves finding approximately 2^{N_p+2} error functions. For large N_p (about 8 to 12), it may be desirable to use a table lookup (e.g., Tables 7-2 and 7-3 of Ref. [4.24]). Such a table lookup approach would require about 400 storage locations and approximately five multiplications per error function.

TABLE 4-4

SUMMARY OF STORAGE, MULTIPLICATIONS, AND CONVERGENCE REQUIREMENTS

Adaptive Channel Estimator Configuration Number	Pulse Shape Storage Requirements (No Interpolation for Timing Estimation)	Total Number of Multiplications Per Iteration	Approximate Number of Iterations for Convergence
1	3M	13	1.6×10^3
2	3M	13	4.0×10^2
3	4M	28	10^4
4	4M	28	2.0×10^3
5	4M	20	4.0×10^3
6	$4M/\Delta_B$	41 (32*)	6.0×10^4
7	$4M/\Delta_B$	41 (32*)	2.0×10^4
8	$3M + (M^2/2)$	12	3.5×10^3
9	$3M + (M^2/2)$	12	1.4×10^3
10	$3M + (M^2/2)$	8	1.4×10^3

*With timing parameter adaptation using only quadratic channel parameters.

M is the number of significant interfering data bits

Δ_B is timing parameter step size

Therefore, assuming N_p equals 12, $2^{14} \times 5 \approx 20{,}000$ multiplications for each error rate calculation. Since there does not appear to be a need to estimate the error rate more frequently than every second, at most 20,000 multiplications per second are required. Twenty thousand multiplies per second correspond to 50 microseconds per multiply. Modern minicomputers, such as the Data General Nova Series or the PDP-11, with hardware multiply/divide, have multiplication times in the range from 5 to 20 microseconds. Thus, it appears that a safety factor of about 2.5 is available if a minicomputer is available to perform the performance assessment.

The above discussion involves 16-bit times 16-bit multiplications/divisions where the exponenets in the lookup tables have been carefully manipulated.

4.6.4 Trial Implementation of Adaptive Channel Estimator

All of the channel estimator configurations require a mixture of specialized digital hardware for simple repetitive high-speed calculations and a small minicomputer for the relatively complex but low-speed calculations required for data evaluation and display. The iterative procedures described in Table 4-4 are performed by a hardware preprocessor.

The hardware preprocessor is different for each estimator configuration. The higher-speed processors can be designed to allow performance of the lower-speed procedures, but this would have no benefit in an operational system. A detailed trial design has been conducted for configuration 1 described in Table 4-2.

The trial design processor performs 200,000 iterations per second. The variables of the continuing iterative procedure are sampled by a minicomputer at a rate of approximately 120 samples per second. The minicomputer then processes and displays the data. The display update rates are selected for the convenience of the operator.

The implementation is presented in Figure 4.38 and its performance is as follows. The channel estimator contains three digital filters which estimate the $S_i(t)$, $i = 0,1,2$, as defined in Eq. (4.11). The $h_T(\cdot)$, $\dot{h}_T(\cdot)$, and $\ddot{h}_T(\cdot)$ are 12-bit constants stored in a read-only memory. This memory can be easily altered. The 16-bit outputs from the three filters are sampled at a 200-kHz rate and processed by a reasonably flexible digital signal processor which performs the calculations defined in Eqs. (4.10) and

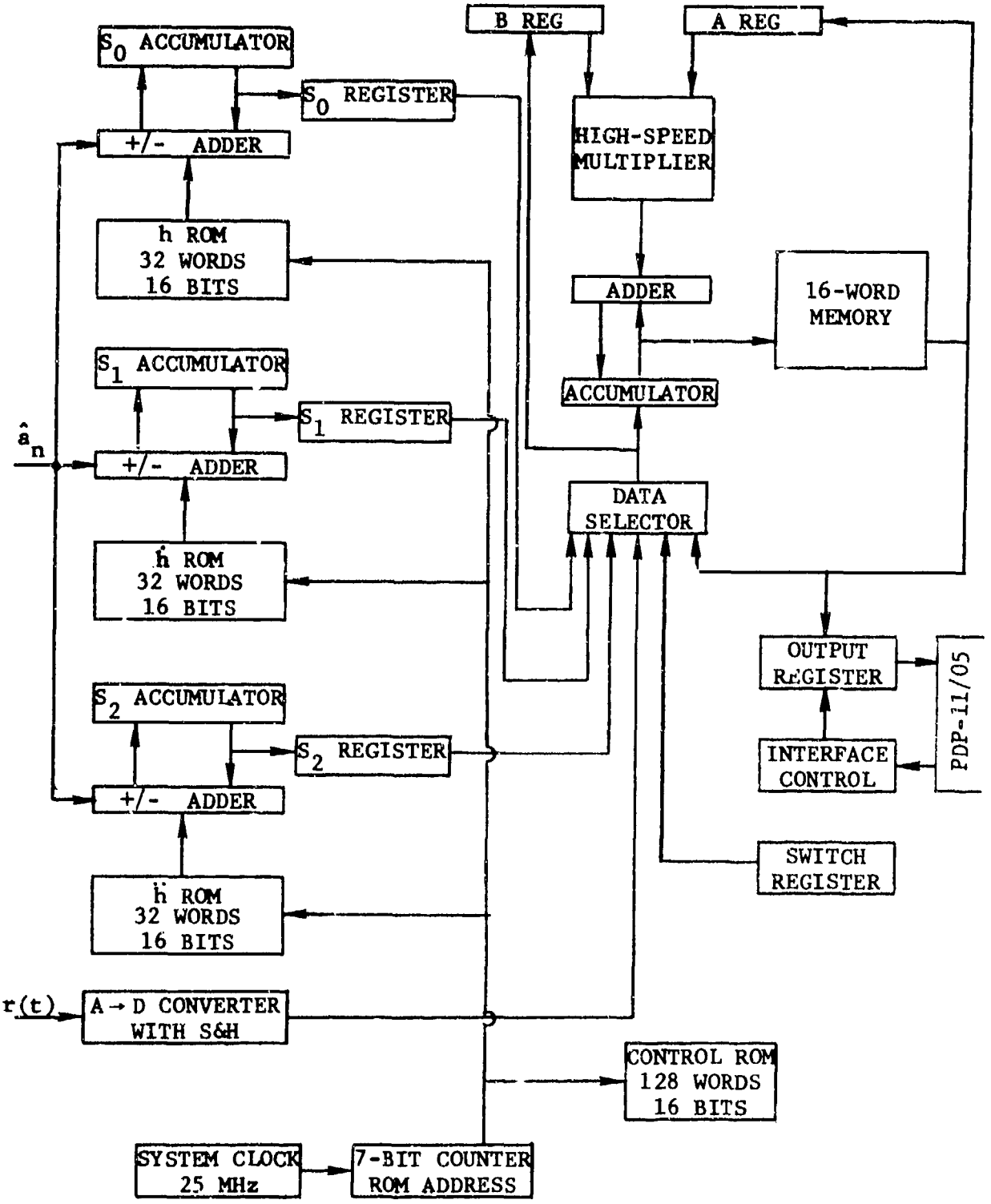

Figure 4.38 Trial Implementation Block Diagram for Nonlinear Adaptive Channel Estimator

(4.17). This processor maintains estimates of P_0, P_1, P_2, and P_3 which are updated every 5 μs. The output from this processor is sampled by a PDP-11/05 minicomputer with the sampling rate entirely under minicomputer control. The minicomputer processes the channel state estimates, using a FORTRAN program, and provides all required performance information on a CRT display.

REFERENCES FOR SECTION 4

[4.1] E. Bedrosian and S. O. Rice, "Distortion and Crosstalk of Linearly Filtered, Angle-Modulated Signals," Proc. IEEE, January 1968, pp. 2 - 13.

[4.2] P. A. Bello and B. Nelin, "The Effects of Frequency Selective Fading on Intermodulation Distortion and Subcarrier Phase Stability in Frequency Modulation Systems," IEEE Trans. on Comm. Systems, March 1964, pp. 87 - 101.

[4.3] T. G. Cross, "Intermodulation Noise in FM Systems Due to Transmission Deviations and AM/PM Conversion," BSTJ, December 1966, pp. 1749 - 1773.

[4.4] G. J. Garrison, "Intermodulation Distortion in Frequency-Division-Multiplex FM Systems - A Tutorial Summary," IEEE Trans. on Comm. Tech., April 1968, pp. 289 - 303.

[4.5] M. L. Lion, "Noise in an FM System Due to an Imperfect Linear Transducer," BSTJ, November 1966, pp. 1537 - 1561.

[4.6] A. Mircea, "Intermodulation Noise Theory," Proc. IEEE (corres.), October 1966, pp. 1463 - 1465.

[4.7] S. O. Rice, "Distortion Produced by Band Limitation of an FM Wave," BSTJ, May-June 1973, pp. 605 - 626.

[4.8] S. O. Rice, "Second and Third Order Modulation Terms in the Distortion Produced when Noise Modulated FM Waves are Filtered, BSTJ, January 1969, pp. 87 - 141.

[4.9] A. J. Rainal, "Computing Distortion in Analog FM Communication Systems," BSTJ, May-June 1973, pp. 627– 648.

[4.10] P. Roma, "More on Intermodulation Noise in FDM-FM Radio Relay Systems," IEEE Trans. on Comm., September 1974, pp. 1361 - 1368.

[4.11] Defense Communications Agency, "Pulse Code Modulation (PCM) Time Division Multiplex (TDM) System Design Verification Test Program," Final Report, February 1972.

[4.12] E. R. Kretzmer, "Binary Data Communication by Partial Response Transmission," Conference Record of 1965 IEEE Annual Convention, pp. 451 - 455.

[4.13] A. Lender, "The Duobinary Technique for High Speed Data Transmission," IEEE Trans. on Comm. and Elect., May 1963, pp. 214 - 218.

[4.14] R. W. Lucky, J. Salz, and E. J. Weldon, Jr., Principles of Data Communication, McGraw-Hill, New York, 1968.

[4.15] A. Sekey, "An Analysis of the Duobinary Technique," IEEE Trans. on Comm. Tech., April 1966, pp. 126 - 130.

[4.16] F. Magee and J. Proakis, "Adaptive Maximum-Likelihood Sequence Estimation for Digital Signaling in the Presence of Intersymbol Interference," IEEE Trans. on Info. Theory, January 1973, pp. 120 - 124.

[4.17] VICOM T Digital Multiplexer, Preliminary Terminal Description, VICOM Telecommunications Division, Vidar Corp., January 1971.

[4.18] P. A. Bello, "Characterization of Randomly Time-Variant Linear Channels," IEEE Trans. on Comm. Systems, December 1963, pp. 360 - 393.

[4.19] A. Gersho, "Adaptive Equalization of Highly Dispersive Channels for Data Transmission," BSTJ, January 1969, pp. 55 - 70.

[4.20] J. G. Proakis and J. H. Miller, "An Adaptive Receiver for Digital Signaling Through Channels with Intersymbol Interference," IEEE Trans. on Info. Theory, Vol. IT-15, July 1969, pp. 484 - 497.

[4.21] T. J. Schonfeld and M. Schwartz, "A Rapidly Converging First-Order Training Algorithm for an Adaptive Equalizer," IEEE Trans. on Info. Theory, Vol. IT-17, July 1971, pp. 431 - 439.

[4.22] A. Ungerboeck, "A Theory on the Convergence Process in Adaptive Equalizers," Proc. Int. Conf. on Comm., 1972, pp. 22-6 - 22-11.

[4.23] A. Gersho, "Adaptive Filtering with Binary Reinforcement," Proc. IEEE Int. Symp. on Info. Theory, February 1972, pp. 94 - 95.

[4.24] M. Abramowitz and I. Stegun, Handbook of Mathematical Functions With Formulas, Graphs, and Mathematical Tables, National Bureau of Standards, Washington, D.C., 1972.

SECTION 5

APPLICATION TO TROPOSCATTER LINKS

Troposcatter links are used in addition to LOS links in the Defense Communication System. They differ in a fundamental way from LOS links in their propagation characteristics. The method of propagation involved is over-the-horizon scattering from inhomogeneities in the atmosphere dielectric constant. Due to this method of propagation the troposcatter link is always fading and dispersive, in contrast to the LOS link, which is usually non-fading and non-dispersive.

The rapidity of fading of a channel is characterized by a parameter called the Doppler spread which is the spectral width of a received carrier (defined in an appropriate sense). For a given link the Doppler spread can vary over an order of magnitude or more due to variations in wind speed and propagation mechanisms within the common volume. For a given beamwidth, the fading rate will generally increase with carrier frequency. For a 1-GHz carrier frequency and a typical set of link parameters, rms Doppler spreads varying from 0.1 - 2 Hz may be expected while an increase in operating frequency to 10 GHz will result in an approximate tenfold increase in this range of Doppler spreads. Doppler spreads for LOS links would be measured in milliherz.

There are very few measurements of multipath spread. From what has been measured, variations in multipath spread appear to be less severe, varying over a range of around 3 to 1. For path lengths and parameters of interest, the predicted average rms multipath spread for DCS links can vary from a very small fraction of a microsecond for the shorter paths to a substantial fraction of a microsecond at the longer paths.

Path losses are high for troposcatter communications and hourly median path loss fluctuations can easily vary by 30 dB or more over a year. Thus, an attempt is made to provide sufficient power at the higher path losses, to obtain some minimum average SNR, say 15 dB, resulting in large swings in hourly median SNR during a year. Standard procedures have been developed by NBS (TN 101 and 102) for estimating path loss characteristics as a function of link parameters, geography, time block, etc.

Large transmitter powers (10 kW for the average link), large antennas (30 to 60-ft diameter dish for the average link), and diversity reception (fourth-order typically for stategic links) are required. To obtain the required large average powers essentially cw operation is required. Both space and frequency diversity are used. Multichannel radio telephony is carried out by FDM/FM (frequency-division-multiplex and frequency modulation). Typically, 60 analog voice channels may be carried by a tropo-scatter link. Presently, data transmission takes place through a voice channel slot or, for higher data rates, through a whole group (12 channels). This procedure is an inefficient mode of data transmission both from the utilization of bandwidth and power and, concurrent with the DCS PCM-TDM upgrade, consideration has been given to more efficient means of high-speed data transmission.

Except for the GRC-143 built by ITT, only experimental models of high-speed TDM modems have been built. These modems may be classified according to whether the signaling pulses have been designed to suffer small distortion from the channel or not. Modems in the former class, with one exception, have been around 1 Mb/s and use incoherent detection techniques. The measured and modeled performance of a few of these modems is presented in [5.1]. The exception is a 3 Mb/s coherent FSK/PSK modem [5.2]. This modem uses synchronized time gates to eliminate portions of received pulses contaminated by intersymbol interference. After the time gates, a maximum likelihood (i.e., minimum probability of error) demodulator is constructed. The 3 Mb/s is achieved by transmitting a 1 μsec pulse having one of four frequencies and one of two phases. Time gates of 1/2 μsec duration are used providing protection against 1/2 μsec of multipath.

Subsequent to the development of the FSK/PSK modem, new techniques have been proposed and are under development which use pulses that can be highly distorted by the propagation medium. The object of these systems is to obtain a performance close to that achievable by a matched filter system where the receiver is matched to the received distorted pulse, and intersymbol interference has been made negligible. Thus, if a particular received pulse is $w_\ell(t)$, for the ℓth diversity channel, the error rate of such a system at the time of reception would depend upon an energy/bit to noise power density ratio of

$$E_b/N_0 \sim \sum_{\ell=1}^{L} \int |w_\ell(t)|^2 \, dt \qquad (5.1)$$

Assuming the troposcatter channel can be modeled by a tapped delay line with K independently fading paths, one may show that approximately

$$\int |w_\ell(t)|^2 \, dt \sim \sum_{k=1}^{K} |g_k^{(\ell)}|^2 \qquad (5.2)$$

where $g_k^{(\ell)}$ is the value of the kth complex gain in the tapped delay line model of the ℓth diversity channel at the time of reception. Because the $\{g_k^{(\ell)}\}$ are fluctuating independently, the matched filter output has the same mathematical properties as the output of a maximal ratio diversity combiner with K paths. Such diversity has gone by several names: in-band, inherent, multipath, and implicity diversity. We shall use the terminology "in-band."

There are three modem techniques under development for achieving this in-band diversity. The one which has been conceived and built by Raytheon involves the transmission of QPSK pulses at a duty cycle of 50%, resulting in a 3-dB power loss at the transmitter. The receiver attempts to set up a filter matched to the transmitted pulse shape and thus achieve the benefits of in-band diversity.

The one presently under development by Sylvania for the Army utilizes QPSK transmission with 100% duty cycle and an adaptive feedback equalizer at the receiver to minimize mean squared error. Data rates up to 12.6 Mb/s are to be achieved. Some simulations [5.3] have indicated that an adaptive equalizer, under some ideal conditions, can yield a performance close to the intersymbol interference-free matched filter receiver. However, the modem actually being built by Sylvania has a backoff of around 5 dB from matched filter performance according to theoretical predictions by Signatron [5.4].

The third approach, currently being implemented by CNR, Inc., is a 100% duty cycle minimum error probability receiver implemented with the use of an adaptive Viterbi algorithm. This modem is predicted to operate at close to the performance of the ideal matched filter receiver. Field testing is scheduled for July 1975.

Assuming that one or more of these can extract the in-band diversity, it is clear that the performance of the modem will vary with the multipath spread since the number of independent paths is approximately K = WL, where W is the bandwidth occupied and L is the multipath spread of the channel. For sufficiently small multipath spread, the in-band diversity will disappear. The demodulator would be designed to handle some maximum multipath spread, as determined from measurements or theoretical predictions. For multipath spreads exceeding the design value, intersymbol interference will appear causing an "irreducible" error probability.

Another form of in-band diversity, which we shall call "time diversity," can be achieved on troposcatter links for any modem by use of coding techniques. This class of techniques has been studied by CNR [5.5], and CNR is currently under contract [5.6] to implement and field test such techniques. The basic concept is one of interleaving bits or blocks of bits to have the coding constraints spread over a time interval encompassing several fades. This technique will improve in performance as the Doppler spread increases, but will show no benefit if the Doppler spread becomes too small.

The advanced modems are all coherent and use some form of channel measurement. If the Doppler spreads become too large, the channel measurements will degrade primarily because of fixed processing delays in the system. Thus, the phase corrections required in coherent processing will lag, causing an uncorrelated component of output to appear. This component acts like an effective additive noise and will result in an irreducible error probability.

Given a properly designed system, excessive multipath and Doppler spread that cause an irreducible error probability to dominate performance should be a rare event. However, even in the usual case where performance is limited by additive noise, it should be clear that for the in-band and time diversity systems the error rate will be determined by the amount of multipath and Doppler spread, since these parameters determine the degree of in-band and time diversity.

The use of the adaptive channel measurement technique at the transmitter with a TQU would be the same in principle for the troposcatter and LOS links. However the application at the receiving end, in the case of the MQU and RQU, would be considerably different than that described for the LOS link. In the first place, the parameterization of the propagation medium would have

to use the tapped delay line model discussed in Section 2.2.2.11 rather than the chain differentiator model. In the second place, since the demodulation process is complex, linear, and coherent for these advanced troposcatter modems, there is no intermodulation distortion introduced by the demodulator when it is operating properly. Complex in-phase and quadrature processing is involved. Thus the structure of the parameterized channel models used at the receiver of the troposcatter link for adaptive channel parameter measurement would differ grossly from the models described in this report for use at the receiver of the LOS link.

Because of the much more rapid fading on troposcatter links the number of iterations required to achieve a given rms parameter measurement error must be kept to an absolute minimum. To track the fades properly, the time span of the iterations should not exceed one millisecond at the higher operating frequencies. Since the highest baud rates involved in troposcatter data transmission are around 6 megabaud, a requirement of 6000 to 9000 iterations implies that the iterations have to occur at about the baud rate. It is unlikely that digital signal processing would be even possible at these rates.

An alternative approach that may be worth considering is based upon the fact that all advanced troposcatter modems must incorporate some form of channel measurement either explicitly or implicitly. These explicit or implicit channel measurements, which must follow the channel fluctuations, could be used as the basis for measurement of channel parameters. In the study, some work was initiated to evaluate this approach with respect to the adaptive equalizer troposcatter modem. However because of the greater importance of the LOS channel and the limited effort available, it was not possible to carry the investigation much further than assembling software for modeling the channel and adaptive equalizer receiver.

REFERENCES FOR SECTION 5

[5.1] P. A. Bello, L. Ehrman, D. S. Arnstein, "Modeling and Data Analysis-Short and Medium Range Troposcatter Tests," Technical Report RADC-TR-69-233, RADC, June 1969, p. 3-25, AD 862-767.

[5.2] P. A. Bello and J. W. Graham, "A High-Speed TDM Coherent FSK/PSK Digital Data Modem for Troposcatter Links," Record of the IEEE 1971 International Conference on Communications, pp. (2-18) to (20-24).

[5.3] P. Monsen, "Digital Transmission Performance on Fading Dispersive Diversity Channels," IEEE Trans. on Comm., Vol. COM-21, No. 1, January 1973.

[5.4] P. Monsen and S. D. Richman, "Adaptive Data Transmission Study," RADC Final Report, AD 768-999, August 1973.

[5.5] "Coding/Mux Overhead Study," Final Report by CNR, Inc. on RADC Contract No. F30602-73-C-0271, RADC-TR-75-71, (AD009174).

[5.6] "Troposcatter Interleaver," (F30602-74-C-0133), Current Contract Between CNR, Inc. and RADC, RADC-TR-75-19, (AD008523).

APPENDIX A

NOISE STATISTICS IN FM LOS SYSTEMS

1. Introduction

In this appendix we consider the problem of determining noise statistics of a duobinary FM LOS system. The SNR's at the discriminator and shaping filter outputs will be determined as a function of carrier-to-noise ratio and IF bandwidth. Furthermore, it will be shown that (neglecting Rice's click noise [1]) the noise at the discriminator output can be separated in two independent components, one Gaussian distributed and the other having a modified Bessel function distribution.

The strengths of the Gaussian and non-Gaussian noise components at the shaping filter output will be determined. Finally, the correlation function for the Gaussian noise component at the shaping filter output is presented. This correlation function was used in the simulation discussed in Section 4.3.3 and in Appendix C.

2. System Description

Figure 1 is a functional block diagram of that portion of the receiver that will be examined in this appendix. The performance of the receiver is as follows. The IF signal is filtered and frequency-demodulated and the resulting baseband signal is passed through a receive shaping filter that reduces the noise and completes the duobinary pulse shaping.

For analysis purposes, the IF filter will be assumed to be an ideal bandpass filter; that is, a frequency response given by

$$G(f) = \begin{cases} 1 \ , & \text{if } |f-f_{IF}| \le \frac{\beta}{2} \\ \\ 0 \ , & \text{otherwise} \end{cases} \qquad (1)$$

(where f_{IF} is the IF frequency) will be assumed.

The receive shaping filter reduces the noise and together with a transmit shaping filter perform the duobinary pulse shaping.

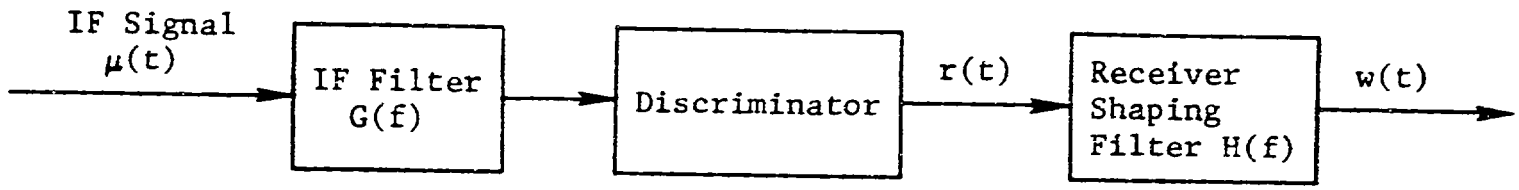

Figure 1 System Block Diagram

The transmit and receive shaping filters will be assumed to have a frequency response given by

$$H(f) = \begin{cases} \sqrt{T}\cos^{\frac{1}{2}}(\pi fT) & , \quad |f| \le \frac{1}{2T} \\ 0 & , \quad \text{otherwise} \end{cases} \tag{2}$$

where T is the symbol duration.

3. Discriminator Noise Theory

Rice [1] has considered the problem of determining the statistical properties of noise at the output of a discriminator. He has shown that under suitable conditions the noise at the discriminator output can be represented as the sum of Gaussian noise and a "click" noise with Poisson arrival times. At input SNR's of greater than 10 - 12 dB, the "clicks" occur so infrequently that they can be considered negligible. For many FM LOS systems, even deep fades (of ~ 40 dB) result in input SNR's greater than 10 - 12 dB and, therefore, for the present analysis we will consider that the click noise can be safely neglected.

The signal at the input to the IF filter is

$$\mu(t) = \mathrm{Re}\left\{\sqrt{\frac{2E}{T}}\, e^{j2\pi\varphi(t)+j2\pi F_{IF}t} + n(t)\right\} \tag{3}$$

where $\phi(t)$ is the baseband duobinary signal, E is the received energy per symbol, and n(t) is the noise. The noise n(t) is assumed to be white, Gaussian, zero-mean, and (two-sided) spectral density of $2N_0$ (N_0 is the one-sided spectral density of the real noise). The received signal power is E/T and the total noise power at the IF filter output is $4N_0\beta$. Hence, the signal-to-noise ratio at the discriminator input is

$$\rho = \frac{E}{4N_0\beta T} \tag{4}$$

For comparison purposes, it is advantageous to define a signal-to-noise ratio that does not depend upon the IF bandwidth. Therefore, we will define a carrier-to-noise ratio by

$$\rho_T = \frac{E}{N_0} \tag{5}$$

This is equivalent to evaluating ρ for an IF bandwidth (β) of $\frac{1}{4T}$.

From (3) we see that we can express $\mu(t)$ as

$$\mu(t) = R \cos\left[2\pi f_{IF} t + 2\pi\varphi(t) + \theta(t)\right] \tag{6}$$

Figure 2 is a graphical interpretation of Eq. (6), where $n_c(t)$ and $n_s(t)$ are the in-phase and quadrature components of $n(t)$ with respect to the frequency $f_{IF}+\dot{\varphi}(t)$. From this figure we note that the noise at the discriminator output is

$$n_D(t) = \frac{A}{2\pi} \frac{d}{dt} \tan^{-1} \frac{n_s(t)}{\sqrt{\frac{2E}{T}} + n_c(t)} \tag{7}$$

where A relates the discriminator input frequency to the output voltage. For our analysis, A is assumed to be a constant over the frequencies of interest and, for notational simplicity, will be normalized to 1. Therefore, n_D is given by

$$n_D(t) = \frac{1}{2\pi} \frac{d}{dt} \tan^{-1} \frac{n_s(t)}{\sqrt{\frac{2E}{T}} + n_c(t)} \tag{8}$$

In previous discriminator noise theory analysis (e.g., [1]), the noise was assumed to be small with respect to $\sqrt{\frac{2E}{T}}$. These assumptions then were used to approximate $n_D(t)$ by

$$\frac{1}{2\pi} \frac{\dot{n}_s(t)}{\sqrt{\frac{2E}{T}}} \tag{9}$$

The present analysis will not make the above simplifying approximation because it is of interest to determine the range of applicability of the above approximation, and the above approximation leads to some over-simplified results. In particular, it

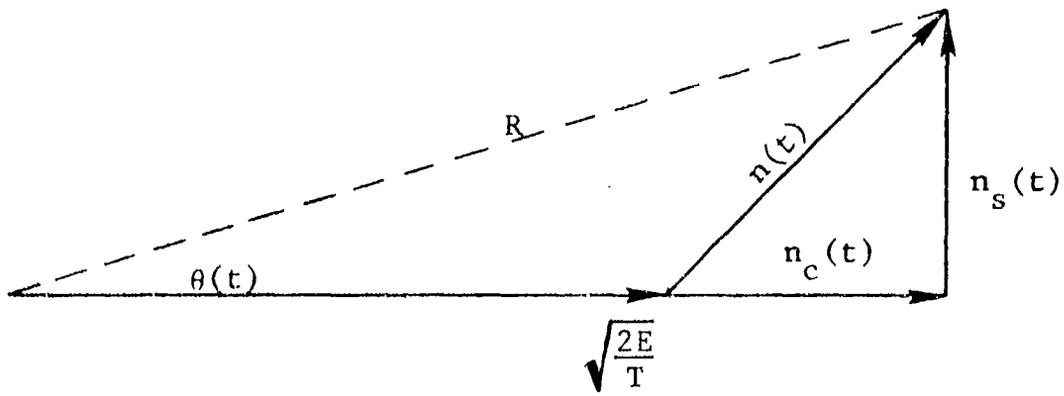

Figure 2 Graphical Interpretation of Equation (6)

will be shown later that use of (9) instead of (8) results in the SNR at the shaping filter output not being dependent on the IF bandwidth for $\beta > \frac{1}{2T}$.

We will assume that the noise is small with respect to $\sqrt{\frac{2E}{T}}$; however, two terms will be used to represent $n_D(t)$. Performing the indicated differentiation of (8) gives

$$n_D(t) = \frac{\frac{1}{2\pi}\left\{\sqrt{\frac{2E}{T}}\,\dot{n}_s(t) + \frac{d}{dt}\,n_s(t)n_c(t)\right\}}{\frac{2E}{T} + \sqrt{\frac{2E}{T}}\,n_c(t) + n_c^2(t) + n_s^2(t)} \tag{10}$$

For $\sqrt{\frac{2E}{T}}$ large with respect to the noise, we can closely approximate the noise at the discriminator output by terms involving $\sqrt{\frac{T}{2E}}$ and $\frac{T}{2E}$. This approximation yields

$$n_D(t) \approx \frac{\frac{1}{2\pi}\,\dot{n}_s(t)}{\sqrt{\frac{2E}{T}}} + \frac{\frac{1}{2\pi}\,n_s(t)\,\dot{n}_c(t)}{\frac{2E}{T}} \tag{11}$$

The first term of this approximation is the approximation given by (9). The second term is the non-Gaussian component.

Since n(t) is Gaussian, $n_s(t)$, $\dot{n}_s(t)$, and $\dot{n}_c(t)$ are also Gaussian. Also, since $n_c(t)$ and $n_s(t)$ are the in-phase and quadrature components of a narrowband Gaussian process whose spectral density in the narrowband is symmetric about its center, then $n_s(t)$ and $\dot{n}_c(t)$ are independent [2]. Furthermore, $\dot{n}_s(t)$ is independent of $\dot{n}_s(t)$ and $\dot{n}_c(t)$. Therefore, the noise at the discriminator output consists of two independent components, one of which is Gaussian and the second is the product of two independent zero-mean Gaussian processes.

We will first consider the Gaussian noise process given by

$$n_G(t) = \frac{\frac{1}{2\pi}\,\dot{n}_s(t)}{\sqrt{\frac{2E}{T}}} \tag{12}$$

Since $n_s(t)$ has zero-mean, it follows that

$$\overline{n_G(t)} = 0 \tag{13}$$

where the overbar denotes ensemble average.

The spectral density of $\dot{n}_s(t)$ is parabolic. In particular, we have

$$P_{\dot{n}_s(t)}(f) = P_{\dot{n}_c(t)}(f) = (2\pi)^2 N_0 f^2 \qquad |f| \leq \frac{\beta}{2} \tag{14}$$

The variance of the Gaussian noise component is

$$\sigma^2_{n_G} = \int_{-\frac{\beta}{2}}^{\frac{\beta}{2}} \frac{N_0 f^2}{\frac{2E}{T}}\, df \tag{15}$$

or

$$\boxed{\sigma^2_{n_G} = \frac{\beta^2}{96\rho}} \tag{16}$$

Equation (16) is the variance of the Gaussian noise component at the output of the discriminator. The variance of the Gaussian noise component at the output of the receive shaping filter is found by integrating its power spectrum.

$$\sigma^2_{n_0} = \int_{-\frac{1}{2T}}^{\frac{1}{2T}} \frac{N_0 f^2 T^2}{2E} \cos \pi f T\, df \tag{17}$$

or

$$\boxed{\sigma^2_{n_0} = \frac{\left[\frac{1}{4} - \frac{2}{\pi^2}\right]}{\pi T^2 4\rho\beta}} \tag{18}$$

where we have assumed that $\beta \geq \frac{1}{2T}$. This assumption is necessary for low distortion transmission of the duobinary signal.

The non-Gaussian noise term [given by the second term of (11)] will now be examined in greater detail. Defining

$$n_1(t) = \frac{\frac{1}{2\pi} n_s(t)\dot{n}_c(t)}{\frac{2E}{T}} \tag{19}$$

it follows that $\overline{n_1} = 0$ and the variance of $n_1(t)$ is

$$\sigma^2_{n_1} = \frac{\overline{n_c^2(t)}}{\frac{2E}{T}} \cdot \frac{\left(\frac{1}{2\pi}\right)^2 \overline{\dot{n}_c^2(t)}}{\frac{2E}{T}} \tag{20}$$

The second term of the above product is given by (16) and the first term can be shown to be equal to $1/8\rho$. Therefore,

$$\boxed{\sigma^2_{n_1} = \frac{\beta^2}{768\,\rho^2}} \tag{21}$$

To find the probability density function of n_1, we first write

$$n_1 = x\,y \tag{22}$$

where x and y are independent, zero-mean, Gaussian processes with standard deviations σ_x and σ_y, respectively. From [3], the probability density function of the product of two random variables is given by

$$f_{n_1}(\gamma) = \int_{-\infty}^{\infty} \frac{1}{|W|} f_{xy}\left(\frac{\gamma}{W}, W\right) dW \tag{23}$$

For the case at hand we have

$$f_{n_1}(\gamma) = \frac{1}{\pi\sigma_x\sigma_y}\int_{-\infty}^{\infty}\frac{1}{W}\exp\left(-\frac{\gamma^2}{2W^2\sigma_x^2}-\frac{W^2}{2\sigma_y^2}\right)dW \tag{24}$$

Using Eq. (3.478-4) on page 342 of [4], it follows that

$$f_{n_1}(\gamma) = \frac{1}{\pi\sigma_x\sigma_y}K_0\left[\frac{|\gamma|}{\sigma_x\sigma_y}\right] \tag{25}$$

where $K_0(\cdot)$ is the spherical modified Bessel function of order zero. For large x, $K_0(x)\approx 1.25\,x^{-\frac{1}{2}}e^{-x}$, while for small x, $K_0(x)\approx -\ell n\ x$.

Since $\sigma_{n_1} = \sigma_x\sigma_y$ and $\sigma_{n_1}^2$ is given by (21), then the probability density function of n_1 can be written as

$$\boxed{f_{n_1}(\gamma) = \frac{16\sqrt{3}\,\rho}{\pi\beta}K_0\left[|\gamma|\ \rho\,\beta^{-1}\,8\sqrt{3}\right]} \tag{26}$$

The statistical properties of the non-Gaussian noise at the output of the receive shaping filter cannot be completely determined because a general technique does not exist for finding the probability density function at the output of a filter in terms of input statistics. However, the variance of the non-Gaussian noise component at the output of the shaping filter can be determined. This is accomplished by first finding the power spectrum of n_1. Note that the correlation function of n_1 is

$$R_{n_1}(\tau) = \frac{T^2}{16E^2\pi^2}\ \overline{n_s(t)\dot{n}_c(t)n_s(t+\tau)n_c(t+\tau)} \tag{27}$$

Since the quadrature component of the narrowband complex Gaussian noise (and its derivative) are independent of the in-phase component (and its derivative), then

$$R_{n_1}(\tau) = \frac{T^2}{16E^2\pi^2} R_{n_s}(\tau)\, R_{\dot{n}_c}(\tau) \tag{28}$$

or, since $R_{\dot{n}_c}(\tau) = R''_{n_c}(\tau)$ [5], we can write

$$R_{n_1}(\tau) = \frac{T^2}{16E^2\pi^2} R_{n_s}(\tau)\, R''_{n_c}(\tau) \tag{29}$$

Since differentiation and multiplication in the τ domain correspond to multiplication by $j2\pi f$ and convolution, respectively, in the f domain, it follows that the power spectrum of n is

$$P_{n_1}(f) = \frac{T^2}{4E^2} \left\{ P_{n_s}(f) \otimes f^2 P_{n_c}(f) \right\} \tag{30}$$

where $\otimes$ denotes convolution and where

$$P_{n_s}(f) = P_{n_c}(f) = \begin{cases} N_0 & , \quad \text{if } |f| \le \frac{\beta}{2} \\ 0 & , \quad \text{otherwise} \end{cases} \tag{31}$$

Using (31) in (30), it follows that the power spectrum of the non-Gaussian noise at the discriminator output is

$$P_{n_1}(f) = \frac{\beta}{768\,\rho^2} \left\{ 1 - \frac{|f|}{\beta} + \frac{6f^2}{\beta^2} - \frac{4|f|^2}{\beta^3} \right\} \quad |f| \le \beta \tag{32}$$

The power spectrum P_N of the non-Gaussian noise at the output of the receive shaping filter [with frequency response given by (2)] is

$$P_N(f) = \begin{cases} T \cos(\pi f T)\, P_{n_1}(f) & , \quad |f| \le \frac{1}{2T} \\ 0 & , \quad \text{otherwise} \end{cases} \tag{33}$$

The variance can be found by integrating $P_N(f)$, which gives

$$\sigma_N^2 = \frac{\beta}{384\,\pi\rho^2}\left[1 - \frac{1.5}{\beta T} + \frac{3}{\pi\beta T} + \frac{1.5}{(\beta T)^2} - \frac{12}{(\pi\beta T)^2} - \frac{0.5}{(\beta T)^3} + \frac{12}{\pi^2(\beta T)^3}\right] \tag{34}$$

Equation (34) gives the variance of the non-Gaussian noise at the output of the receive shaping filter.

4. Signal Fluctuations

In this section the rms signal fluctuations at the discriminator output and at the receive shaping filter will be determined. The transmit filter will be assumed to have the frequency response of the receive filter [see Eq. (2)]. With $g(\tau)$ the transmitter pulse shape, the baseband signal at the input to the frequency modulator is

$$x(t) = \sum_{n=-\infty}^{\infty} a_n\, g(t - nT) \tag{35}$$

For duobinary FM, the data sequence can take either one of two levels. In particular, the data sequence can assume

$$a_n = \pm \frac{\delta\sqrt{T}}{(0.762)} \tag{36}$$

where δ is the nominal frequency deviation. For a 12.6 Mb/s modem and a 14-MHz 99% bandwidth, δT was found to be given by 0.245.

From [6], the rms signal fluctuations at the output of the discriminator were found to be given by

$$\delta_f = \sqrt{1.095}\,\delta \tag{37}$$

The signal fluctuations at the shaping filter output can be found by noting that the signal passed through the receive shaping filter is

$$v(t) = \sum_{k=-\infty}^{\infty} a_k \, s(t - kT) \tag{38}$$

where the transmit and receive shaping filters both have frequency responses given by Eq. (2) and where the Fourier transform of s(t) is

$$S(f) = |H(f)|^2 \tag{39}$$

From (38) it follows that

$$\overline{v(t)} = 0$$

$$\overline{v^2(t)} = \frac{1}{T} \overline{a_k^2} \int S^2(t) \, dt \tag{40}$$

From Eq. (36), Parseval's theorem, and using the filter frequency response given by (2), the variance of the signal at the receive filter output is

$$\overline{v^2(t)} = \frac{\delta^2}{(0.762)^2} \int_{-\frac{1}{2T}}^{\frac{1}{2T}} T^2 \cos^2(\pi f T) \, df \tag{41}$$

and evaluating the above integral gives

$$\boxed{\overline{v^2(t)} = 0.861 \, \delta^2 T} \tag{42}$$

In the next section, Eqs. (37) and (42) will be used (along with the noise variances found in Section 3) to determine SNR's at the discriminator and receive shaping filter outputs.

5. Signal-to-Noise Ratios

It was shown in Section 3 above that the noise at the output of the discriminator has two independent components. One component is Gaussian with zero-mean and variance given by (16). The second component has a spherical modified Bessel function distribution with zero-mean and variance given by (21). The rms signal fluctuations at the discriminator output is given by (37). From (16) and (37), the signal to Gaussian noise ratio at the discriminator output is

$$\boxed{SNR_G = \frac{105.12\ \delta^2\rho}{\beta^2}} \tag{43}$$

From (21) and (37), the signal to non-Gaussian noise ratio at the discriminator output is

$$\boxed{SNR_{NG} = \frac{840\ \delta^2\rho^2}{\beta^2}} \tag{44}$$

Equations (43) and (44) are plotted in Figure 3 for several IF bandwidths. As shown in this figure, the SNR of the Gaussian noise is greater than 10 dB above the SNR of the non-Gaussian noise for E/N_0 greater than 10 dB.

At the output of the receive shaping filter, the Gaussian noise component has variance given by (18). The signal has fluctuations given by (42). From (18) and (42), the SNR (due to the Gaussian noise component) at the shaping filter output is

$$\boxed{SNR_{GO} = 228.4\ \delta^2 T^3 \beta\rho} \tag{45}$$

The variance of the non-Gaussian noise component at the shaping filter output is given by (34). From (34) and (42),

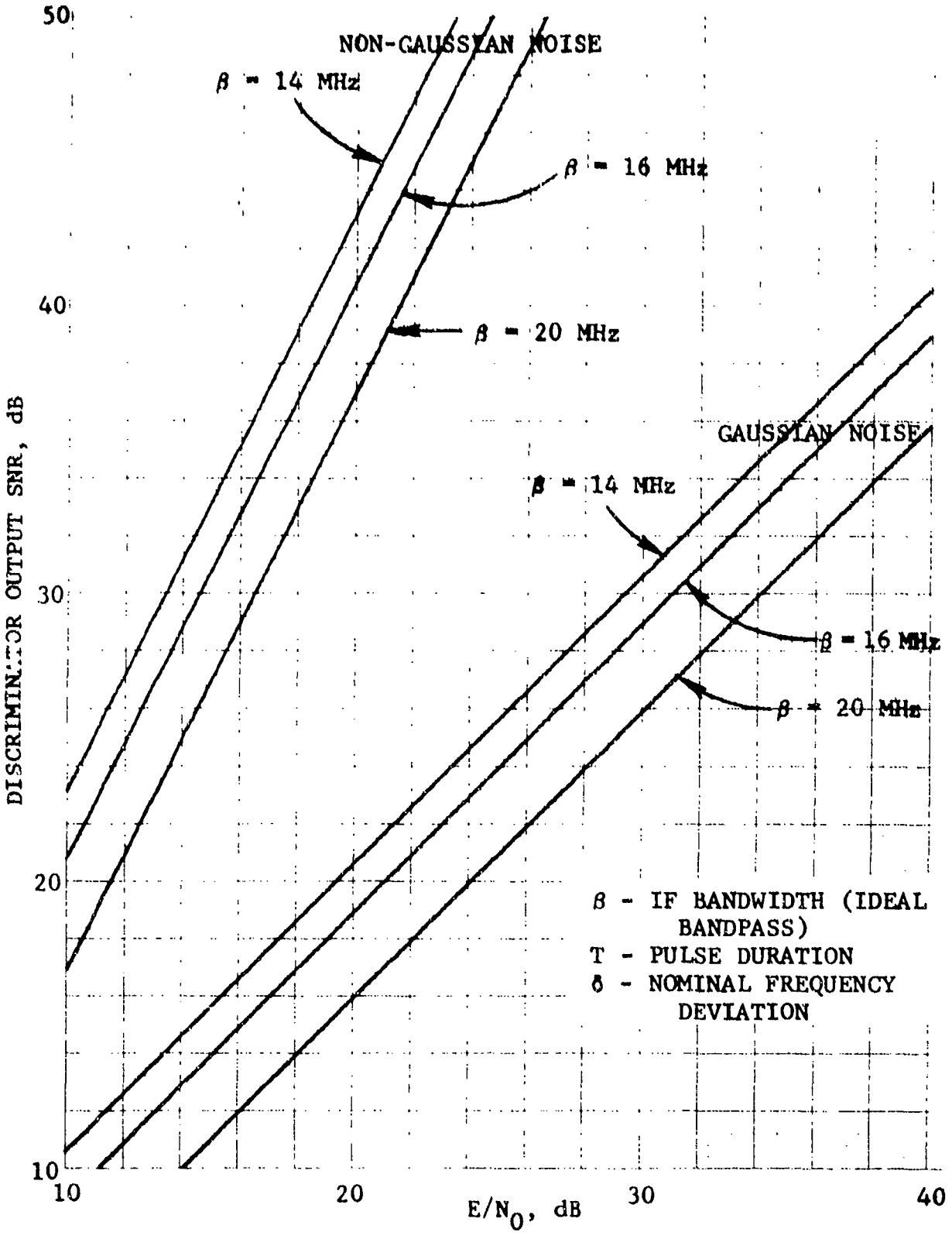

Figure 3 Discriminator Output SNR's
(1/T = 12.6 Mb/s; δT = 0.245)

the SNR (due to the non-Gaussian noise component) at the shaping filter output is

$$\boxed{SNR_{NO} = 50.44 \frac{\delta^2 T \rho^2}{\beta} A(\beta T)} \tag{46}$$

where $A(\beta T)$ is the coefficient of β/ρ^2 given in (34).

Figure 4 presents the SNR's at the output of the shaping filter. As shown in this figure, increasing the IF bandwidth decreases the output SNR due to the non-Gaussian noise component. However, the signal to Gaussian noise ratio does not depend upon the IF bandwidth.

6. Correlation Function of Gaussian Noise

In Section 3 above, it was shown that the Gaussian noise at the output of the shaping filter is not white, but has spectral density

$$\frac{N_0 f^2 T^2}{2E} \cos \pi f T \qquad |f| \le \frac{1}{2T} \tag{47}$$

This will lead to correlated noise samples in the detector. It is of interest to determine the correlation of these samples at various sampling offsets. This can be done by Fourier transforming (47), which can be used to find the correlation coefficient of the Gaussian noise. In particular, we have (for $x \neq \pm 1$) found that the correlation coefficient of the Gaussian noise is

$$\rho(\tau) = \frac{\frac{4\pi x}{\left(x^2 - 1\right)^2} \sin\left(\frac{\pi x}{2}\right) + \left[\frac{-\pi^2}{2(x^2 - 1)} + \frac{12x^2 + 4}{\left(x^2 - 1\right)^3}\right] \cos\left(\frac{\pi x}{2}\right)}{\frac{\pi^2}{2} - 4} \tag{48}$$

where $x = \frac{2\tau}{T}$. At $x = \pm 1$, $\rho \pm \frac{T}{2} = \frac{\pi\left[\frac{\pi^2}{6} - 1\right]}{2\pi^2 - 16}$.

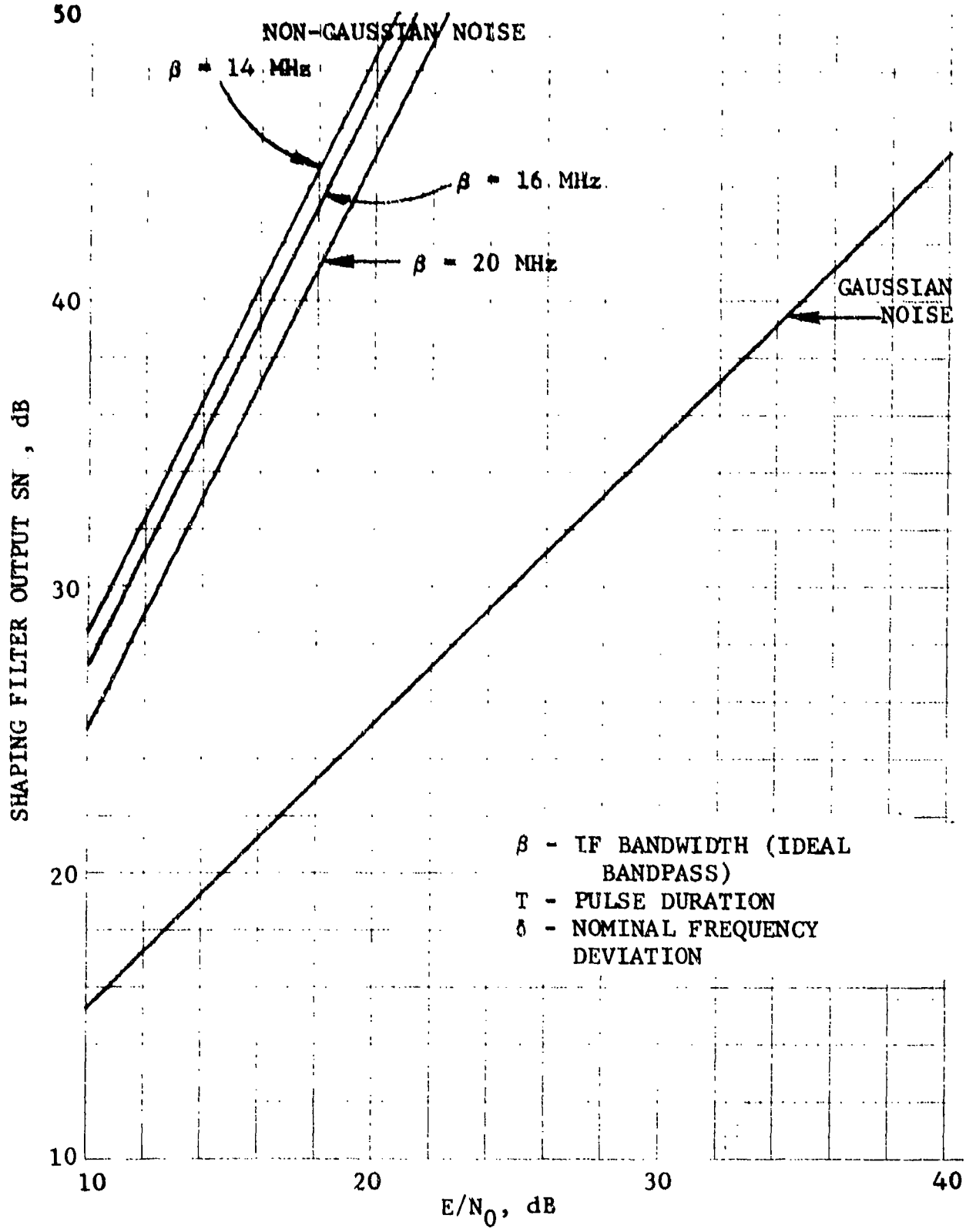

Figure 4 Shaping Filter Output SNR's
(1/T = 12.6 Mb/s; δT = 0.245)

The correlation coefficient for $\tau \geq 0$ [note that $\rho(\tau)$ is even) of the Gaussian noise component at the shaping filter output is presented in Figure 5. As shown in this figure, a noise sample is strongly correlated with four adjacent noise samples.

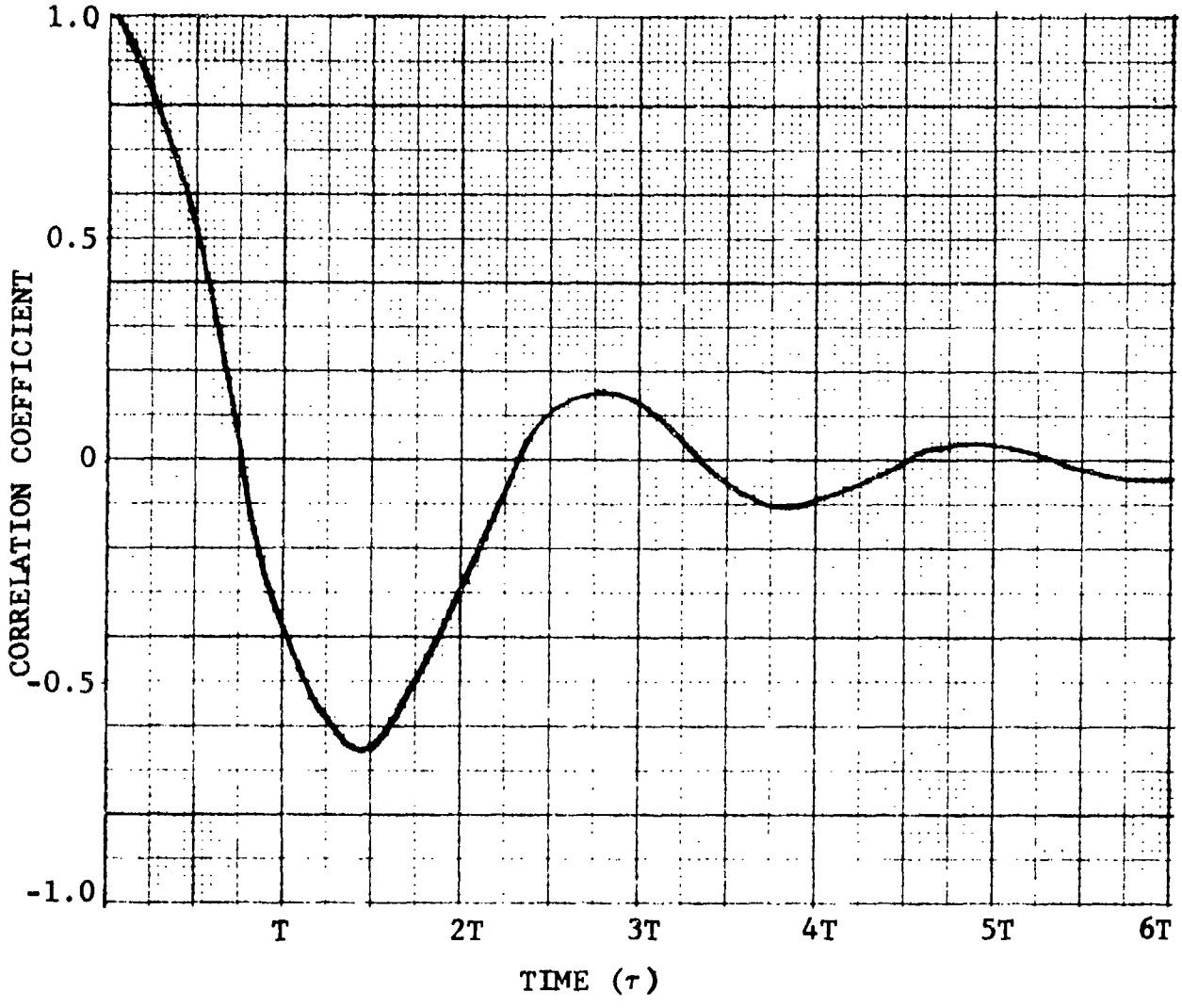

Figure 5 Correlation Function of Gaussian Noise at Output of Receive Shaping Filter [$\rho(\tau)$ even]

REFERENCES FOR APPENDIX A

[1] S. O. Rice, "Noise in FM Receivers," in Time Series Analysis, M. Rosenblatt, ed., John Wiley & Sons, 1963, Chapter 25.

[2] A. J. Viterbi, Principles of Coherent Communication, McGraw-Hill, New York, 1966.

[3] J. M. Wozencraft and I. M. Jacobs, Principles of Communication Engineering, John Wiley & Sons, New York, 1965.

[4] I. Gradshteyn and I. Ryzhik, Table of Integrals Series and Products, Academic Press, New York, 1972.

[5] A. Papoulis, Probability, Random Variables, and Stochastic Processes, McGraw-Hill, New York, 1965.

[6] P. A. Bello, et al., "Line-of-Sight Technical Investigation," Final Report on Contract F30602-73-C-0244, by CNR, Inc., for Rome Air Development Center, June 1974, RADC-TR-74-330, (AD006104).

APPENDIX B

DESCRIPTION OF CHANNEL MODELS USED IN THE COMPUTATION OF EXAMPLES

1. Introduction

In computing examples and in simulating the proposed non-linear adaptive channel estimator, we will assume that the channel can be modeled by a finite number of discrete paths. This model has been proposed for the LOS channels and has been able to predict some of the measured phenomena for this link [1].

For an N-path channel, the time-varying channel transfer function [2] can be expressed as:

$$T(f,t) = \sum_{i=1}^{N} \alpha_i(t)\, e^{-j2\pi\xi_i(t)[f+f_0]} \qquad (1)$$

where f_0 is the carrier frequency, and $\alpha_i(t)$ and $\xi_i(t)$ are the amplitude and delay of the i^{th} path, respectively.

For this report, the two- and three-path channel models were used. The use of these models allowed us to generate the actual received signal (using the method described in Appendix C), and to evaluate the performance of the proposed non-linear adaptive channel estimator.

2. Two-Path Channel

To determine the distortion depicted by Figs. 4 - 7 of App. C, a 2-path channel model [N=2 in Eq. 1] was used. For these examples, a delay difference $|\xi_1 - \xi_2|$ of 2 ns and a relative amplitude $\frac{\alpha_2}{\alpha_1}$ of 1.01 was used. The phase difference of the two paths (at f = 0) is then

$$\Delta\psi = 2\pi f_0 \cdot (2 \text{ ns}) \qquad (2)$$

Assuming $f_0 = 8$ GHz, then $\Delta\psi = 32\pi$ radians. Therefore, the phase difference of the two paths is very large (~ 16 revolutions)

and any phase difference (modulo 2π) can be obtained by very small ($\lesssim \pm 3\%$) variations in f_0 or the delay difference. For this reason, a delay difference of 2 ns was used for all fade levels required to generate Figs. 4 - 7 of Appendix C, and appropriate phase shifts were inserted to produce fades to the require depths.

3. Three-Path Channel

In [1] and [3], a multiple-path LOS channel model was derived using a geometric optics calculation of propagation in the presence of an elevated layer of steep negative refractive index gradient. A three-path structure was found to be most likely.

As one example of the structure calculated it was found that the amplitude of each of two multipath components was 1.25 times the amplitude of the direct path and they arrived at the receiver 1.6 and 2.2 nanoseconds after the direct path. Therefore, using the direct path in (1), (i=1), as a reference $\xi_1=0$, $\xi_2 = 1.6$ ns, $\xi_3 = 2.2$ ns, $\alpha_1=1$, $\alpha_2=\alpha_3=1.25$. The three-path multipath structure is typical of that predicted on 30-mile links. The values of delay and amplitude have been calculated using a LOS channel model (see Fig. 2.23 of [1]) in which a thick layer of steep negative refractive index gradient (-420 N units/km) exists just above one terminal. This terminal is assumed to be 100 feet above the other.

As in the case of the two-path channel model, the delays were held constant for all fade levels. Actually, changes in delay (and/or carrier frequency) are necessary to obtain different fade levels, but since only a small delay change ($\leq \pm 4\%$) would be required, we elected to omit these changes in favor of obtaining results for a fixed delay model with inserted phase shifts.

4. Channel Parameters

4.1 Introduction

In order to determine the effectiveness of the nonlinear adaptive channel estimator to estimate channel parameters, we must find the values of these parameters for the particular channel model being used. In this section we will determine the quadratic and cubic channel model parameters to be estimated for an N-path channel.

From (1) for an N-path channel, the time-varying channel transfer function can be expressed as

$$T(f,t) = \sum_{i=1}^{N} \alpha_i(t)\, e^{-j2\pi\xi_i(t)[f+f_0]} \tag{3}$$

The received data signal q(t) is related to the transmitted spectrum Z(f) by

$$q(t) = \int Z(f)\, T(f,t)\, e^{j2\pi ft}\, df \tag{4}$$

To determine the channel parameters to be estimated, it is necessary to expand T(f,t) in a power series in f. Since the existence of a mean delay ξ_0 produces a factor $\exp\{-j2\pi f\xi_0\}$ in T(f,t) which can fluctuate with f quite rapidly, it is desirable to expand only that portion of T(f,t) which does not include this factor. Then

$$T(f,t) = T_0(f,t)\, e^{-j2\pi f\xi_0} \tag{5}$$

where $T_0(f,t)$ is the time-varying channel transfer function after the mean delay has been removed. The selection of ξ_0 to obtain the best estimate of q(t) using the fewest terms in expanding $T_0(f,t)$ is considered in Section 4.4 below. From (3) and (5), $T_0(f,t)$ for the N-path model is

$$T_0(f,t) = \sum_{i=1}^{N} \alpha_i(t)\, e^{-j2\pi f_0\xi_i(t) - j2\pi f[\xi_i(t)-\xi_0]} \tag{6}$$

Defining a complex gain of the i^{th} path by

$$\beta_i(t) = \alpha_i(t)\, e^{-j2\pi f_0\xi_i(t)} \tag{7}$$

and a relative delay of the i^{th} path by

$$\eta_i(t) = \xi_i(t) - \xi_0 \tag{8}$$

then

$$T_0(f,t) = \sum_{i=1}^{N} \beta_i(t)\, e^{-j2\pi f \eta_i(t)} \tag{9}$$

Expanding $T_0(f,t)$ in a power series gives

$$T_0(f,t) = \sum_{n=0}^{\infty} T_n(t)\, (2\pi j)^n\, f^n \tag{10}$$

where for the N-path channel $T_n(t)$ can be easily found from (7) to be given by

$$T_n(t) = \frac{(-1)^n}{n!} \sum_{i=1}^{N} \beta_i(t)\, \left[\eta_i(t)\right]^n \tag{11}$$

Substituting (5) and (10) into (4), it follows that

$$q(t) = \sum_{n=0}^{\infty} T_n(t)\, (2\pi j)^n \int f^n\, Z(f)\, e^{j2\pi f(t-\xi_0)}\, df \tag{12}$$

A filter with transfer function $(2\pi jf)^n$ is an n^{th}-order differentiator. Therefore, (12) can be written as

$$q(t) = \sum_{n=0}^{\infty} T_n(t)\, \frac{d^n\, z(t-\xi_0)}{d\, t^n} \tag{13}$$

In the case of a frequency-modulated signal

$$z(t) = e^{j\varphi(t)} \tag{14}$$

where $x(t) = \dot{\varphi}(t)$ is the frequency modulation and $\varphi(t)$ is the corresponding phase modulation. Equations (11) and (13) will be used in Sections 4.2 and 4.3 below to find channel model approximations.

4.2 Quadratic Channel Model Parameters

In this section we will find the output of the discriminator as a function of x(t) (the frequency modulation) and its derivatives and cross terms, where only signal terms with units of sec^{-1}, sec^{-2}, and sec^{-3} are retained. This analysis parallels that presented by Bello and Nelin in [4]. To accomplish this objective requires that q(t) [as given by (13)] be approximated by

$$q(t) \approx \sum_{n=0}^{2} T_n(t) \frac{d^n z(t-\xi_0)}{dt^n} \tag{15}$$

Since $x(t) = \dot{\phi}(t)$ and using (14), it follows that

$$\frac{d z(t-\xi_0)}{dt} = j\, x(t-\xi_0)\, z(t-\xi_0)$$

$$\frac{d^2 z(t-\xi_0)}{dt^2} = \left[j\, \dot{x}(t-\xi_0) - x^2(t-\xi_0)\right] z(t-\xi_0) \tag{16}$$

Substituting (16) into (15) and using (14) gives

$$q(t) = e^{j\varphi(t-\xi_0)} \Big\{ T_0(t) + j\, T_1(t)\, x(t-\xi_0) + \left[j\, \dot{x}(t-\xi_0) - x^2(t-\xi_0)\right] T_2(t) \Big\} \tag{17}$$

For the LOS channel of interest, the time variations of the channel are much slower than the time variations of x(t). Therefore, one may regard the channel as fixed when finding the discriminator output. Expressing q(t) as

$$q(t) = e^{j[\varphi(t-\xi_0)+B(t-\xi_0)]} \tag{18}$$

then the discriminator output r(t) is given by

$$r(t) = \dot{\phi}(t - \xi_0) + \dot{B}(t - \xi_0) \tag{19}$$

From (17), it can be shown that [recalling that $x(t) = \dot{\phi}(t)$]

$$r(t) = P_0 x(t - \xi_0) + P_1 \dot{x}(t - \xi_0) + P_2 \ddot{x}(t - \xi_0) + P_3 x(t - \xi_0)\dot{x}(t - \xi_0) \tag{20}$$

where

$$P_0 = A$$

$$P_1 = A\ \mathrm{Re}\left\{\frac{T_1(t)T_0^*(t)}{|T_0(t)|^2}\right\}$$

$$P_2 = A\ \mathrm{Re}\left\{\frac{T_2(t)T_0^*(t)}{|T_0(t)|^2}\right\}$$

$$P_3 = A2\left[\mathrm{Re}\left\{\frac{T_1(t)T_0^*(t)}{|T_0(t)|^2}\right\}\ \mathrm{Im}\left\{\frac{T_1(t)T_0^*(t)}{|T_0(t)|^2}\right\} - \mathrm{Im}\left\{\frac{T_2(t)T_0^*(t)}{|T_0(t)|^2}\right\}\right] \tag{21}$$

and where A is a constant.

Equation (20) is an approximate expression for the output of the discriminator obtained by using the quadratic channel model. The channel parameters $\{P_i\}$ are the parameters estimated by the nonlinear adaptive channel estimator.

The coefficient $T_0(t)$ is seen from Eq. (10) to be the value of the time-varying channel transfer function at the center of the band. Throughout this study, the fade depth has been defined as the depth of fade in the center of the band. That is, fade depth is related to $|T_0(t)|$. (Note that this means there could be a deeper fade at some other frequency within the 14 MHz band of interest).

It is of interest to determine the range of values that the channel parameters assume for the three-path channel model discussed in Section 3 above. To better represent the results, we will express $T_0(t)$ by

$$T_0(t) = |T_0(t)|e^{j\theta(t)} \tag{22}$$

where ξ_0 was selected as the delay of the direct path and where θ is the channel phase relative to the direct path at the center. For a given fade depth, $|T_0(t)|$, θ can vary from 0 - 360° corresponding to different degrees of frequency selectivity. Using (11) and (21), it is possible to express the channel parameters for a given fade level as a function of θ (except for another geometry in which we replace θ by $-\theta$ and P_2 by $-P_2$).

Figures 1 through 12 give the range of parameter values for 25-, 30-, 35-, and 40-dB fades. It was found, for the channel model considered, that the main effect of varying the fade level was to scale the amplitudes of the P_i's. In these figures P_0 was assumed to be 1 and the P_i's are in units of bit intervals (12.6 Mbs system).

In Section 4.5 examples illustrating the performance of a duo-binary FM LOS system during multipath fading were presented. The three-path channel model discussed in Section 3 above was used with two different values of channel phase (θ) selected. As illustrated by Figs. 1 to 12, choosing two values of θ from the range $[0,2\pi]$ results in many combinations of channel parameters P_i. Since small values of P_i (for a given fade level) indicate a small distortion and large P_i higher distortion, it was decided to present error rate examples which (for the three-path channel model of Section 3 above) would bound the performance for most choices of channel phase.

After examining Figs. 1 to 12 it was decided that using a channel phase (θ) of 286° would give smaller values of parameters while a channel phase of 166° would give highest values of the parameters. The parameter values for the "good" and "bad" channels can be found for different fade levels by using Figs. 1 to 12 and finding θ (theta) values of 166° and 286°.

Examples illustrating the degree of frequency selectivity and the amount of delay distortion for the "bad" and "good" channels were computed for 25-, 30-, 32-, 35-, and 40-dB fades using the three-path channel model of Section 3 above. The frequency selectivity is illustrated by a plot of $|T(f,t)|$ (in dB

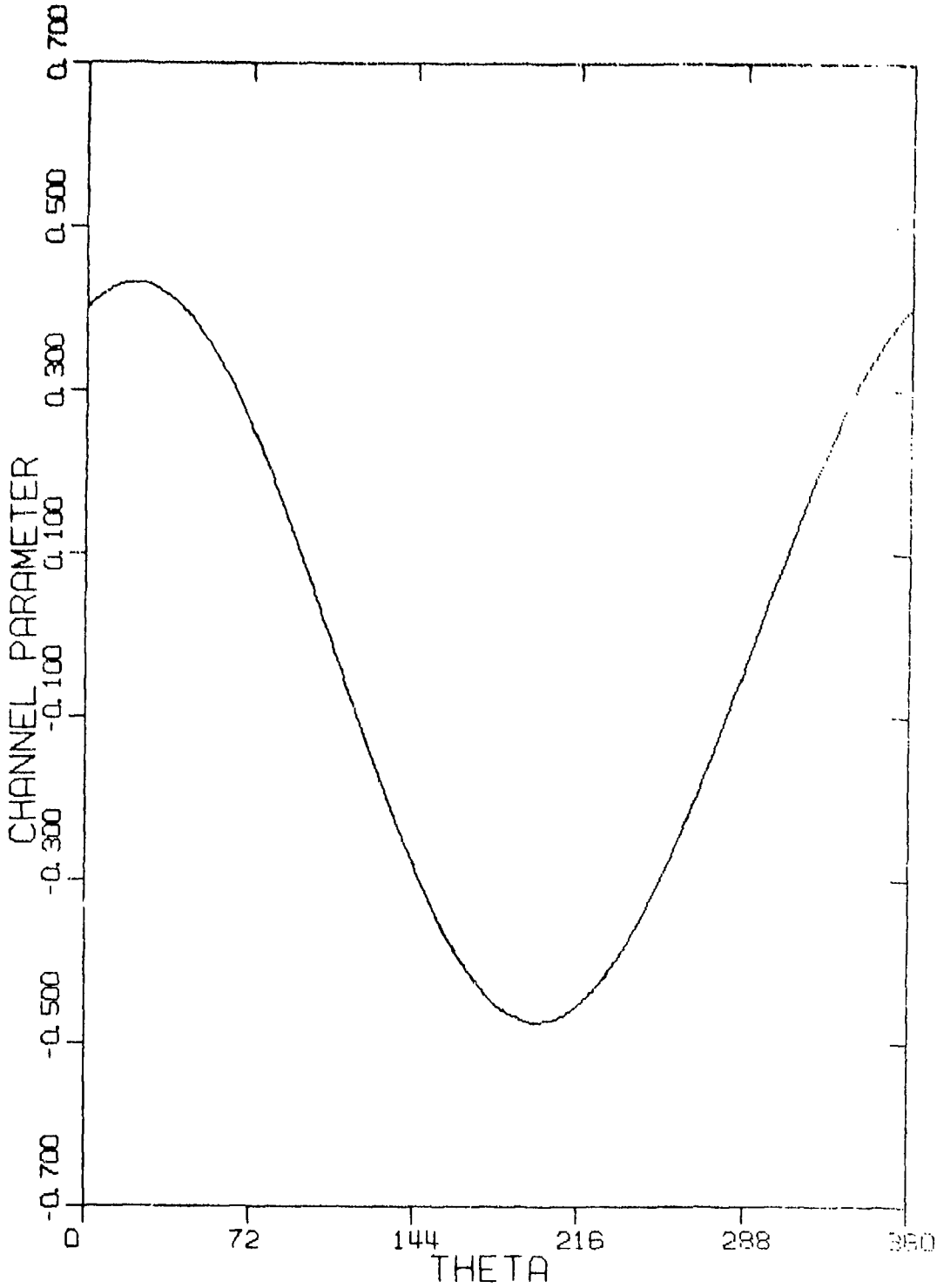

Figure 1 Channel Parameter P_1 for 25-dB Fade (Three-Path Model)

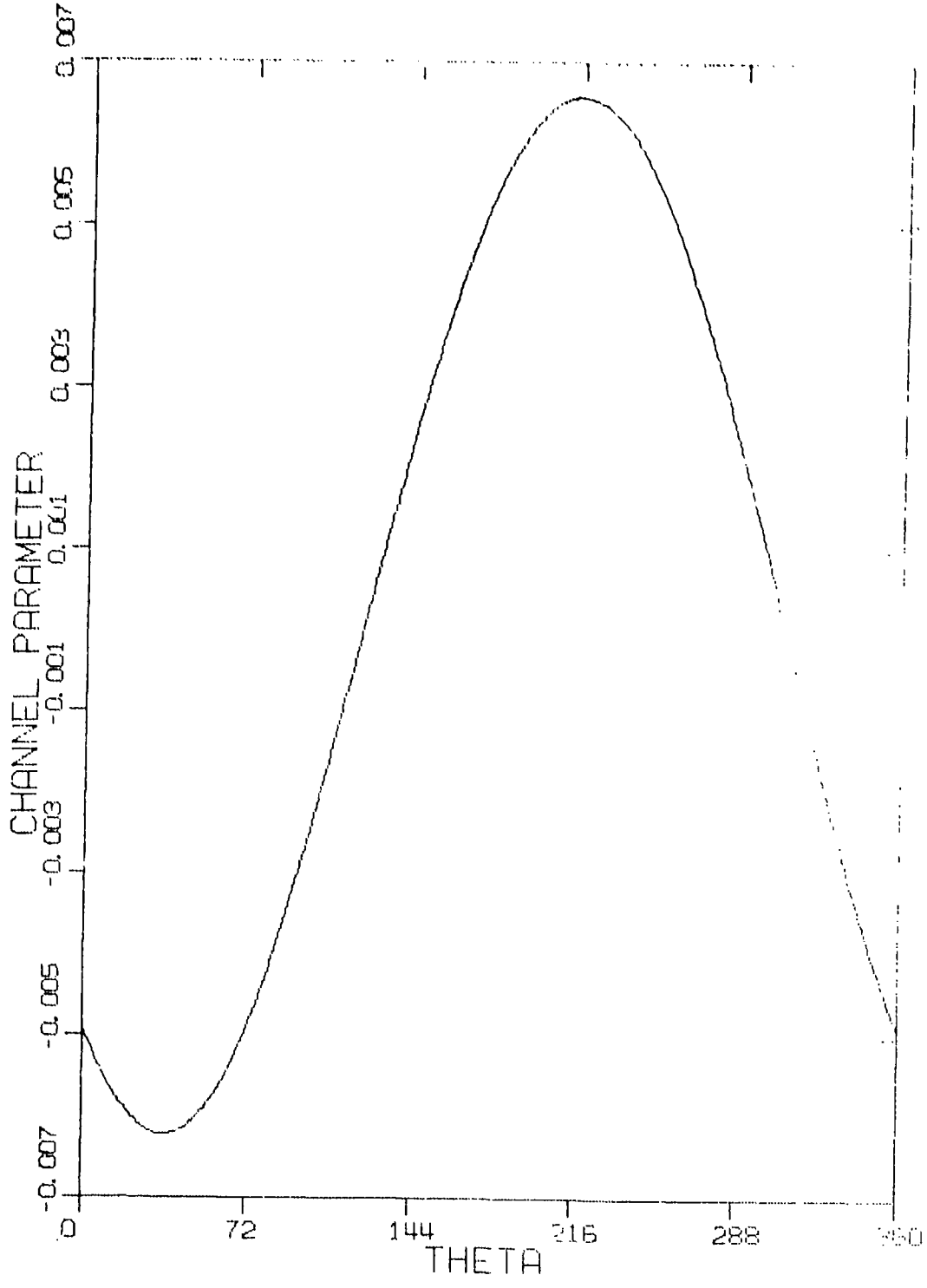

Figure 2 Channel Parameter P_2 for 25-dB Fade (Three-Path Model)

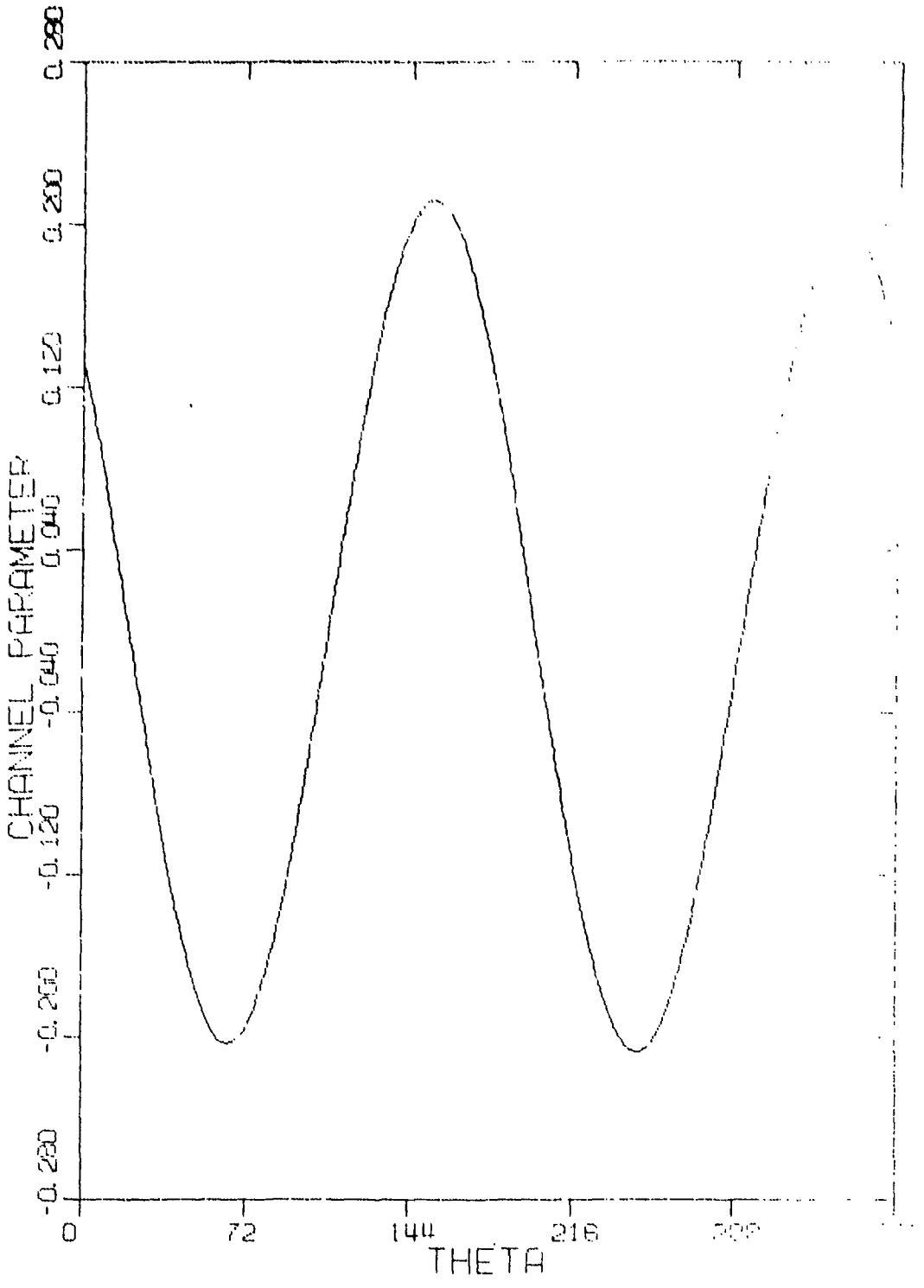

Figure 3 Channel Parameter P_3 for 25-dB Fade (Three-Path Model)

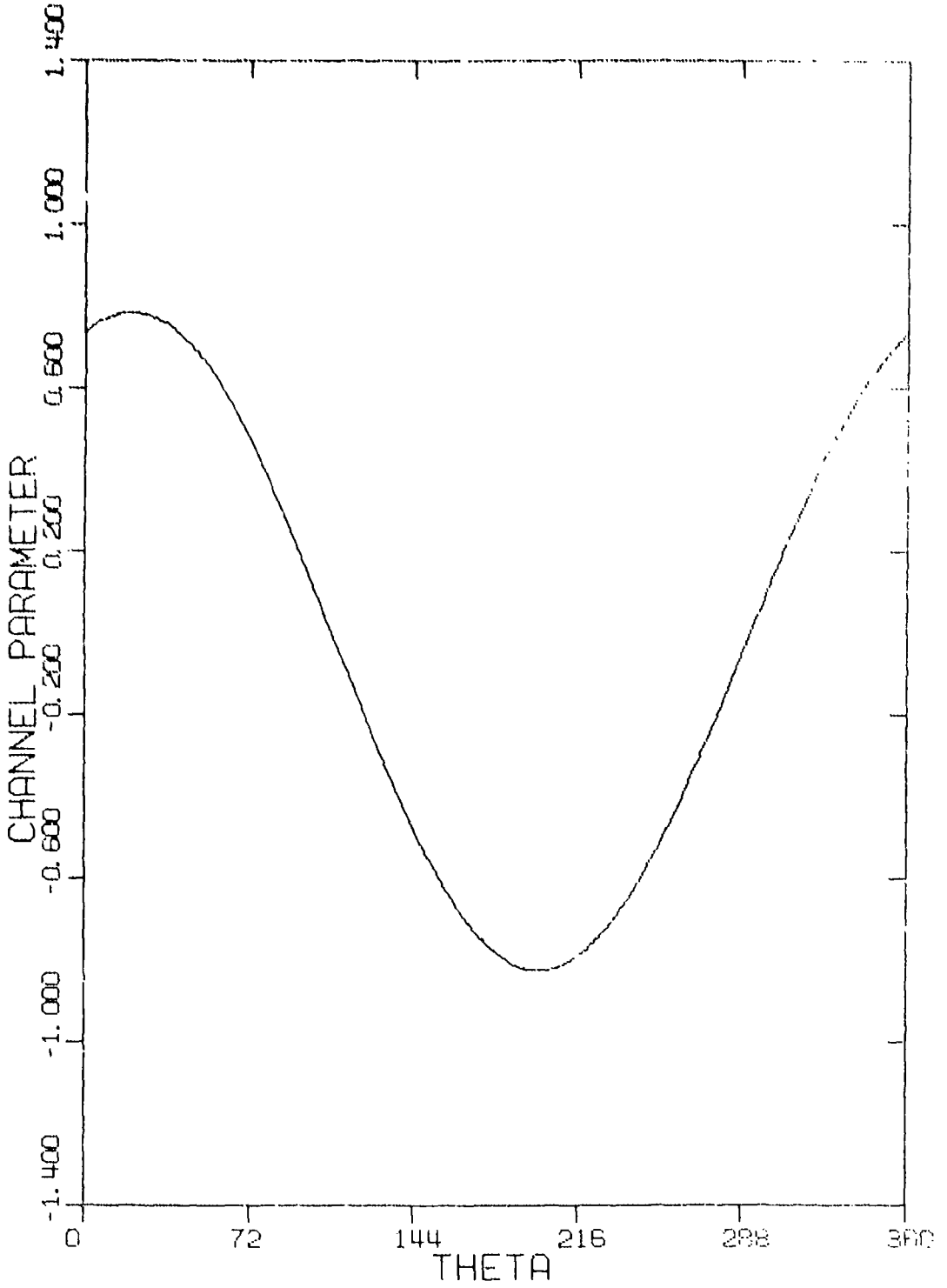

Figure 4 Channel Parameter P_1 for 30-dB Fade (Three-Path Model)

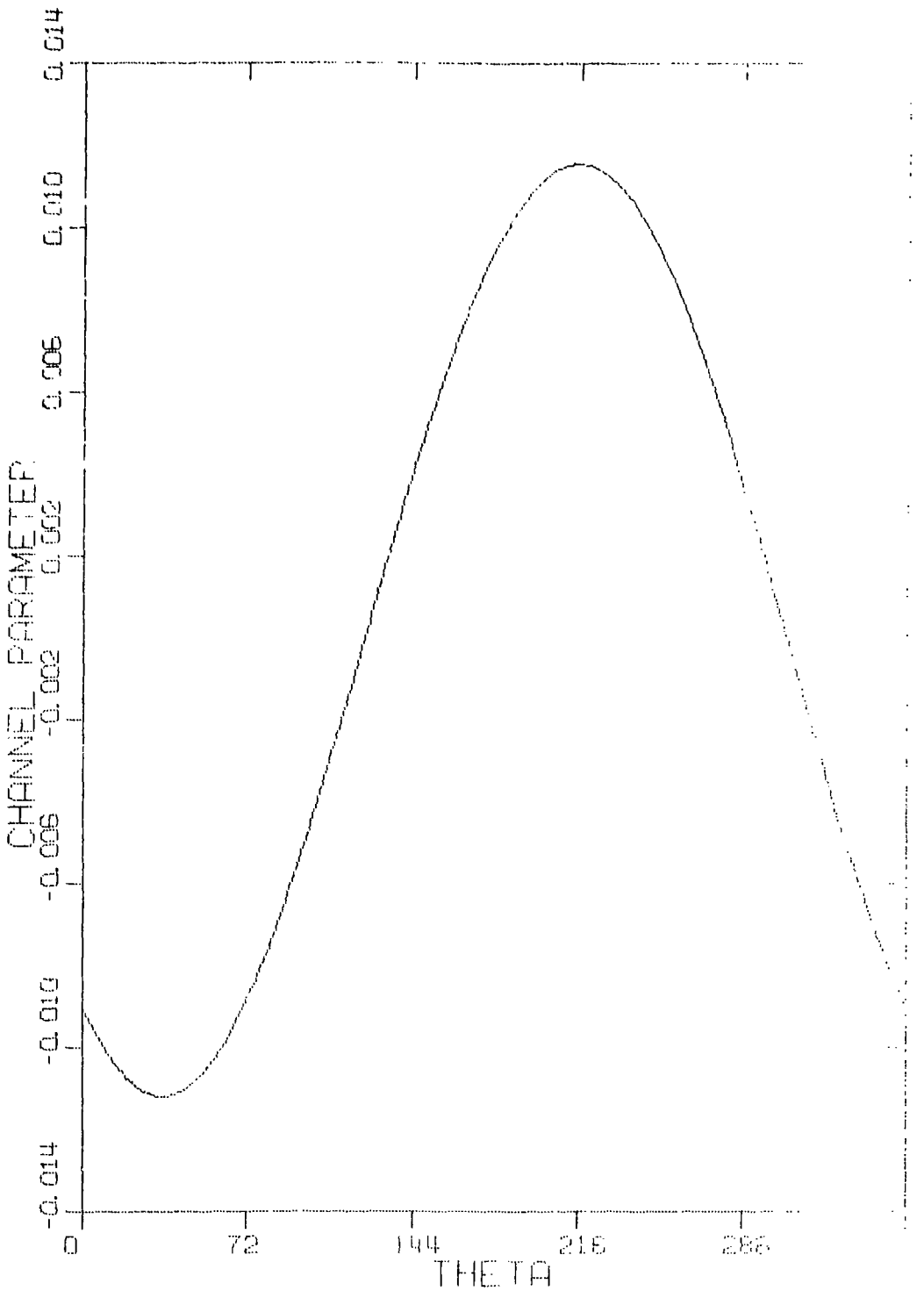

Figure 5 Channel Parameter P_2 for 30-dB Fade (Three-Path Model)

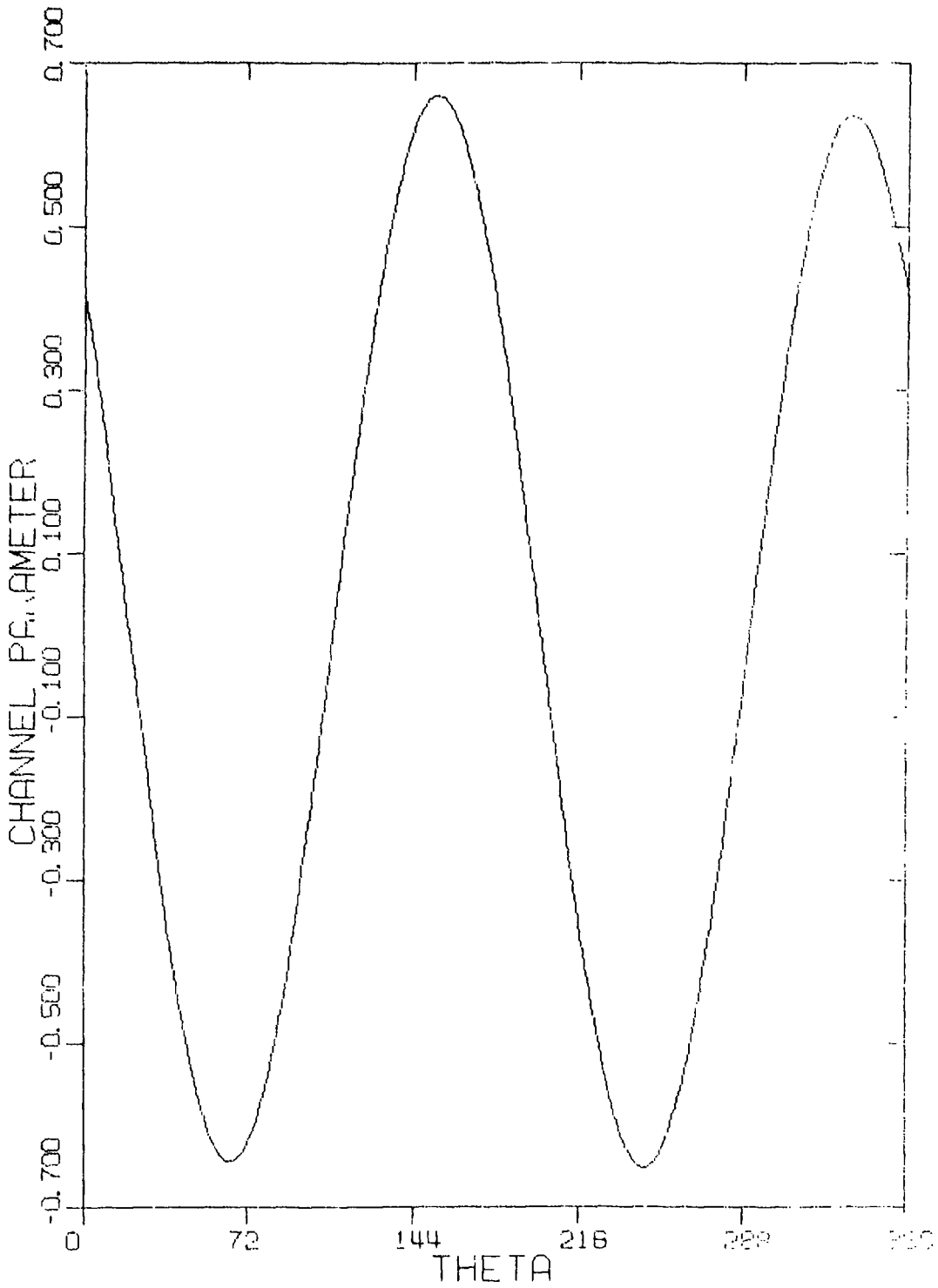

Figure 6 Channel Parameter P_3 for 30-dB Fade (Three-Path Model)

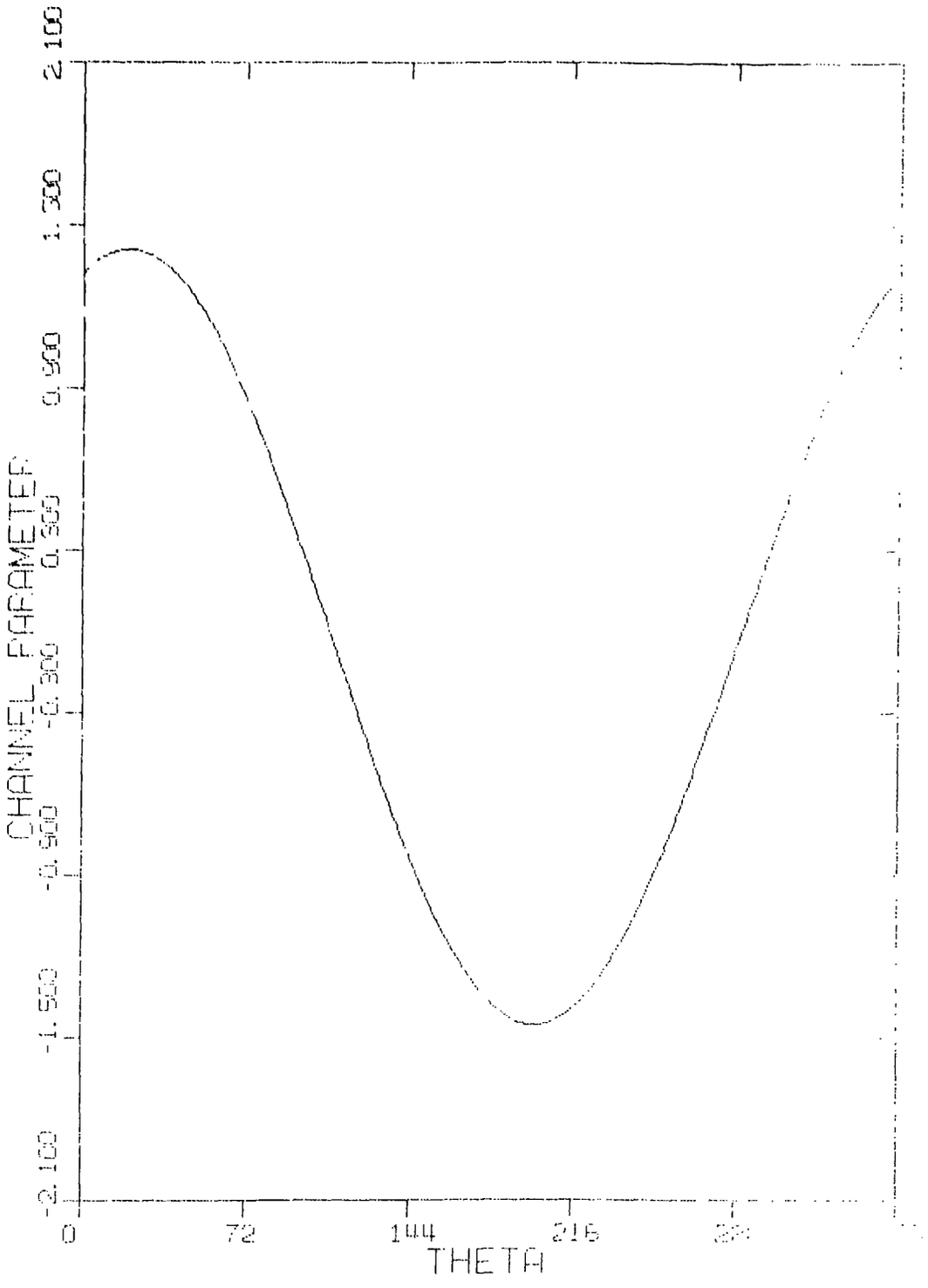

Figure 7 Channel Parameter P_1 for 35-dB Fade (Three-Path Model)

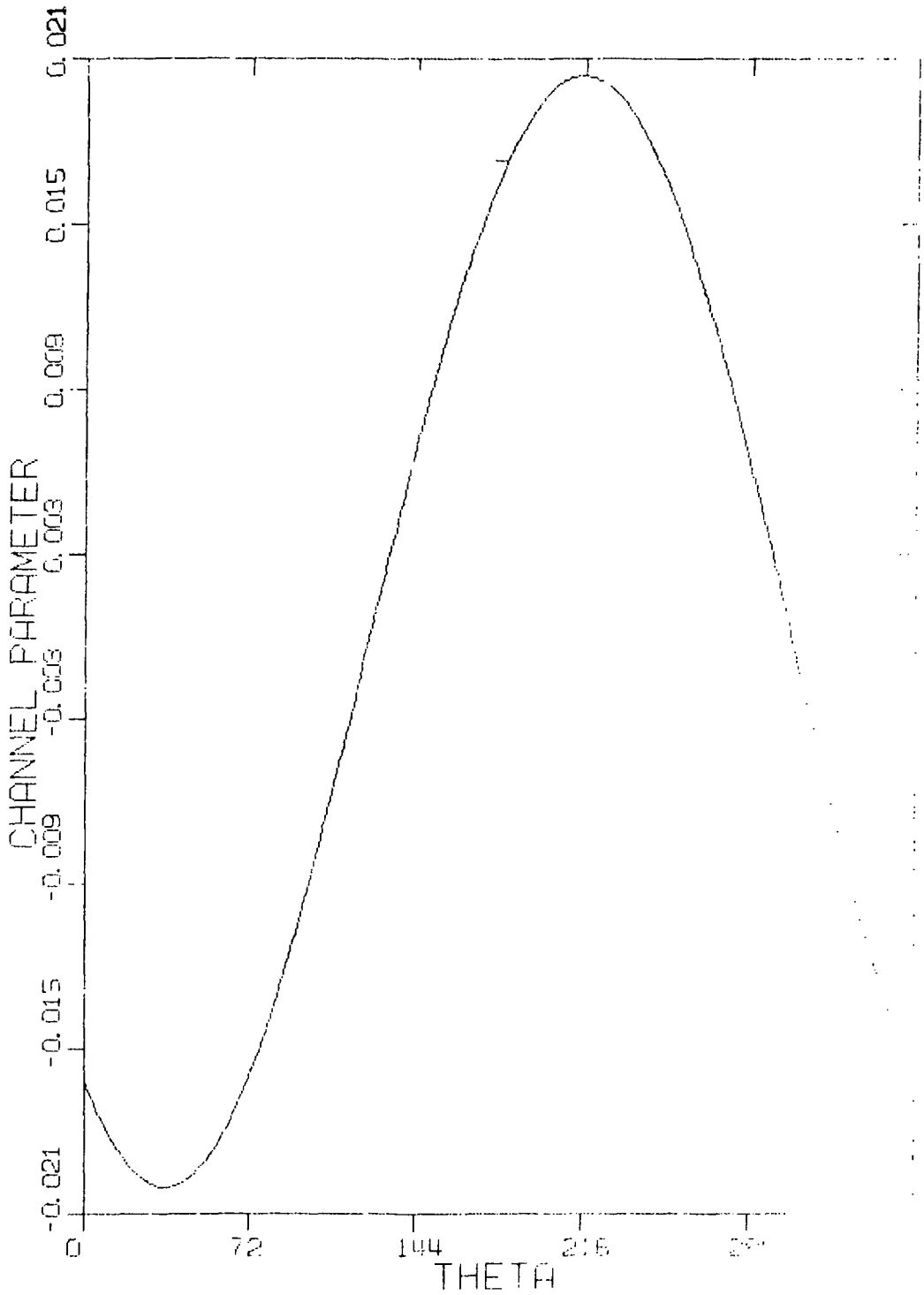

Figure 8 Channel Parameter P_2 for 35-dB Fade (Three-Path Model)

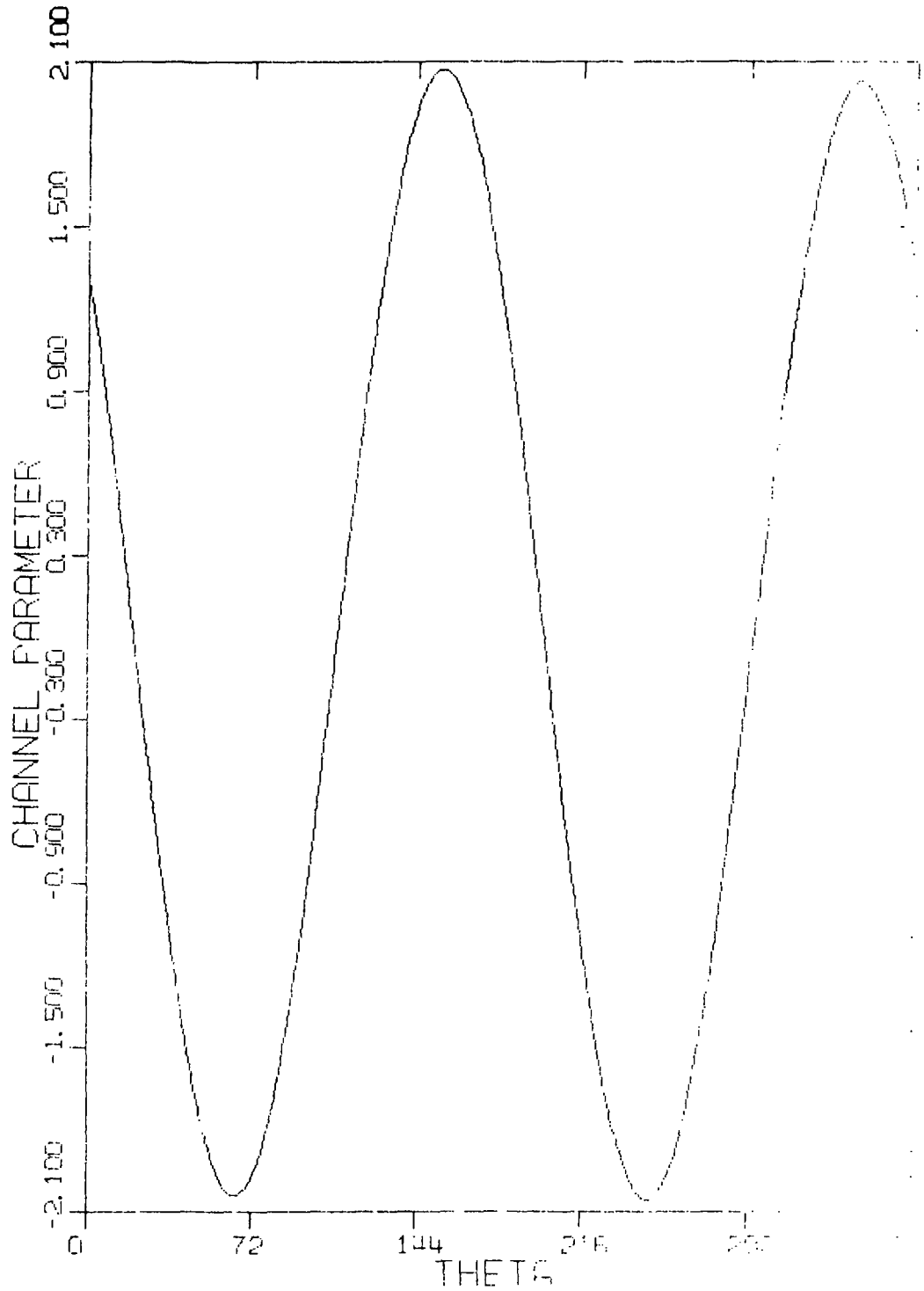

Figure 9 Channel Parameter P_3 for 35-dB Fade (Three-Path Model)

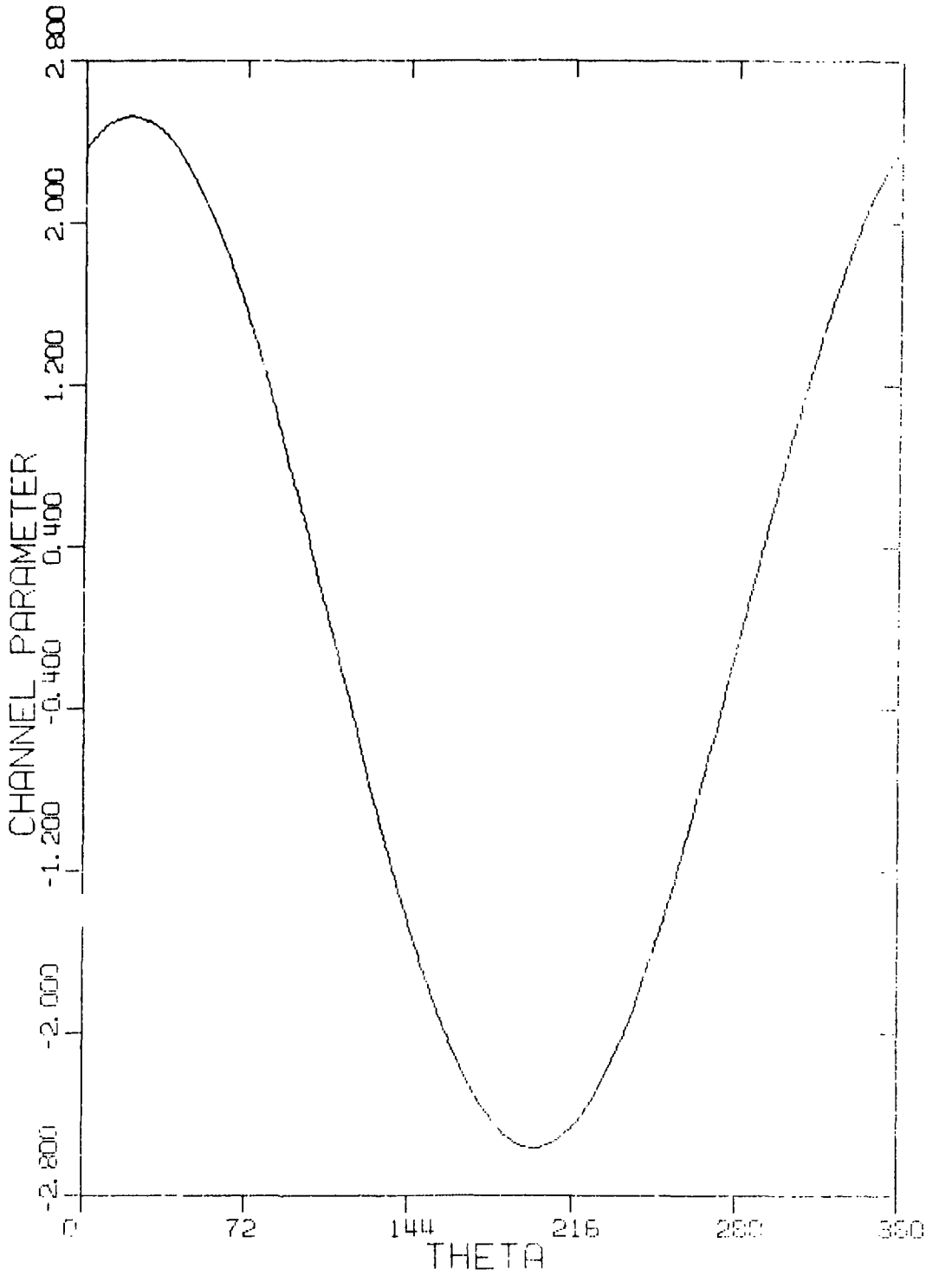

Figure 10 Channel Parameter P_1 for 40-dB Fade (Three-Path Model)

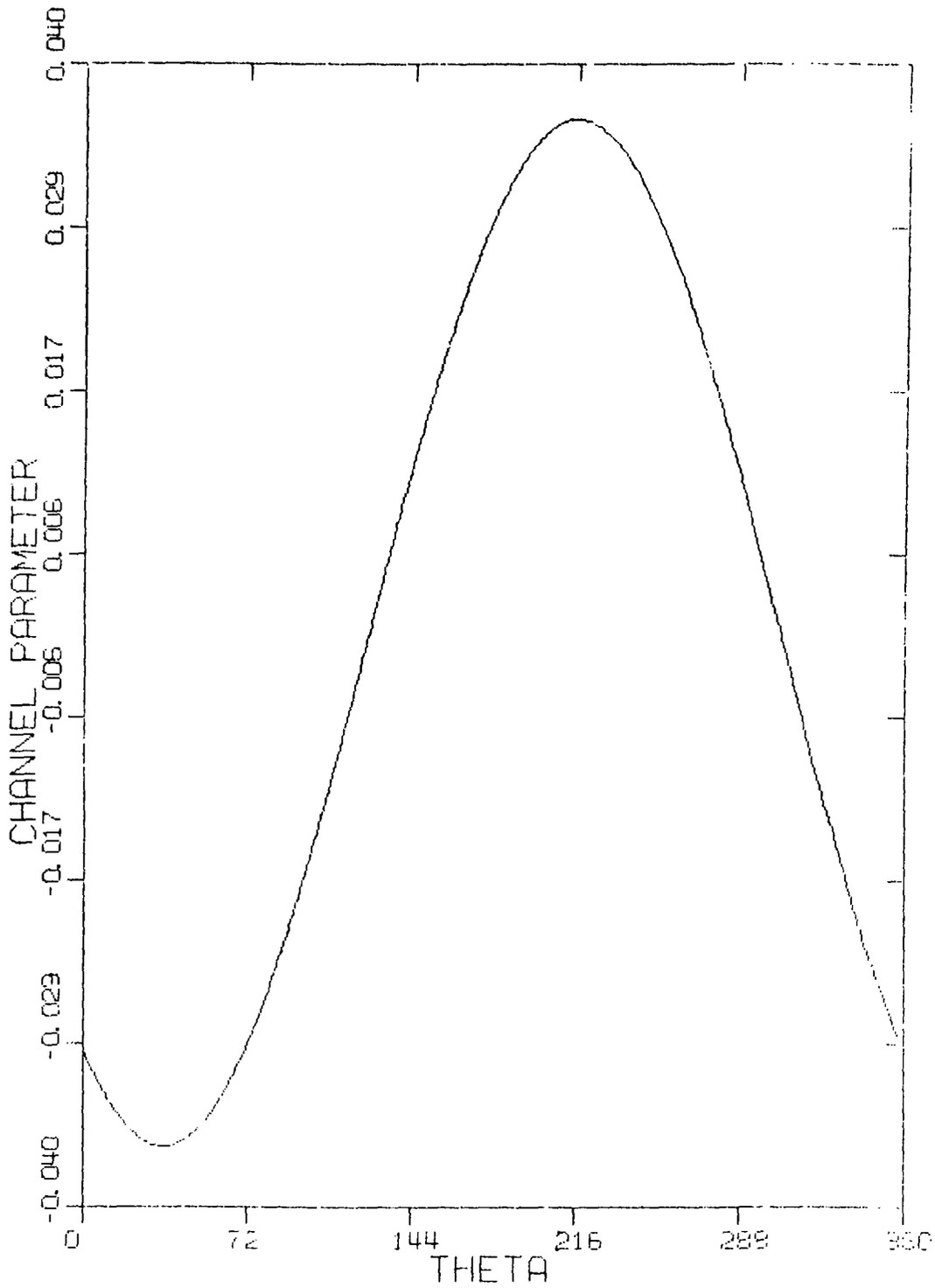

Figure 11 Channel Parameter P_2 for 40-dB Fade (Three-Path Model)

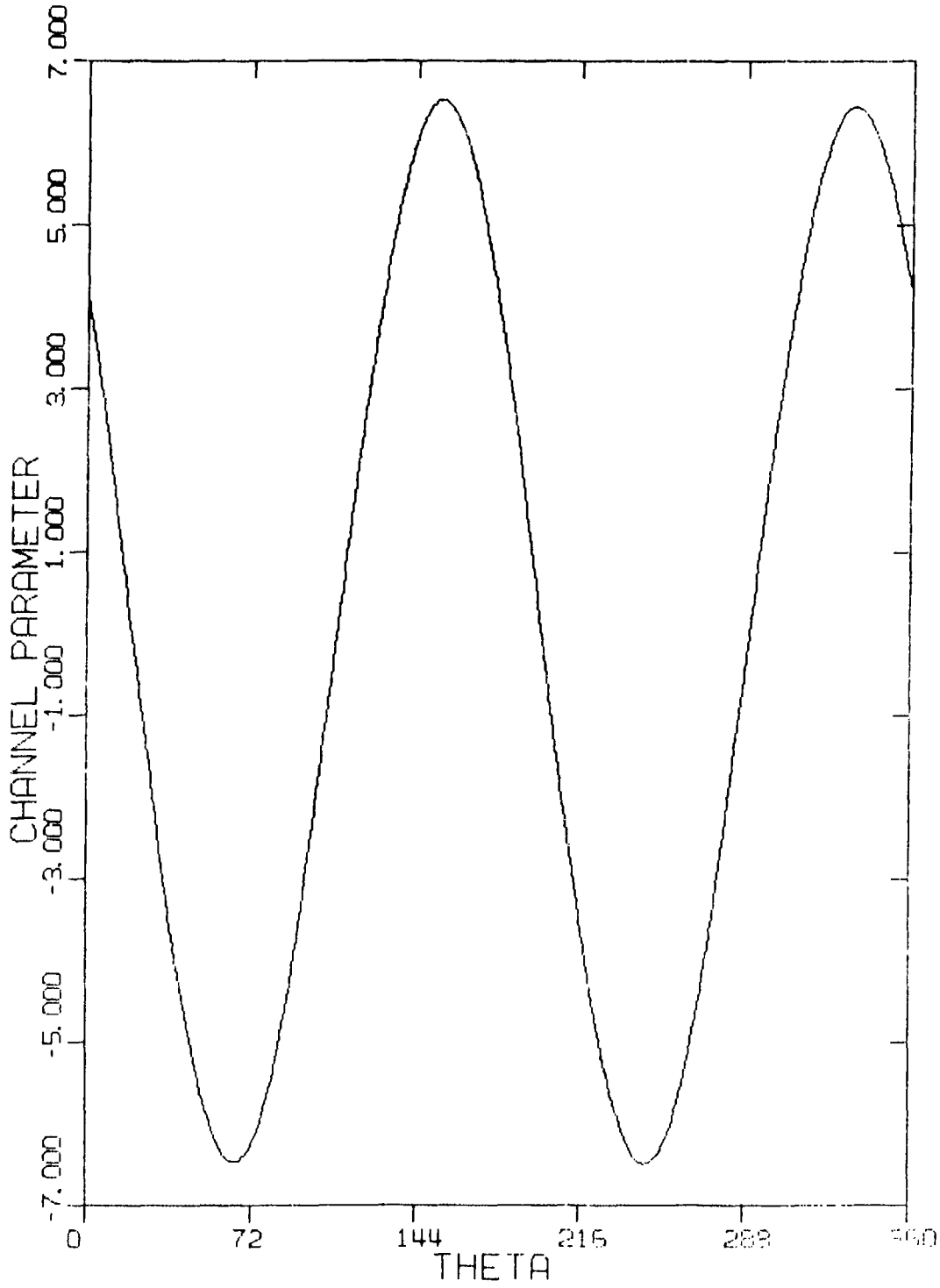

Figure 12 Channel Parameter P_3 for 40-dB Fade (Three-Path Model)

relative to the direct path) and group delay ($-1/2\pi$ x slope of $\not\propto T(f,t)$) versus frequency.

Figures 13 to 32 show the frequency selectivity and delay distortion for the "bad" and the "good" channels. As shown in these figures, there is the curious result that the "good" channel is more frequency selective. This is noted by comparing the amplitude versus frequency plots (at the same fade depth) for the two channels. Furthermore, the peak delay distortion is much larger for the "good" channel than for the "bad" channel! This is seen by comparing delay distortion versus frequency plots for the same fade depth and the two channel models.

Therefore, although the "good" channel is more frequency selective than the "bad" channel and has larger delay distortion, the fact that channel parameters P_1, P_2, P_3 are smaller for the "good" channel result in lower error rates for the "good" channel. One possible explanation for the superior performance of the "good" channel is that the delay distortion is restricted to a narrower band of frequencies which is severely attenuated. This apparently results in less intersymbol interference.

4.3 Cubic Channel Model

Although the quadratic channel model presented in the previous section is sufficient to model the channel during many fading conditions, it may not be adequate to model certain faults or to model the channel during very deep fades. The cubic channel model is derived in exactly the same manner except that q(t) is approximated by

$$q(t) \approx \sum_{n=0}^{3} T_n(t) \frac{d^n z(t-\xi_0)}{dt^n} \tag{23}$$

Proceeding in a manner similar to (16) - (20), the discriminator output can be approximated for the cubic channel model by

$$\begin{aligned} r(t) = {} & P_0 x(t-\xi_0) + P_1 \dot{x}(t-\xi_0) + P_2 \ddot{x}(t-\xi_0) \\ & + P_3 x(t-\xi_0)\dot{x}(t-\xi_0) + P_4 \ddot{x}(t-\xi_0) + P_5 x^2(t-\xi_0)\dot{x}(t-\xi_0) \\ & + P_6 \dot{x}^2(t-\xi_0) + P_7 x(t-\xi_0)\ddot{x}(t-\xi_0) \end{aligned} \tag{24}$$

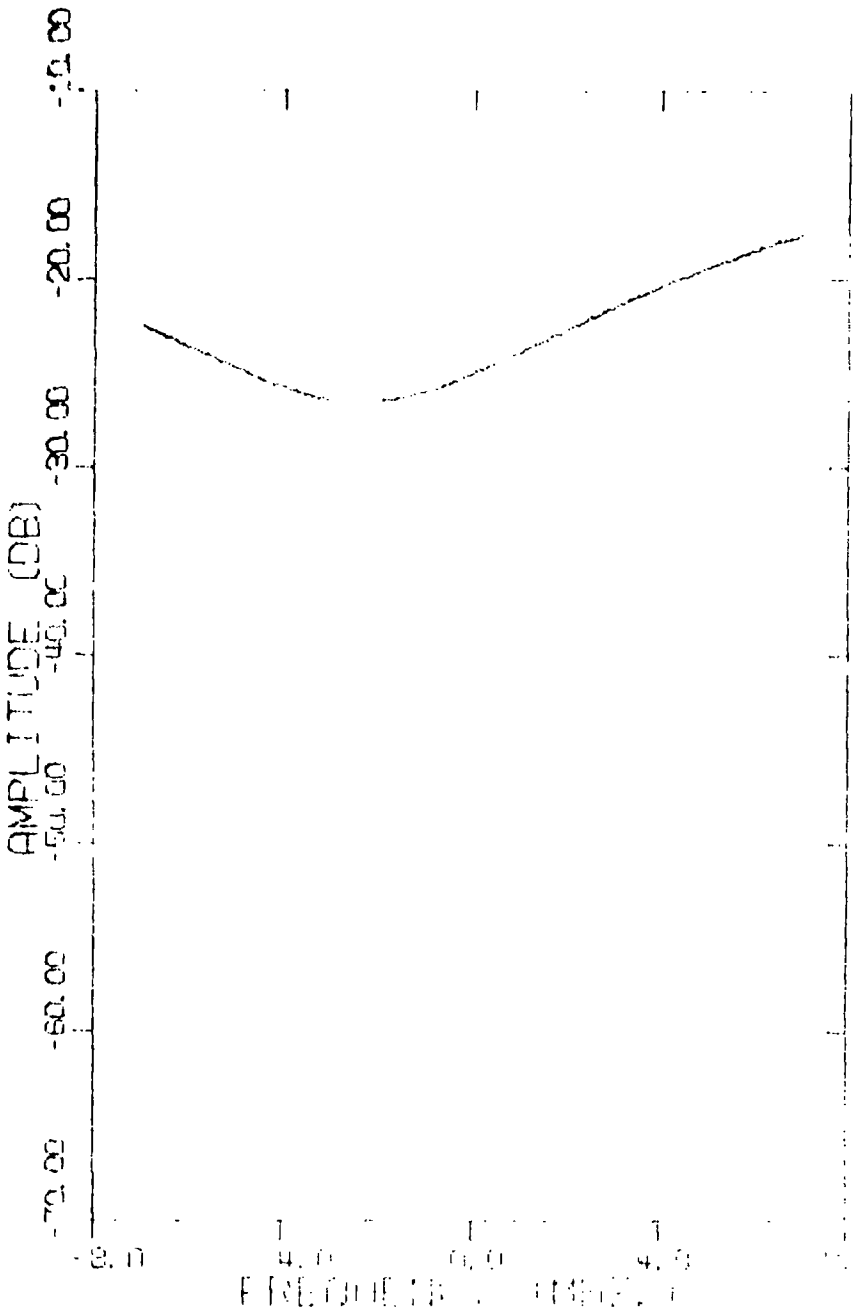

Figure 13 Amplitude Vs. Frequency for 25 dB Fade ("Bad" Channel)

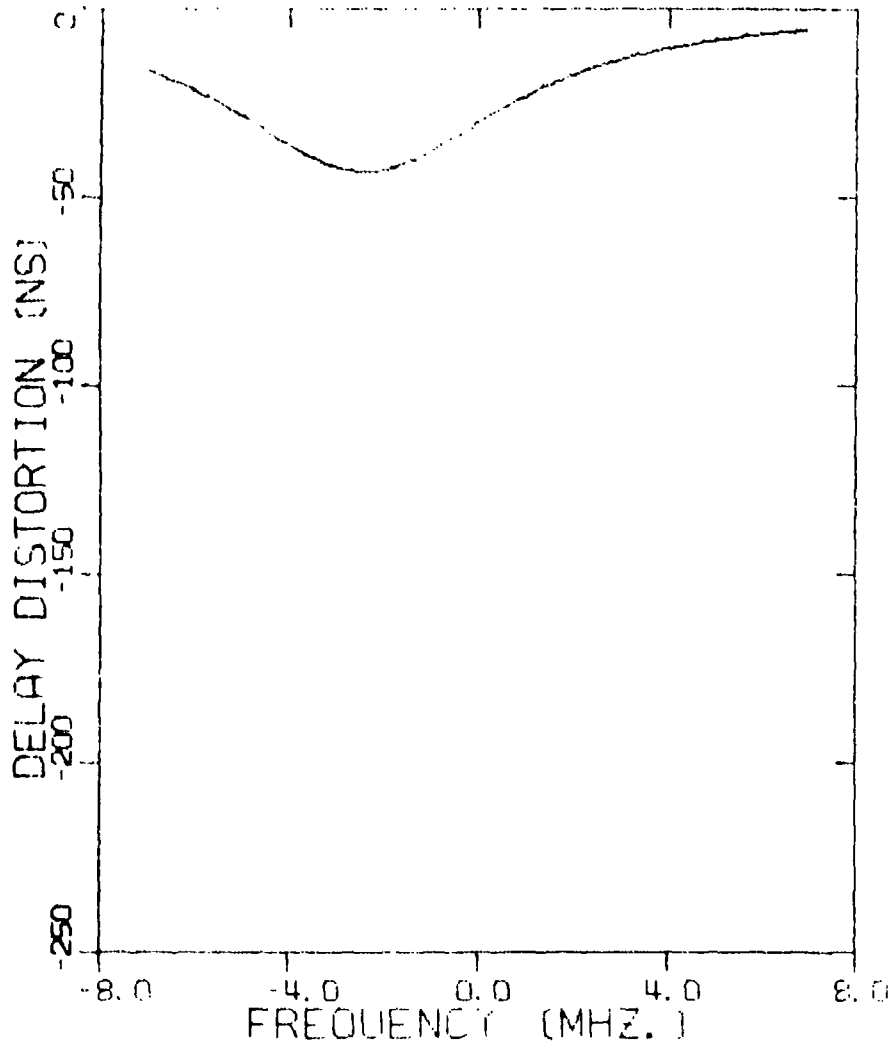

Figure 14 Group Delay Vs. Frequency for 25 dB Fade ("Bad" Channel)

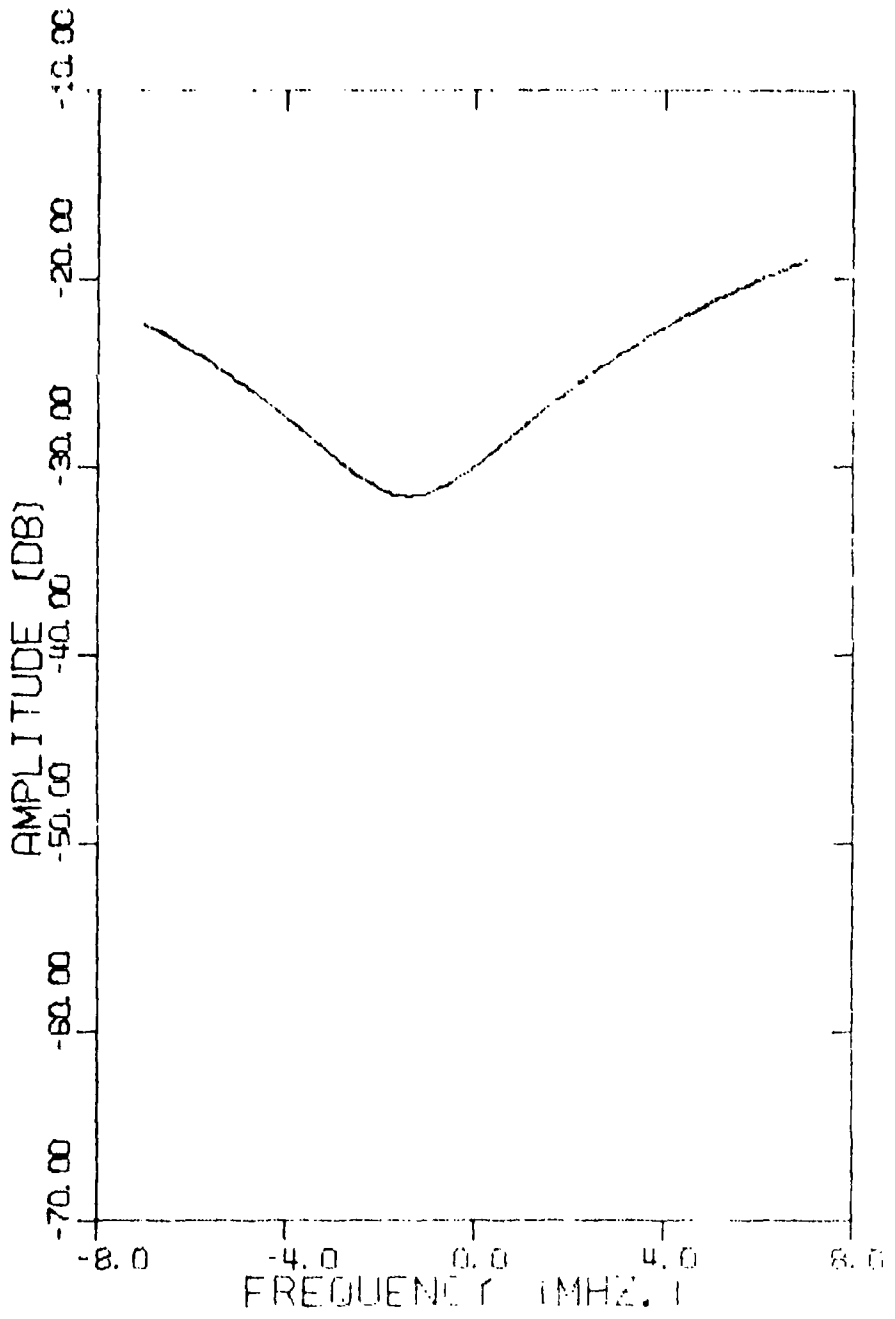

Figure 15 Amplitude Vs. Frequency for 30 dB Fade ("Bad" Channel)

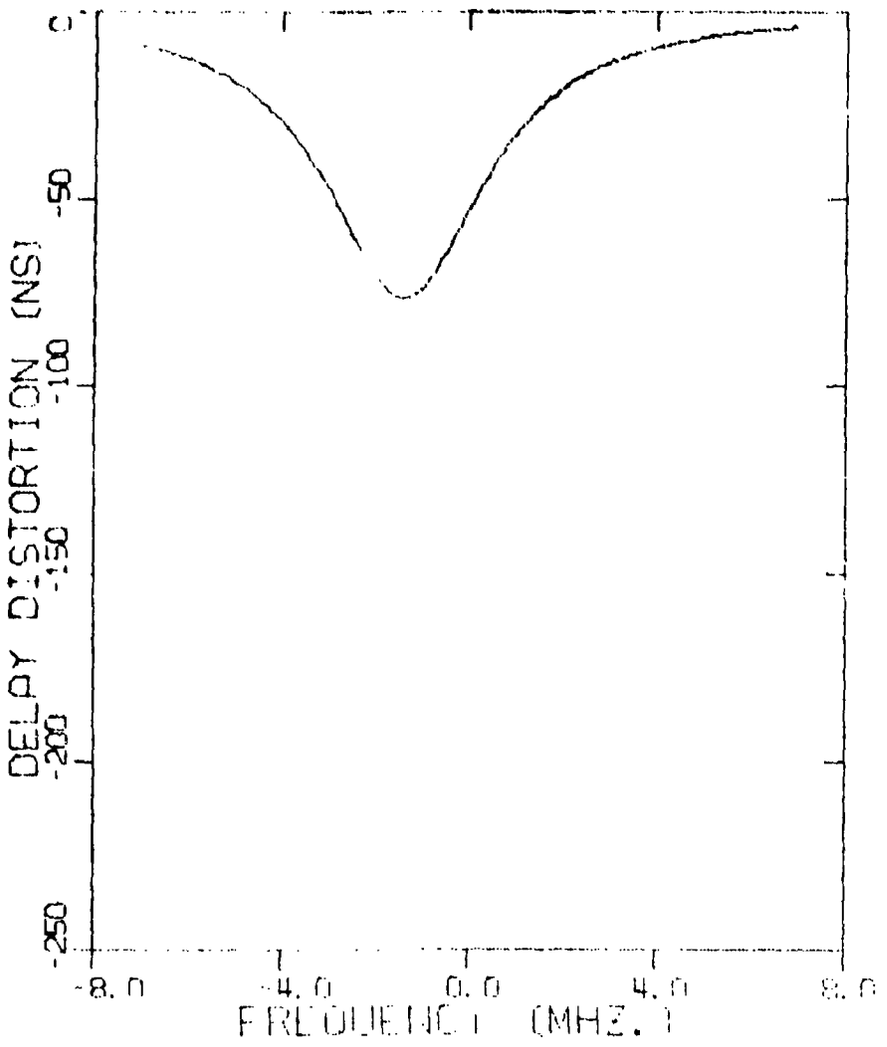

Figure 16 Group Delay Vs. Frequency for 30 dB Fade ("Bad" Channel)

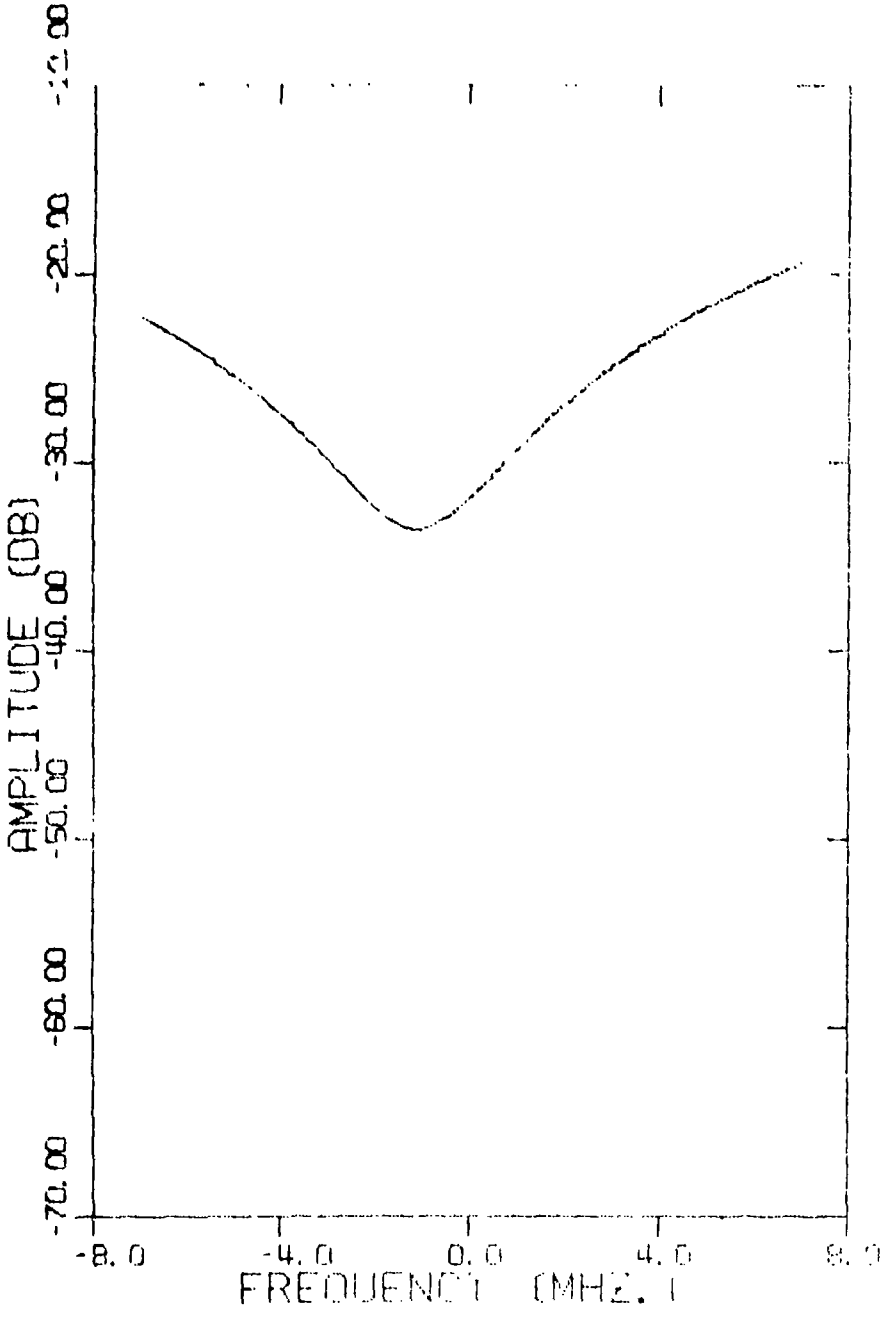

Figure 17 Amplitude Vs. Frequency for 32 dB Fade ("Bad" Channel)

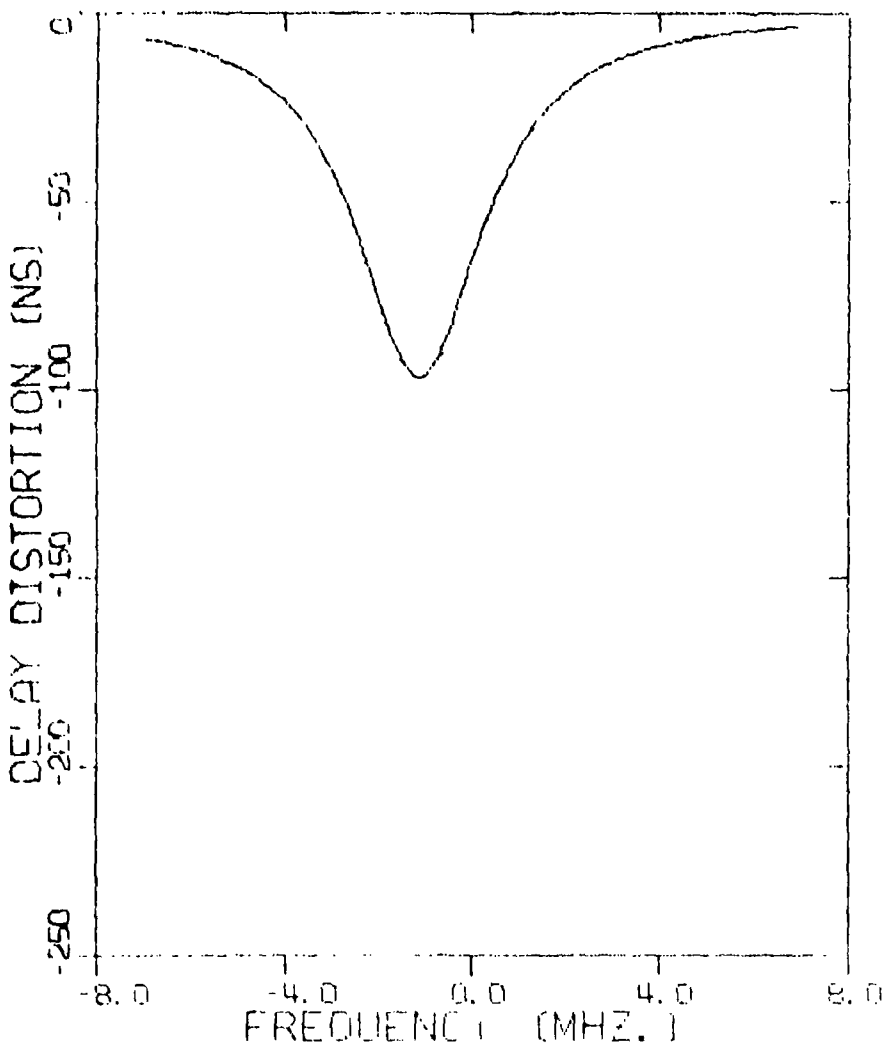

Figure 18 Group Delay Vs. Frequency for 32 dB Fade ("Bad" Channel)

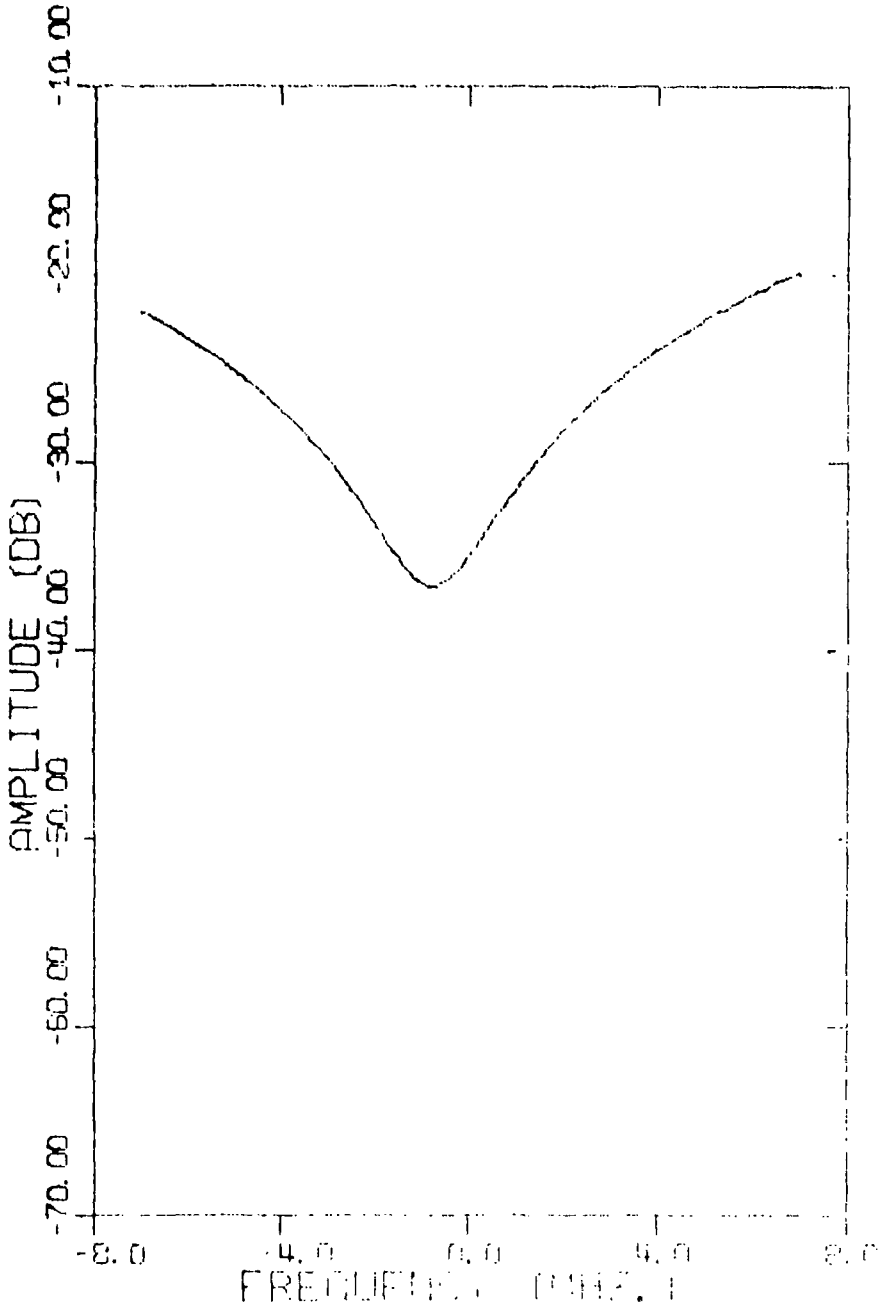

Figure 19 Amplitude Vs. Frequency for 35 dB Fade ("Bad" Channel)

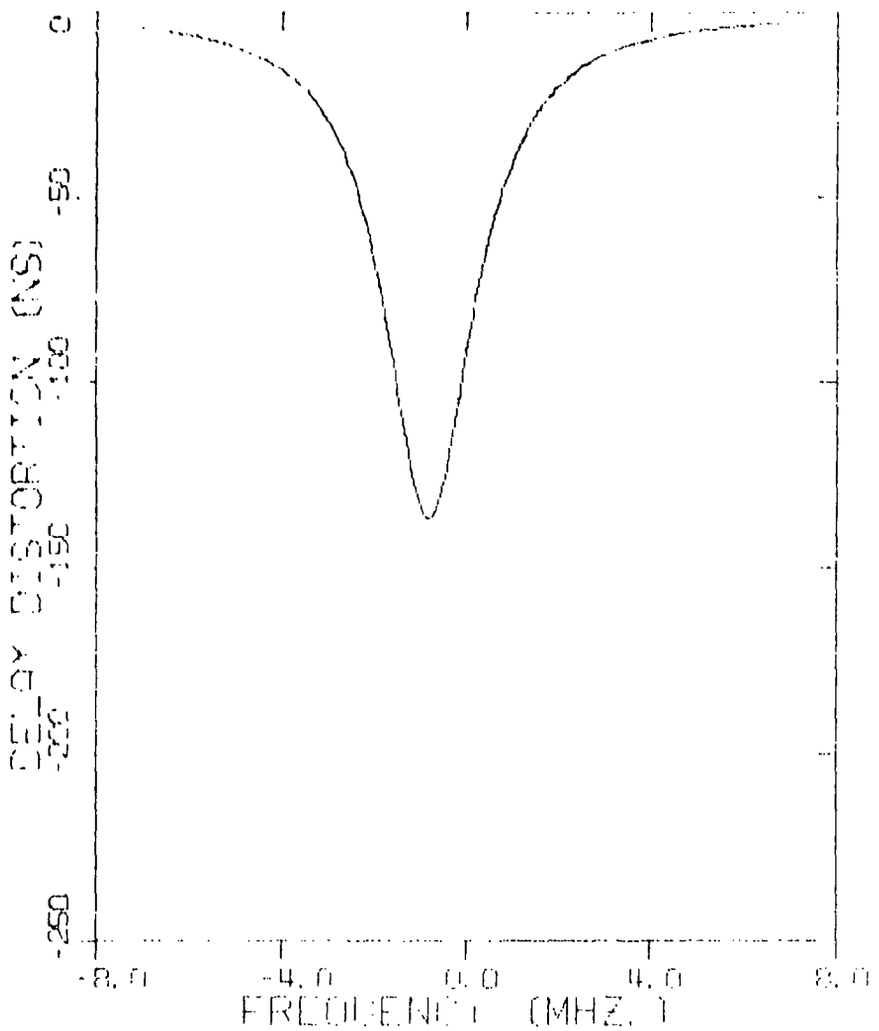

Figure 20 Group Delay Vs. Frequency for 35 dB Fade ("Bad" Channel)

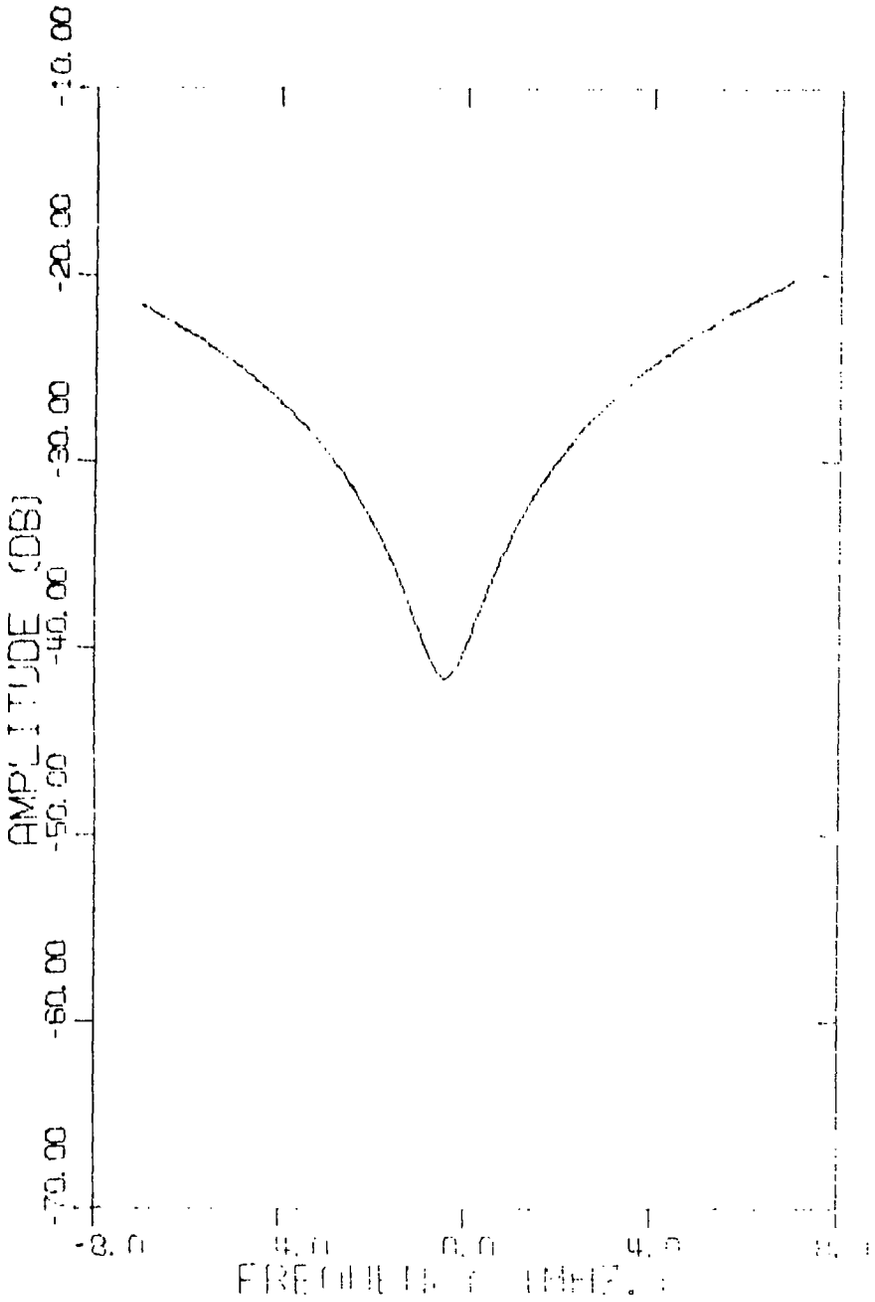

Figure 21 Amplitude Vs. Frequency for 40 dB Fade ("Bad" Channel)

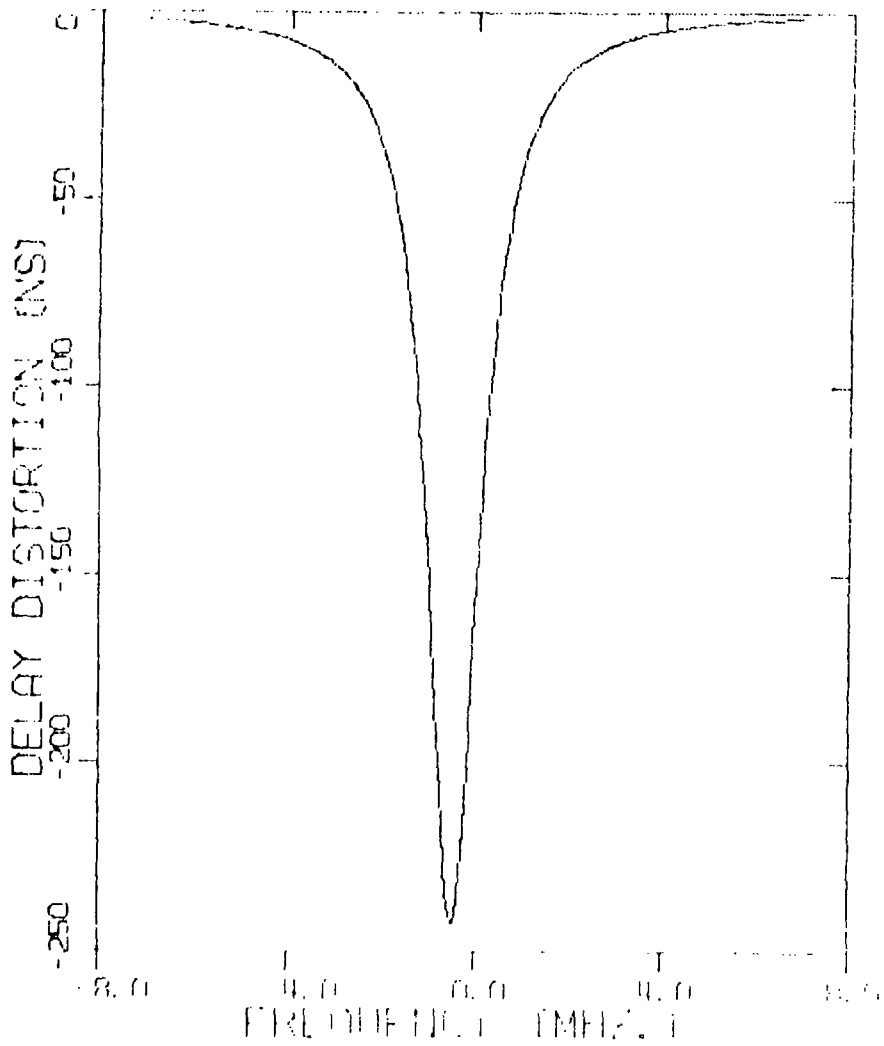

Figure 22 Group Delay Vs. Frequency for 40 dB Fade ("Bad" Channel)

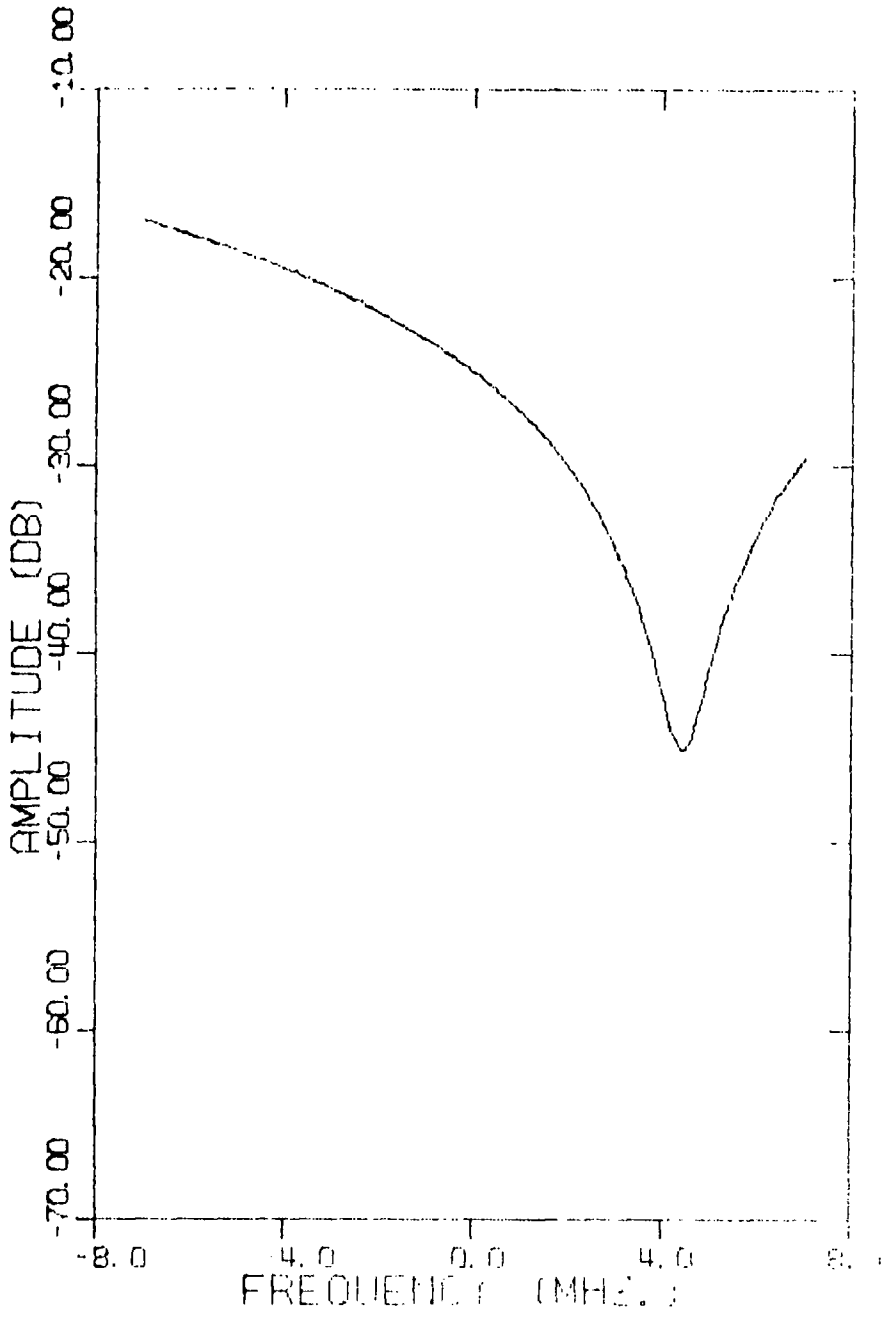

Figure 23 Amplitude Vs. Frequency for 25 dB Fade ("Good" Channel)

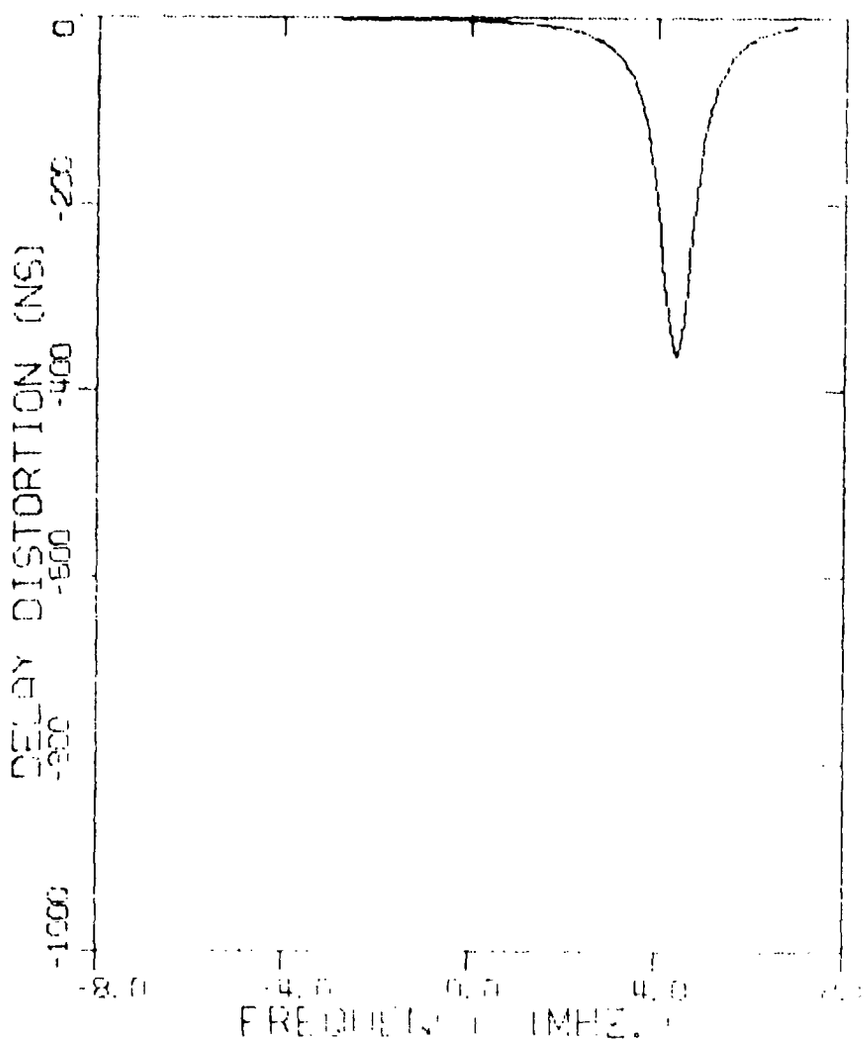

Figure 24 Group Delay Vs. Frequency for 25 dB Fade ("Good" Channel)

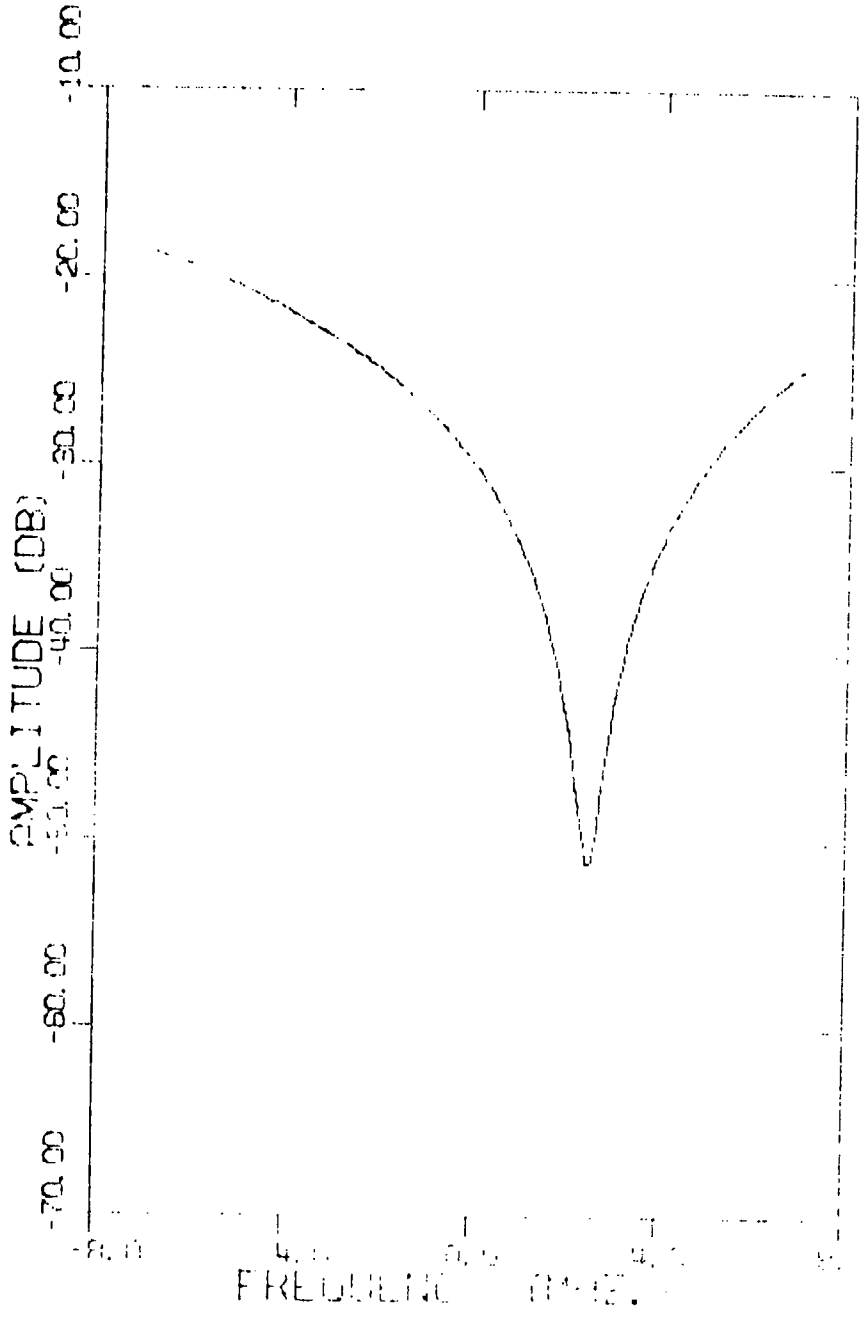

Figure 25 Amplitude Vs. Frequency for 30 dB Fade ("Good" Channel)

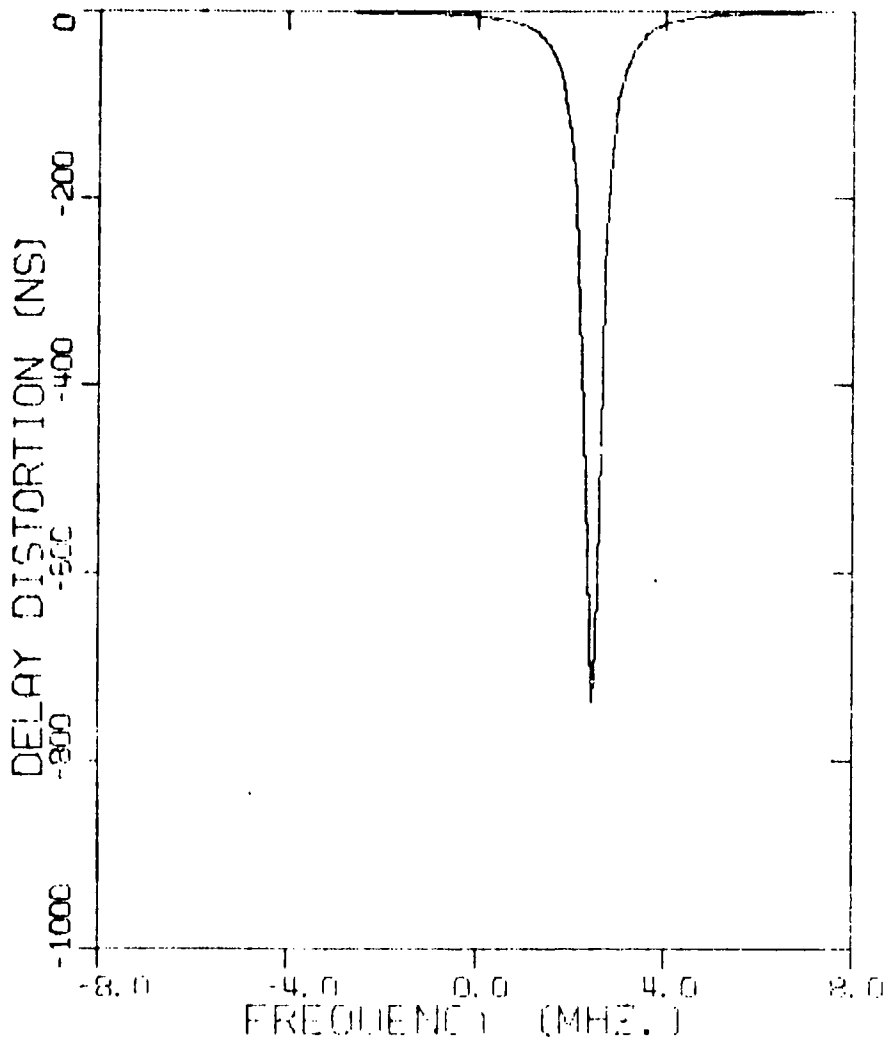

Figure 26 Group Delay Vs. Frequency for 30 dB Fade ("Good" Channel)

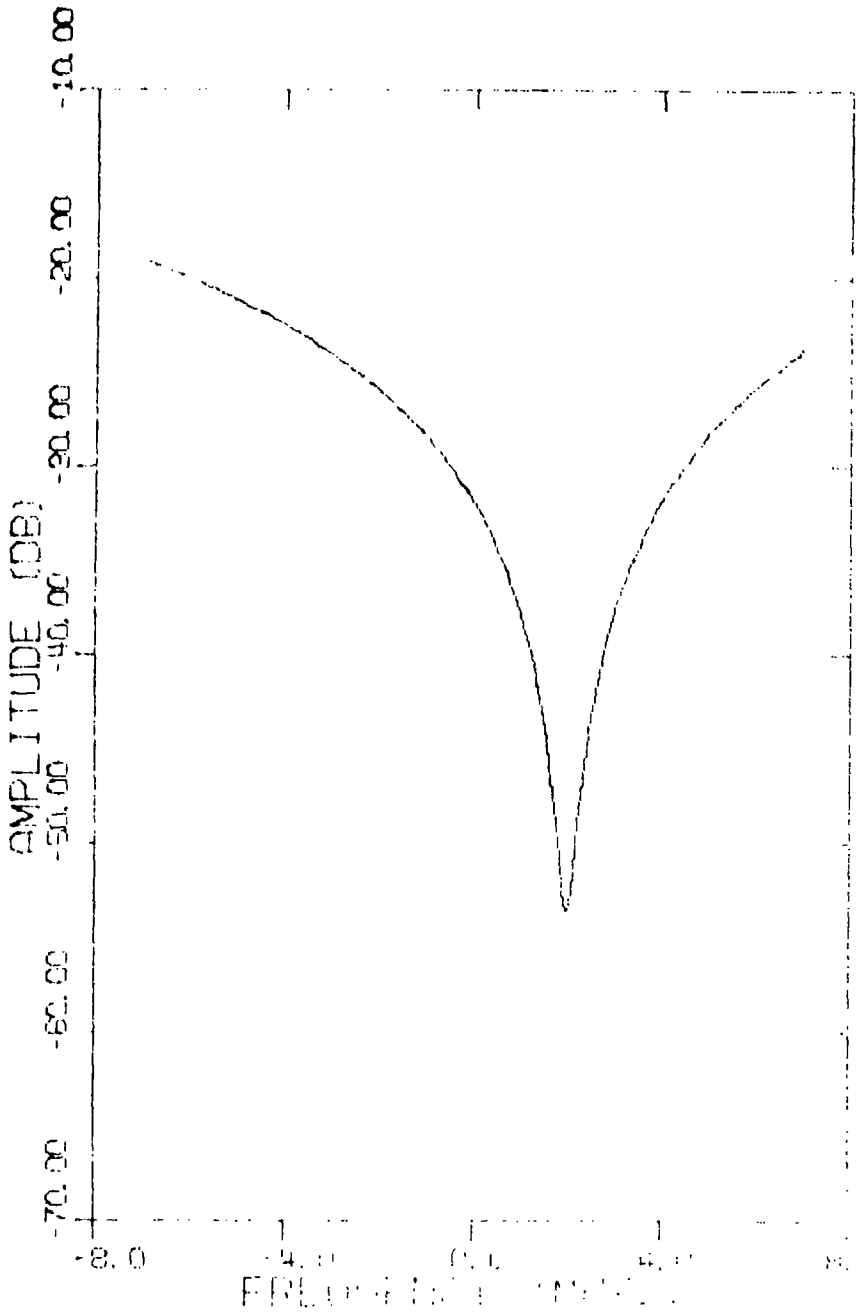

Figure 27 Amplitude Vs. Frequency for 32 dB Fade ("Good" Channel)

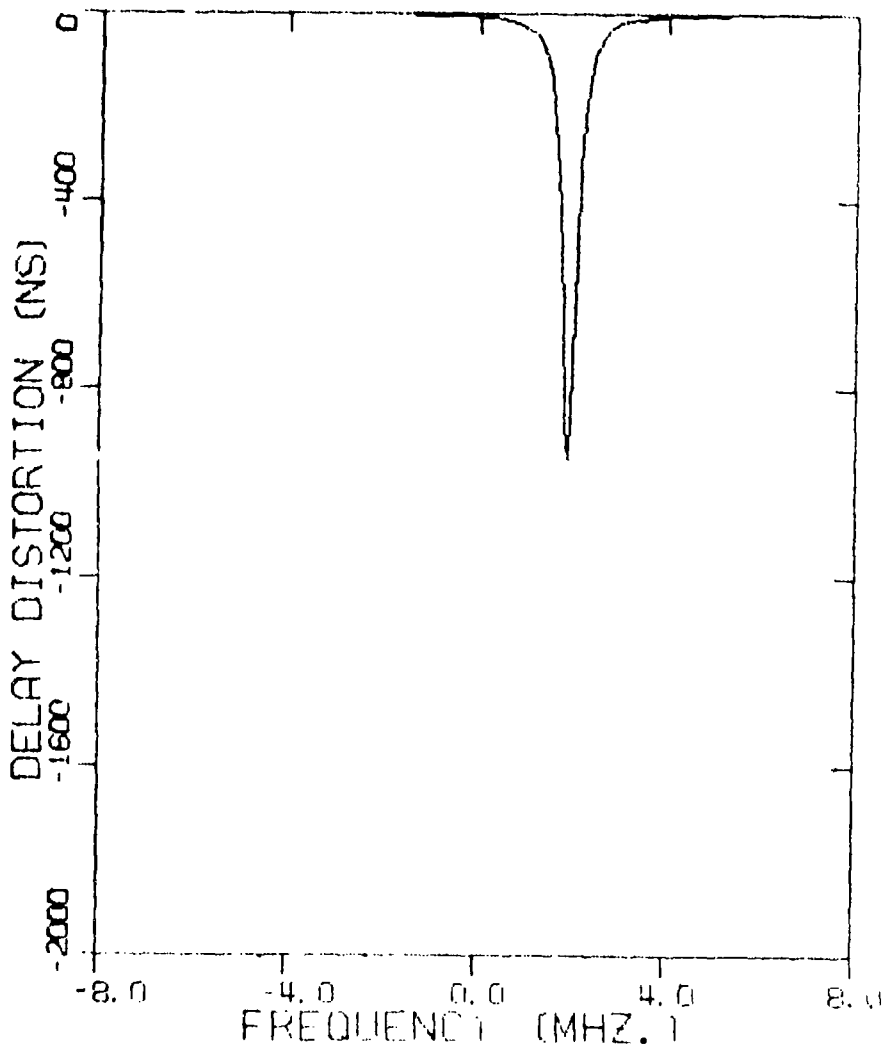

Figure 28 Group Delay Vs. Frequency for 32 dB Fade ("Good" Channel)

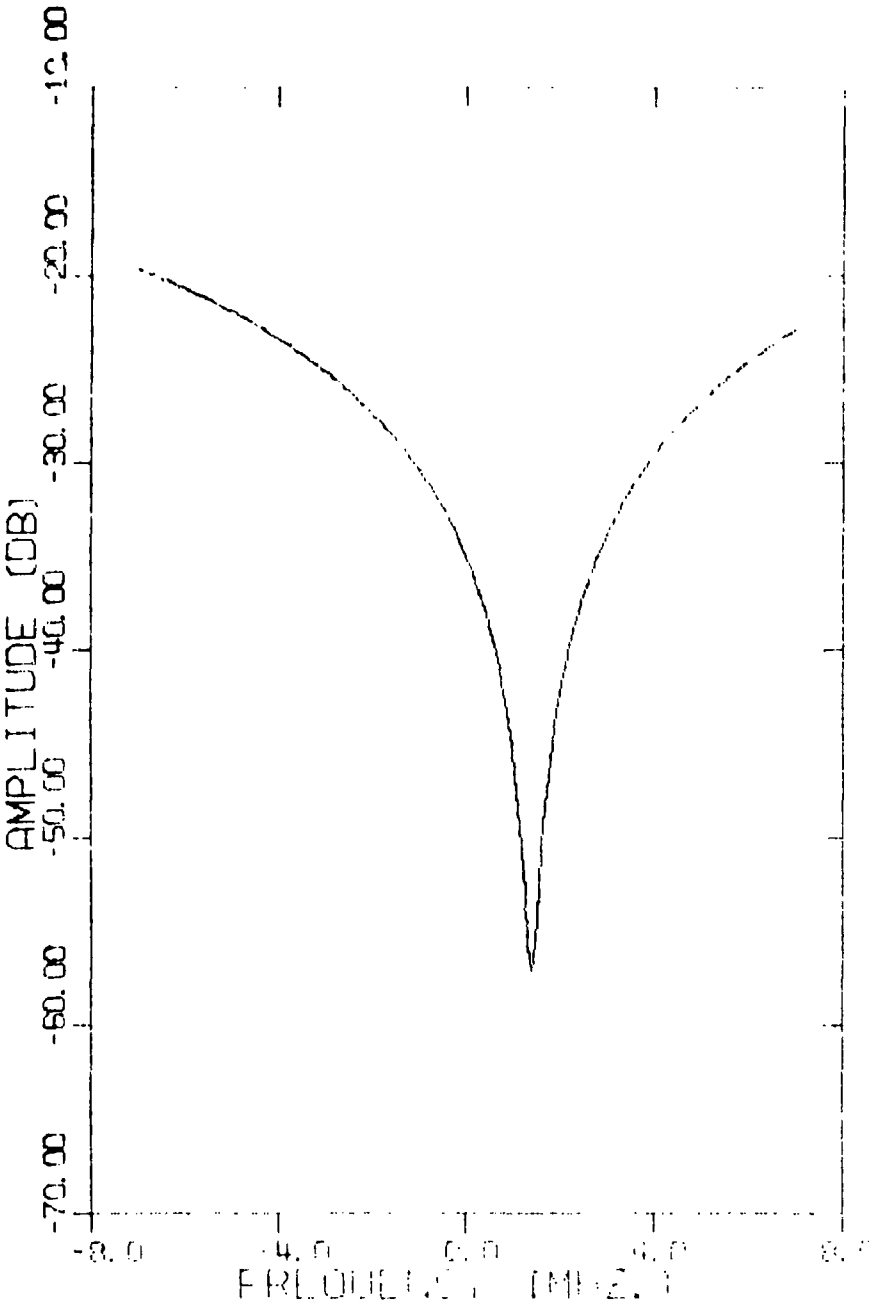

Figure 29 Amplitude Vs. Frequency for 35 dB Fade ("Good" Channel)

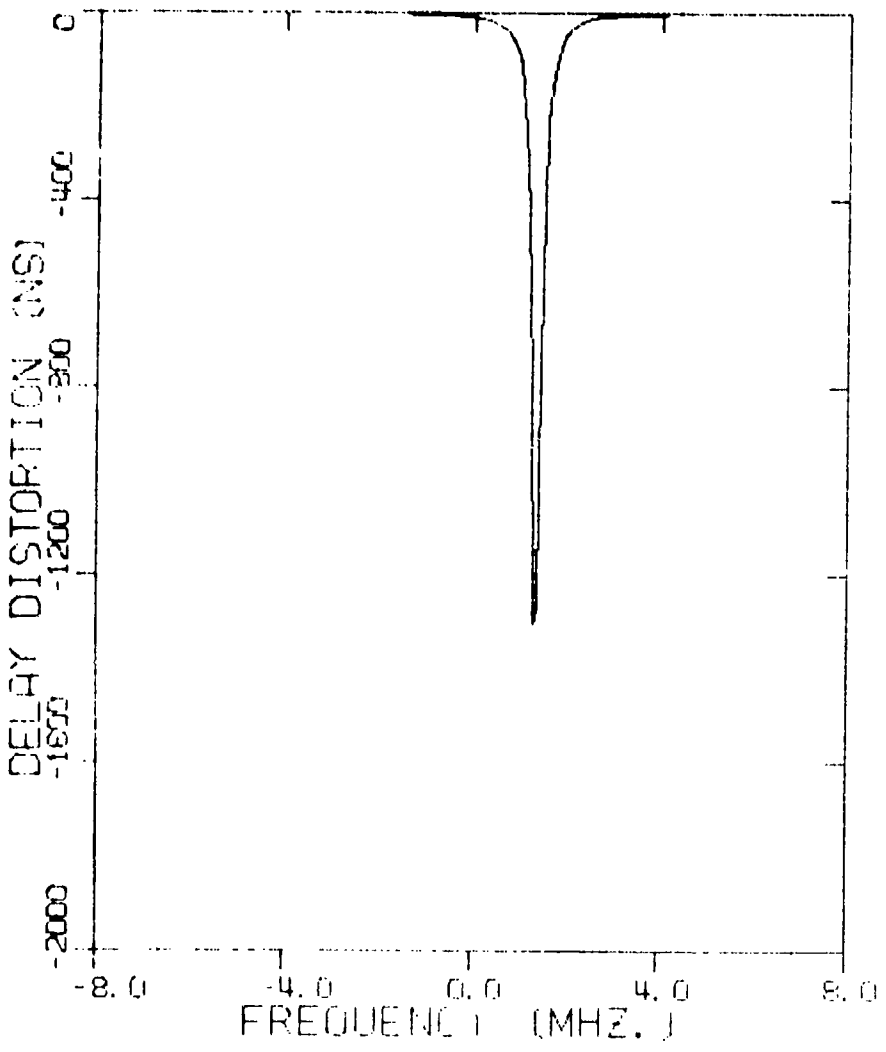

Figure 30 Group Delay Vs. Frequency for 35 dB Fade ("Good" Channel)

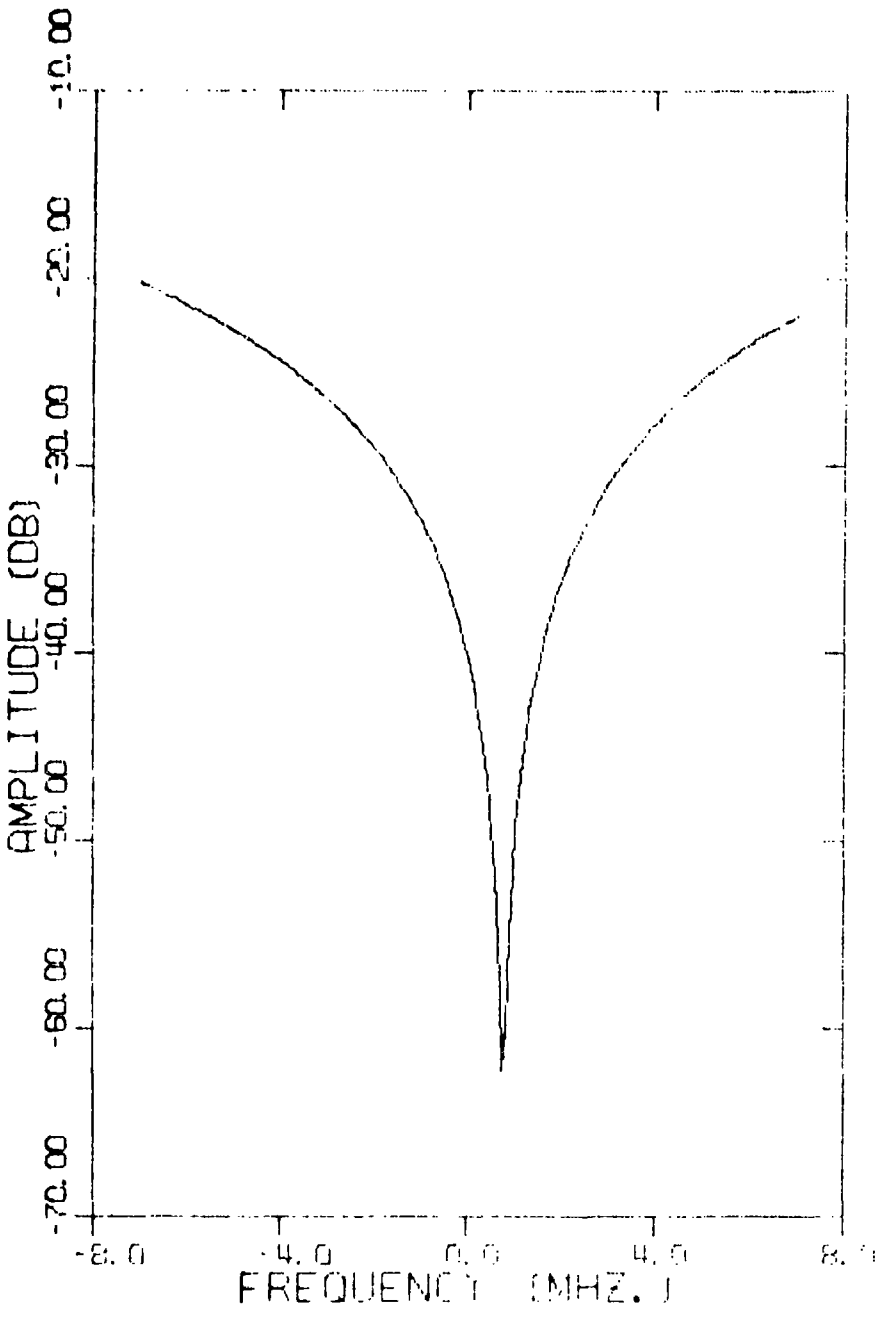

Figure 31 Amplitude Vs. Frequency for 40 dB Fade ("Good" Channel)

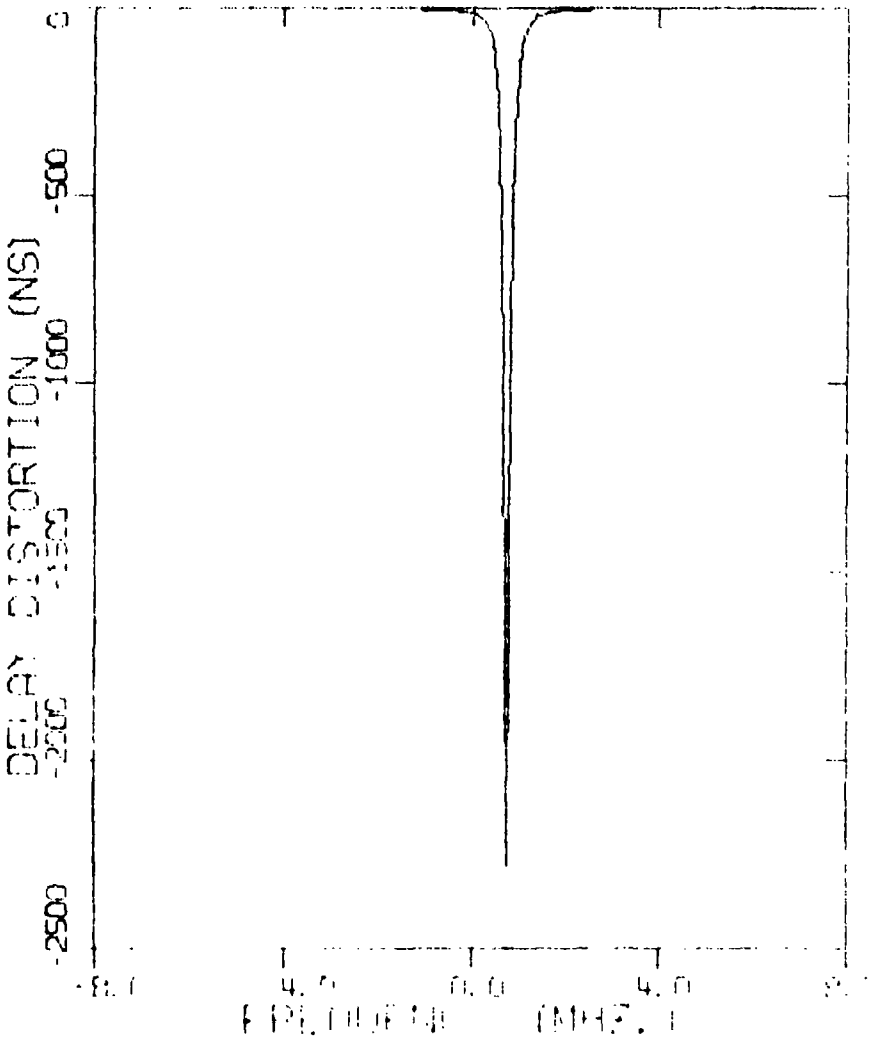

Figure 32 Group Delay Vs. Frequency for 40 dB Fade ("Good" Channel)

where P_i, $i = 0,1,2,3$, are given by (21) and where

$$P_4 = \mathrm{Re}\left\{\frac{T_0^*(t)T_3(t)}{|T_0(t)|^2}\right\}$$

$$P_5 = -3\mathrm{Re}\left\{\frac{T_0^*(t)T_3(t)}{|T_0(t)|^2}\right\} - 3\,\mathrm{Im}\left\{\frac{T_0^*(t)T_1(t)}{|T_0(t)|^2}\right\}\ \mathrm{Im}\left\{\frac{T_0^*(t)T_2(t)}{|T_0(t)|^2}\right\}$$

$$+ 3\mathrm{Re}\left\{\frac{T_0^*(t)T_1(t)}{|T_0(t)|^2}\right\}\ \mathrm{Re}\left\{\frac{T_0^*(t)T_2(t)}{|T_0(t)|^2}\right\} - \mathrm{Re}^3\left\{\frac{T_0^*(t)T_1(t)}{|T_0(t)|^2}\right\}$$

$$+ 3\mathrm{Im}^2\left\{\frac{T_0^*(t)T_1(t)}{|T_0(t)|^2}\right\}\ \mathrm{Re}\left\{\frac{T_0^*(t)T_1(t)}{|T_0(t)|^2}\right\}$$

$$P_6 = P_7 = -3\,\mathrm{Im}\left\{\frac{T_0^*(t)T_3(t)}{|T_0(t)|^2}\right\} + \mathrm{Re}\left\{\frac{T_0^*(t)T_1(t)}{|T_0(t)|^2}\right\}\ \mathrm{Im}\left\{\frac{T_0^*(t)T_2(t)}{|T_0(t)|^2}\right\}$$

$$+ \mathrm{Re}\left\{\frac{T_0^*(t)T_2(t)}{|T_0(t)|^2}\right\}\ \mathrm{Im}\left\{\frac{T_0^*(t)T_1(t)}{|T_0(t)|^2}\right\} \qquad (25)$$

Therefore, by using Eqs. (21) and (25) we can estimate the discriminator output using either a quadratic or cubic channel model.

REFERENCES FOR APPENDIX B

[1] P. A. Bello, et al., "Line-of-Sight Technical Investigation," Final Report on Contract F30602-73-C-0244 by CNR, Inc., for RADC, June 1974, RADC TR 74-330, (AD006104).

[2] P. A. Bello, "Characterization of Randomly Time-Variant Linear Channels," IEEE Trans. on Comm. Systems, December 1963, pp. 360 - 393.

[3] P. A. Bello, et al., "Line-of-Sight Wideband Propagation," Final Report on Contract F30602-73-C-0013 by CNR, Inc., for RADC, May 1973, RADC-TR-73-167, (AD762939).

[4] P. A. Bello and B. D. Nelin, "The Effects of Frequency Selectivity Fading on Intermodulation Distortion and Subcarrier Phase Stability in Frequency Modulation Systems," IEEE Trans. on Comm. Systems, March 1964, pp. 87 - 101.

[5] P. A. Bello, "Time-Frequency Duality," IEEE Trans. on Inf. Theory, January 1964, pp. 18 - 33.

APPENDIX C

DISTORTION IN FM LOS SYSTEMS CALCULATED FROM TWO- AND THREE-PATH CHANNEL MODELS

1. Introduction

In this appendix we address the problem of evaluating the frequency selectivity-induced distortion for a duobinary FM LOS system. For analysis purposes, two-path and three-path channel models were considered. For these channel models, the distortion at the shaping filter output and at the discriminator output was determined.

The purpose of this analysis is to develop expressions for the received baseband signal which are required for the simulations discussed in Section 4.3.5. These simulations were used to evaluate the performance of the adaptive channel estimator.

2. System Description

For our analysis we consider a duobinary FM LOS system of the type presented in Figure 1. The performance of the system is as follows. A data sequence $\{a_n\}$ modulates a train of impulses which is filtered to form $x(t)$, the input to the frequency modulator. The frequency modulator output is transmitted over the channel, bandpass-filtered in the receiver, and frequency-demodulated. To complete the duo-binary pulse shaping and reduce the noise in the receiver, the discriminator output is passed through a receive shaping filter.

In Section 3 below we will show that the output of the discriminator can be expressed as the sum of three terms: a signal term, a distortion term, and a noise term. The noise in a FM duobinary LOS system has been considered in detail in Appendix A. In this appendix we will derive expressions for the frequency-selectivity induced distortion.

3. Selectivity-Induced Distortion for a Two-Path Channel

In this section we will use a two-path channel model to determine the distortion introduced by the frequency selectivity of the channel. A two-path channel model is used because an

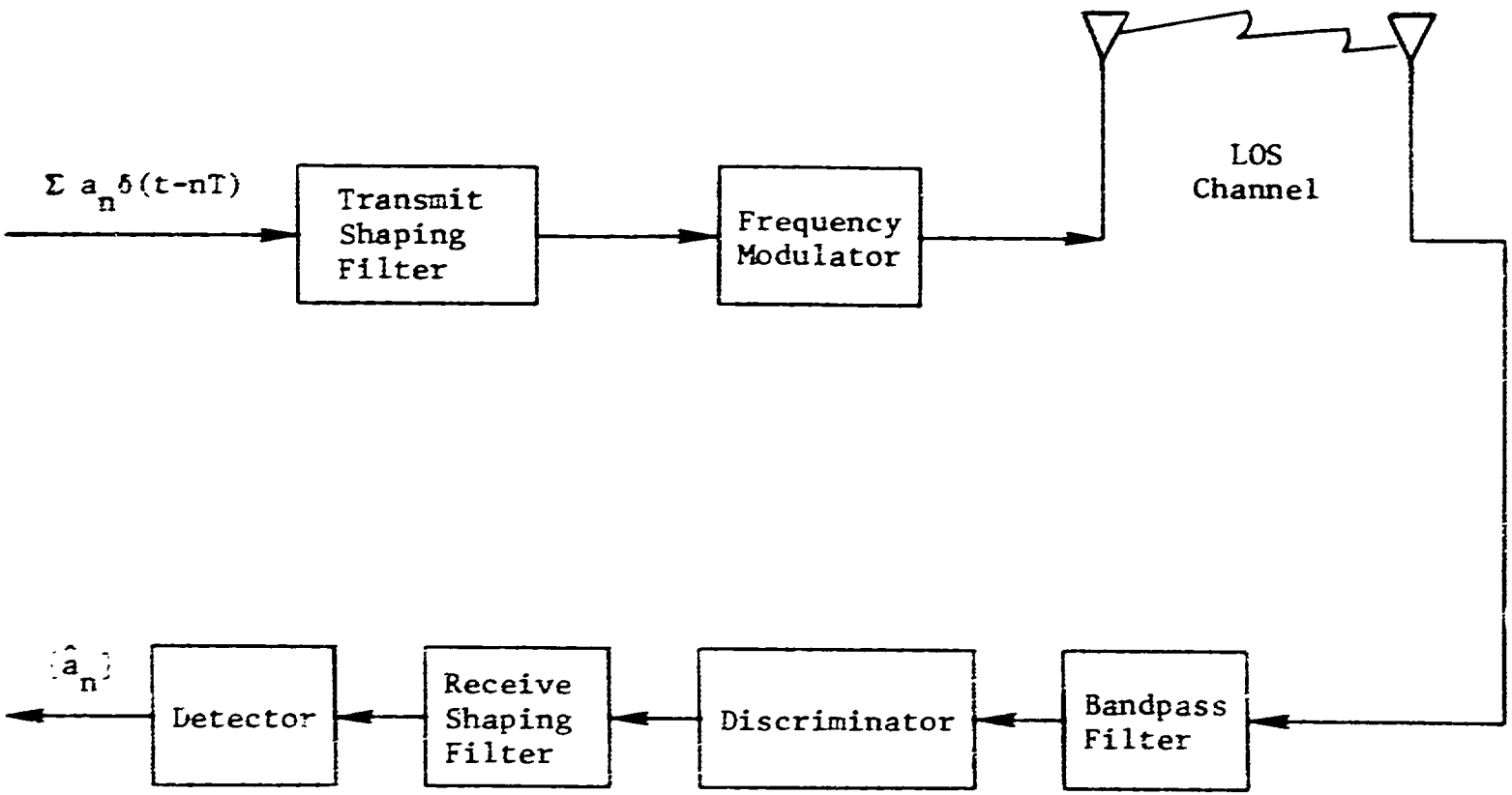

Figure 1 System Block Diagram

exact expression can be obtained for the received baseband signal.

For a two-path channel model, the time-varying channel impulse response is given by

$$g(t,\xi) = \sum_{i=1}^{2} \alpha_i(t)\, e^{-j2\pi f_0 \tau_i(t)}\, \delta\left[\xi - \tau_i(t)\right] \tag{1}$$

where $\tau_i(t)$ and $\alpha_i(t)$ are the time-varying delay and gain of the i^{th} path, respectively. Since the time variations of a LOS channel are much slower than the data rate, then over many data bits the channel may be considered fixed. Therefore, the time dependence in (1) will be dropped. Furthermore, without loss of generality, we can assume that the direct path (assumed to be path 1) has gain 1 and delay 0. For path 2, we will define

$$\alpha_2\, e^{-j2\pi f_0 \tau_2} \triangleq \mu + ju \tag{2}$$

where we have dropped the time dependence. Therefore, without loss of generality, we can assume that $g(t,\xi)$ can be expressed as

$$g(\xi) = \delta(\xi) + (\mu + ju)\,\delta(\xi - \tau_2) \tag{3}$$

over a time interval of many data bits.

The received data signal is related to the transmitted data signal by [1]

$$q(t) = \int z(t-\xi)\, g(\xi)\, d\xi \tag{4}$$

Substituting (3) into (4) and performing the indicated convolution gives

$$q(t) = z(t) + (\mu + ju)\, z(t - \tau_2) \tag{5}$$

For FM systems, the transmitted data signal is

$$z(t) = e^{j\varphi(t)} \tag{6}$$

where $\varphi(t)$ is the baseband data signal. From (5) and (6), the received data signal is

$$q(t) = e^{j\varphi(t)}\left\{1 + (\mu + ju)\, e^{j\left[\varphi(t-\tau_2)-\varphi(t)\right]}\right\} \tag{7}$$

Defining $\Delta\varphi$ by

$$\Delta\varphi \triangleq \varphi(t-\tau_2) - \varphi(t) \tag{8}$$

then $q(t)$ can be expressed as

$$q(t) = e^{j\varphi(t)}\left\{\left[1 + \mu\cos(\Delta\varphi) - u\sin(\Delta\varphi)\right] + j\left[u\cos(\Delta\varphi) + j\mu\sin(\Delta\varphi)\right]\right\} \tag{9}$$

or

$$q(t) = A(t)\, e^{j\left[\varphi(t)+B(t)\right]} \tag{10}$$

where

$$A^2(t) = \left[1 + \mu\cos(\Delta\varphi) - u\sin(\Delta\varphi)\right]^2 + \left[u\cos(\Delta\varphi) + \mu\sin(\Delta\varphi)\right]^2 \tag{11}$$

$$B(t) = \tan^{-1}\left|\frac{u\cos(\Delta\varphi) + \mu\sin(\Delta\varphi)}{1 + \mu\cos(\Delta\varphi) - u\sin(\Delta\varphi)}\right| \tag{12}$$

The purpose of the IF filter is to reduce the noise at the discriminator input. The bandwidth of this filter should be wide enough so that the received signal is passed nearly undistorted.

Differentiating the phase of (10) and including noise, the discriminator output is

$$r(t) = \dot{\varphi}(t) + \dot{B}(t) + n_D(t) \tag{13}$$

where $n_D(t)$ is the noise term.

Since $\dot{\varphi}(t)$ is the desired signal, $\dot{B}(t)$ is the distortion at the discriminator output introduced by the multipath-induced frequency selectivity. $\dot{B}(t)$ can be found by differentiating (12); after some simplification, this gives

$$\dot{B}(t) = (\Delta\dot{\varphi})\left[\frac{-u\sin(\Delta\varphi) + \mu\cos(\Delta\varphi) + \mu^2 + u^2}{\mu^2 + u^2 + 1 + 2\mu\cos(\Delta\varphi) - 2u\sin(\Delta\varphi)}\right] \tag{14}$$

It should be mentioned that, although we call $\dot{B}(t)$ distortion, part of the effect of the multipath is the introduction of a time-varying group delay, which is not really distortion. This time-varying group delay is discussed in Section 4.5.

The distortion at the output of the receive shaping filter is

$$D(t) = \int_{-\infty}^{\infty} h_R(\tau)\ \dot{B}(t-\tau)\, d\tau \tag{15}$$

In Section 6 below, we will present statistical properties of the signal at the discriminator and receive filter outputs. These were obtained via a simulation. These properties will aid in determining the effect of the distortion upon error rates for FM duobinary LOS modems.

The distortion given by (14) can be expressed in terms of the baseband signal by expanding $\varphi(t-\tau_2)$ in a Taylor series about $\varphi(t)$; in particular,

$$\varphi(t-\tau_2) = \varphi(t) - \tau_2\dot{\varphi}(t) + \frac{\tau_2^2}{2}\ddot{\varphi}(t) - \ldots \tag{16}$$

From the definition of $\Delta\phi$ given by (8), it follows that

$$\Delta\phi = -\tau_2\dot{\phi}(t) + \frac{\tau_2^2}{2}\ddot{\phi}(t) - \ldots$$

$$\Delta\dot{\phi} = -\tau_2\ddot{\phi}(t) + \frac{\tau_2^2}{2}\dddot{\phi}(t) - \ldots \qquad (17)$$

For duobinary FM, the baseband signal is

$$x(t) = \dot{\phi}(t) = \sum_{n=-\infty}^{\infty} a_n h_T(t - nT) \qquad (18)$$

where $h_T(t)$ is the impulse response of the transmit shaping filter. From (17) and (18), $\Delta\phi$ and $\Delta\dot{\phi}$ can be expressed in terms of the data and transmit shaping filter impulse response.

4. Use of Quadratic Channel Model to Estimate Distortion

In Section 3 above, the two-path channel model was used to evaluate the distortion (at the discriminator and receive filter output) in a duobinary FM modem. The distortion will now be evaluated using the parameters of the quadratic channel model.

Bello and Nelin [1] have determined the distortion at the output of a discriminator introduced by the frequency selectivity of the channel. In their analysis, a quadratic approximation to the time-varying transfer function of the channel was used. Section 4 of Appendix B derives the channel parameters for a quadratic and cubic approximation to the time-varying transfer function of the channel. From Eqs. (60) - (62) of Ref. [1], their estimate of the distortion is

$$\hat{B}(t) = \dot{x}(t)P_1 + \ddot{x}(t)P_2 + x(t)\dot{x}(t)P_3 \qquad (19)$$

where

$$P_1 = \mathrm{Re}\left\{\frac{T_1(t)T_0^*(t)}{|T_0(t)|^2}\right\}$$

$$P_2 = \mathrm{Re}\left\{\frac{T_2(t)T_0^*(t)}{|T_0(t)|^2}\right\}$$

$$P_3 = 2\left[\mathrm{Re}\left\{\frac{T_1(t)T_0^*(t)}{|T_0(t)|^2}\right\} \cdot \mathrm{I_m}\left\{\frac{T_1(t)T_0^*(t)}{|T_0(t)|^2}\right\} - \mathrm{I_m}\left\{\frac{T_2(t)T_0^*(t)}{|T_0(t)|^2}\right\}\right]$$

(20)

and where $T_n(t)$ are coefficients in an f-power series expansion of $T(f,t)$, the time-varying channel transfer function [2]. For the two-path channel model considered in Section 3 above, the above coefficients are given by

$$T_0(t) = 1 + \mu + ju$$

$$T_1(t) = \tau_2(\mu + ju)$$

$$T_2(t) = \frac{1}{2}\tau_2^2(\mu + ju) \qquad (21)$$

From (20) and (21), the channel parameters P_i for the two-path channel are given by

$$P_1 = -\tau_2 \frac{\mu^2 + u^2 + \mu}{(1+\mu)^2 + u^2}$$

$$P_2 = \frac{\tau_2^2\left(\mu^2 + u^2 + \mu\right)}{2\left[(1+\mu)^2 + u^2\right]}$$

$$P_3 = \frac{\tau_2^2\left[u\left(\mu^2 + u^2 - 1\right)\right]}{\left[(1+\mu)^2 + u^2\right]^2} \qquad (22)$$

Comparing $\hat{B}(t)$ given by (14) and $\hat{\dot{B}}(t)$ given above, it can be shown that if $\dot{B}(t)$ is expanded into a series involving $x(t)$ and its derivatives, then P_1, P_2, and P_3 are the coefficients of $x(t)$, $\dot{x}(t)$, and $x(t)\dot{x}(t)$, respectively.[3] Therefore, higher-order products of $x(t)$ and its derivatives result in errors in using $\hat{\dot{B}}(t)$ to estimate $\dot{B}(t)$.

5. Selectivity-Induced Distortion for a Three-Path Channel

In Section 3 above, a two-path channel model was used to find the distortion at the discriminator and receive shaping filter outputs. It has been shown [3] that the LOS channel can be frequently modeled as a two- or three-path channel. In this section we extend the analysis of the above-mentioned channel to the case of a three-path channel. This analysis is analogous to the two-path analysis and is presented for completeness and because of the importance of the three-path channel model in LOS systems.

For a three-path channel, the time-varying impulse response of the channel is

$$g(t,\xi) = \sum_{i=1}^{3} A_i(t)\, \delta\left[\xi - \tau_i(t)\right] \tag{23}$$

where $A_i(t)$ is the time-varying complex gain of the i^{th} path and $\tau_i(t)$ is its delay. Without loss of generality we can assume

$$A_1(t) = 1$$

$$A_2(t) = u + jv$$

$$A_3(t) = y + jz \tag{24}$$

where a "frozen" channel has been assumed since the channel variations are on a time scale order of magnitude slower than the symbol duration.

The received signal is given by

$$q(t) = \int z(t-\xi)\, g(t,\xi)\, d\xi \tag{25}$$

Combining the above equations gives

$$q(t) = e^{j\varphi(t)}\left[1 + (\mu + ju)\, e^{j\Delta\varphi_2} + (y + jz)\, e^{j\Delta\varphi_3}\right] \tag{26}$$

where $\Delta\varphi_i = \varphi(t-\tau_i) - \varphi(t)$. Simplifying gives

$$q(t) = A(t)\, e^{j[\varphi(t)+B(t)]} \tag{27}$$

where B(t) is the phase distortion.

B(t) can be expressed as

$$B(t) = \tan^{-1}\left\{\frac{v\cos\Delta\varphi_2 + u\sin\Delta\varphi_2 + z\cos\Delta\varphi_3 + y\sin\Delta\varphi_3}{1 + u\cos\Delta\varphi_2 - v\sin\Delta\varphi_2 + y\cos\Delta\varphi_3 - z\sin\Delta\varphi_3}\right\} \tag{28}$$

The output of the discriminator is

$$\dot{\varphi}(t) + \dot{B}(t) + n_D(t) \tag{29}$$

where $\dot{\varphi}(t)$ is the signal, $\dot{B}(t)$ is the distortion, and $n_D(t)$ is the noise.

$\dot{B}(t)$ can be easily found from (28) by noting that if

$$F(x) = \tan^{-1}\left\{\frac{g(x)}{h(x)}\right\} \tag{30}$$

then

$$\frac{dF(x)}{dx} = \frac{h(x)\frac{dg(x)}{dx} - g(x)\frac{dh(x)}{dx}}{g^2(x) + h^2(x)} \tag{31}$$

To find $\dot{B}(t)$, $\Delta\rho_2$ and $\Delta\rho_3$ must be evaluated using

$$\Delta\rho_2 = -\tau_2\dot{\phi}(t) + \frac{\tau_2^2}{2}\ddot{\phi}(t) - \ldots$$

$$\Delta\rho_3 = -\tau_3\dot{\phi}(t) + \frac{\tau_3^2}{2}\ddot{\phi}(t) - \ldots \tag{32}$$

where $\dot{\phi}(t)$ is given by (18).

6. Examples

As is shown in Section 4.5.2, the channel selectivity produces a time-varying delay at the output of the discriminator. Ideally, a bit synchronizer would track this delay. A simulation was developed which uses a random bit stream to generate the signal at the output of the receive filter. For a 25-dB fade and the channel that is called a "bad" channel in Appendix B, the mean zero crossing was found. Convergence of the sampling time to the mean zero crossing is sometimes the criterion used to design bit synchronizers [4].

A histogram of this signal sampled at the mean zero crossing offset is shown in Fig. 2. For comparison, if the mean delay is not tracked, then the samples of the receive filter output would have a histogram given by Fig. 3. As can be seen by Fig. 3, if the mean delay is not tracked, errors will be made without noise. From Fig. 2 we note that the channel selectivity has resulted in a SNR loss, as illustrated by the spread about the three signal levels and the reduction in three-level eye opening. However, due to the high SNR during a 25-dB fade, very low error rates are expected if the mean delay is tracked.

The histograms presented in Figures 2 and 3 are each the result of using 10,000 samples of the receive filter output which is then quantized to 128 levels. The number of occurrences in

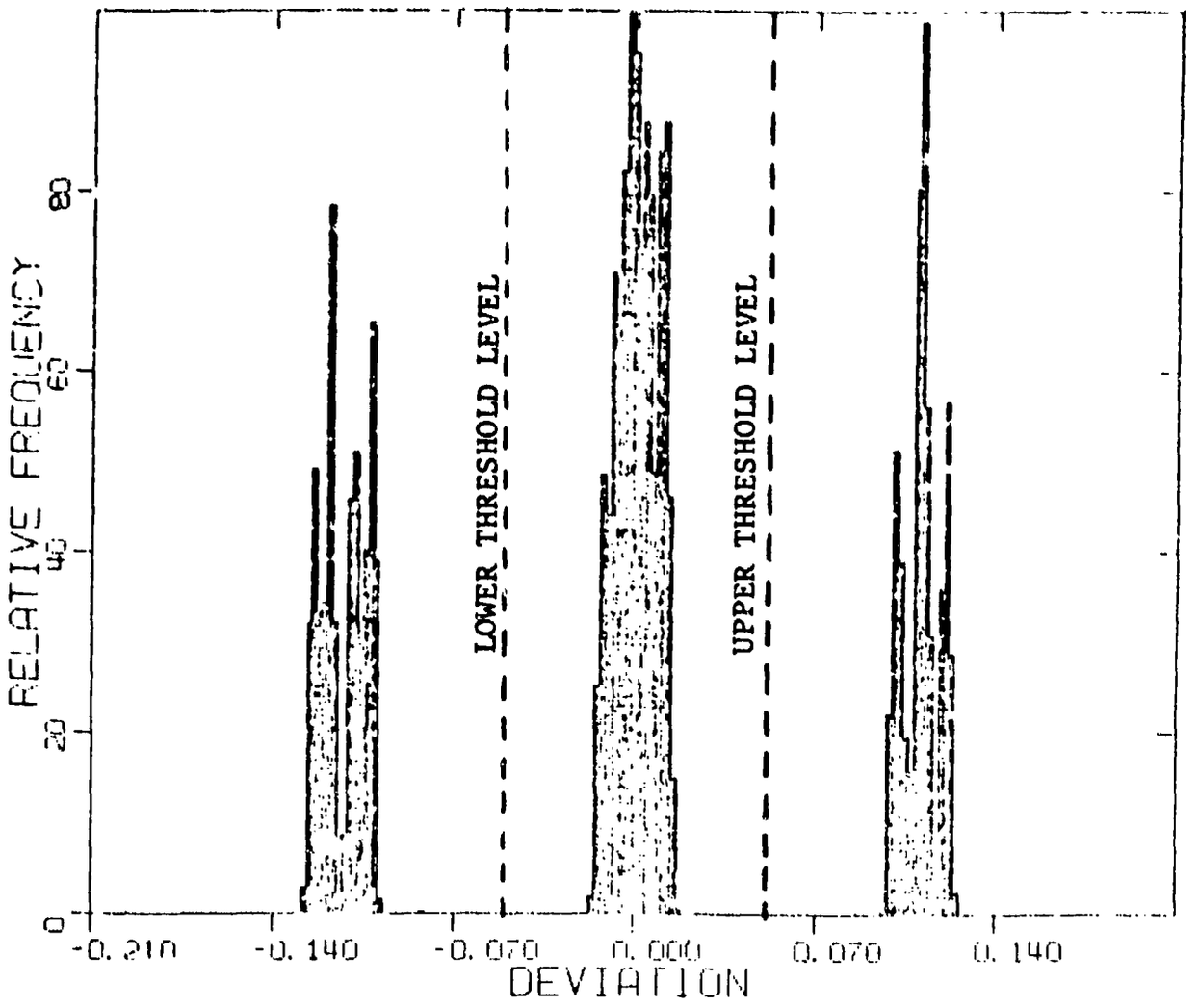

Figure 2 Histogram of Receive Filter Output at Mean Zero Crossing of "Eye" Pattern (25-dB Fade, "Bad" Channel)

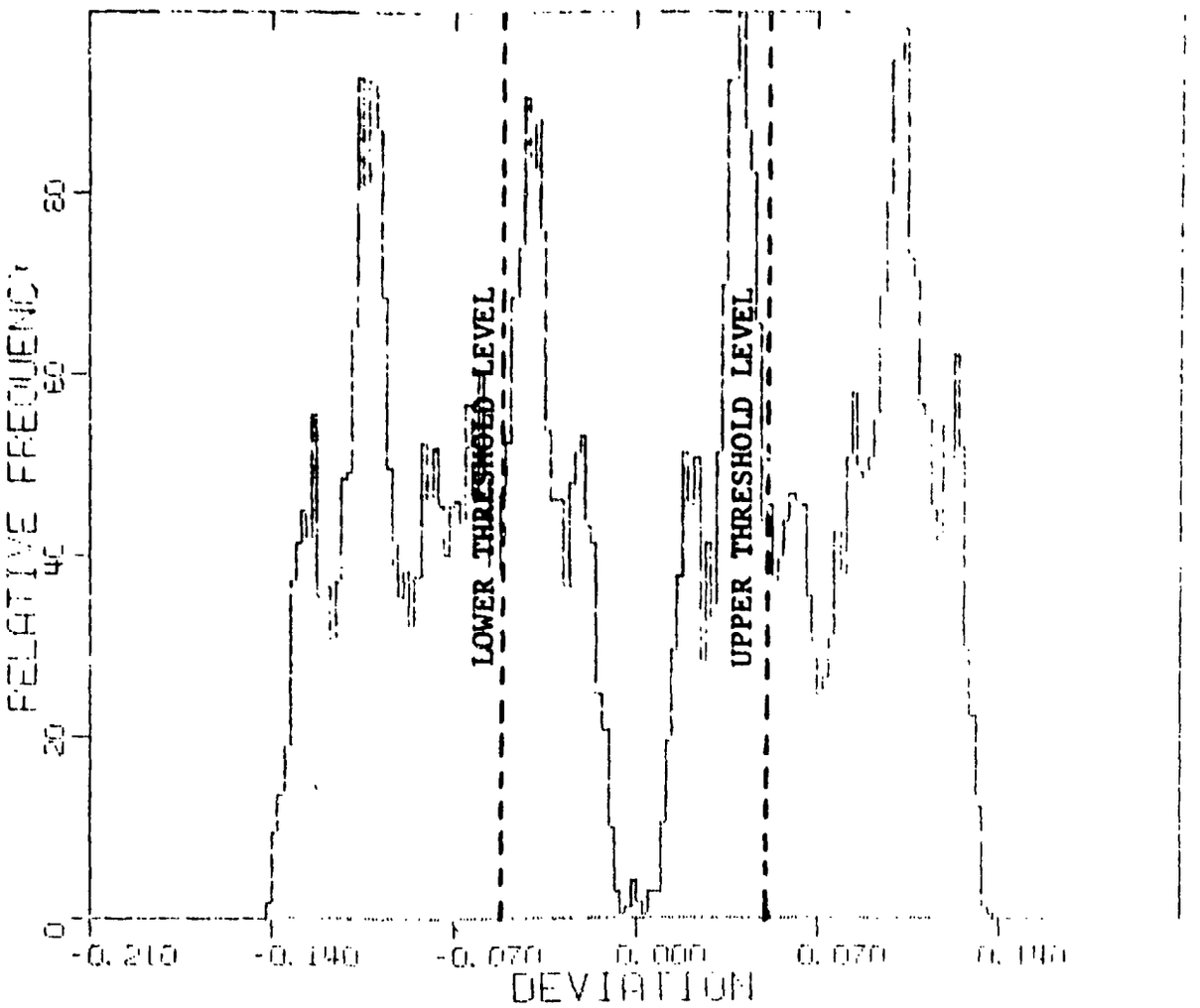

Figure 3 Histogram of Receive Filter Output at Mean Zero Crossing for "Eye" Pattern in the Absence of Multipath (25-dB Fade, "Bad" Channel)

each level is scaled such that the level that occurred most frequently has a relative frequency of 100.

Using the two-path channel discussed in Appendix B, the histogram of the shaping filter output (without tracking mean path delay) was found for 10-, 20-, 30-, and 35-dB fades. These histograms are presented in Figs. 4 to 7. Since Figs. 4 and 5 shows that the shaping filter output at those fade levels is limited to three narrow bands, then for the channel model considered, fades less than 20 dB are essentially flat fades. From Fig. 6, the duobinary 0 (center level) has separated into two segments ($a_{k-1} = +d$, $a_k = -d$ and $a_{k-1} = -d$, $a_k = +d$) due to the time-varying delay. At a 35-dB fade, the interference is very severe, as illustrated by Fig. 7.

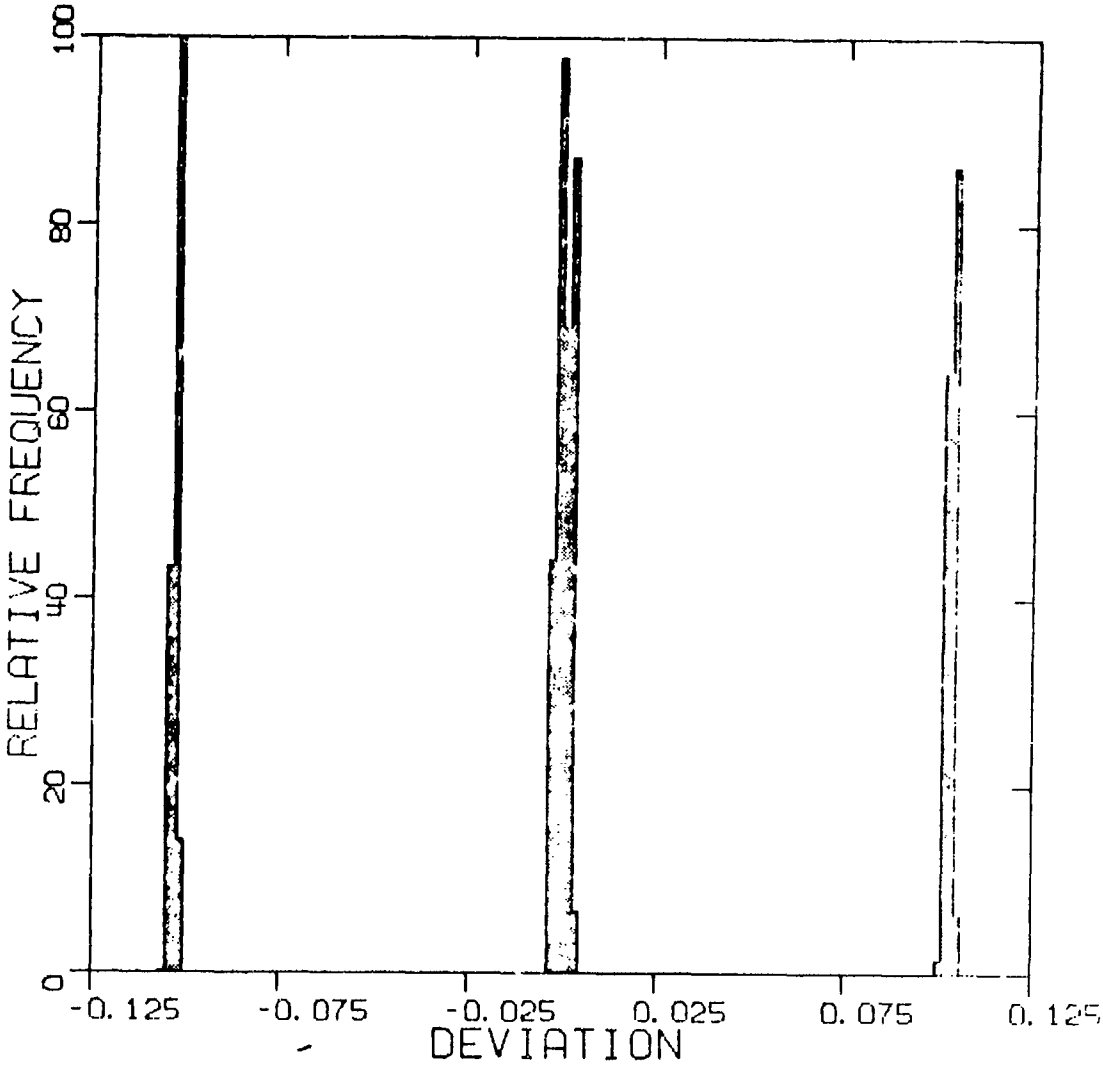

Figure 4 Histogram of Shaping Filter Output for 10-dB Fade (Two-Path Channel, Not Tracking Delay)

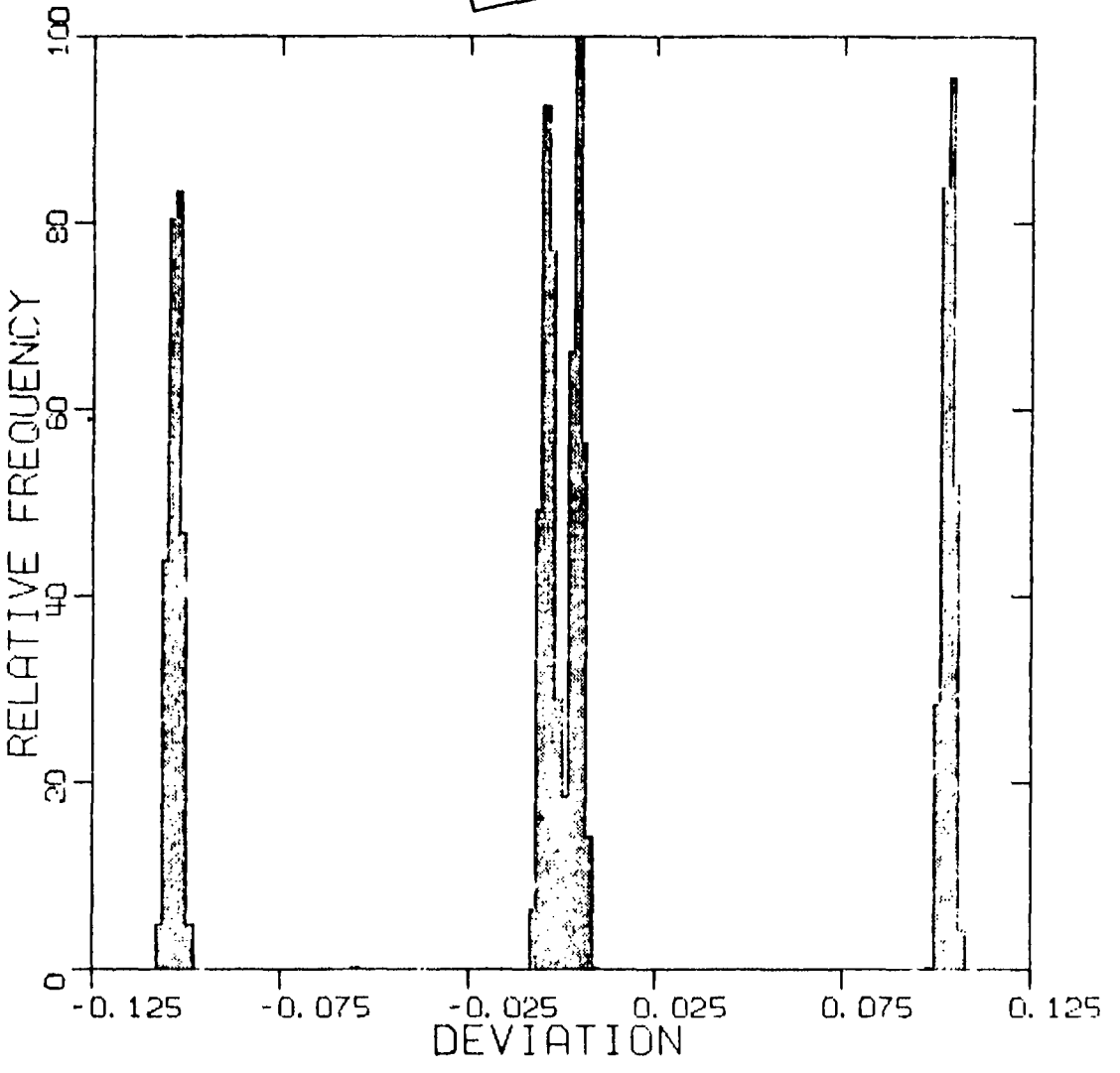

Figure 5 Histogram of Shaping Filter Output for 20-dB Fade (Two-Path Channel, Not Tracking Delay)

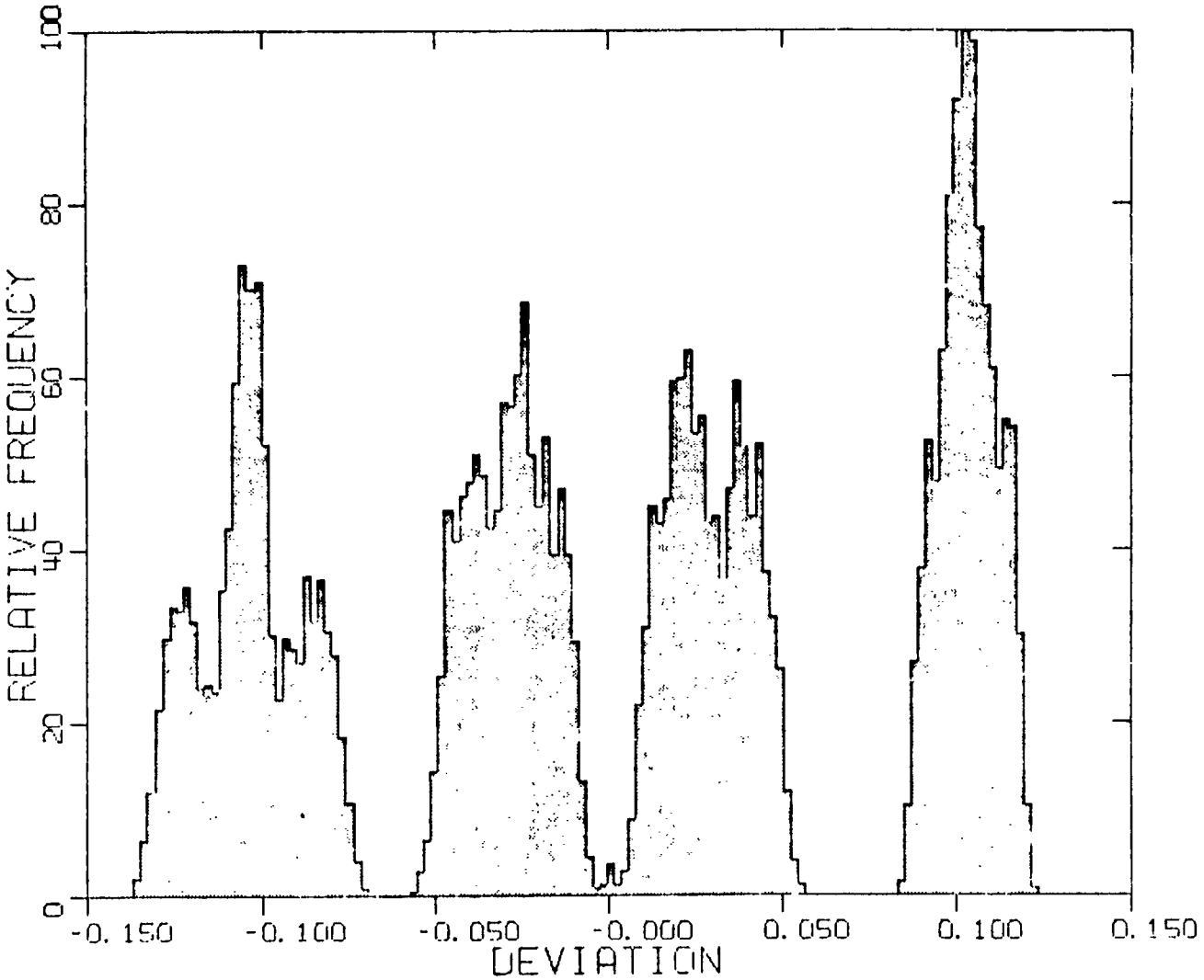

Figure 6 Histogram of Shaping Filter Output for 30-dB Fade (Two-Path Channel, Not Tracking Delay)

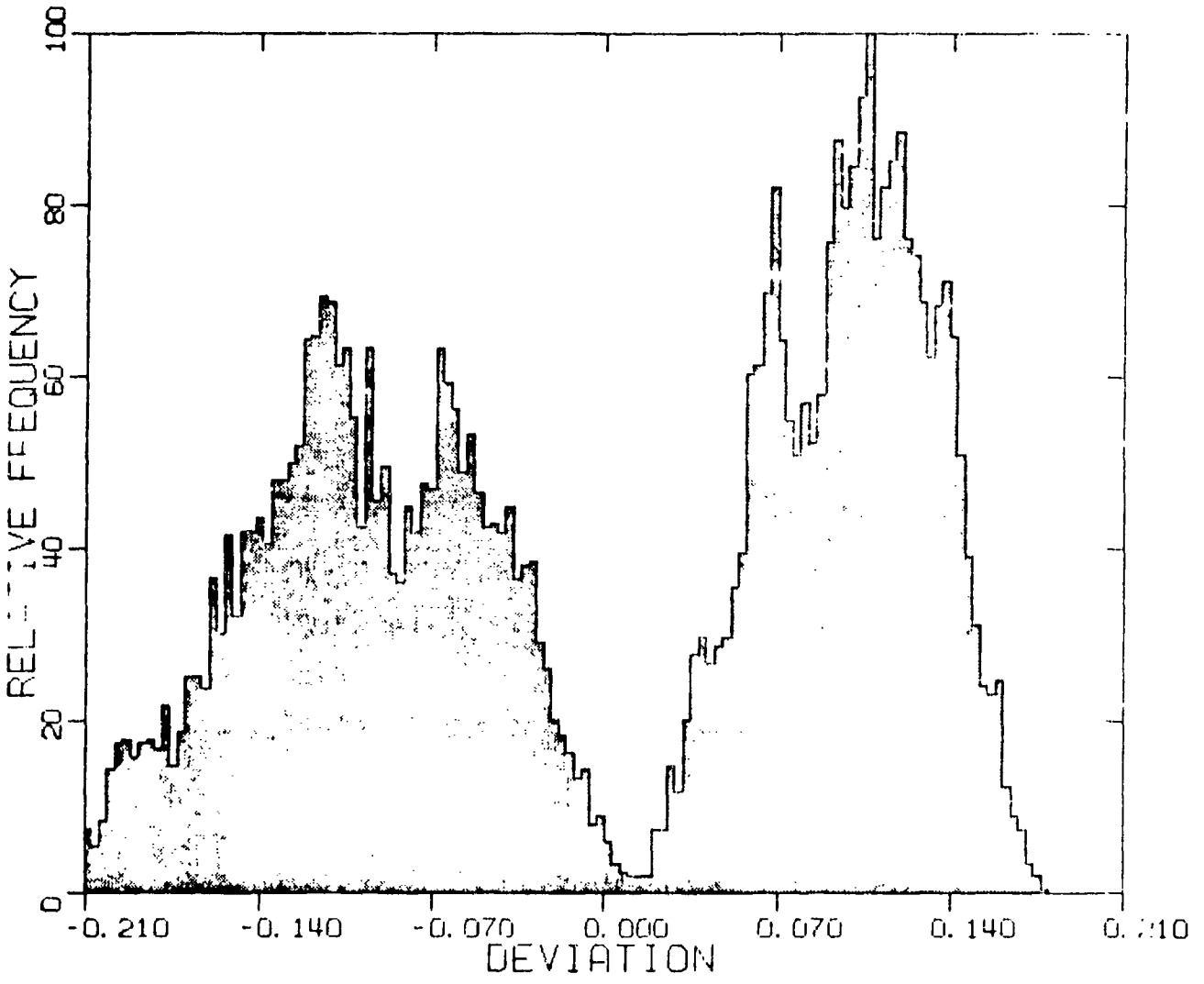

Figure 7 Histogram of Shaping Filter Output for 35-dB Fade (Two-Path Channel, Not Tracking Delay)

REFERENCES FOR APPENDIX C

[1] P. A. Bello and B. D. Nelin, "The Effects of Frequency Selective Fading on Intermodulation Distortion and Subcarrier Phase Stability in Frequency Modulation Systems," IEEE Trans. on Comm. Systems, March 1964, pp. 87 - 101.

[2] P. A. Bello, "Characterization of Randomly Time-Variant Linear Channels," IEEE Trans. on Comm. Systems, December 1963, pp. 360 - 393.

[3] P. A. Bello, et al., "Line-of-Sight Technical Investigation," Final Report on Contract F30602-73-C-0244 by CNR, Inc., for RADC, June 1974, RADC-TR-74-330, (AD006104).

[4] W. R. Bennett and J. R. Davey, Data Transmission, McGraw-Hill, New York, 1965.

APPENDIX D

SHAPING FILTER OUTPUT

1. Introduction

In this appendix we derive expressions for the signal at the output of the shaping filter as a function of the transmit and receive filter impulse responses and the channel parameters. It will be assumed that the discriminator and shaping filter outputs can be accurately represented by a quadratic channel model (see Appendix B).

2. System Description

The system to be analyzed is presented in Figure 1. In this figure the data is filtered in order to perform some shaping of the baseband spectrum prior to transmission. H_T is the transmit shaping filter. The input to the frequency modulator is

$$x(t) = \sum a_n h_T(t - nT) \tag{1}$$

where a_n is the two-level ($\pm d$) NRZ data sequence and $h_T(\cdot)$ is the impulse response of the transmit filter.

Using the result from [1], we can represent the output of the frequency discriminator in terms of the input to the frequency modulator. This representation assumes a small amount of frequency selectivity and uses the f-power series model derived in [2] and discussed in Section 3.2.2.1.2. Therefore, the signal at the output of the discriminator can be approximated by

$$r(t) = P_0 x(t) + P_1 \dot{x}(t) + P_2 \ddot{x}(t) + P_3 x(t)\dot{x}(t) \tag{2}$$

where, for notational simplicity, the group delay of the system, excluding that introduced by the channel disturbances, has been assumed to be compensated for, and where the P_i are the quadratic channel model parameters which are discussed in detail in Appendix B. From (1) it immediately follows that

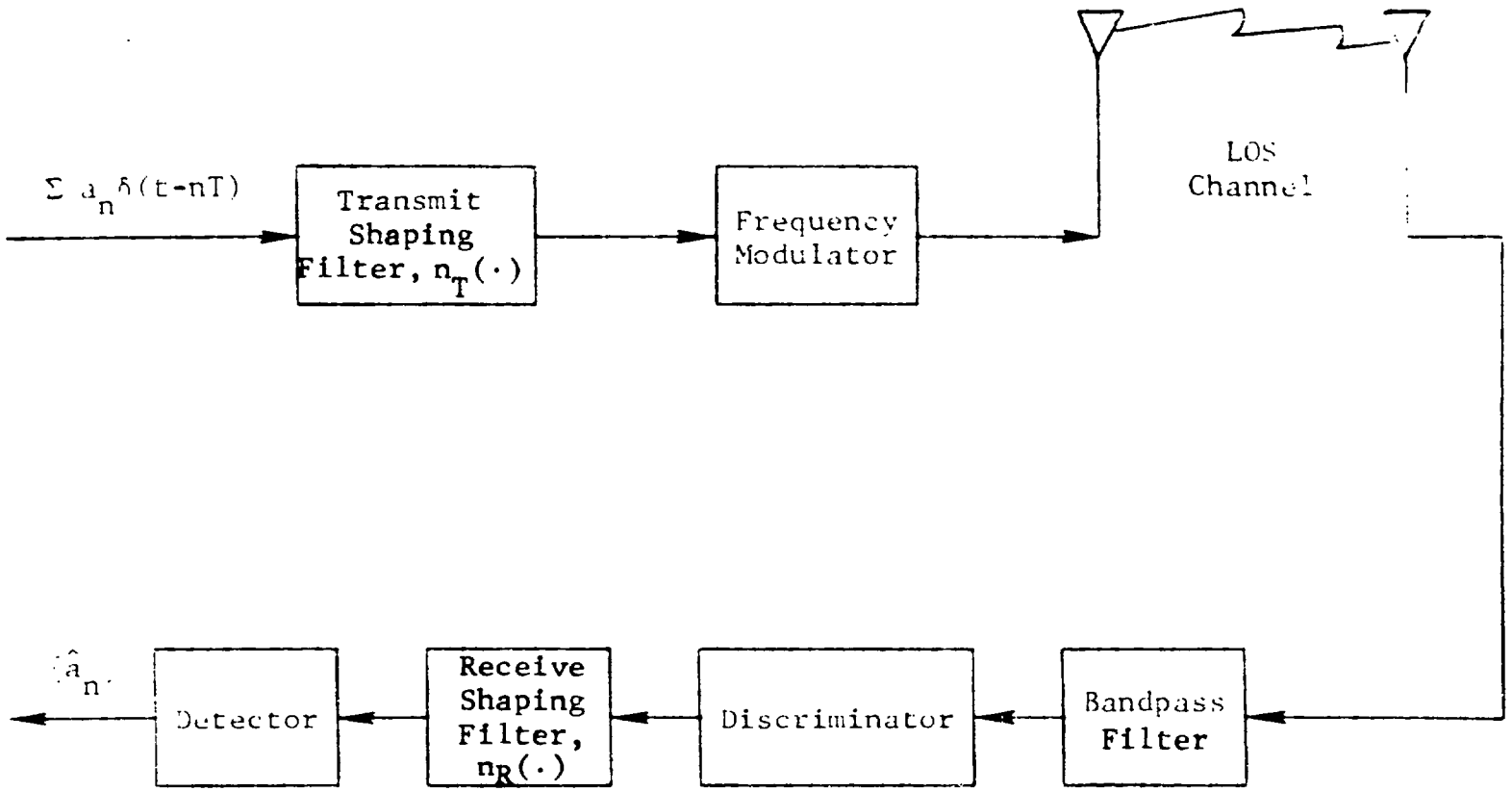

Figure 1 Duobinary FM LOS System

$$\dot{x}(t) = \sum a_n \dot{h}_T(t - nT)$$

$$\ddot{x}(t) = \sum a_n \ddot{h}_T(t - nT) \qquad (3)$$

The output of the receive shaping filter can be expressed in terms of the discriminator output by

$$w(t) = \int_{-\infty}^{\infty} h_R(\tau)\, r(t - \tau)\, d\tau + \int_{-\infty}^{\infty} h_R(\tau) n_D(t-\tau)\, d\tau \qquad (4)$$

where $n_D(t)$ is the noise at the discriminator output.

Using (1) through (4), it follows that

$$w(t) = \sum_{q=0}^{3} P_q\, y_q(t) + n(t) \qquad (5)$$

where n(t) is the shaping filter output noise and $y_q(t)$ are given by

$$y_0(t) = \sum_n a_n \int_{-\infty}^{\infty} h_R(\tau)\, h_T(t - nT - \tau)\, d\tau$$

$$y_1(t) = \sum_n a_n \int_{-\infty}^{\infty} h_R(\tau)\, \dot{h}_T(t - nT - \tau)\, d\tau$$

$$y_2(t) = \sum_n a_n \int_{-\infty}^{\infty} h_R(\tau)\, \ddot{h}_T(t - nT - \tau)\, d\tau$$

$$y_3(t) = \sum_n \sum_m a_n a_m \int_{-\infty}^{\infty} h_R(\tau)\, h_T(t - nT - \tau) \cdot \dot{h}_T(t - mT - \tau)\, d\tau \qquad (6)$$

Substituting (6) in (5) gives

$$w(t) = P_0 \sum_n a_n \int_{-\infty}^{\infty} h_R(\tau)\, h_T(t - nT - \tau)\, d\tau$$

$$+ P_1 \sum_n a_n \int_{-\infty}^{\infty} h_R(\tau)\, \dot{h}_T(t - nT - \tau)\, d\tau$$

$$+ P_2 \sum_n a_n \int_{-\infty}^{\infty} h_R(\tau)\, \ddot{h}_T(t - nT - \tau)\, d\tau$$

$$+ P_3 \sum_n \sum_m a_n a_m \int_{-\infty}^{\infty} h_R(\tau) h_T(t - nT - \tau) \dot{h}_T(t - mT - \tau)\, d\tau \qquad (7)$$

$$+ n(t)$$

When the k^{th} three-level data variable is detected, no error is made if

$$\hat{b}_k = a_k + a_{k-1} \qquad (8)$$

Therefore, it is of interest to express $w(kT + \tau_0)$ given by (7) in terms of a_k and a_{k-1}. Collecting terms involving a_k, a_{k-1}, and $a_k a_{k-1}$ it follows from (7) that

$$w(kT + \tau_0) = a_k G_1(k, \tau_0) + a_{k-1} G_2(k, \tau_0) + a_k a_{k-1} G_3(k, \tau_0)$$

$$+ G_4(k, \tau_0) + n(kT + \tau_0) \qquad (9)$$

where

$$G_{11}(k, \tau_0) = P_0 \int h_R(\tau) h_T(\tau_0 - \tau)\, d\tau + P_1 \int h_R(\tau) \dot{h}_T(\tau_0 - \tau)\, d\tau$$

$$+ P_2 \int h_R(\tau) \ddot{h}_T(\tau_0 - \tau)\, d\tau \qquad (10)$$

$$G_{12}(k,\tau_0) = P_3 \sum_{\substack{m\neq k \\ m\neq k-1}} a_m \left\{ \int h_R(\tau) h_T(\tau_0 - \tau) \dot{h}_T(kT + \tau_0 - mT - \tau)\, d\tau \right.$$

$$\left. + \int h_R(\tau) h_T(kT + \tau_0 - mT - \tau) \dot{h}_T(\tau_0 - \tau)\, d\tau \right\}$$

$$G_1(k,\tau_0) = G_{11}(k,\tau_0) + G_{12}(k,\tau_0)$$

$$G_{21}(k,\tau_0) = P_0 \int h_R(\tau) h_T(T + \tau_0 - \tau)\, d\tau + P_1 \int h_R(\tau) \dot{h}_T(T + \tau_0 - \tau)\, d\tau$$

$$+ P_2 \int h_R(\tau) \ddot{h}_T(T + \tau_0 - \tau)\, d\tau$$

$$G_{22}(k,\tau_0) = P_3 \sum_{\substack{m\neq k \\ m\neq k-1}} a_m \left\{ \int h_R(\tau) h_T(T + \tau_0 - \tau) \dot{h}_T(kT + \tau_0 - mT - \tau)\, d\tau \right.$$

$$\left. + \int h_R(\tau) h_T(kT + \tau_0 - mT - \tau) \dot{h}_T(T + \tau_0 - \tau)\, d\tau \right\}$$

$$G_2(k,\tau_0) = G_{21}(k,\tau_0) + G_{22}(k,\tau_0)$$

$$G_3(k,\tau_0) = P_3 \left\{ \int h_R(\tau) h_T(\tau_0 - \tau) \dot{h}_T(T + \tau_0 - \tau)\, d\tau \right.$$

$$\left. + \int h_R(\tau) h_T(T + \tau_0 - \tau) \dot{h}_T(\tau_0 - \tau)\, d\tau \right\} \qquad (10) \text{ (Cont'd)}$$

$$G_{41}(k,\tau_0) = \sum_{\substack{m\neq k \\ m\neq k-1}} a_m \Big[P_0 \int h_R(\tau) h_T(kT + \tau_0 - mT - \tau)\, d\tau + P_1 \int h_R(\tau) \dot{h}_T(kT + \tau_0 - mT - \tau)\, d\tau + P_2 \int h_R(\tau) \ddot{h}_T(kT + \tau_0 - mT - \tau)\, d\tau \Big]$$

$$G_{42}(k,\tau_0) = P_3 \sum_{m} \int h_R(\tau) h_T(kT - mt + \tau_0 - \tau) \dot{h}_T(kT + \tau_0 - mT - \tau)\, d\tau$$

$$G_{43}(k,\tau_0) = P_3 \sum_{\substack{m\neq k,k-1 \\ n\neq k,k-1 \\ m\neq n}} \sum_{} a_n a_m \int h_R(\tau) h_T(kT + \tau_0 - nT - \tau) \cdot \dot{h}_T(kT + \tau_0 - mT - \tau)\, d\tau$$

$$G_4(k,\tau_0) = G_{41}(k,\tau_0) + G_{42}(k,\tau_0) + G_{43}(k,\tau_0) \qquad (10)$$
(Cont'd)

To evaluate the three-level error rate using the procedure presented in Section 4.5, we must express the shaping filter output [as defined by (4.41)] conditional upon a_k, a_{k-1} in the form given by Eq. (4.48). Since a_k, a_{k-1} equal $\pm a$, there are four cases that need to be considered. They are:

$$w_k(d,d,\tau_0) = dG_{11}(k,\tau_0) + dG_{21}(k,\tau_0) + d^2G_3(k,\tau_0) + G_{42}(k,\tau_0) + dG_{12}(k,\tau_0) + dG_{22}(k,\tau_0) + G_{41}(k,\tau_0) + G_{43}(k,\tau_0) + n(kT + \tau_0) \qquad (11)$$

$$w_k(d,-d,\tau_0) = dG_{11}(k,\tau_0) - dG_{21}(k,\tau_0) - d^2G_3(k,\tau_0) + G_{42}(k,\tau_0)$$
$$+ dG_{12}(k,\tau_0) - dG_{22}(k,\tau_0) + G_{41}(k,\tau_0) + G_{43}(k,\tau_0)$$
$$+ n(kT+\tau_0)$$

$$w_k(-d,d,\tau_0) = -dG_{11}(k,\tau_0) + dG_{21}(k,\tau_0) - d^2G_3(k,\tau_0) + G_{42}(k,\tau_0)$$
$$- dG_{12}(k,\tau_0) + dG_{22}(k,\tau_0) + G_{41}(k,\tau_0) + G_{43}(k,\tau_0)$$
$$+ n(kT+\tau_0)$$

$$w_k(-d,-d,\tau_0) = -dG_{11}(k,\tau_0) - dG_{21}(k,\tau_0) + d^2G_3(k,\tau_0) + G_{42}(k,\tau_0)$$
$$- dG_{12}(k,\tau_0) - dG_{22}(k,\tau_0) + G_{41}(k,\tau_0) + G_{43}(k,\tau_0)$$
$$+ n(kT+\tau_0) \qquad (11)$$
(Cont'd)

Comparing (10) and (11) with (4.48) of Section 4.5, the following can be verified:

$$\sum_{\substack{\ell\neq k,k-1\\ p\neq k,k-1,\ell}}\sum a_\ell a_p E_{\ell p}^{(k)}(\tau_0) = G_{43}(k,\tau_0)$$

$$C(m,n,\tau_0) = mG_{11}(k,\tau_0) + nG_{21}(k,\tau_0) + mnG_3(k,\tau_0) + G_{42}(k,\tau_0)$$

$$\sum_{\ell\neq k,k-1} a_\ell D_{\ell k}(m,n,\tau_0) = mG_{12}(k,\tau_0) + nG_{22}(k,\tau_0) + G_{41}(k,\tau_0) \qquad (12)$$

Lastly, in determining the effect of $G_{43}(k,\tau_0)$ upon the three-level error rate, we can write

$$C_{43}(k,\tau_0) = P_3 \sum_{\substack{m\neq k,k-1 \\ n\neq k,k-1 \\ m>n}} \sum a_n a_m g_{nm} \tag{13}$$

where g_{nm} follows from (10), and by reordering n and m

$$G_{43}(k,\tau_0) = P_3 \sum C_n h_n \tag{14}$$

where $\{h_n\}$ can be put in a one-one correspondence with $\{g_{nm}/d\}$ and C_n is an i.i.d. sequence taking on $\pm d$ with equal probability. Furthermore, C_n and a_n are uncorrelated and, for numerical purposes, we will assume them also to be independent. Thus, the nonlinear intersymbol interference (ISI) has been reduced to a constant and linear ISI, which can be treated analytically and numerically.

REFERENCES FOR APPENDIX D

[1] P. A. Bello and B. D. Nelin, "The Effects of Frequency Selective Fading on Intermodulation Distortion and Subcarrier Phase Stability in Frequency Modulation Systems," IEEE Trans. on Comm. Systems, March 1964, pp. 87 - 101.

[2] P. A. Bello, "Characterization of Randomly Time-Variant Linear Channels," IEEE Trans. on Comm. Systems, December 1963, pp. 360 - 393.

APPENDIX E

RELATIONSHIP BETWEEN TWO- AND THREE-LEVEL ERROR RATES FOR DUOBINARY SYSTEMS

1. Introduction

In this appendix we address the problem of determining the relationship between two-level errors and three-level errors in a duobinary system without precoding. With precoding, a three-level error almost always (except if a $\pm 2d$ is detected as a $\mp 2d$, where the three levels are $\pm 2d, 0$) results in a two-level error. Therefore, we will restrict our attention to the nonprecoded case. The error propagation of nonprecoded binary data sequences will be examined.

In Section 5 below, the effect of correlated noise samples will be illustrated.

2. System Description

A nonprecoded duobinary system will be considered in this appendix. For this system, a two-level ($\pm d$) data sequence $\{a_n\}$ pulse amplitude modulates a train of pulses in such a manner that a controlled amount of intersymbol interference [1] is allowed. In the receiver, a three-level sequence is generated from the output of the receive shaping filter [2] according to the rule:

$$\hat{b}_k = \begin{cases} +2d & , \text{ if } W(kT) \geq \alpha \\ 0 & , \text{ if } |W(kT)| < \alpha \\ -2d & , \text{ if } W(kT) \leq -\alpha \end{cases} \tag{1}$$

where α is the threshold level and $W(t)$ is the output of the receive shaping filter.

Ideally, the three-level sequence would be given by [2]

$$b_n = a_n + a_{n-1} \tag{2}$$

and a three-level error is made if

$$\hat{b}_n \neq b_n \tag{3}$$

After detection of the three-level sequence using (1), the two-level sequence is generated using

$$\hat{a}_n = \begin{cases} +d, & \text{if } \hat{b}_n = 2d \\ -d, & \text{if } \hat{b}_n = -2d \\ -\hat{a}_{n-1}, & \text{if } \hat{b}_n = 0 \end{cases} \tag{4}$$

and a two-level error is made if

$$\hat{a}_n \neq a_n \tag{5}$$

As can be seen from (4), if a_{n-1} was in error and $b_n = \hat{b}_n = 0$, then a_n will also be in error, thus indicating that errors can propagate. This propagation effect will be examined in detail in Section 3 below.

3. Relationship of Three-Level and Two-Level Errors

In this section we will determine the relationship between three-level and two-level errors for a nonprecoded duobinary system. In order to determine this relationship analytically, the following assumptions will be made:

(1) There will not be a three-level error until the propagation effects of the previous three-level error are completed.

(2) When a three-level $\pm 2d$ is in error, it will be detected as a 0.

(3) The probability of error for the present three-level data variable does not depend upon the future data sequence.

(4) The data $\{a_n\}$ is an independent, identically distributed sequence taking on the values $\pm d$ with equal probability.

Assumption (1) is expected to be valid as long as the error rate is not very high (greater than about 10^{-1} or 10^{-2}). Assumption (2) should be valid for the cases of interest. Assumption (3) is made to simplify the analysis; however, as illustrated in Section 4.5, for selective fading there is intersymbol interference and, thus, the probability of error for the present three-level data variable does depend upon the future data sequence. If the intersymbol interference is specified, the probability of error for the present three-level error conditioned upon the future data sequence can be found and used to weight the number of future two-level data bits in error; that is, the errors shown in Figures 1 - 3 can be used to find the expected number of two-level errors. Assumption (4) is a commonly made assumption and should be valid for data transmission or digitized voice.

3.1 +2d Error

In this section we will determine the propagation effects when a $\hat{b}_n = 0$ is detected and a_n and a_{n-1} both equal d. From Eq. (2), $b_n = 2d$. A trellis showing the possible data sequences is shown in Figure 1. In this figure, a data sequence is shown until the errors can no longer propagate. Also in this figure, the E's indicate a two-level error. Thus, the expected number of E's would give the expected number of two-level errors per three-level error conditioned upon $\hat{b}_n = 0$, $b_n = +2d$.

It is shown in this figure that a_n will be detected in error. From assumptions (2) and (4), a_{n+1} will be in error one half of the time, a_{n+2} will be in error one quarter of the time, etc. Thus, the expected number of two-level errors per three-level error conditioned upon $\hat{b}_n = 0$, $b_n = +2d$ is

$$1 + \frac{1}{2} + \frac{1}{4} + \ldots = 2 \qquad (6)$$

3.2 -2d Error

In a similar manner to that presented in Section 3.1 above, it can be shown that the expected number of two-level errors per three-level error conditioned upon $\hat{b}_n = 0$, $b_n = -2d$ is 2.

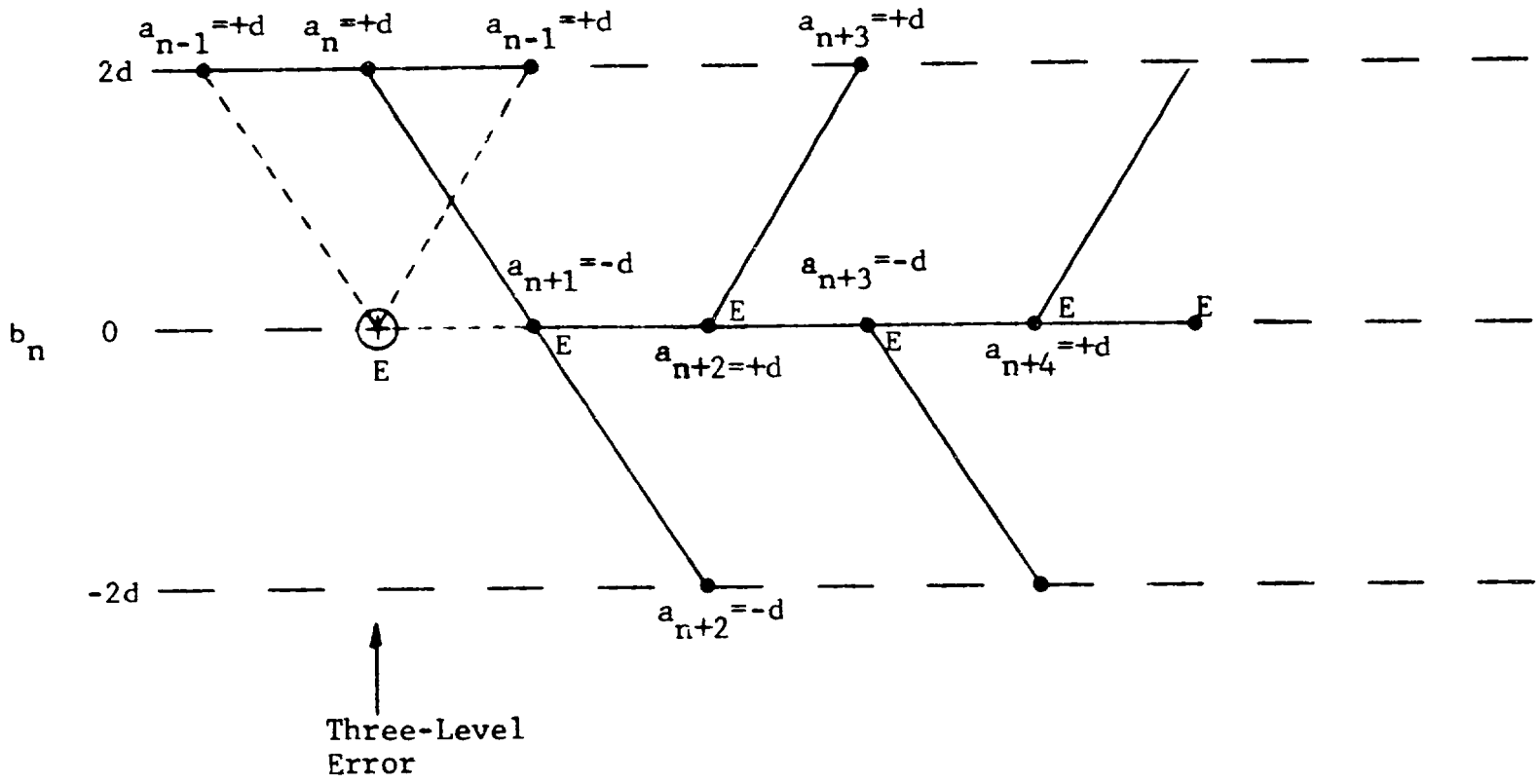

Figure 1 Error Trellis for $b_n = +2d$ Error

3.3 0 Error

The expected number of two-level errors per three-level error will be determined for the case for which $b_n = 0$, $\hat{b}_n \neq 0$. There are four possible data configurations for this case. They are:

(1) $a_{n-1} = +d, \quad a_n = -d, \quad \hat{b}_n = +2d$

(2) $a_{n-1} = +d, \quad a_n = -d, \quad \hat{b}_n = -2d$

(3) $a_{n-1} = -d, \quad a_n = +d, \quad \hat{b}_n = +2d$

(4) $a_{n-1} = -d, \quad a_n = +d, \quad \hat{b}_n = -2d$

The trellis for case (1) is presented in Figure 2, where the E's indicate two-level errors. From this figure and assumption (4), it is easy to see that the expected number of two-level errors per three-level error is 2. Furthermore, case (4) is a dual of case (1) and, thus, will also have on the average 2 two-level errors per three-level error.

The trellis for case (2) is presented in Figure 3. From this case, it is seen that no two-level errors result. Furthermore, since case (3) is the dual of case (2), no two-level errors will result from case (3).

In the following section, the two-level and three-level error rates will be determined.

4. Error Rate Relationships

In this section we will use the results of the previous section to relate the two-level and three-level error rates.

From Eq. (3), the three-level error rate is

$$P_3 = \text{Prob.}\{\hat{b}_n \neq b_n\} \tag{7}$$

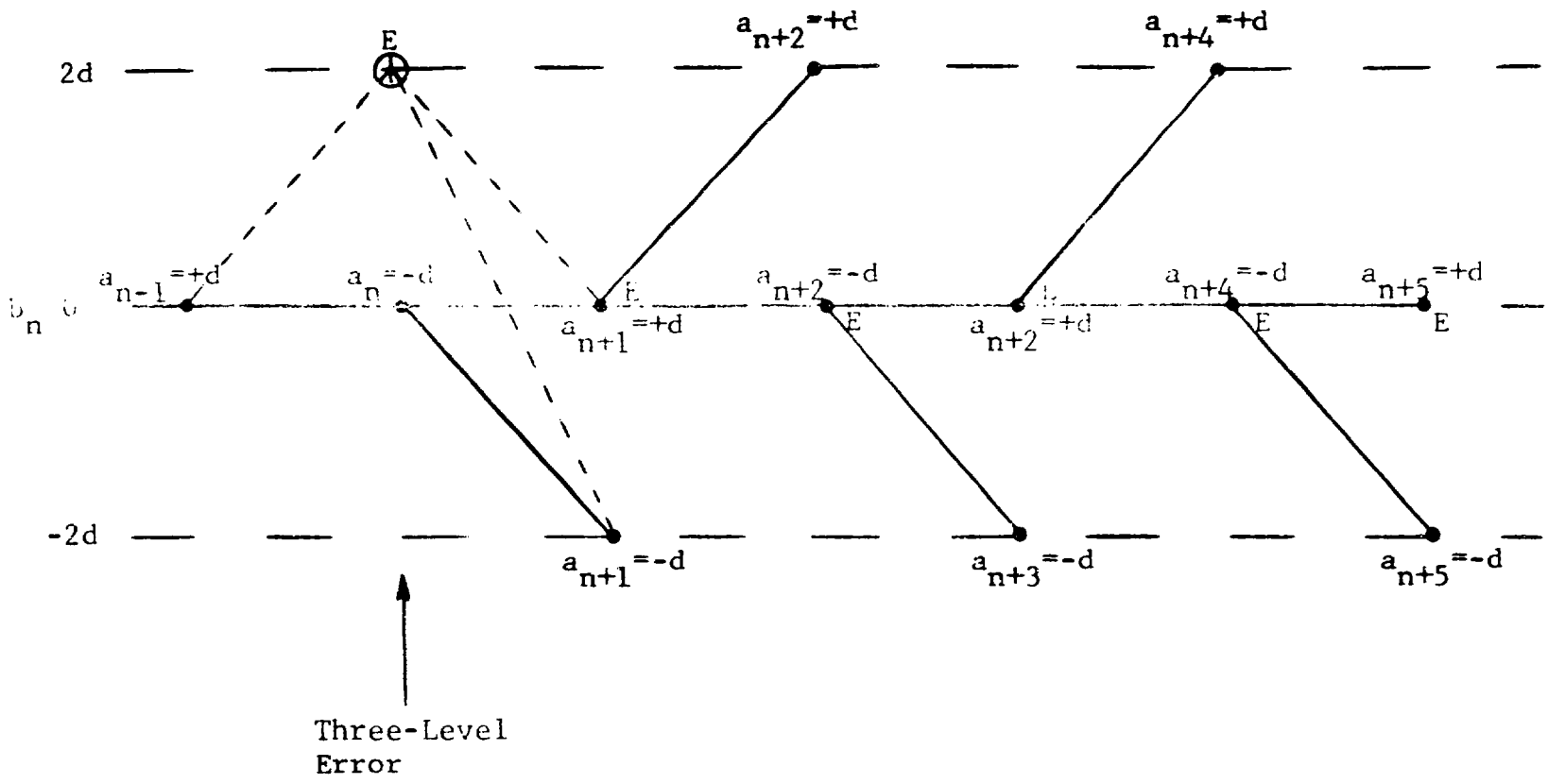

Figure 2 Error Trellis for $b_n = 0$ ($\hat{b}_n = +2d, a_n = -d$)

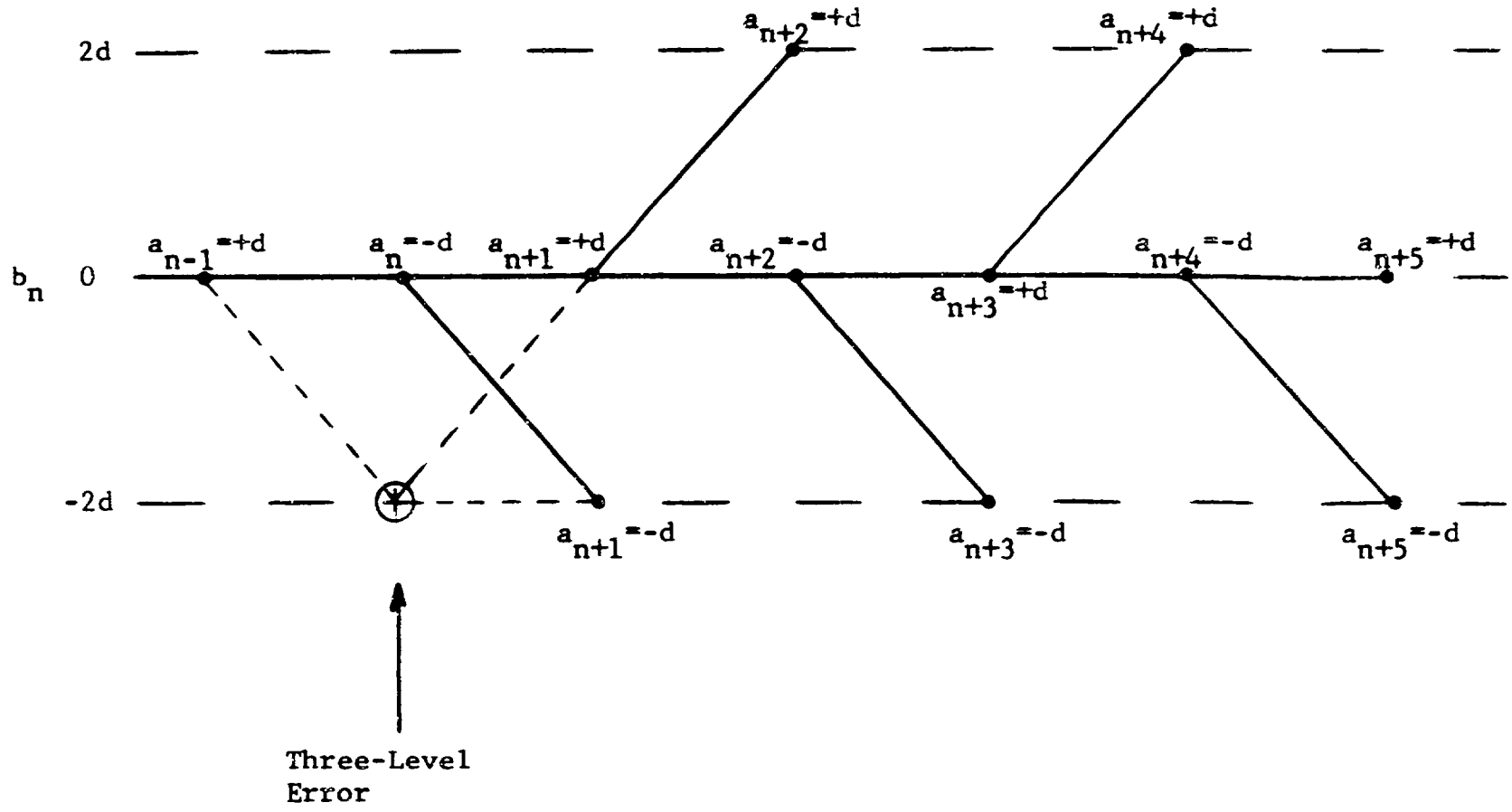

Figure 3 Error Trellis for $b_n = 0$ Error ($\hat{b}_n = -2d, a_n = -d$)

Using assumptions (2) to (4), P_3 can then be expressed as

$$P_3 = \frac{1}{2}\,\text{Prob.}\{\hat{b}_n = +2d \mid b_n = 0\} + \frac{1}{2}\,\text{Prob.}\{\hat{b}_n = -2d \mid b_n = 0\}$$
$$+ \frac{1}{4}\,\text{Prob.}\{\hat{b}_n = 0 \mid b_n = +2d\} + \frac{1}{4}\,\text{Prob.}\{\hat{b}_n = 0 \mid b_n = -2d\} \tag{8}$$

From Eq. (5), the two-level error rate is

$$P_2 = \text{Prob.}\{\hat{a}_n \neq a_n\} \tag{9}$$

Using assumptions (1) through (4) and the results of Section 3 above, P_2 can be approximated by

$$P_2 = \frac{1}{4} \cdot 2 \cdot \text{Prob.}\{\hat{b}_n = +2d \mid a_n = -d, a_{n-1} = +d\}$$
$$+ \frac{1}{4} \cdot 2 \cdot \text{Prob.}\{\hat{b}_n = -2d \mid a_n = +d, a_{n-1} = -d\}$$
$$+ \frac{1}{4} \cdot 2 \cdot \text{Prob.}\{\hat{b}_n = 0 \mid b_n = +2d\}$$
$$+ \frac{1}{4} \cdot 2 \cdot \text{Prob.}\{\hat{b}_n = 0 \mid b_n = -2d\} \tag{10}$$

Ideally, the above conditional probabilities would be equal; however, in a selectively fading FM LOS system, the probabilities will differ (see Section 5.6). For the ideal case, we have

$$P_3 = \frac{3}{2} \cdot \text{Prob.}\{n > d\}$$
$$P_2 = 2 \cdot \text{Prob.}\{n > d\} \tag{11}$$

where the probabilities given in (8) and (10) are all assumed equal to Prob.$\{n > d\}$, which can be thought of as the probability of the noise exceeding the three-level threshold.

From (11) it follows that, for the ideal case,

$$P_2 = \frac{4}{3} P_3 \tag{12}$$

It should be reiterated that, for the selectively fading FM system, Eqs. (8) and (10) must be used to relate the two-level and three-level error rates. Defining

$$P(A) = \frac{1}{2}\left[\text{Prob.}\left\{\hat{b}_n = 0 \mid b_n = +2d\right\} + \text{Prob.}\left\{\hat{b}_n = 0 \mid b_n = -2d\right\}\right]$$

$$P(B) = \frac{1}{2}\left[\text{Prob.}\left\{\hat{b}_n = +2d \mid a_n = -d, a_{n-1} = +d\right\} + \text{Prob.}\left\{\hat{b}_n = -2d \mid a_n = +d, a_{n-1} = -d\right\}\right]$$

$$P(C) = \frac{1}{2}\left[\text{Prob.}\left\{\hat{b}_n = +2d \mid b_n = 0\right\} + \text{Prob.}\left\{\hat{b}_n = -2d \mid b_n = 0\right\} - P(B)\right] \tag{13}$$

it follows from (8) and (10) that

$$P_3 = \frac{1}{2} P(A) + P(B) + P(C)$$

$$P_2 = P(A) + P(B) \tag{14}$$

Therefore, the general form of (12) is

$$P_2 = \frac{P(A) + P(B)}{\frac{1}{2} P(A) + P(B) + P(C)} \cdot P_3 \tag{15}$$

The special form of (15) given by (12) follows by noting that, for the ideal case, $P(C) = 0$ and $P(A) = P(B)$.

5. Generation of Correlated Noise Samples

In this section we address the problem of generating Gaussian noise samples with a correlation coefficient given by

$$\rho(k) = \frac{\left[-\frac{\pi^2}{8k^2 - 1} + \frac{48k^2 + 4}{\left(4k^2 - 1\right)^3} \right] \cos k\pi}{\frac{\pi^2}{2} - 4} \tag{16}$$

Equation (16) is the correlation coefficient for the Gaussian noise at the shaping filter output evaluated at $\tau = kT$ (see Figure 5 and Eq. (8) of Appendix A).

To generate the noise samples, we must truncate $\rho(k)$ at some value of k (say M). M would be chosen such that $|\rho(k)| \ll 1 \forall\ k > M$. Once M is chosen, we define

$$R_k = \sigma_n^2 \rho(k) \qquad k = 0,1,\ldots,M \tag{17}$$

as the correlation function of the noise samples, where σ_n is the noise standard deviation.

Assuming that the previous M noise samples $\{x_i;\ i = 1,\ldots,M\}$ have been generated, then the present noise sample can be generated from a Gaussian random number generator with mean

$$a_1 x_1 + a_2 x_2 + \ldots + a_M x_M \tag{18}$$

and variance

$$R_0 = a_1 R_1 + a_2 R_2 + \ldots + a_M R_M \tag{19}$$

and where a_i, $i = 1,\ldots,M$ are given by

$$\begin{bmatrix} a_1 \\ \vdots \\ a_M \end{bmatrix} = \begin{bmatrix} R_0 & R_1 & \cdots & R_{M-1} \\ R_1 & R_0 & & \\ \vdots & & \ddots & \\ R_{M-1} & \cdots & R_1 & R_0 \end{bmatrix}^{-1} \begin{bmatrix} R_1 \\ \vdots \\ R_M \end{bmatrix} \qquad (20)$$

The mathematical basis of Eqs. (5) through (7) is given in Eqs. (8.78) and (8.80) of Ref. [3]. From (18) and (19), the previous noise samples only influence the mean of the present noise sample. Furthermore, since the R_k are know a priori, the set $\{a_i\}$ can be generated beforehand.

6. Examples

Examples were considered to verify the preceding analysis, determine the range of validity of the assumptions, and to determine the effects of correlated noise samples.

Figures 4 through 6 show results of simulations in comparison with the predicted results. For these examples, an ideal system was used and, thus, Eq. (12) is applicable.

From Figures 5 and 6, we seen that the simulations verify the analysis even for high error rates. However, in Figure 4, the predicted and simulated results do not agree too well. This is probably due to one three-level error affecting the propagation of errors resulting from a previous three-level error. That is, assumption (1) is not valid for this high an error rate.

Also, from these simulations, correlated noise samples have a very slight effect upon the relationship of two-level and three-level error rates.

7. Concluding Comment

We should mention that the assumptions presented in Section 3 above may not always be valid. In particular, assumption (3) could significantly alter the ratio of two-level errors to three-level errors. An analysis without this assumption would require specifying the probability of the three-level errors conditioned upon each data sequence or, at least, upon a truncated version of this sequence.

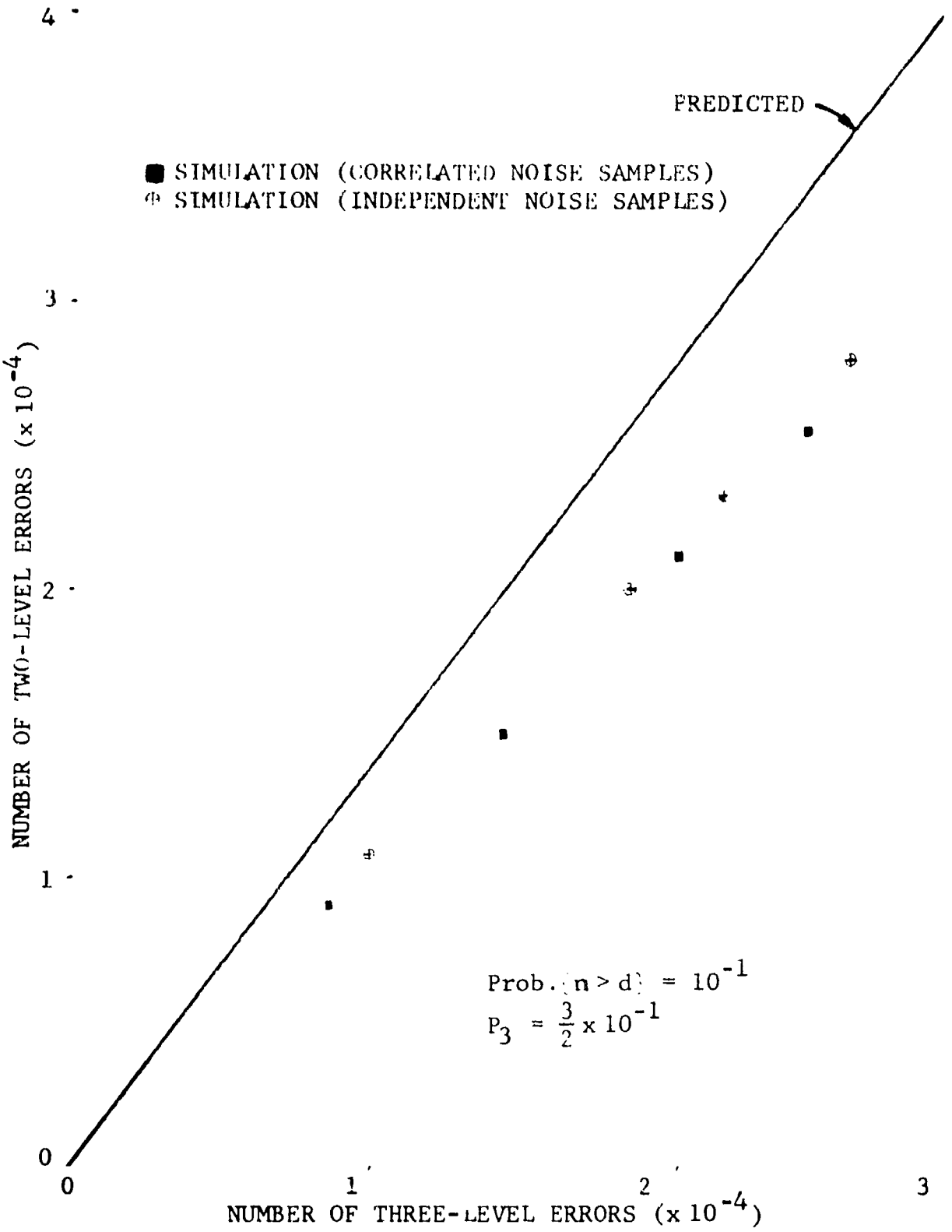

Figure 4 Relationship Between Number of Two-Level and Three-Level Errors

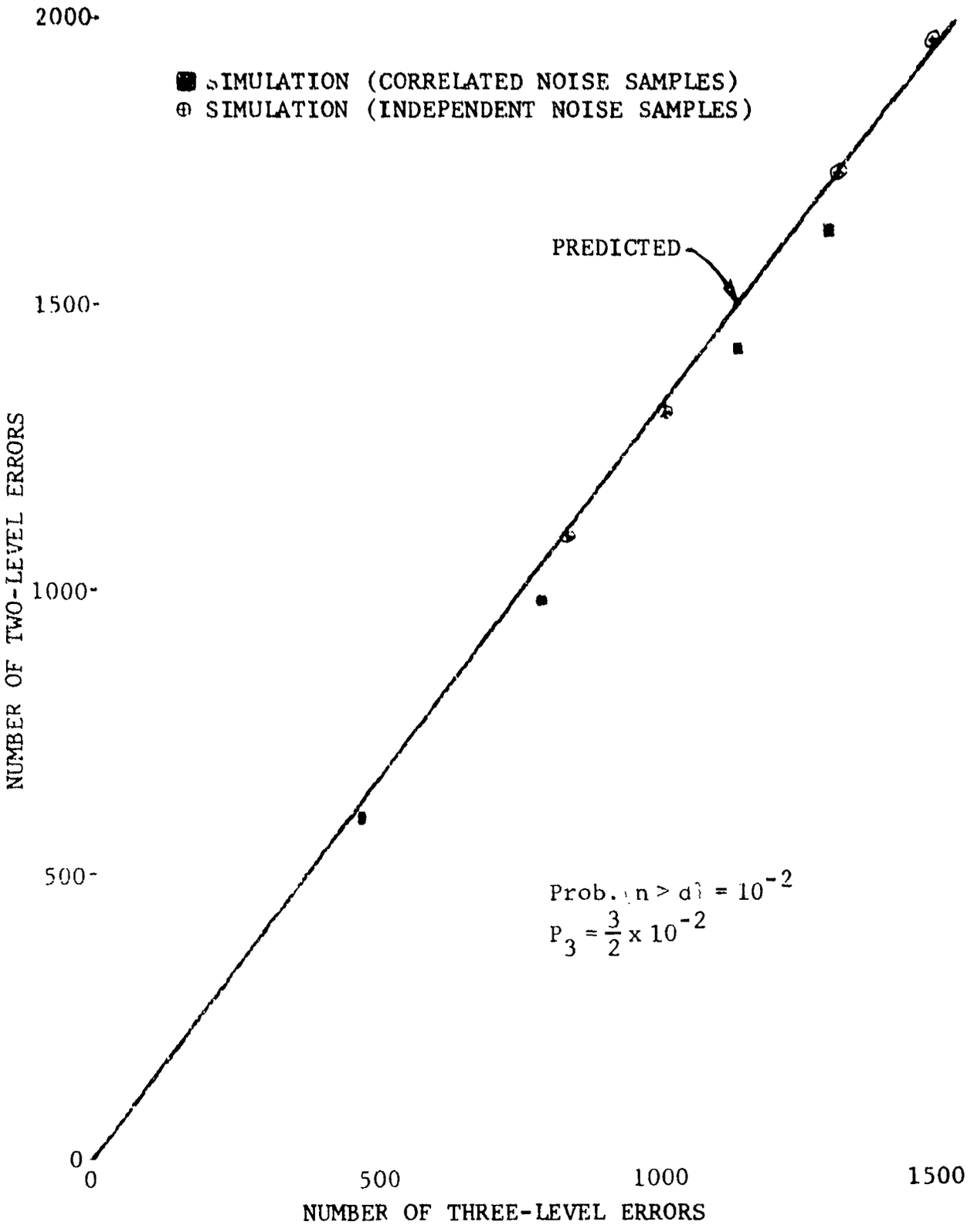

Figure 5 Relationship Between Number of Two-Level and Three-Level Errors

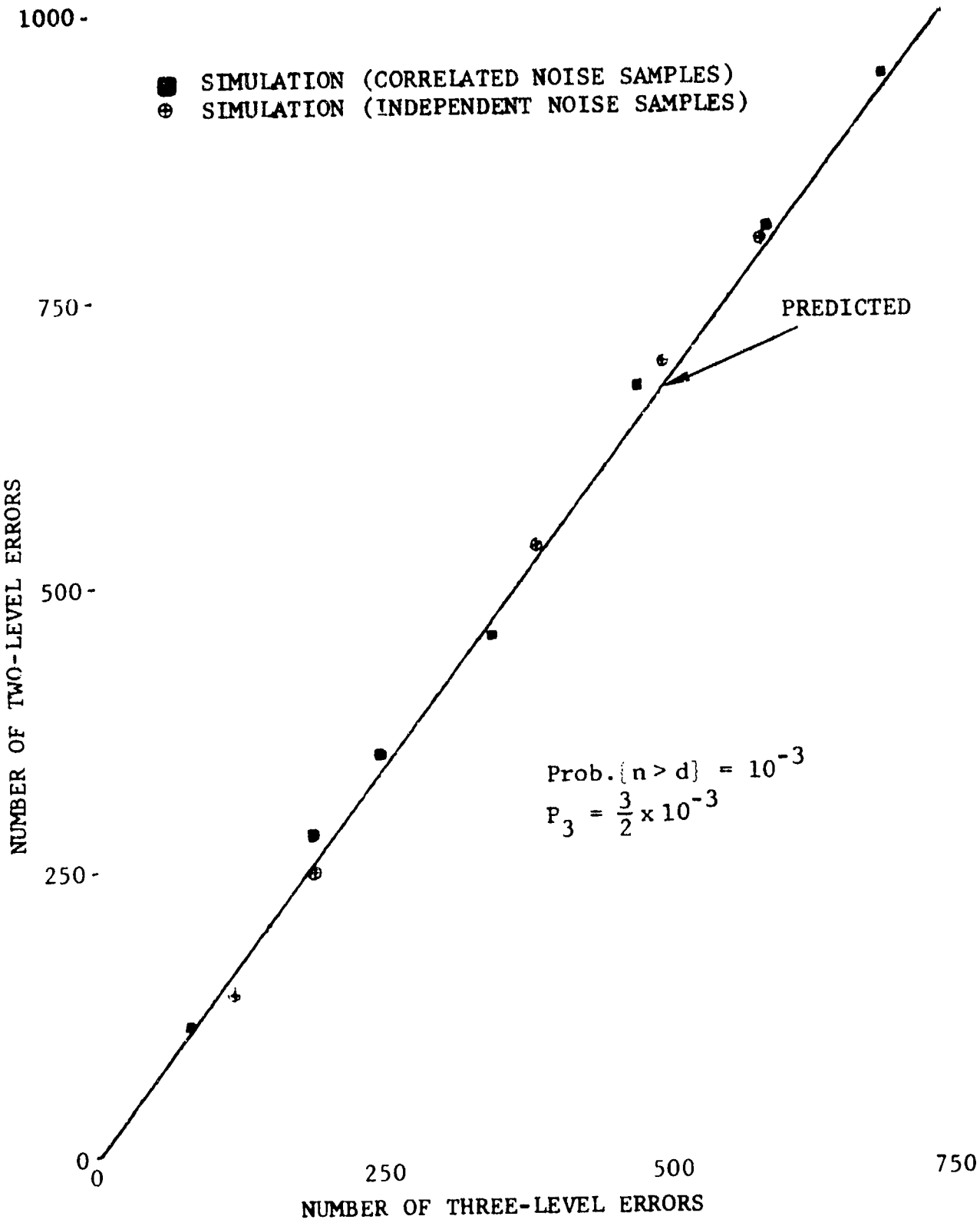

Figure 6 Relationship Between Number of Two-Level and Three-Level Errors

REFERENCES FOR APPENDIX E

[1] A. Lender, "The Duo-Binary Technique for High Speed Data Transmission," IEEE Trans. on Comm. and Electronics, May 1963, pp. 214 - 218.

[2] R. Lucky, J. Salz, and W. Weldon, Principles of Data Communication, McGraw-Hill, New York, 1968.

[3] A. Papoulis, Probability, Random Variables, and Stochastic McGraw-Hill, New York, 1965.

APPENDIX F

PULSE SHAPE INFORMATION REQUIRED BY CHANNEL ESTIMATOR SIMULATIONS

1. Filter Impulse Response

With $h_T(\cdot)$ the impulse response of the transmit filter, then from Eq. (4.11) of Section 4.3.2.1, in order to determine the discriminator output using the quadratic channel model requires $h_T(kT-\xi_g)$, $\dot{h}_T(kT-\xi_g)$, and $\ddot{h}_T(kT-\xi_g)$. For the cubic channel model, $\dddot{h}_T(kT-\xi_g)$ will also be required. Reference [1] recommends that the transfer function of the transmit and receive filters be given by

$$h_T(f) = h_R(f) = \begin{cases} [2T\cos(\pi f t)]^{\frac{1}{2}}, & \text{if } |f| \le \frac{1}{2T} \\ 0, & \text{otherwise} \end{cases} \tag{1}$$

Therefore, it follows that

$$h_R(\tau) = h_T(\tau) = \frac{2^{1/2}}{\pi T^{1/2}} \int_{-\pi/2}^{\pi/2} \cos^{1/2} y \cos\left(\frac{2\tau}{T} y\right) dy \tag{2}$$

$$\dot{h}_T(\tau) = -\frac{2^{3/2}}{\pi T^{3/2}} \int_{-\pi/2}^{\pi/2} y \cos^{1/2} y \cos\left(\frac{2\tau}{T} y\right) dy \tag{3}$$

$$\ddot{h}_T(\tau) = -\frac{2^{5/2}}{\pi T^{5/2}} \int_{-\pi/2}^{\pi/2} y^2 \cos^{1/2} y \cos\left(\frac{2\tau}{T} y\right) dy \tag{4}$$

$$\dddot{h}_T(\tau) = \frac{2^{7/2}}{\pi T^{7/2}} \int_{-\pi/2}^{\pi/2} y^3 \cos^{1/2} y \sin\left(\frac{2\tau}{T} y\right) dy \tag{5}$$

For use in the simulations and error rate calculations described in Section 4, the above integrals were evaluated numerically.

2. Statistical Analysis of Signal Functions

The use of the variance equalization and the determination of the adaptive channel estimator step size require the calculation of the variance of the $S_q(t)$, where $S_q(t)$ is given by Eqs. (4.11) and (4.13) of Section 4.3.2.1, or of $y_q(t)$ given by Eq. (4.14) of Section 4.3.2.1. To calculate the variance, the NRZ data $\{a_n\}$ was assumed to form independent, identically distributed sequence taking on the values ± 1 with equal probability. With this assumption on the data, the variance of $S_q(t)$ can be found to be given by

$$\sigma^2_{S_0(t)} = \sum_n h_T^2(t - \xi_g - nT) \tag{6}$$

$$\sigma^2_{S_1(t)} = \sum_n \dot{h}_T^2(t - \xi_g - nT) \tag{7}$$

$$\sigma^2_{S_2(t)} = \sum_n \ddot{h}_T^2(t - \xi_g - nT) \tag{8}$$

$$\sigma^2_{S_3(t)} = \sum_{\substack{m \\ m \neq n}} \sum_n \Big\{ \dot{h}_T^2(t - \xi_g - nT) h_T^2(t - \xi_g - mT) + \dot{h}_T(t - \xi_g - nT) \cdot \dot{h}_T(t - \xi_g - mT) h_T(t - \xi_g - nT) h_T(t - \xi_g - mT) \Big\} \tag{9}$$

$$\sigma^2_{S_4(t)} = \sum_n \dddot{h}_T^2(t - \xi_g - nT) \tag{10}$$

$$\sigma^2_{S_5(t)} = \sum_n h_T^4(t - \xi_g - nT)\dot{h}_T^2(t - \xi_g - nT)$$

$$+ \sum_{\substack{n \\ n\neq m}}\sum_m h_T^4(t - \xi_g - nT)\dot{h}_T^2(t - \xi_g - mT)$$

$$+ 6 \sum_{\substack{n \\ n\neq m}}\sum_m h_T^2(t - \xi_g - nT)h_T^2(t - \xi_g - mT)\dot{h}_T^2(t - \xi_g - mT)$$

$$+ 8 \sum_{\substack{n \\ n\neq m}}\sum_m h_T^3(t - \xi_g - nT)\dot{h}_T(t - \xi_g - nt)h_T(t - \xi_g - mT)\dot{h}_T(t-\xi_g-mT)$$

$$+ 3 \sum_{\substack{n \\ n\neq m\neq p\neq n}}\sum_m\sum_p h_T^2(t - \xi_g - nT)h_T^2(t - \xi_g - mT)\dot{h}_T^2(t - \xi_g - pT)$$

$$+ 12 \sum_{\substack{n \\ n\neq m\neq p\neq n}}\sum_m\sum_p h_T^2(t - \xi_g - nT)h_T(t - \xi_g - mT)\dot{h}_T(t - \xi_g - mT)$$

$$\cdot h_T(t - \xi_g - pT)\dot{h}_T(t - \xi_g - pT) \qquad (11)$$

$$\sigma^2_{S_6(t)} = 2 \sum_{\substack{n \\ m\neq m}}\sum_m \dot{h}_T^2(t - \xi_g - nT)\dot{h}_T^2(t - \xi_g - mT) \qquad (12)$$

$$\sigma^2_{S_7(t)} = \sum_{\substack{n \\ n\neq m}}\sum_m \Big[\dot{h}_T^2(t - \xi_g - nT)h_T^2(t - \xi_g - mT) + \ddot{h}_T(t - \xi_g - nT)$$

$$\cdot \ddot{h}_T(t - \xi_g - mT)h_T(t - \xi_g - nT)h_T(t - \xi_g - mT)\Big] \qquad (13)$$

The variance of the $y_q(t)$ given by Eq. (4.11) of Section 4.3.2.1 can also be found. For $q = 0, 1, 2, 3$, the variances are given by

$$\sigma^2_{y_0(t)} = \sum_n \left| \int_{-\infty}^{\infty} h_R(\tau) h_T(t - \xi_g - nT - \tau) d\tau \right|^2 \tag{14}$$

$$\sigma^2_{y_1(t)} = \sum_n \left| \int_{-\infty}^{\infty} h_R(\tau) \dot{h}_T(t - \xi_g - nT - \tau) d\tau \right|^2 \tag{15}$$

$$\sigma^2_{y_2(t)} = \sum_n \left| \int_{-\infty}^{\infty} h_R(\tau) \ddot{h}_T(t - \xi_g - nT - \tau) d\tau \right|^2$$

$$\sigma^2_{y_3(t)} = \sum_{\substack{n \\ n \neq m}} \sum_m \left[\left| \int_{-\infty}^{\infty} h_R(\tau) h_T(t - \xi_g - nT - \tau) \dot{h}_T(t - \xi_g - mT - \tau) d\tau \right|^2 \right.$$

$$+ \left| \int_{-\infty}^{\infty} h_R(\tau) h_T(t - \xi_g - nT - \tau) \dot{h}_T(t - \xi_g - mT - \tau) d\tau \right|$$

$$\left. \cdot \left| \int_{-\infty}^{\infty} h_R(v) h_T(t - \xi_g - mT - v) \dot{h}_T(t - \xi_g - nT - v) dv \right| \right] \tag{16}$$

The variances of the $y_i(t)$ for $i = 4$ to 7 can be found by using (14), (17), and the coefficients in Eq. (11). In particular, the varaince of $y_4(t)$ can be found by replacing $h_T(\cdot)$ by $\dot{h}_T(\cdot)$ in (14); the variance of $y_6(t)$ can be found by replacing $h_T(\cdot)$ by $\dot{h}_T(\cdot)$ in Eq. (17); the variance of $y_7(t)$ can be found by replacing $\dot{h}_T$ by $\ddot{h}_T$ in (17). The variance of $y_5(t)$ can be found from the coefficients in (11). For notational simplicity we define

$$H(n,m,p) = \int_{-\infty}^{\infty} h_T(\tau) h_T(t - \xi_g - nT - \tau) h_T(t - \xi_g - mT - \tau)$$

$$\cdot \dot{h}_T(t - \xi_g - pT - \tau) \, d\tau \tag{18}$$

It follows that (after a little manipulation)

$$\sigma^2_{y_5(t)} = \sum_{n} H^2(n,n,n) + \sum_{\substack{n \\ n\neq m}}\sum_{m} H^2(n,n,m)$$

$$+ \sum_{\substack{n \\ n\neq m}}\sum_{m} \Big[2H(n,n,m)H(m,m,m) + 4H^2(n,m,m)$$

$$+ 4H(n,n,n)H(n,m,m) + 4H(n,m,n)H(n,n,m)\Big]$$

$$+ \sum_{\substack{n \\ n\neq m\neq p\neq n}}\sum_{m}\sum_{p} \Big[2H(n,n,p)H(m,m,p) + 4H^2(n,m,p)$$

$$+ 4H(n,n,m)H(m,p,p) + 4H(n,p,p)H(n,m,m)$$

$$+ 4H(n,m,p)H(n,p,m)\Big] \qquad (19)$$

REFERENCE FOR APPENDIX F

[1] R. W. Lucky, J. Salz, and E. J. Weldon, Principles of Data Communication, McGraw-Hill, New York, 1968.

APPENDIX G

CHANNEL PARAMETER ESTIMATION BIAS DUE TO BIT ERRORS

In this appendix we will examine the bias in estimating channel parameters due to errors in detecting the data sequence. The purpose of this analysis is to determine an approximate range of error rates over which the adaptive channel estimator of Section 4 can be considered to perform satisfactorily. For this analysis it will be assumed that a quadratic channel model is sufficient to model the discriminator output. Therefore, the discriminator output can be closely approximated [see Eq. (4.10)] by

$$r(t) = \sum_{q=0}^{3} P_q F_q(t) + n(t) \tag{1}$$

where $n(t)$ is the noise, P_q are the channel parameters and $F_q(t)$ are given by

$$F_0(t) = \sum_n a_n h_T(t-nT)$$

$$F_1(t) = \sum_n a_n \dot{h}_T(t-nT)$$

$$F_2(t) = \sum a_n \ddot{h}_T(t-nT)$$

$$F_3(t) = F_0(t) \cdot F_1(t) \tag{2}$$

where the mean path delay has been neglected.

In Eq. (2), $\{a_n\}$ is the binary data sequence, and $h_T(\cdot)$ is the impulse response of the transmit filter. The adaptive channel estimator that estimates the discriminator output would use the detected data sequence $\{\hat{a}_n\}$ to form an estimate of $r(t)$. The estimate of $r(t)$ is given by

$$\hat{r}(t) = \sum_{q=0}^{3} \hat{P}_q(t) S_q(t) \tag{3}$$

where $\hat{P}_q(t)$ is the estimate of P_q and

$$S_0(t) = \sum_n \hat{a}_n h_T(t-nT)$$

$$S_1(t) = \sum_n \hat{a}_n \dot{h}_T(t-nT)$$

$$S_2(t) = \sum_n \hat{a}_n \ddot{h}_T(t-nT)$$

$$S_3(t) = S_0(t) \cdot S_1(t) \tag{4}$$

To update the estimate of the channel parameters, an error signal would be formed by

$$\epsilon(t) = r(t) - \hat{r}(t) \tag{5}$$

Using the LMS adaptation algorithm [see Eq. (4.19)], the k+1'th estimate of the channel parameters would be found by

$$\hat{P}_q(kT+T) = \hat{P}_q(kT) + 2\Delta\epsilon(kT)S_q(kT) \quad \text{for} \quad q = 0,1,2,3 \tag{6}$$

where Δ is the step size. Substituting Eqs. (1), (3), and (5) into Eq. (6) gives

$$\hat{P}_q(kT+T) = \hat{P}_q(kT) + 2\Delta \left\{ \sum_{\ell=0}^{3} [P_\ell F_\ell(kT) - \hat{P}_\ell(kT)S_\ell(kT)] + n(kT) \right\}$$

$$\cdot S_q(kT) \quad \text{for} \quad q = 0,1,2,3 \tag{7}$$

To find the bias introduced by the data errors we average Eq. (7) over the data and noise. This gives

$$\overline{\hat{P}_q(kT+T)} = \overline{\hat{P}_q(kT)} + 2\Delta \left\{ \sum_{\ell=0}^{3} P_\ell \, \overline{F_\ell(kT)S_q(kT)} - \overline{\hat{P}_\ell(kT)S_\ell(kT)S_q(kT)} \right.$$

$$\left. + \overline{n(kT)S_q(kT)} \right\} \quad \text{for} \quad q = 0,1,2,3 \tag{8}$$

where the overbar denotes average over noise and data.

For steady state (large k) $\overline{\hat{P}_q(kT+T)} = \overline{\hat{P}_q(kT)}$ for $q = 0,1,2,3$. Furthermore, if we assume that most data errors are the result of multipath induced distortion and that $\overline{n(kT)} = 0$, then $n(kT)$ and $S_q(kT)$ should be nearly uncorrelated and $\overline{n(kT)S_q(kT)}$ can be neglected. Lastly, if a small step size Δ is used then $\hat{P}_\ell(kT)$ and $S_\ell(kT)S_q(kT)$ should be uncorrelated. With the above assumptions, Eq. (8) yields the following set of equations.

$$\sum_{\ell=0}^{3} P_\ell \, \overline{F_\ell(kT)S_q(kT)} \approx \sum_{\ell=0}^{3} \overline{P_\ell(kT)} \; \overline{S_\ell(kT)S_q(kT)}$$

$$\text{for} \quad q = 0,1,2,3 \text{ and } k \text{ large} \qquad (9)$$

If the transmitted data $\{a_n\}$ forms an independent, identically distributed sequence taking on the values $\pm d$ with equal probability, then the set of equations given by Eq. (9) can be expressed as

$$\begin{bmatrix} b_1 & b_2 & b_3 \\ b_2 & b_4 & b_5 \\ b_3 & b_5 & b_5 \end{bmatrix} \begin{bmatrix} \overline{\hat{P}_0(k)} \\ \overline{\hat{P}_1(k)} \\ \overline{\hat{P}_2(k)} \end{bmatrix} \approx (1-2P_e) \begin{bmatrix} b_1 & b_2 & b_3 \\ b_2 & b_4 & b_5 \\ b_3 & b_5 & b_6 \end{bmatrix} \begin{bmatrix} P_0 \\ P_1 \\ P_2 \end{bmatrix} \qquad (10)$$

and

$$\overline{\hat{P}_3(kT)} \; (b_2^2 + a_2) \approx P_3\{b_2^2 + a_2[1-4P_e + 3P_e^2]\}, \text{ for } k \text{ large} \qquad (11)$$

where P_e is the probability that $a_n \neq \hat{a}_n$ and

$$b_1 = \sum_n h_T^2(nT)$$

$$b_2 = \sum_n \dot{h}_T(nT)h_T(nT)$$

$$b_3 = \sum_n \ddot{h}_T(nT)h_T(nT)$$

$$b_4 = \sum_n \dot{h}_T^2(nT)$$

$$b_5 = \sum_n \ddot{h}_T(nT)\dot{h}_T(nT)$$

$$b_6 = \sum_n \ddot{h}_T^2(nT)$$

$$a_2 = b_2^2 + b_1 b_4 - 2 \sum_n h_T^2(nT)\dot{h}_T^2(nT) \qquad (12)$$

The matrix of b's presented in Eq. (10) is the correlation matrix of $S_q(kT)$, $q = 0,1,2$ and is positive definite. Multiplying both sides of Eq. (10) by the inverse of this correlation matrix gives

$$\overline{\hat{P}_q(kT)} \approx (1-2P_e)P_q \quad , \quad \text{for } q = 0,1,2 \text{ and } k \text{ large} \qquad (13)$$

Therefore, the bias in estimating channel parameters P_0, P_1, P_2 is given by $-2P_eP_q$. To determine the bias of the estimate of channel parameter P_3 we return to Eq. (11) and note that normally $a_2 \gg b_2^2$ which results in

$$\overline{\hat{P}_3(kT)} \approx P_3(1-4P_e + 3P_e^2) \quad , \; k \text{ large} \qquad (14)$$

Examining Eqs. (13) and (14) we note that if the bias is to be kept less than 10% for P_q, $q = 0,1,2,3$ the error rate should be less than 0.025.

The simulation discussed in Section 4.3.5.2 was used to verify the preceding analysis. In this simulation random errors were generated and the statistics of the parameter estimates determined. The results of these simulations are presented in Tables 1 to 4. For the simulation runs summarized in the tables, it should be noted that the measured mean value of the channel parameter estimates was closer to the mean value predicted by Eqs. (13) and (14) than to the actual value for all but one case (P_2 of Table 4). The agreement of theory and simulation indicate that Eqs. (13) and (14) can be used with some confidence in predicting channel parameter estimation bias.

TABLE 1

SUMMARY OF CHANNEL PARAMETER ESTIMATION
(P_e = 0.0903, NORMALIZED STEP SIZE = 0.01, NOISE ADDED)

Channel Parameter	Actual Parameter Value	Predicted Mean	Measured Mean	Measured Standard Deviation
P_0	1.0	0.8194	0.7670	0.1149
P_1	-0.8678	-0.7111	-0.7814	0.0557
P_2	0.0097	0.0079	-0.0079	0.0415
P_3	0.9574	0.6350	0.6612	0.2512

LMS Algorithm
"Bad" Channel
Variance Equalization
32 dB Fade
Quadratic Channel Model
Statistics Over 2500 Iterations

TABLE 2

SUMMARY OF CHANNEL PARAMETER ESTIMATION
(P_e = 0.0903, NORMALIZED STEP SIZE = 0.001, NOISE ADDED)

Channel Parameter	Actual Parameter Value	Predicted Mean	Measured Mean	Measured Standard Deviation
P_0	1.0	0.8194	0.7768	0.0334
P_1	-0.8678	-0.7111	-0.7824	0.0119
P_2	0.0097	0.0079	-0.0051	0.0077
P_3	0.9574	0.6350	0.6357	0.0443

LMS Algorithm
"Bad" Channel
Variance Equalization
32 dB Fade
Quadratic Channel Model
Statistics Over 2500 Iterations

TABLE 3

SUMMARY OF CHANNEL PARAMETER ESTIMATION
(P_e = 0.0903, NORMALIZED STEP SIZE = 0.001, NO NOISE)

Channel Parameter	Actual Parameter Value	Predicted Mean	Measured Mean	Measured Standard Deviation
P_0	1.0	0.8194	0.7753	0.0330
P_1	-0.8678	-0.7111	-0.7829	0.0136
P_2	0.0097	0.0079	-0.0059	0.0077
P_3	0.9574	0.6350	0.6381	0.0438

LMS Algorithm
"Bad" Channel
Variance Equalization
32 dB Fade
Quadratic Channel Model
Statistics Over 2500 Iterations

TABLE 4

SUMMARY OF CHANNEL PARAMETER ESTIMATION
(P_e = 0.0101, NORMALIZED STEP SIZE = 0.001, NOISE ADDED)

Channel Parameter	Actual Parameter Value	Predicted Mean	Measured Mean	Measured Standard Deviation
P_0	1.0	0.9798	0.9746	0.0123
P_1	-0.8678	-0.8503	-0.8525	0.0055
P_2	0.0097	0.0095	0.0113	0.0035
P_3	0.9574	0.9190	0.8328	0.0431

LMS Algorithm
"Bad" Channel
Variance Equalization
32 dB Fade
Quadratic Channel Model
Statistics Over 2500 Iterations